UNIVERSITY OF CALIFORNIA,
IRVINE

Resolving the History of the Earth's Atmospheric Radiocarbon for Calibration and Carbon Cycle Studies

DISSERTATION

submitted in partial satisfaction of the requirements
for the degree of

DOCTOR OF PHILOSOPHY

in Earth System Science

by

Alexandra L Noronha

Dissertation Committee:
Dr. Kathleen Johnson, Chair
Dr. John Southon
Dr. Claudia Czimczik
Dr. Ellen Druffel

2014

TABLE OF CONTENTS

LIST OF FIGURES

Page

LIST OF TABLES

Page

ACKNOWLEDGMENTS

Chapter 2:, is a reproduction of an article as it appears in Paleoceanography 2010. Magana, Alexandra L.; Southon, John R.; Kennett, James P; Roark, E. Brendan; Sarnthein, Michael; Stott, Lowell D., American Geophysical Union, 2010. The dissertation author is the primary investigator and author of this paper.

Chapter 4:, is a reproduction of an article as it appears in Quaternary Science Reviews 2012. Southon, John R.; Noronha, Alexandra L.; Cheng, Hai; Edwards, R. Lawrence; Wang, Yongjin, Elsevier, 2012. The dissertation author is one of the primary investigators and authors of this paper.

Chapter 5:, is a reproduction of an article as it appears in Earth and Planetary Science Letters 2014. Noronha, Alexandra L.; Johnson, Kathleen R.; Hu, Chaoyang; Ruan, Jiaoyang; Southon, John R.; Ferguson, Julie E., Elsevier, 2014. The dissertation author is the primary investigator and author of this paper.

Chapter 6:, in part, is being prepared for publication. Noronha, Alexandra L.; Johnson, Kathleen R.; Southon, John R.; Hu, Chaoyang; Ruan, Jiaoyang; McCabe-Glynn, Staryl, The dissertation author is the primary investigator and author of this paper.

The appendix:, is a reproduction of an article as it appears in Radiocarbon 2010. Southon, John R.; Magana, Alexandra L., University of Arizona, 2010. The dissertation author is one of the primary investigators and authors of this paper.

I am grateful for the financial support I received through a National Science Foundation East Asia Pacific Summer Institute Fellowship (2011).

I have been exceptionally lucky to have many mentors over the course of my academic career, without which I would not be submitting this finished work. Before UCI, as an undergrad geology student at UC Santa Barbara, the work I did under the mentorship of Jim Kennett and Frank Spera made me realize how central the accuracy of the radiocarbon calibration curve is to so much of what we know about Earth's recent history. I thank them both for their generosity with their time, and in helping set me on my way as a young scientist.

Accordingly, I came to UC Irvine because I wanted to work on radiocarbon calibration, and John's willingness to take me on as a student gave me the opportunity to engage with

calibration work in a way that would not have been possible anywhere else. I am so grateful for the countless hours and apparently infinite patience John has had for me over these past six years. John has always been available to talk through any of the thoughts that are bouncing around my head, and his generosity has been absolutely central to my success.

Similarly, Kathleen has been endlessly patient and supportive - seeing me through from a student on my first trip to China, doubting the wisdom of my choices, to today as we continue to work on truly exciting research together. I'm so glad to have been a part of her nascent lab at UCI. She has always pushed me just the right amount to get out of my comfort zone, and it's with those nudges that I've had many of my most proud successes over these past years.

I'd like to thank the numerous others at UCI ESS who have made my time at UCI so fruitful - Ellen Druffel, Claudia Czimczik, Xiaomei Xu, Guaciara dos Santos, Julie Ferguson, Shelia Griffin, my fellow graduate students, and postdocs, that I've had the pleasure of getting to know, my many collaborators, and the members of the community that I have met at conferences and short courses.

And, of course, I must thank Rodrigo. From the being my steadfast partner and an endless source of support, to the hours he spent patiently helping me to learn to write better code - Rodrigo contributed much to my success and makes me a better person in countless ways. From when we met as couple of freshman, to today as we head out on our next big adventure, I'm so glad it was you that was building a life with me.

CURRICULUM VITAE

Alexandra L Noronha

EDUCATION

Doctor of Philosophy in Earth System Science **2014**

University of California Irvine *Irvine, CA*

Bachelor of Science in Geological Sciences **2007**

University of California, Santa Barbara *Santa Barbara, CA*

REFEREED JOURNAL PUBLICATIONS

Assessing influences on speleothem dead carbon variability over the Holocene: implications for speleothem-based radiocarbon calibration **2014**

Earth and Planetary Science Letters

The New Zealand Kauri (Agathis Australis) Research Project: A Radiocarbon Dating Intercomparison of Younger Dryas Wood and Implications for IntCal **2013**

Radiocarbon

A high-resolution record of atmospheric ^{14}C based on Hulu Cave speleothem H82 **2012**

Quaternary Science Reviews

Resolving the cause of large differences between deglacial benthic foraminifera radiocarbon measurements in Santa Barbara Basin **2010**

Paleoceanography

A Comparison of Cellulose Extraction and ABA Pretreatment Methods for AMS ^{14}C Dating of Ancient Wood **2010**

Radiocarbon

ABSTRACT OF THE DISSERTATION

Resolving the History of the Earth's Atmospheric Radiocarbon for Calibration and Carbon Cycle Studies

By

Alexandra L Noronha

Doctor of Philosophy in Earth System Science

University of California, Irvine, 2014

Dr. Kathleen Johnson, Chair

Reconstructing the history of Earth's atmospheric radiocarbon (^{14}C) through the detection limit has been a long term goal of the scientific community, because of the usefulness of ^{14}C as a chronometer for records of Quaternary Earth history, and because variations in atmospheric ^{14}C are, in part, recorders of changes in Earth's carbon cycle. This dissertation represents the result of work that aims to reconstruct the history of Earth's atmospheric ^{14}C, both through studies of intervals of interest to the climate-carbon feedback cycle in the deglacial interval, and through attempting to develop speleothem records of atmospheric ^{14}C in older intervals where knowledge of atmospheric ^{14}C is currently lacking. The major results of this dissertation include a record of deglacial ventilation ages in the Santa Barbara Basin. This record demonstrates that the hypothesized "old water" mass thought to have been responsible for the deglacial atmospheric CO_2 rise and concurrent $\Delta^{14}C$ decline is unlikely to have existed in the Santa Barbara Basin. Also included in this dissertation is the result of work to reconstruct atmospheric ^{14}C during the Younger Dryas climate event based on New Zealand kauri. The remainder of the dissertation is composed of works that aim to develop

speleothem-based records of atmospheric ^{14}C, and to understand carbon incorporation in speleothems. These works demonstrate that there do exist some speleothems, most notably Hulu Cave H82, that have low and stable dead carbon incorporation and are are valuable sources of records of atmospheric ^{14}C. Records speleothem ^{14}C from Heshang Cave HS4 suggest that increases in precipitation drives increases in speleothem dead carbon incorporation through shifting carbonate dissolution to a more closed system regime, though decreases in precipitation do not appear to drive proportional decreases in speleothem dead carbon. Modern monitoring of cave carbon cycling at Heshang Cave and modeling of speleothem bomb peak records indicates that speleothem carbon is likely derived primarily from decomposition of down-washed soil organic matter in the deep vadose zone, and that organic matter in karst settings may be much older than organic matter in sites studied previously.

Chapter 1

Introduction

1.1 Introduction

Ice core records of the past 800 ka record glacial/interglacial cycles in atmospheric pCO_2, and show a tight relationship between atmospheric pCO_2, ice volume, and global temperature. However, in spite of the clear importance of atmospheric pCO_2 as a driver of global climate, the mechanism driving glacial/interglacial cycles of atmospheric pCO_2 is still largely unknown. Understanding the drivers of glacial/interglacial atmospheric pCO_2 is perhaps the most important question in paleoclimatic research, and the continued development of our understanding of the relationship between the global carbon cycle and climate change in this current period of rapid anthropogenically driven climate change is essential.

The reconstruction of a radiocarbon (^{14}C) record that directly samples atmospheric CO_2 through the last glacial cycle, tied to a robust independent timescale, has been a long-time goal of the scientific community for two key reasons. First, ^{14}C measurements are used to create chronologies for records of Earth systems history, but dates must be calibrated to a calendar age to correct for offsets between ^{14}C age and calendar age due to changes in the

production rate and partitioning of ^{14}C in the Earth system. Second, these same fluctuations in atmospheric ^{14}C that present a complication to ^{14}C based calendar chronology are valuable records of the changes in Earth's carbon cycle. The focus of this dissertation is to contribute to the effort to improve the understanding of the history of the Earth's atmospheric ^{14}C, on a variety of timescales, as well as intervals of importance in the carbon-climate feedback cycle, for both the improvement of understanding the history of Earth's carbon cycle and the ^{14}C calibration curve.

1.2 Current state of knowledge of the history of Earth's atmospheric ^{14}C

Soon after the development of the ^{14}C dating method, for which Willard Libby was given the Nobel Prize for Chemistry in 1960, it was recognized that "^{14}C time" deviates from calendar time (Suess and Linick, 1990). This deviation arises from the assumption of constant past atmospheric ^{14}C concentrations made in the calculation of conventional ^{14}C age. Atmospheric ^{14}C concentrations have changed significantly over the past 50 ka, driven by both changes in both the production rate of ^{14}C in the upper atmosphere, and the distribution of carbon in reservoirs of the Earth system and rates of exchange between these reservoirs. The long term decreasing trend is due to a long period of decreased shielding effect of the geomagnetic dipole field, and most of the high frequency changes are due to magnetic fluctuations of solar origin (Bard, 1998). Climatically driven changes in the Earth's carbon cycle are also apparent in records of atmospheric ^{14}C, especially during the deglacial interval.

Because ^{14}C is an important source of calendar chronologies, the current knowledge of atmospheric ^{14}C is conveniently summarized by the calibration curve, IntCal (Reimer *et al.*, 2013). Records of ^{14}C dendrochronological dated tree ring are considered the most robust

records of atmospheric ^{14}C because they directly incorporate atmospheric CO_2 during photosynthesis and have high-resolution independent chronologies. Tree ring records from central and northern Europe are the basis of the most recent IntCal13 ^{14}C calibration curve to 13.9 ka (Reimer *et al.*, 2013). Before this time, regional climate conditions were less hospitable to trees, and the tree ring records are no longer the basis of ^{14}C calibration curves, although there are some floating tree ring chronologies that cover earlier intervals (e.g. Turney *et al.*, 2007; Muscheler *et al.*, 2008; Kromer *et al.*, 2004; Hua *et al.*, 2009; Hogg *et al.*, 2013b).

The only true non-tree ring record of atmospheric ^{14}C extending beyond 13.9 ka is a record from Lake Suigestu, Japan, which is based on macrofossils paired with a varve counting chronology (Kitagawa and van der Plicht, 1998a, 1998b, 2000, Staff et al., 2010, Bronk Ramsey et al., 2012) and covers the interval 0-52.8 ka. The Lake Suigetsu record presented by Kitagawa and van der Plitch (1998a, 1998b, 2000) showed significant divergences from other atmospheric ^{14}C reconstructions prior to $\sim$25 ka, which was found to be due to incomplete core retrieval during sampling (Staff *et al.*, 2010). A new set of overlapping cores was taken and a new, high-resolution record with an improved chronology has been constructed. This new record displays large scatter in the ^{14}C ages due to small sample sizes in the interval $>$28 ka, as well as large uncertainty in the layer-counting age model (Bronk Ramsey *et al.*, 2012). Nonetheless, the Lake Suigetsu ^{14}C record provides a valuable "backbone" for the atmospheric ^{14}C record, which is refined by a variety of other ^{14}C records.

In the absence of true atmospheric records, the majority of calibration efforts have been focused on marine sediment records with a constant correction applied to account for the marine reservoir effect - the offset between the concentration of ^{14}C in the ocean and the atmosphere. The marine records included in IntCal13 include both marine sediment and coral records. The marine sediment records are based on foraminifera from the Cariaco Basin (Hughen *et al.*, 2006), the Iberian Margin (Bard *et al.*, 2004), and the Pakistan Margin (Bard *et al.*, 2013) tuned to the Hulu Cave speleothem $\delta^{18}O$ record (Wang *et al.*, 2001) to

establish a calendar chronology for the unvarved sections. The coral records are U-Th dated and are sourced from from both the tropical Pacific (Bard *et al.*, 1990, 1998a, 2004; Edwards *et al.*, 1993; Burr *et al.*, 1998, Burr *et al.*, 2004, Cutler *et al.*, 2004, Durand *et al.*, 2013) and tropical Atlantic (Fairbanks *et al.*, 2005).

The newest addition to IntCal is speleothem-based records of atmospheric ^{14}C. Speleothem are cave carbonate deposits, which have long been used in paleoclimate research, and have recently been of great interest as records of atmospheric ^{14}C. Records from submerged speleothems from the Bahamas (Beck *et al.*, 2001 and Hoffmann *et al.*, 2010) as well as a record presented in this dissertation from Hulu Cave (Southon *et al.*, 2012) were included in IntCal13.

1.3 ^{14}C as a tracer of the deglacial carbon cycle

During the last deglaciation, the interval spanning from to Last Glacial Maximum ($\sim$ 21 ka) to the beginning of the Holocene (11.7 ka) atmospheric pCO_2 increased by 80 ppm, while atmospheric $\Delta^{14}C$ decreased by 400‰. These changes were not monotonic, but instead the bulk of the rise occurred during two abrupt climate stadial events - Heinrich Event 1, a period also referred to as the "Mystery Interval" (Denton *et al.*, 1999), and the Younger Dryas (YD). Reconstructions of Earth's magnetic field strength show that the field has strengthened over the last 40 ka, which lowers the production rate of ^{14}C (Laj *et al.*, 2002). Changing production rate can account for some, but not all, of the decline in atmospheric ^{14}C, the remainder is thought to be largely driven by changes in ocean ventilation (Broecker and Barker, 2007).

The current hypothesis for the source of the large increase in atmospheric pCO_2 and concurrent decrease in atmospheric ^{14}C during the Mystery Interval is the so called "old water"

hypothesis. The old water hypothesis suggests that during the last glacial period, the abyssal ocean was poorly ventilated, leading to the isolation of a deep water mass in which ^{14}C decay dominated. At the termination of the glaciation this old water mass was upwelled at intermediate depths and mixed with the rest of the ocean, leading to increasing differences followed by sudden reductions in the difference between surface and bottom water ages. These differences in ^{14}C ages are apparent in differences between benthic and planktonic foraminifera. Chapter 2 of this dissertation presents the published manuscript of a study of benthic-planktonic ^{14}C age differences in the Santa Barbara Basin, CA during the Mystery Interval Magana *et al.* (2010). A previous study by Sarnthein *et al.* (2007) showed large benthic-planktonic ^{14}C age differences in the Santa Barbara Basin during the last deglaciation. If these measurements could be confirmed, they would provide valuable information about the transport pathway and upwelling pattern of the old water mass. The result of this work shows that large interspecies differences in benthic taxa exist, and ultimately show no evidence of a ^{14}C depleted water mass in the basin during the Mystery Interval.

Although being critically important for understanding carbon cycle changes, at present knowledge of atmospheric ^{14}C during the YD interval is quite limited. In the most current IntCal, there is a "gap" in the tree ring records where the interval 11.8 - 12.2 ka is defined by only 3 points. The highest resolution record in this interval is the marine-based Cariaco Basin record, but recent studies have shown that the reservoir age in the Cariaco Basin changed drastically during the YD. These changes in reservoir ages highlight the need for high-resolution, true atmospheric records during the YD interval in order to understand the feedbacks between the carbon cycle and climate during abrupt climate change, as well as for establishing chronologies for YD paleoclimatic and paleoecological records.

Chapter 3 of this dissertation represents work that was done to develop a record of atmospheric ^{14}C covering the YD interval based on subfossil kauri extracted from bogs in Northern New Zealand. The chapter describes the preliminary results of the work on the YD Kauri

undertaken at UCI. Work on this project is still underway as a collaboration between several labs as reported by Hogg *et al.* (2013b). The results tentatively show that the majority of the centennial scale variations in atmospheric ^{14}C during the YD interval can be explained by changes in ^{14}C production rate.

1.4 Development of speleothem-based records of atmospheric ^{14}C

Chapters 4-6 of this dissertation concern the use of speleothems as records of atmospheric ^{14}C. Recently, there has been interest in using speleothems to create records for ^{14}C calibration (e.g. Beck *et al.*, 2001; Weyhenmeyer *et al.*, 2003; Dorale *et al.*, 2008; McDermott *et al.*, 2008; Hoffmann *et al.*, 2010; Southon *et al.*, 2012). Speleothems hold some key advantages over floating tree rings, varved chronologies, and marine records:

1. They can be precisely and absolutely dated using U-Th methods (Richards and Dorale, 2003)
2. Their fast growth rates, highly resolvable stratigraphy, and excellent preservation allow for high-resolution ^{14}C measurement over the entire ^{14}C dating range
3. They may be a more direct recorder of atmospheric ^{14}C than marine records
4. They are widely used for paleoclimate reconstruction (Fairchild *et al.*, 2006) so access to numerous U-Th dated samples is possible and will allow for replication of records and direct comparison with climate proxy data.

There are, however, several complicating factors affecting speleothem-based ^{14}C calibrations that stem from the way that speleothems are formed.

Formation of speleothem calcite is driven by CO_2 degassing of cave drip water that has accumulated carbon from the soil and bedrock. Meteoric waters equilibrate with soil CO_2 to form carbonic acid:

$$CO_2 + H_2O \longrightarrow H_2CO_3$$

This weak acid causes dissolution of the cave host limestone bedrock as water moves through the epikarst:

$$H_2CO_3 + CaCO_3 \longrightarrow Ca^{2+} + 2\,HCO_3^-$$

Because of lower pCO_2 of cave air relative to the drip water, CO_2 degassing is initiated as drip water moves into the cave:

$$Ca^{2+} + 2\,HCO_3^- \longrightarrow CO_2 + H_2O + CaCO_3$$

Consequently, ^{14}C in speleothem calcite is offset from contemporaneous atmospheric ^{14}C because a proportion of speleothem carbon comes from soil CO_2 derived from decomposition old soil organic matter (SOM) and from ^{14}C-free "dead carbon" from the bedrock. The offset between speleothem ^{14}C and contemporaneous atmospheric ^{14}C has been referred to in a variety of different ways in the literature, including the published manuscripts in this dissertation. In the published manuscript presented in Chapter 4, the offset is referred to as the dead carbon fraction (DCF), which is an offset in ^{14}C years. In Chapters 5 and 6 the offset is referred to as the dead carbon proportion (DCP) as a percentage as defined by (Genty and Massault, 1997), but also as a "correction" or "offset" with units of ^{14}C years.

Despite the potential for variable DCP to complicate speleothem-based reconstructions of atmospheric ^{14}C, speleothem ^{14}C records have, as is demonstrated in this dissertation, been used to provide valuable constraints on the calibration curve during intervals where true atmospheric ^{14}C data are limited. An example of the usefulness of speleothem-based records for improving our understanding of atmospheric ^{14}C is the results of combining the true

atmospheric measurements from Lake Suigetsu, with the robust calendar chronologies of speleothem ^{14}C records. While the Lake Suigetsu record has the advantage of being a true atmospheric ^{14}C record, the inherent uncertainty in varve counting chronology limits the certainty of the calendar chronology in older sections. Speleothem records provide the advantage of having robust absolute calendar chronologies based on U-Th dating and comparison between speleothem-based records of atmospheric ^{14}C provides a way to correct for the drift in the Lake Suigetsu varve counting chronology (Bronk Ramsey *et al.*, 2012).

Chapter 4 of the dissertation represents a published manuscript of a record of atmospheric ^{14}C based on the Hulu Cave speleothem H82 that was included in IntCal13. DCP in H82 is remarkably low and stable, suggesting the great potential of speleothem-based ^{14}C calibration. While the H82 record demonstrates the utility of speleothem-based records of atmospheric ^{14}C, it also highlights the importance of developing an understanding of speleothem DCP. Understanding the controls of the variability in, or stability of, dead carbon incorporation is a necessary prerequisite to being able to reliably interpret speleothem ^{14}C records as records of atmospheric ^{14}C.

Accordingly, Chapter 5 is a study that seeks to understand variability in dead carbon incorporation in a Holocene speleothem, HS4 from Heshang Cave, China. The Holocene represents the interval where atmospheric ^{14}C is best known based on dendrochronologically dated trees, allowing for precise identification of changes in speleothem DCP. HS4 is a good candidate to understand variability in speleothem dead carbon incorporation over a wide range of climatic conditions, as Heshang Cave lies in the East Asian Summer Monsoon region, a location that has likely experienced large changes in precipitation in response to changing Northern Hemisphere summer insolation over the Holocene. This study showed an increase in speleothem DCP during the warmer, wetter, mid-Holocene interval. The decrease in DCP during the colder, drier, 8.2 ka event was not proportional to the increases

in the mid-Holocene, suggesting that speleothem DCP may be less sensitive to decreases in precipitation than increases.

Chapter 6 is a study of modern soil carbon processes at Heshang Cave. This chapter argues that the shape of the 20^{th} century atmospheric ^{14}C bomb peak recorded in speleothems indicates that speleothem carbon is not derived from CO_2 in the shallow soils commonly found in karst terrains, but instead from decomposition of soil organic matter deep in the vadose zone. This hypothesis may help to explain some of the stability observed in speleothem DCP despite large changes in climate, as the deep vadose zone is insulated against large changes in climate at the Earth's surface.

Chapters 5 and 6 are the beginning of a more complete understanding of the controls of speleothem DCP, and the role of soil carbon in karst settings in the global carbon cycle. Chapter 7, the final chapter of this dissertation, suggests some of the directions that future research in understanding speleothem DCP and carbon cycling in karsts might take.

Chapter 2

Resolving the cause of large differences between deglacial benthic foraminifera radiocarbon measurements in Santa Barbara Basin

2.1 Abstract

To better understand the deglacial upwelling pattern in the east Pacific, we have made radiocarbon (^{14}C) measurements on benthic foraminifera and macrofauna from a 3.5 m long interval in ODP Core 893A from Santa Barbara Basin, California, representing early deglaciation. This work serves to investigate the source of apparent disagreement between radiocarbon data sets from Leibnitz Laboratory, Kiel University (Kiel) and Carbon Center for Accelerator Mass Spectrometry, Lawrence Livermore National Laboratory (LLNL). These data sets are based on measurements of mixed benthic and mixed planktonic foraminifera. Interlaboratory

^{14}C results are similar for the planktonic foraminiferal analyses; however, Kiel measurements on mixed benthic foraminifera are much older than mixed benthic measurements from equivalent depths measured at LLNL. Our new results show distinct ^{14}C differences between taxa, with *Pyrgo sp.* giving ages consistently older than Kiel measurements on mixed benthic taxa, while ages for *Nonionellina sp.*, *Buliminella sp.*, *Uvigerina sp.*, and benthic macrofauna were much younger, even younger than the LLNL mixed benthic data. The new data supports benthic-planktonic age offsets of no more than 300 years, indicating that bottom waters within the basin remained significantly younger during early deglaciation than some previous results have suggested and are thus consistent with sedimentary and faunal evidence for well-oxygenated conditions.

2.2 Introduction

Foraminiferal benthic-planktonic (B-P) radiocarbon (^{14}C) age differences have provided key information in reconstructing changes in ventilation rates of the deep ocean over the last glacial cycle. Recently, extreme radiocarbon depletions have been observed in benthic foraminifera from early deglacial intervals of marine sedimentary cores from Baja California (MV99-MC19/GC31/PC08 23.5 °N, 111.6 °W; 705 m water depth) (Marchitto *et al.*, 2007), and the Galapagos Islands (VM21-30 1 °13‘S 89 °410W; 617 m water depth) (Stott *et al.*, 2009). These old benthic ^{14}C ages may be evidence of a water mass, previously isolated in the deep ocean, moving through the Pacific at intermediate depths during deglaciation. Marchitto *et al.* (2007) linked these changes with a low-Δ^{14}C excursion in Eastern Pacific lower thermocline waters, and hypothesized that they represented ventilation via the Southern Ocean of a previously isolated glacial deep water mass (Adkins *et al.*, 2002), with massive release of sequestered CO_2. Breakdown of deep ocean stratification may have led to upwelling in the Southern Ocean and outgassing of this water mass between 17.5 and 14.5 kyr. This

outgassing is thought to be the cause of the deglacial 190‰ decline in atmospheric $\Delta^{14}C$ and concurrent 40 ppm rise in atmospheric pCO_2 (Broecker and Barker, 2007). If confirmed, this hypothesis of deep ocean carbon sequestration would provide a simple explanation for much of the glacial drawdown of atmospheric pCO_2. Several recent studies have reported B-P differences of Last Glacial Maximum deep waters that are significantly larger than Holocene values (Galbraith *et al.*, 2007; Robinson *et al.*, 2005; Sarnthein *et al.*, 2007; Skinner *et al.*, 2010). However, evidence for an abyssal water mass of sufficient size and $\Delta^{14}C$ depletion to account for the bulk of the deglacial $\Delta^{14}C$ drop is still lacking (Broecker, 2009), and the Southern Ocean upwelling locations and pathways of the upwelled water into the ocean interior remains enigmatic (De Pol-Holz *et al.*, 2010; Rose *et al.*, 2010).

Measurements carried out by Sarnthein *et al.* (2007) at the Leibnitz Laboratory at Kiel University (Kiel) showed B-P ^{14}C age differences of ∼2,000 yrs in a deglacial interval spanning 28-31.5 m below seafloor (mbsf) in Santa Barbara Basin (SBB) Ocean Drilling Program Core 893A. Applying a late Holocene ^{14}C marine reservoir correction of ∼650 years (Ingram and Southon, 1996), this depth interval corresponds to the period ∼18-17 kyr cal BP, which is consistent with the presence of very old water in the basin during early deglaciation. This event appears to precede the period of greatest $\Delta^{14}C$ depletions off Baja California, but Sarnthein *et al.* (2007)postulated a much larger deglacial reservoir correction than previously used, which brings the Baja California and SBB events into synchronicity. These Kiel measurements, however, disagree sharply with a previous set of ^{14}C data measured at Lawrence Livermore National Laboratory (LLNL) on SBB foraminifera from the same interval in 893A (Hendy *et al.*, 2002). Shown in 2.1, ^{14}C measurements on mixed planktonic taxa from both Kiel and LLNL are in close agreement, but LLNL measurements on mixed benthic taxa do not display the same ^{14}C depletion shown by the Kiel data.

If the mixed benthic measurements made at Kiel can be confirmed to be representative of the age of the bottom water in SBB during this interval, then SBB would represent the

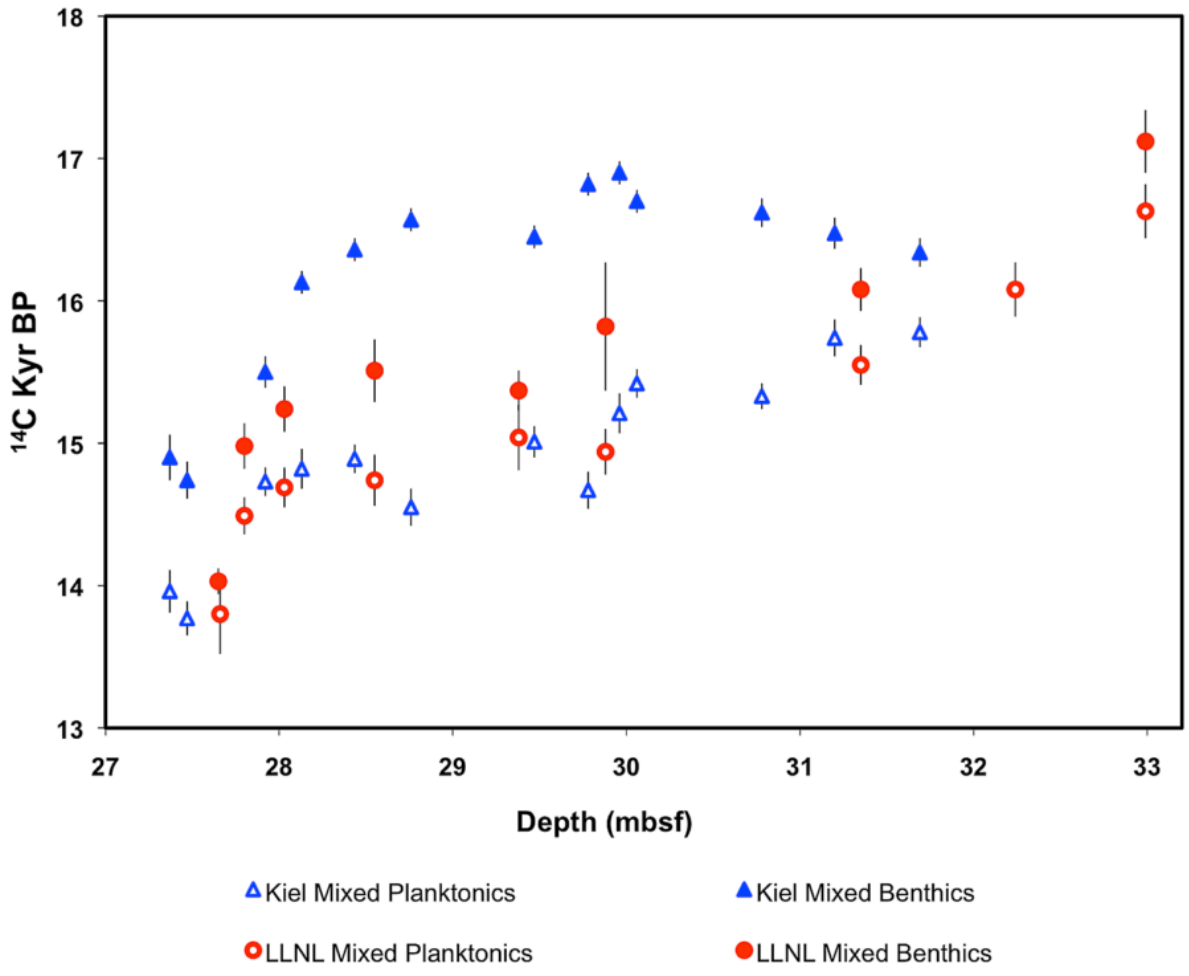

Figure 2.1: The ^{14}C results from mixed-assemblage foraminifera samples measured at Kiel and LLNL in previous studies.

most northerly location of the ^{14}C depleted intermediate water mass so far observed. Resolving the discrepancy in B-P differences between these measurements is therefore critical to understanding the transport path and upwelling pattern of this proposed water mass. To investigate the source of the differences in these data sets, and to improve our knowledge of ^{14}C in the SBB water column during deglaciation, we have conducted further ^{14}C measurement on 41 single taxa benthic samples, 6 mixed planktonic taxa samples, and 12 benthic gastropod and bivalve shell samples. Additionally, $\delta^{13}C$ measurements were made on aliquots reserved from 28 of the single taxa benthic foraminiferal samples.

2.3 Methods

Ocean Drilling Program core 893A was collected in 1993 from the Santa Barbara Basin, California (34°17′N, 120°2′W, 576.5 m water depth) during Part 2 of Leg 146. Sediment samples used in this project were sampled at 2 cm resolution in 2004, quickly disaggregated, dried, and stored in glass vials at University of California Santa Barbara. To identify any potential diagenetic explanations for the apparent disagreement between the data sets, we analyzed benthic foraminifera using a Scanning Electron Microscope (SEM) equipped with an EDX (Energy Dispersive X-ray spectrometer). SEM images reveal that the samples have not undergone diagenetic $CaCO_3$ (calcium carbonate) replacement, though they do contain overgrowths and crystals that were identified visually as $CaSO_4$ (gypsum) and confirmed using EDX to determine sulfur. The conversion of $CaCO_3$ material to $CaSO_4$ is a common observation in organic rich sediment cores and in this case was likely a consequence of the long time between 893A core collection and the sample washing to concentrate foraminifera. The presence of such overgrowths and crystals has no impact on the ^{14}C measurements, and although the formation of gypsum is sometimes associated with the destruction of foraminifera, the SEM images showed no evidence of etching. Samples for the LLNL and Kiel data sets

were picked with effort to select pristine specimens, discarding samples that contained pyrite or significant discoloration. In this new study we resampled vials of 893A sediment that had already been picked for foraminifera for at least two previous projects, including the Kiel measurements. The remaining foraminifera in the samples generally occur in the size class <250µm and >150µm, and often contained pyrite. Care was taken to exclude specimens contaminated with tar, but because the samples have been heavily sampled previously, all other specimens were collected regardless of their quality. *Pyrgo sp.* was particularly abundant and large, often >425µm. All benthic foraminiferal forms present in large enough abundance to yield a single taxa ^{14}C measurement (>0.15 mg bulk foraminifera) were picked and analyzed for ^{14}C and $\delta^{13}C$. Six mixed planktonic samples from within the interval where the previous data sets disagreed were also picked and measured for ^{14}C as were 12 shell samples of small deep water gastropods and bivalves.

Pretreatment chemistry and accelerator mass spectrometer (AMS) ^{14}C measurements on the new samples were carried out at University of California, Irvine (UCI) using methods similar to those employed previously at LLNL and Kiel. Briefly, carbonate samples at all three laboratories were pretreated by leaching (using H_2O_2 at Kiel and dilute HCl at UCI and LLNL), hydrolyzed with H_3PO_4, and converted to graphite by iron-catalyzed hydrogen reduction. ^{14}C results were corrected for sample size dependent backgrounds based on results from small modern samples and ^{14}C-dead blanks (spar calcite at LLNL and UCI, and Eemian foraminifera at Kiel).

Stable isotope measurements were carried out at the University of Southern California (USC). Foraminiferal samples were crushed in glass slides and pretreated according to the standard USC protocol based on methods described by Barker *et al.* (2003). Bulk subsamples of 10-15 individuals were reserved from 23 of the single benthic taxa foraminifera samples used for ^{14}C analysis (9 *Nonionellina sp.*, 1 *Buliminella sp.*, 10 *Pyrgo sp.*, and 3 *Uvigerina sp.* samples) and analyzed on a VG Prism mass spectrometer. Precision based on repeated measurements

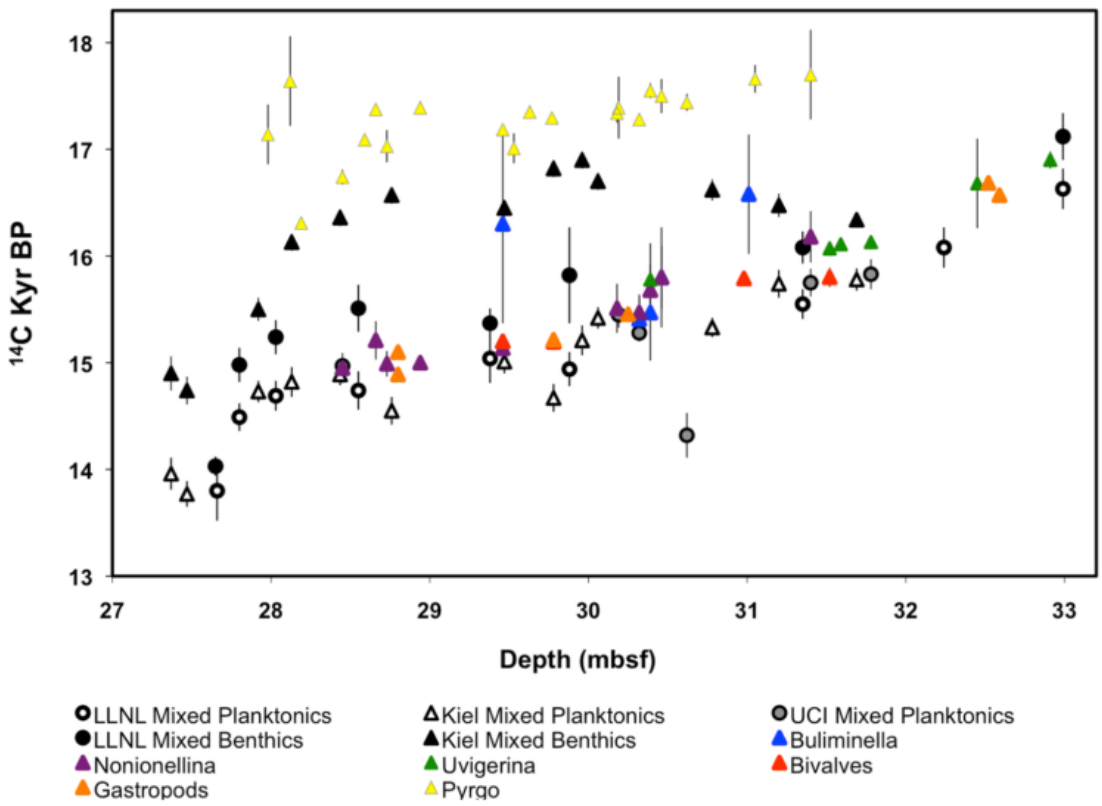

Figure 2.2: The ^{14}C results from this investigation, with data points from previous studies.

of an internal USC lab standard is 0.1‰. An additional 5 single specimens of Pyrgo were individually analyzed to determine isotopic variability within the 2 cm sampling intervals.

2.4 Results

Apart from one unexplained outlier at 30.6 m, AMS ^{14}C data from LLNL, Kiel and UCI on mixed planktonic samples are in good agreement, indicating that sample preparation and measurement techniques at the three labs are closely equivalent (Table 1 and 2.2). Our new results on benthic foraminifera show distinct large ^{14}C differences between taxa, with *Pyrgo sp.* giving ages 2,000-2,500 years older than the planktonics, and measurements on *Nonionellina sp.*, *Buliminella sp.*, and *Uvigerina sp.* yielding ages younger even than the

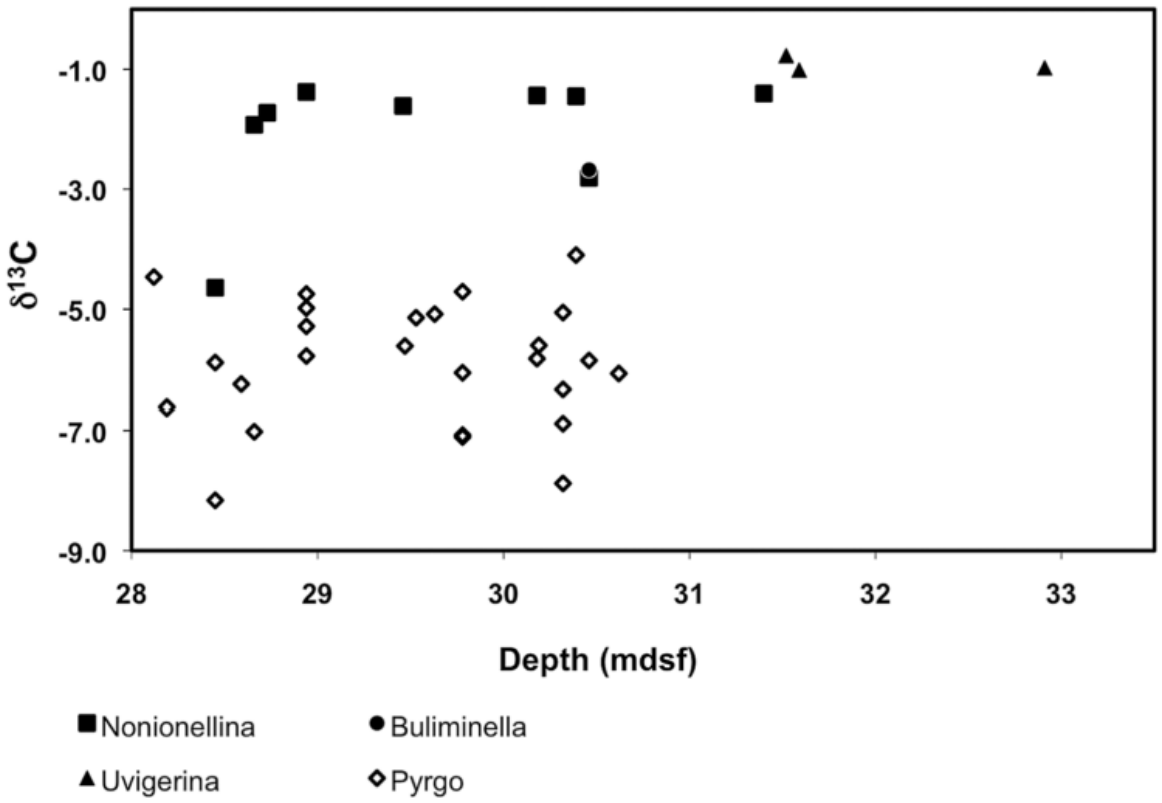

Figure 2.3: The δ^{13}C results from this study. Data are reported in standard delta notation as per mil deviations from the Vienna Pee Dee belemnite standard.

LLNL mixed benthic data (Table 1 and 2.2). With few exceptions, the new measurements on single taxa benthic foraminiferal samples and single benthic macrofauna result in B-P offsets typically 300 years or less. Two measurements on *Buliminella sp.* samples at 29.5 and 31.0 m gave ages similar to mixed benthic data from Kiel, but were both extremely small samples and have correspondingly large 1σ uncertainties on the measurements of $\pm$ 930 and $\pm$ 560 years, respectively.

δ^{13}C values for the 28-31.5 m interval show large variations between taxa (Table 1 and 2.3). The δ^{13}C measurements on individual *Pyrgo sp.* tests within single 2 cm sampling intervals varied widely between about -4 and -8‰, and bulk *Pyrgo sp.* measurements (10-15 individuals combined) also showed large scatter. Bulk sample measurements on other taxa showed higher δ^{13}C values between -1 and -3‰ throughout the interval, apart from

one *Nonionellina sp.* result at $-4.6‰$, and thus were clearly distinct from the *Pyrgo sp.* data and less variable.

2.5 Discussion

This new ^{14}C data suggest that measurements from both Kiel and LLNL on mixed benthics are biased old in the 28 to 31.5m interval, by about 1,500 and 300 years, respectively. Given the very high sedimentation rate in SBB, ($\sim$4 m/1000 ^{14}C years) and the good agreement between ages on single taxa benthic foraminiferal samples and individual benthic macrofauna, the possibility seems remote of significant mixing of material of different ages in the sediment. This suggests that the younger benthic ages are correct and that the offsets between mixed benthic samples result from some taxa, *Pyrgo sp.* and almost certainly other infaunal forms, being biased anomalously old, probably because of calcification in old pore waters.

The benthic samples measured at LLNL (examined by J.K. and B.R.) were made up predominantly of *Bolivina sp.* and *Uvigerina sp.* Although new measurements on *Uvigerina sp.* samples in this study are closely equivalent to those of corresponding mixed planktonics, only one of our *Uvigerina sp.* samples (at 30.4 m) came from the interval of apparent disagreement. It is therefore possible that *Bolivina* and perhaps also *Uvigerina sp.* ages were biased older during the interval of apparent disagreement. Mixed benthic samples measured at Kiel were made up of a larger diversity of taxa, and notes of what was included are sparse, but checks on sampling notes (by J.K.) indicate that at least two of the samples measured at Kiel contained *Pyrgo sp.* The foraminifera were picked from vials that had already been extensively sampled, and therefore *Pyrgo sp.* were included to help make up the necessary weights for AMS ^{14}C measurements. Visual inspection of vial samples shows that *Pyrgo sp.* were very uncommon or absent above 28m and below 31.5m. The interval of abundant and very old *Pyrgo sp.* corresponds closely to the region where the LLNL and Kiel results

disagree. It therefore seems highly likely that inclusion of *Pyrgo sp.* in the Kiel samples contributed to the anomalously old results. Since Pyrgo was not present in at least one sample within the section, it appears likely that other infaunal taxa including *Bolivina* sp. also contributed to the anomalously old results.

Kennett *et al.* (2000) interpreted low δ^{13}C values in benthic foraminifera in SBB as evidence that CH_4 contributed to isotopically depleted sediment pore waters where infaunal species calcified. During intervals of increased CH_4 fluxes through basin sediments, strong CH_4 gradients within near-surface sediments will be reflected in the δ^{13}C of benthic foraminifera. However, these fluxes of CH_4 are thought to be caused by warming of SBB bottom water leading to clathrate destabilization during interstadials, which in 893A are characterized by laminated sediments and a dominance of dysoxic benthic foraminifera assemblages, indicating poor bottom water ventilation. In contrast, sediments throughout the interval covered by this study are massive, and contain oxic benthic foraminiferal assemblages (Cannariato *et al.*, 1999) that attest to high bottom water oxygen levels. Thus, while CH_4 oxidation may indeed have contributed to the low Δ^{14}C and δ^{13}C values measured on *Pyrgo sp.* and other infaunal taxa in this study, it seems unlikely that it played a dominant role.

With the exception of *Pyrgo sp.*, δ^{13}C values observed among the taxa from the deglacial section of the 893A core are consistent with those of modern foraminifera that have been analyzed from the SBB. Stott *et al.* (2002) measured very steep gradients of pore water δ^{13}C in core top sediments at two SBB locations remote from methane seeps, with δ^{13}C as low as -5.1‰ at 2.5 cm depth, and showed that these depletions are consistent with remineralization of particulate organic carbon (POC) deposited within the basin today (δ^{13}C $= -22$‰). Pyrgo is a deep infaunal taxa that has been observed elsewhere to inhabit a large depth range (0-3 cm) in the sediment column (Linke and Lutze, 1993). Core top Pyrgo murrhina δ^{13}C values measured at other locations are $\sim$1‰ lighter than calcite precipitated in equilibrium with bottom water, corresponding to a 1‰ enrichment in *Pyrgo sp.* tests

relative to δ^{13}C of bottom water ΣCO_2 (Graham *et al.*, 1981; Romanek *et al.*, 1992). If similar offsets apply in SBB, the very depleted and highly variable *Pyrgo sp.* δ^{13}C results (-4 to -8‰) correspond to δ^{13}C values in pore water ΣCO_2 of about -5 to -9‰ and could be explained by a modest increase in SBB sediment δ^{13}C gradient compared to today and/or an extension of *Pyrgo sp.* habitat deeper into the sediments. We suggest that the isotopic results in this interval of 893A probably reflect a deglacial interval of higher than normal oxygen levels in SBB bottom waters (and likely, changes in other environmental conditions). Effects of increased diffusion of oxygen into the sediments on the subsurface microbial community promoted increases in the remineralization of refractory POC, leading to a reduction in pore water Δ^{14}C and to increased near-surface δ^{13}C gradients, while allowing *Pyrgo sp.* and other infaunal taxa to calcify at greater depths with isotopically depleted pore waters.

If CH_4 was not a major factor influencing the pore water Δ^{14}C, this mechanism requires an alternative source of old carbon within the SBB sediments. Several studies have identified mechanisms delivering geologically derived (^{14}C-free) or "preaged" POC to SBB and other California Margin sediments, that could potentially survive burial and be remineralized at depth. These include fluvial input of old terrestrial POC, either directly (Masiello and Druffel, 2001; Komada *et al.*, 2004; Drenzek *et al.*, 2009) or indirectly via lateral transport of reworked coastal sediments (Hwang *et al.*, 2005); and adsorption of aged marine Dissolved Organic Carbon (DOC) on to sinking POC (Hwang *et al.*, 2006). Redeposited tar from surface hydrocarbon slicks originating from seeps within the SBB (Hill *et al.*, 2006) may also have provided a source of old carbon for remineralization, since tar was visibly present on some sediment grains and foraminifera in the studied interval, though concentrations were low compared to the very high tar levels observed in more recent deglacial SBB sediments (Hill *et al.*, 2006).

Throughout this interval, isotopic offsets ($\Delta\delta^{13}$C and $\Delta\Delta^{14}$C, respectively) between *Pyrgo sp.* and other benthic taxa were -5‰ and of -250‰. These offsets provide a constraint on the δ^{13}C and Δ^{14}C of the pore water source materials responsible for the drastic increase in *Pyrgo sp.* age, and we attempt a simple mass balance to identify the most likely cause of the offset between epifaunal and infaunal species. Modern tar samples from SBB have an average δ^{13}C of -23‰ (Kvenvolden and Hostettler, 2004) and a Δ^{14}C of -1000‰. Modern preaged terrestrial material has δ^{13}C of about -25‰ and Δ^{14}C as low as -550‰ (Komada *et al.*, 2004), and DOC in the California Margin has an average δ^{13}C of -22‰ and Δ^{14}C of approximately -500‰ at 500m water depth (Bauer and Druffel, 1998).

For simplicity we ignore all vital effects and differences in the basin between modern and deglacial periods. Modern epifaunal foraminifera in the SBB have an average δ^{13}C of -2‰ (Holsten *et al.*, 2004), and we take Δ^{14}C as -150‰ for SBB bottom water based on GEOSECS results from stations 201 and 347 (Ostlund and Stuiver, 1980). Using a source material δ^{13}C of -22‰, we find that achieving a $\Delta\delta^{13}$C of -5‰ and $\Delta\Delta^{14}$C -250‰ relative to modern epifaunal foraminifera with δ^{13}C of -2‰ and Δ^{14}C of -150‰, would require a source material with a Δ^{14}C value of -1150‰ that accounted for 25% of the pore water carbon. While this Δ^{14}C value is not physically possible, the calculation does show that an extremely ^{14}C depleted source is required to account for the offsets observed in this study. Therefore, the most consistent simple explanation for *Pyrgo sp.* isotopic depletion is tar as the primary additional source of pore water carbon, with minimal input of preaged terrestrial material or adsorbed old DOC.

The conditions leading to the observed offset in benthic species in this study are somewhat unique to the SBB, and hardly ubiquitous to the global ocean. SBB is a suboxic and highly productive setting, with a very high sedimentation rate, which together allow for enhanced preservation of organic material in the basin. This preservation and the occurrence of well-oxygenated periods such as the interval in this study, allow for the presence and calcification

of deep infaunal foraminifera at sediment depths where pore water $\Delta^{14}C$ can be sharply affected by old remineralized carbon. The abundance and extreme ^{14}C depletion of organic deposits in SBB sediments results in exceptionally large offsets that would not be observed in a basin with less organic matter preservation, smaller oxygenation variations, and younger sedimentary organic carbon.

We found no evidence in this study of anomalously old ^{14}C ages in *Uvigerina sp.*, the taxa measured in most of the benthic samples from the Galapagos and Gulf of California sites where the presence of old intermediate water has previously been inferred. However, we note that sediments from a core taken off Central California (F2-92-P3 35 °27.4′N, 121 °36.3′W, 800 m water depth) revealed a spread of 2,500 years between ^{14}C ages for *Bolivina spissa*, *Uvigerina peregrina* and *Bolivina argentea* (*B. argentea* > *U. peregrina* > *B. spissa*) during one early Holocene interval (van Geen *et al.*, 1996), though another comparison on sediments from the deglacial interval showed good agreement between ages for the three taxa. Given the large differences observed between taxa in the present study, the possibility of interspecies age differences in benthic taxa from other locations should not be ignored. While SBB may be an extreme case, it is important to consider the possible effects of ^{14}C depleted material in different oceanic settings when interpreting ^{14}C data in studies of paleoceanography. We urge investigators to treat ^{14}C ages on mixed benthics with due caution, and to supplement them with ^{14}C and $\delta^{13}C$ measurements on single taxa epifaunal or shallow infaunal taxa wherever possible.

2.6 Conclusion

Our new data show no evidence for large B-P ^{14}C offsets in Santa Barbara Basin. They indicate that in the deglacial interval where large B-P differences were previously thought to have occurred, ^{14}C ages for basin bottom waters were at most 300 years older than surface

waters, and sometimes less. Dates on planktonic foraminifera from this study are consistent with previous results that show ^{14}C plateaus in the SBB record, which Sarnthein *et al.* (2007) have correlated with ^{14}C results from other locations to deduce the existence of very large atmosphere-surface ocean ^{14}C offsets during deglaciation. Thus, we cannot rule out the possibility that the surface and bottom waters in SBB were both highly ^{14}C depleted relative to the contemporary atmosphere. However, this would require intense upwelling coupled with minimal equilibration of the upwelled water

2.7 Acknowledgments

We thank M. Rincon for $\delta^{13}C$ analyses; J. Zheng and M. Sung for assistance with SEM photography and EDX analysis; and W. Beaumont, K. Beverly, N. Yi, and K. Thompson for laboratory assistance. P.M. Grootes kindly helped with specifying Kiel laboratory treatments of foraminifers. We thank Luke Skinner, an anonymous reviewer, and Christopher Charles for valuable suggestions.

Table 2.1: Carbon-14 Data for ODP 893A Showing Deglacial Mixed Planktonic and Mixed Benthic Results From Hendy *et al.* (2002)and Sarnthein *et al.* (2007), Plus New ^{14}C Data From This Study[a]

Depth (m below seafloor)	Core Section	Core Depth (cm)	Sample Description	Lab	^{14}C (years)	±	$\delta^{13}C$
24.18	3H5	9-12	Mixed benthic taxa	LLNL	12760	80	
			Mixed planktonic taxa	LLNL	12340	70	
24.76	3H5	67-69	Mixed planktonic taxa	Kiel	12630	60	
25.33	3H5	124-126	Mixed planktonic taxa	Kiel	12940	65	
25.54	3H5	145-147	Mixed planktonic taxa	Kiel	12960	75	
25.81	3H6	144-146	Mixed benthic taxa	Kiel	13890	150	
26.36	3H6	96-99	Mixed benthic taxa	LLNL	13520	90	
			Mixed planktonic taxa	LLNL	12990	170	
26.42	3H6	105-107	Mixed benthic taxa	Kiel	13620	70	
26.8	3H6	140-142	*Pyramidellidae* or *Turridae*	UCI	13615	30	
26.81	3H6	144-146	Mixed planktonic taxa	Kiel	13400	120	
27.37	3H7	50-52	Mixed benthic taxa	Kiel	14900	160	
			Mixed planktonic taxa	Kiel	13960	150	
27.47	3H7	60-62	Mixed benthic taxa	Kiel	14740	130	
			Mixed planktonic taxa	Kiel	13770	120	
27.65	3H7	79-81	Mixed benthic taxa	LLNL	14030	160	
			Mixed planktonic taxa	LLNL	13800	280	
27.8	4H1	8-11	Mixed benthic taxa	LLNL	14980	160	
			Mixed planktonic taxa	LLNL	14490	130	

27.92	4H1	21-23	Mixed benthic taxa	Kiel	15500	110	
			Mixed planktonic taxa	Kiel	14730	100	
27.98	4H1	26-28	*Pyrgo sp.*	UCI	17140	280	
28.03	4H1	32-34	Mixed benthic taxa	LLNL	15240	220	
			Mixed planktonic taxa	LLNL	14690	140	
28.12	4H1	40-42	*Pyrgo sp.*	UCI	17640	420	−4.5
28.13	4H1	42-44	Mixed benthic taxa	Kiel	16130	80	
			Mixed planktonic taxa	Kiel	14820	140	
28.19	4H1	47-49	*Pyrgo sp.*	UCI	16310	60	−6.6
28.44	4H1	93-95	Mixed benthic taxa	Kiel	16360	80	
			Mixed planktonic taxa	Kiel	14890	100	
28.45	4H1	96-98	Mixed planktonic taxa	UCI	14970	60	
			Nonionellina sp.	UCI	14950	140	−4.6
			Pyrgo sp.	UCI	16740	70	−5.9, −8.2
28.55	4H1	105-107	Mixed benthic taxa	LLNL	15510	140	
			Mixed planktonic taxa	LLNL	14740	180	
28.59	4H1	110-112	*Pyrgo sp.*	UCI	17090	50	−6.2
28.66	4H1	117-119	*Nonionellina sp.*	UCI	15210	180	−1.9
			Pyrgo sp.	UCI	17375	45	−7
28.73	4H1	124-126	*Nonionellina sp.*	UCI	14990	120	−1.7
			Pyrgo sp.	UCI	17030	150	
28.76	4H1	126-128	Mixed benthic taxa	Kiel	16570	80	
			Mixed planktonic taxa	Kiel	14550	130	
28.8	4H1	131-133	*Cadulus Californicus*	UCI	14890	60	
			Gastropod	UCI	15100	30	
28.94	4H1	145-147	*Nonionellina sp.*	UCI	15000	50	−1.4
			Pyrgo sp.	UCI	17390	60	−4.7, −5.0, −5.3, −5.8
29.38	4H2	5-7	Mixed benthic taxa	LLNL	15370	450	
			Mixed planktonic taxa	LLNL	15040	230	
29.46	4H2	12-14	*Buliminella sp.*	UCI	16300	930	
			Nonionellina sp.	UCI	15135	50	−1.6
			Cardiidae or *carditidae*	UCI	15200	30	
			Pyrgo sp.	UCI	17185	50	
29.47	4H2	14-16	Mixed benthic taxa	Kiel	16450	80	
			Mixed planktonic taxa	Kiel	15010	110	
			Pyrgo sp.				-5.6
29.53	4H2	19-21	*Pyrgo sp.*	UCI	17010	140	−5.1
29.63	4H2	33-35	*Pyrgo sp.*	UCI	17350	60	−5.1
29.78	4H2	47-49	*Pyrgo sp.*	UCI	17295	50	−4.7, −6.1, −7.1, −7.1
			Mixed benthic taxa	Kiel	16820	80	
			Mixed planktonic taxa	Kiel	14670	130	
			Cardiidae or *carditidae*	UCI	15205	30	
			Cardiidae or *carditidae*	UCI	15195	25	
			Boreotrophon	UCI	15215	25	
29.88	4H2	55-57	Mixed benthic taxa	LLNL	15820	150	
			Mixed planktonic taxa	LLNL	14940	160	
29.96	4H2	63-65	Mixed benthic taxa	Kiel	16900	80	
			Mixed planktonic taxa	Kiel	15210	140	
30.06	4H2	73-75	Mixed benthic taxa	Kiel	16700	80	
			Mixed planktonic taxa	Kiel	15420	100	
30.18	4H2	89-91	*Nonionellina* sp.	UCI	15510	230	−1.4
			Pyrgo sp.	UCI	17340	90	−5.8
30.25	4H2	96-98	*Cadulus Californicus*	UCI	15455	25	
30.32	4H2	103-105	Mixed planktonic taxa	UCI	15280	60	

			Buliminella sp.	UCI	15410	210	
			Nonionellina sp.	UCI	15470	170	
			Pyrgo sp.	UCI	17280	60	−5.1, −6.9, −7.9, −6.3
30.39	4H2	110-112	*Buliminella sp.*	UCI	15470	450	
			Nonionellina sp.	UCI	15680	170	−1.5
			Uvigerina sp.	UCI	15780	340	
			Pyrgo sp.	UCI	17550	70	−4.1
30.46	4H2	117-119	*Buliminella sp.*	UCI	15800	470	−2.7
			Nonionellina sp.	UCI	15800	290	−2.8
			Pyrgo sp.	UCI	17500	160	−5.9
30.62	4H2	138-140	Mixed planktonic taxa	UCI	14320	210	
			Pyrgo sp.	UCI	17440	80	−6.1
30.78	4H2	145-147	Mixed benthic taxa	Kiel	16620	100	
			Mixed planktonic taxa	Kiel	15330	90	
30.98	4H3	21-23	*Cardiidae* or *carditidae*	UCI	15790	70	
31.01	4H3	24-26	*Buliminella sp.*	UCI	16580	560	
31.05	4H3	28-30	*Pyrgo sp.*	UCI	17660	130	
31.2	4H3	42-44	Mixed benthic taxa	Kiel	16475	110	
			Mixed planktonic taxa	Kiel	15740	130	
31.35	4H3	57-60	Mixed benthic taxa	LLNL	16080	220	
			Mixed planktonic taxa	LLNL	15550	140	
31.4	4H3	63-65	Mixed planktonic taxa	UCI	15750	130	
			Nonionellina sp.	UCI	16180	240	−1.4
			Pyrgo sp.	UCI	17700	420	
31.52	4H3	77-79	*Uvigerina sp.*	UCI	16070	70	−0.8
			Cardiidae or carditidae	UCI	15800	90	
31.59	4H3	84-86	*Uvigerina sp.*	UCI	16110	60	−1
31.69	4H3	91-93	Mixed benthic taxa	Kiel	16340	100	
			Mixed planktonic taxa	Kiel	15780	105	
31.78	4H3	106-108	Mixed planktonic taxa	UCI	15830	140	
			Uvigerina sp.	UCI	16130	60	
30.91	4H3	14-16	Mixed planktonic taxa	UCI	15450	120	
			Pyrgo sp.	UCI	17390	290	−5.6
32.24	4H4	3-5	Mixed planktonic taxa	LLNL	16080	190	
32.45	4H4	24-26	*Uvigerina sp.*	UCI	16680	420	
32.52	4H4	31-33	*Cadulus Californicus*	UCI	16685	30	
32.59	4H4	38-40	*Boreotrophon*	UCI	16570	40	
32.91	4H4	73-75	*Uvigerina sp.*				−1
32.99	4H4	90-93	Mixed benthic taxa	LLNL	17120	90	
			Mixed planktonic taxa	LLNL	16630	190	

[a]LLNL ^{14}C results originally published in Ingram and Kennett (1995) were recalculated in Hendy *et al.* (2002) to properly correct for the presence of ^{14}C-dead carbon as well as modern carbon in ^{14}C small-sample processing backgrounds. All data have been placed on the Hendy *et al.* (2002) depth scale for ODP 893A: void-corrected depths within each ODP core section were calculated based on Merrill and Beck (1995), and

these are keyed to the section-top depths of Behl (1995). We have followed Hendy *et al.* (2002) in correcting the Behl (1995) depths for 1.5 m and 0.75 m of missing core at the 1H-2H and 2H-3H section boundaries, respectively, and in our use of 27.7 m for the top of 4H1 rather than the adjusted Behl (1995) depth of 25.8 + 2.25 m (see the 4H1 depths shown in Hendy *et al.* (2002) (Table 3).)

Chapter 3

Preliminary results of ^{14}C measurements of New Zealand Kauri (*Agathis australis*) covering the Younger Dryas Interval

3.1 Introduction

The Younger Dryas (YD) was an abrupt return to glacial-like conditions 12.9-11.7 ka that punctuated the transition to warmer interglacial conditions during the termination of the last glacial period. It has long been viewed as the canonical, abrupt climate change event, and accordingly is one of the most studied climatic events in recent Earth history. The interval saw large changes in atmospheric ^{14}C, the causes of which are still not well known and is the topic of intense debate. The event is thought to have been caused by a reduction in North Atlantic Deep Water formation and the strength of the ocean thermohaline circulation,

causing a reduction in deep-ocean ventilation. These changes in ocean circulation would likely affect ventilation rates and therefore atmospheric ^{14}C. Changes in the production rate owing to changes in solar activity and geomagnetic field intensity also likely influenced atmospheric ^{14}C during the interval.

Reconstruction of atmospheric ^{14}C during the YD interval is important for understanding the Earth's carbon-climate feedback cycle, both as a record of changes in the global carbon cycle and for calibration of ^{14}C dates that establish the chronology for climatic and ecological records during the interval. This YD interval is critical for calibration purposes, as it links the tree ring ^{14}C record with the floating European Late-glacial Pine (Kromer *et al.*, 2004) and Central European Late-glacial Master (Kaiser *et al.*, 2012) chronologies. At present, the portion of the ^{14}C calibration curve based on tree rings extends to 13.9 kyr BP, but at present there are minimal (3 points) ^{14}C measurements in the interval 11.8 - 12.2 ka. While this entire interval is anchored with dendrochronology, it was previously defined by a Swiss larch tree ring record, Ollon505, which was removed from IntCal13 after it was found to be misplaced. Accurate dendrochronology of the European tress in this interval is challenged by short records with little overlap, which highlights the need to obtain trees with robust dendrochronology in this interval. Hua *et al.* (2009) made an important contribution towards improving the ^{14}C calibration during the YD interval by extending the European absolute tree-ring chronology from 12.4 to 12.6 ka and linking it with a 617-yr long record of tree rings of Huon Pine from Tasmania, Australia. However the Huon record, which was composed of only 4 logs, could not be cross-matched using ring width and therefore relied on ^{14}C wiggle-matching alone, inducing uncertainty in the calendar chronology.

To improve the linkage of the floating tree ring records and develop a record of atmospheric ^{14}C spanning the YD with a robust internal chronology, a research project has been ongoing to measure ^{14}C in the New Zealand Kauri (*Agathis australis*) (Hogg *et al.*, 2013b). Kauri logs buried in bogs scattered over a 300-km stretch of northern New Zealand represent one of the

world's foremost atmospheric archives for the last 60 kyr (Turney *et al.*, 2007). Some of the logs have diameters of over 4 m and individual ages of more than 2 kyr, and the anaerobic conditions in the bogs result in remarkable preservation of the wood (Ogden *et al.*, 1992 and Palmer *et al.*, 2006). This chapter presents the results of ^{14}C analyses made at the University of California, Irvine (UCI) on New Zealand Kauri covering the YD interval. This work is part of a larger collaboration at several institutions and a ^{14}C intercomparison of measurements made at five institutions (UCI, University of Waikato, University of Oxford, University of Heidelberg, and the Swiss Federal Institute of Technology Zurich), which was described in a publication in the IntCal13 special issue of *Radiocarbon* (Hogg *et al.*, 2013b).

3.2 Methods

A total of 144 decadal samples were pretreated to produce hollocellulose using a protocol that was developed for this project and is described in detail in (Southon and Magana, 2010). The method is based on the Jayme-Wise cellulose extraction method (Green, 1963), which is one of the more commonly used methods for cellulose extraction for isotope measurements. A batch processing protocol for Jayme-Wise cellulose extraction, developed by Leavitt and Danzer (1993) and commonly used for stable isotope measurements, involves 3 steps to isolate α-cellulose, each step followed by multiple water washes:

1. Cleaning: treatment in a Soxhlet system with toluene and ethanol to remove waxes, fats, oils, resins, and other compounds soluble in organic solvents.

2. Isolation of holocellulose: bleaching with a mixture of sodium chlorite and acetic acid to remove lignins.

3. Isolation of α-cellulose: treatment with strong base followed by a neutralizing acetic acid wash.

The conventional treatment for organic samples in ^{14}C labs is an acid-base-acid (ABA) treatment, where organic samples are treated at 60 °C-90 °C with 1N HCl and 1N NaOH, with the base washes repeated until the solutions remain clear. Cellulose extraction is most often preferred for on wood samples over ABA in order to remove carbon that has been translocated within the tree. Because we are measuring decadal samples and in an interval where interannual differences are smaller than the analytical error, the purpose of pretreatment to cellulose is less to remove carbon that was translocated within in the tree, and more to serve as a more rigorous treatment than ABA to remove exogenous carbon. To establish a protocol that optimizes time and minimizes backgrounds for this study of YD kauri, we compared several variations of the Jayme-Wise cellulose extraction method with ABA pretreatment.

We found that while ^{14}C results are often indistinguishable between wood pretreated with ABA only and wood pretreated to holocellulose, there exists some wood for which ABA pretreatment is ineffective and cellulose extraction is necessary. We found no improvement in backgrounds by isolation of alpha-cellulose over holocellulose and therefore adopted a protocol for pretreatment of YD kauri as follows:

1. ABA: ∼30 mg of shaved wood is pretreated in individual test tubes with a standard ABA pretreatment at 60 °C-90 °C.

2. Isolation of holocellulose: Samples are bleached in individual test tubes with a mixture of equal parts (normally 3 ml) 1N sodium chlorite and 1N HCl for 3 hours at 60 °C-90 °C. If necessary, a second treatment is applied.

3. Drying: After washing several times in Milli-Q water (15 min, 70 °C) to pH >6, samples are dried on the heat block at 60 °C-70 °C.

The results of the work that established this protocol were published in the Proceedings of the 20th International Radiocarbon Conference (Southon and Magana, 2010), and at the time

of publication we believed that we had identified the cause of observed higher ^{14}C values of holocellulose blanks relative to blanks treated with only ABA as an old contaminated batch of sodium chlorite. However, in subsequent tests the higher ^{14}C of samples pretreated to holocellulose persisted, and testing new bottles of sodium chlorite sold by 4 different brands (Fig 3.1) showed that the the cause was likely to not be the old bottle of sodium chlorite. This suggests that the process of holocellulose extraction can cause contamination with modern carbon, which is an unexpected result, though one that has been observed previously (X. Xu and H. Kitagawa personal communication).

We have made two modifications to the original protocol that appears to prevent the higher ^{14}C in holocellulose. The first is bleaching for 3 hours only, instead of overnight, and the second is drying samples in air instead of a vacuum oven (Fig 3.2). They both appear to improve the blank, but the reason is not clear. In our protocol, holocellulose extraction is done in Milli-Q water in the presence of excess acid, which should prevent contamination by organic and modern atmospheric CO_2 regardless of the length of the bleaching step is done for. We can see no compelling reason why drying in a vacuum oven would cause contamination with modern carbon, but we suspect that the vacuum oven removes more water than is done by air drying, which allows atmosphere access to more/different activation sites. We have tried letting the vacuum oven up to N_2 instead of atmospheric air, but we observed the ^{14}C enrichment of holocellulose. Although we cannot find the source of the enrichment, air drying is ultimately the preferred method not only because of the better backgrounds, but also because it produces a final product that is more coherent and easier to handle than vacuum drying.

After pretreatment to holocellulose, samples were combusted, cryogenically purified, and converted to graphite using standard methods.

To understand the role of changing production rate versus carbon cycle changes, we compare this new record with the GISP2 ^{10}Be record. ^{14}C and ^{10}Be are both cosmogenic isotopes,

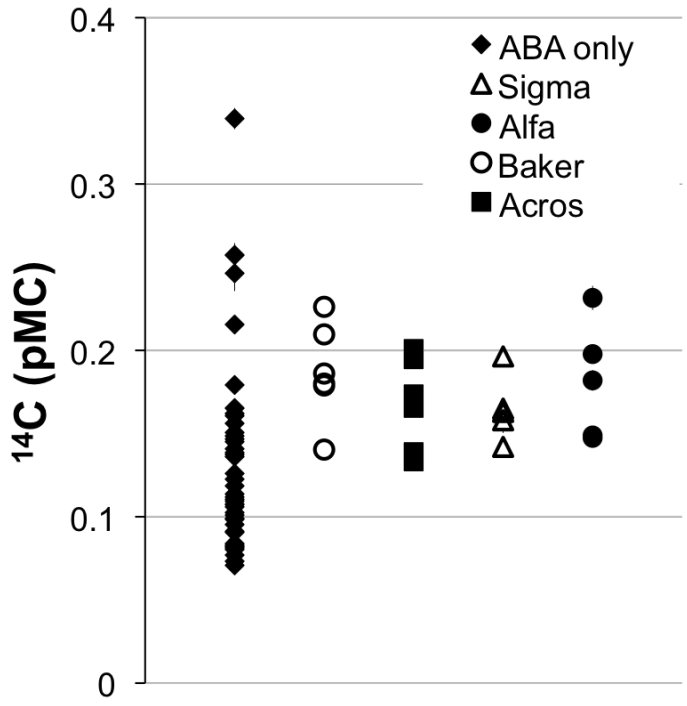

Figure 3.1: ^{14}C results (pMC) for samples pretreated to holocelluose using different brands of sodium chlorite.

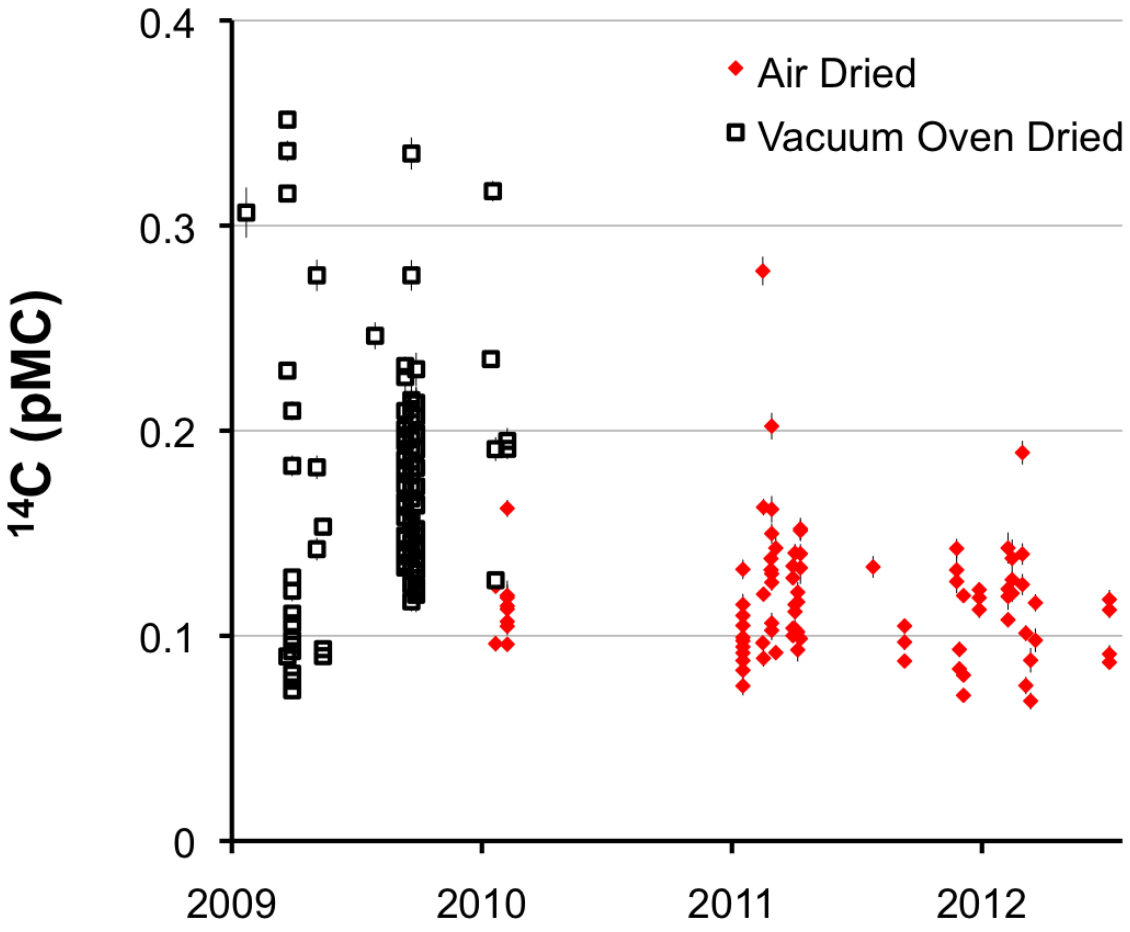

Figure 3.2: ^{14}C results (pMC) for samples pretreated to holocelluose dried in air and a vacuum oven.

produced in the upper atmosphere by cosmic rays secondaries, but unlike carbon, beryllium does not participate in a complex global geochemical cycling. Beryllium becomes attached to aerosols and is deposited within 1-2 yrs (Raisbeck *et al.*, 1981), though the correlation between ice core δ^{18}O and ^{10}Be indicates that deposition rates are affected by climate (Beer *et al.*, 1993). When corrected for changes in deposition rates, ice core records of ^{10}Be can be thought of as records of cosmogenic isotope production rates. The ^{10}Be record shown in Figure 3.7 has been corrected for both dry and wet deposition using a simple deposition model as described in Alley *et al.* (1995) and Finkel and Nishiizumi (1997).

Shown in Fig 3.7, the YD kauri ^{14}C record was detrended by subtracting the long term trend, which was estimated by smoothing the tree rings included in IntCal13 with a low pass filter (1/1000 yr). The GISP2 timescale has been adjusted by 60 yrs to account for the offset between the GISP2 chronology and the tree ring chronology in this interval (Muscheler *et al.*, 2008 and Finkel and Nishiizumi, 1997). For simplicity, the ^{10}Be record has been has been shifted an additional 15-20 yrs to account for the offset driven by carbon cycling (Beer *et al.*, 1993 and Stuiver and Quay, 1980) and linearly scaled to fit the detrended ^{14}C record. In future works, the more rigorous way to identify changes in the carbon cycle during the YD interval would be to run ^{10}Be record through a carbon cycle model as others have done (e.g. Muscheler *et al.*, 2008). However, this would be challenging as the exact magnitude of changes in atmospheric ^{14}C driven by changes in the carbon cycle during this interval are currently not well known, and most modeling studies have difficulty simulating a decline in atmospheric ^{14}C (Matsumoto and Yokoyama, 2013).

3.3 Results and Discussion

Radiocarbon results presented in this chapter are the mean of replicate ^{14}C measurements. The record has been robustly cross dated as described in Hogg *et al.* (2013b), but is not

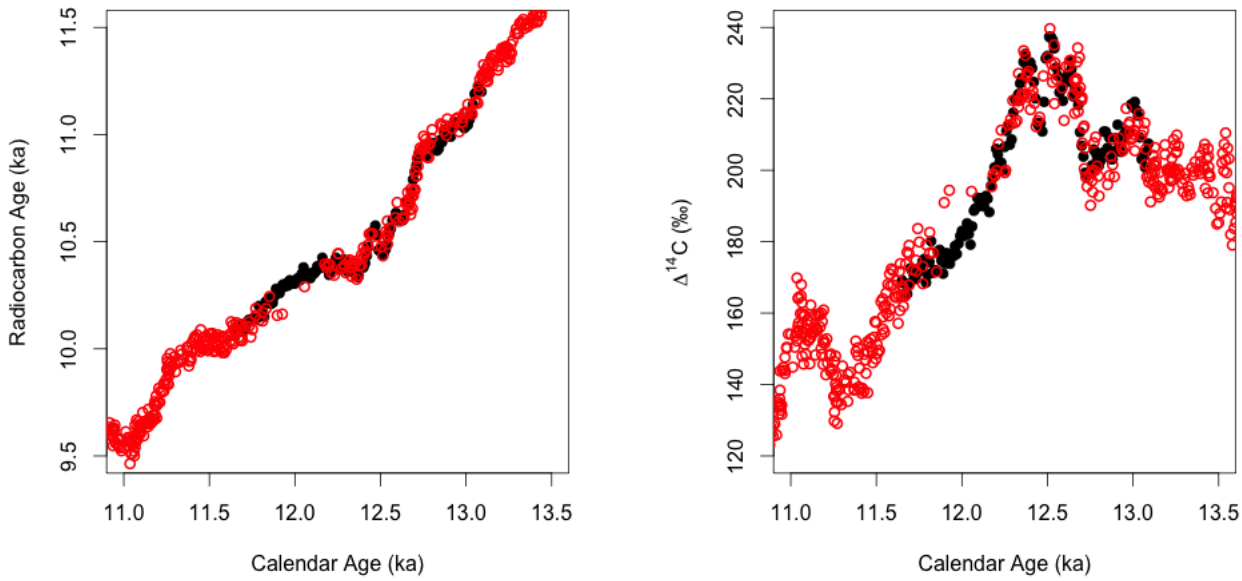

Figure 3.3: YD Kauri (black) wiggle matched to the tree rings included in IntCal13 (Reimer *et al.*, 2013) (red) in units of both ^{14}C yrs and Δ^{14}C. The youngest ring has been placed at 11,650 yr BP.

anchored to the master tree rings. At present, the overlap between the record and the master tree rings is short, making the correct placement of the record in calendar time uncertain. Efforts are underway to extend the record on the younger end, but for the purposes of this chapter, a tentative placement has been made based on ^{14}C wiggle matching. A constant north-south (N-S) offset of 40 yrs has been applied (McCormac *et al.*, 2002) and the record has been visually wiggle matched to the IntCal13 tree ring record. The wiggle matches places the first yr at 11,650 yr BP.

Figure 3.3 shows the record placed in the context of the tree ring records included in IntCal13 in both ^{14}C yrs and Δ^{14}C. The record is in disagreement with the three points in the gap that this record fills, and no placement can be made that is in good agreement with both the younger and older sections of the gap and these three points. That inability to find a good fit highlights the need to extend the record toward the younger end to increase the confidence of the placement of the record and identify the source of the disagreement between this new

record and the tree ring records included in IntCal13. If we assume the placement of the YD kauri is correct, the most likely potential sources of the disagreement are changing N-S offset over the interval or an error in the dendrochronology of one of the records. To explain the offset entirely in terms of N-S offset, N-S offset would have had to increase to almost 200 yrs during this interval, which is far higher than the observed range of 8-80 yrs (McCormac *et al.*, 2002). The current working hypothesis for the YD atmospheric ^{14}C decrease is venting of a ^{14}C depleted water mass in the Southern Ocean, which could drive changes in the N-S offset though such a significant increase may not be possible.

As a simple test of the potential of an increase in N-S offset as the cause of this disagreement, we consider the change in the N-S offset in the post-industrial, pre-bomb, atmosphere. To explain the offsets in the YD in terms of changes in N-S offset, the maximum N-S offset in the YD interval would be 175 yrs, which is an increase from the constant offset applied here of 45 yrs of 130 yrs. In the post-industrial, pre-bomb era, as shown in Fig 3.4, ∼60 gigatons of ^{14}C-free carbon was emitted into the Northern Hemisphere in 50 yrs (1900-1950) (Boden and Andres, 2013). In this interval the N-S offset went from an pre-industrial average of ∼45 yrs to ∼40 yrs in the opposite direction - that is in 1950 the N Hemisphere atmospheric $^{14}CO_2$ age was 40 yrs older than the S Hemisphere. The rapid release of 60 gigatons of ^{14}C-free carbon shifted the N-S offset by ∼85 yrs in the post-industrial era. Assuming a simple scaling can be applied, a release of ∼90 gigatons of ^{14}C-free carbon would be necessary to explain the disagreement in the two records entirely in terms of a change in N-S offset.

This approach involves many assumptions, the most clearly incorrect that the post-industrial carbon cycle is the same as the YD carbon cycle, as well as that the carbon released in the YD was of ^{14}C-free carbon. Additionally, the interval increased N-S offset in the YD is at least 160 yrs, which would require that the total amount of carbon was larger in order to sustain the offset for the entire interval. Atmospheric pCO_2 increased 15 ppm in the post-industrial era considered here (Etheridge *et al.*, 1996), while atmospheric pCO_2 rose 30 ppm over the

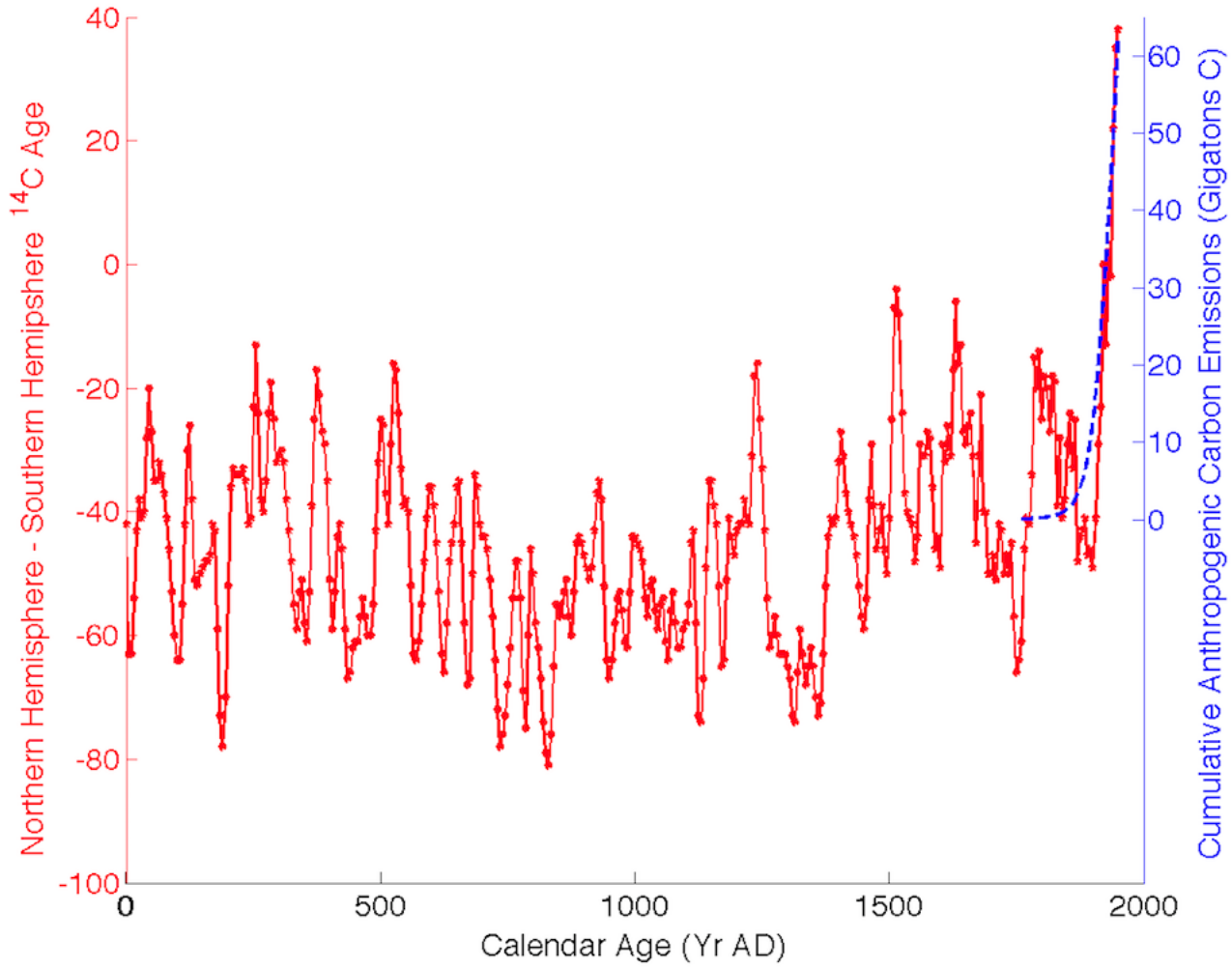

Figure 3.4: N-S offset during the Common Era (0-1950 AD) based on the difference between IntCal13 (Reimer *et al.*, 2013) and SHCal13 (Hogg *et al.*, 2013a) (red), plotted with the cumulative anthropogenic carbon emissions (Boden and Andres, 2013) (blue).

course of the entire YD interval, beginning ∼12.8 ka, and atmospheric pCO_2 only increased 3 ppm in the interval of disagreement. Accordingly, it seems unlikely that the entirety of the offset can be explained in terms of increasing N-S offset, though a more rigorous modeling approach would be necessary to more precisely determine flux of old carbon in the Southern Ocean necessary to cause a N-S offset of 175 yrs in the YD, and if it is consistent with observations of atmospheric pCO_2 in the interval.

Comparison with other atmospheric ^{14}C records (Huon Pine and Lake Suigetsu) and atmospheric proxy records (Hulu Cave) in this interval (shown in Figure 3.5) does not show clear indication of the source of the disagreement. The Huon Pine record does not extend to this section, and the uncertainty and variability in other records are high while simultaneously the sampling resolution is low. Given the previously mentioned misplacement of the Swiss larch, it appears that dendrochronology of the European tress in this interval is uncertain, suggesting the potential that the source of the disagreement is more likely to be based in an error in dendrochronology or the ^{14}C measurement, though changing N-S offset cannot be completely ruled out and would be consistent with venting of a ^{14}C depleted water mass in the Southern Ocean.

However as shown in Fig 3.6 the agreement between the IntCal13 tree ring records and marine ^{14}C records (Cariaco Basin and corals) in the "gap" is better than the agreement between the marine ^{14}C records and the YD kauri, which suggests that the IntCal13 trees are correctly placed. As is clear in Fig 3.6, some marine reservoir ages changed significantly at the onset of the YD, and consequently these records have been excluded from IntCal in this interval. But the agreement between the Cariaco Basin ^{14}C and the IntCal13 tree ring records suggests that while Cariaco Basin reservoir age changed at the onset of the YD, it may have returned to pre-YD values by the later stages of the YD and the reservoir corrected Cariaco Basin record may reflect a more global signal during the late YD interval. The agreement between the Cariaco Basin and the IntCal13 records, which disagrees with the YD kauri record as it is currently placed highlights the need to robustly anchor the kauri record and obtain Northern Hemisphere records covering this interval.

The overall agreement between the scaled ^{10}Be production record and the detrended atmospheric ^{14}C records is good, though there are some differences (Fig 3.7). Notably the records diverge between 11.2-11.5 ka as well as at the single ^{10}Be points at 12 and 12.2 ka. There are also exist apparent offsets between the records, where ^{10}Be appears to be older than the

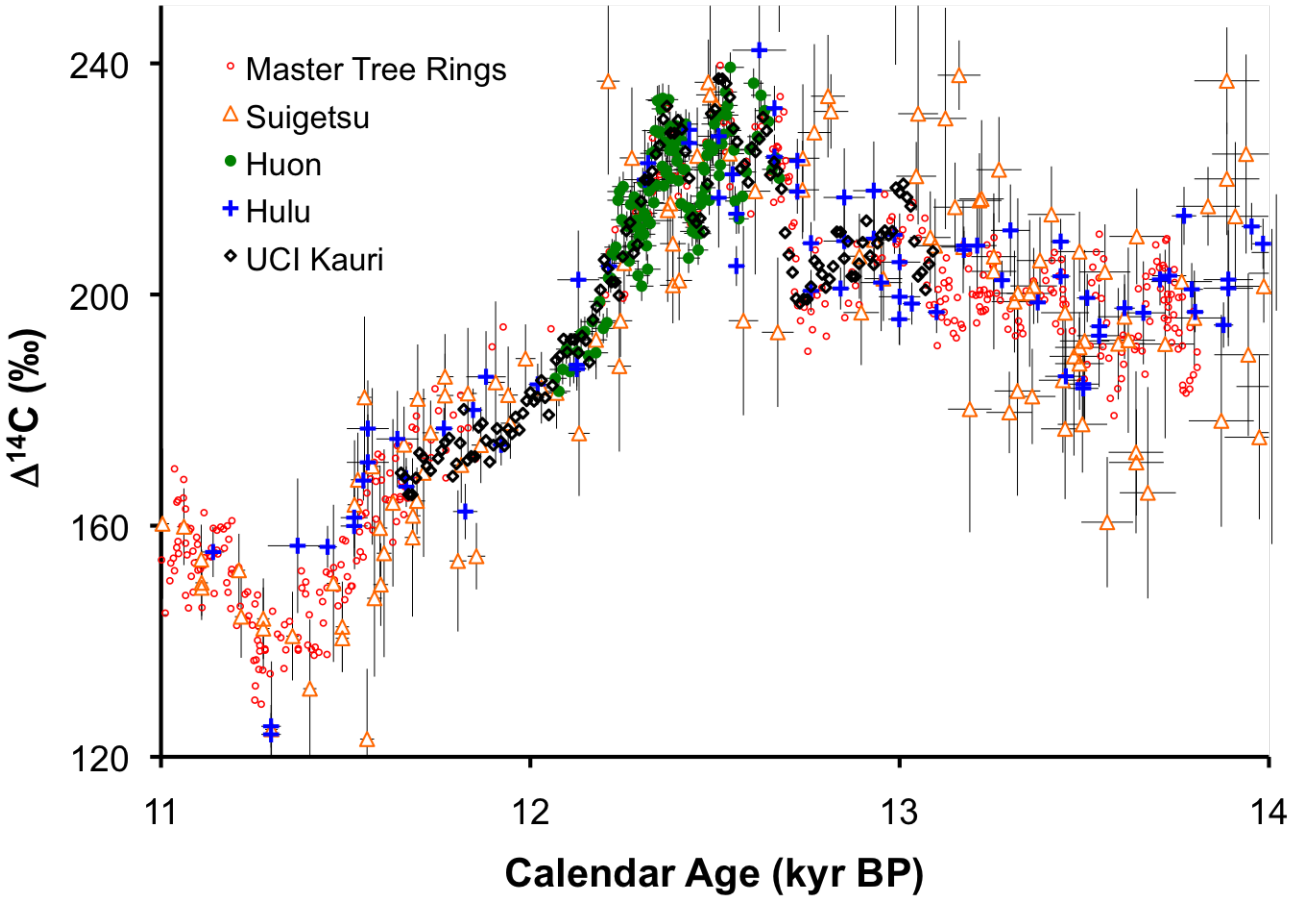

Figure 3.5: YD kauri record as placed in Figure 3.3, with atmospheric records including IntCal13 tree rings, Lake Suigetsu (Bronk Ramsey *et al.*, 2012) macrofossils, and the Huon Pine (Hua *et al.*, 2009). Also included is the Hulu Cave, H82, speleothem-based record (Southon *et al.*, 2012).

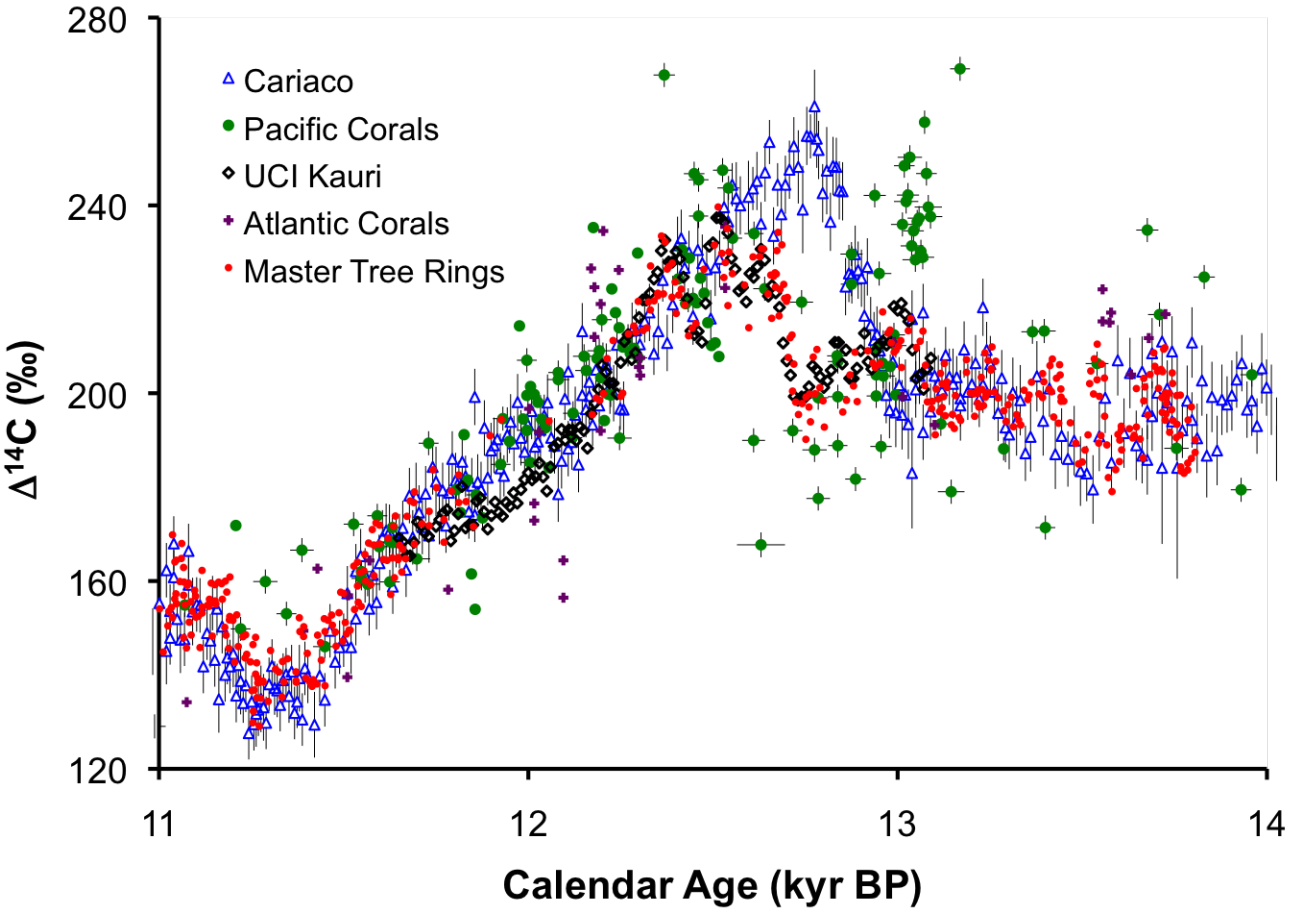

Figure 3.6: YD kauri record plotted with IntCal13 tree rings and IntCal13 marine records (Reimer *et al.*, 2013). Marine records have been corrected using a constant pre-bomb reservoir age. Systematic differences between the tree ring records and the marine records suggest changes in marine reservoir ages at the onset of the YD.

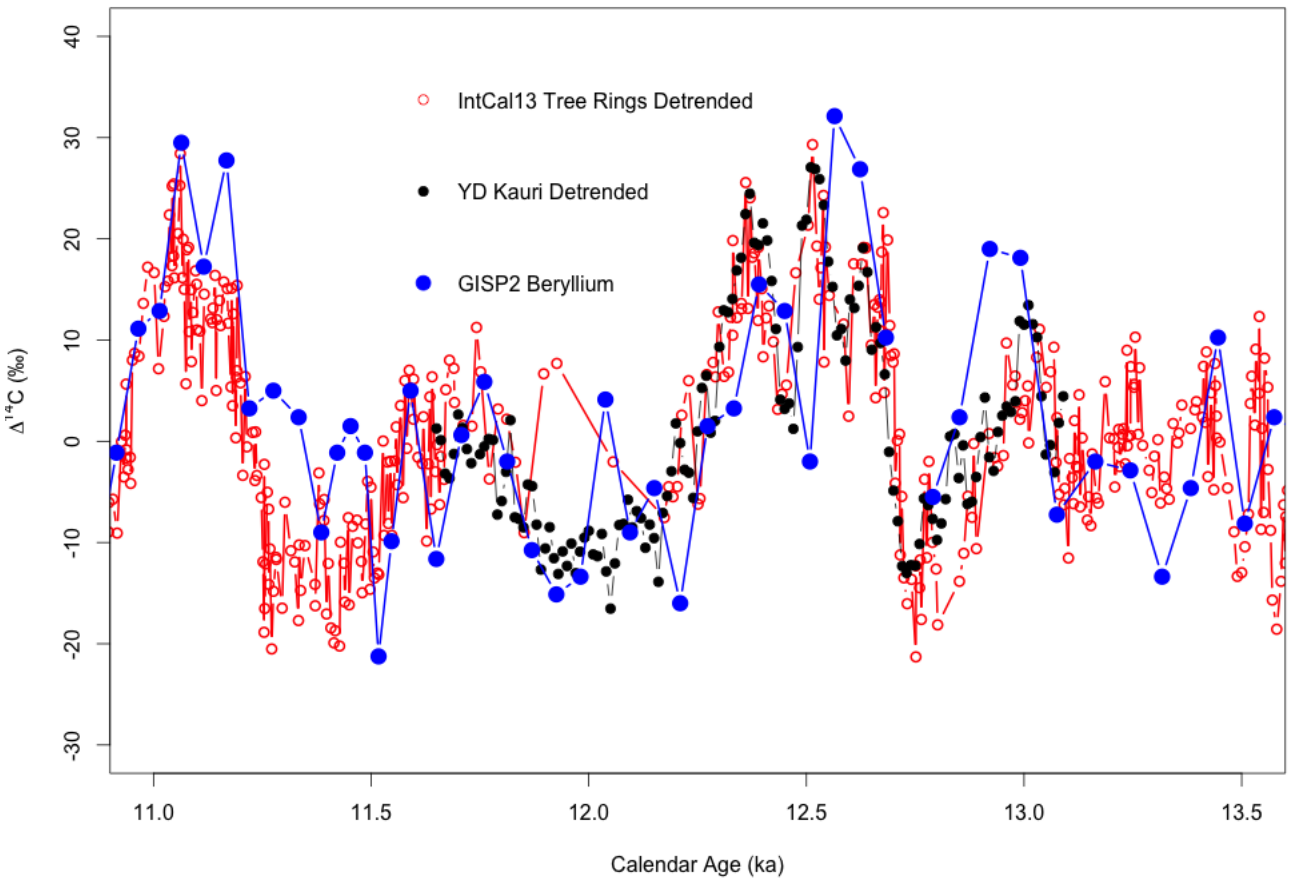

Figure 3.7: YD Kauri and tree rings included in IntCal13 detrended and plotted with a scaled record of atmospheric ^{10}Be production rates.

^{14}C between 12.4 and 12.6 kya and ^{10}Be is younger than ^{14}C starting around 12.9 ka. These offsets are likely a result of the smoothing window used. The 1000 yr smoothing flattens the "bump" in atmospheric ^{14}C in this interval, which increases the difference between the ^{14}C record and smoothed record at both ends of the rise and fall, causing an apparent offset between the ^{10}Be and the detrended ^{14}C record that would not be as prominent if a shorter smoothing window was used.

The ^{10}Be production record does not capture all of the three distinct rises and falls at the YD onset in ^{14}C, but this is likely a consequence of the sampling resolution of the ^{10}Be record. The overall good agreement between the ^{10}Be production record and atmospheric ^{14}C record suggests that much of the change in atmospheric ^{14}C during the YD interval can be explained by changes in atmospheric production rate only. This result is in contrast with the conclusion of Hua *et al.* (2009) who concluded that carbon cycle changes are necessary to explain the increase in atmospheric ^{14}C at the onset of the YD. This result is due to the differences in approaches to detrending the atmospheric tree ring ^{14}C records. Hua *et al.* (2009) and Muscheler *et al.* (2008) both detrended tree ring records using a simple linear fit to the 10-14 ka interval, versus the 1/1000 yr smoothing used here. This difference indicates that the long term trend likely contains information about changes in the carbon cycle during the YD, but by subtracting it here we can see that the short term variations in atmospheric ^{14}C can potentially be explained by production rate only.

3.4 Conclusion

The preliminary results of this new record of atmospheric ^{14}C during the Younger Dryas interval highlights questions about the chronology of the IntCal13 tree ring records and potentially carbon cycle changes around ∼12 ka BP. Comparison between the GISP2 ^{10}Be record and this new YD record suggests that much of the change in atmospheric ^{14}C during

the YD can be explained with production alone, though it is likely, given the large changes in marine reservoir ages during the YD, that there exists millennial scale changes in atmospheric ^{14}C that can be attributed to carbon cycle changes which were removed through detrending. Firmly anchoring the YD kauri record to the master tree ring record will help to answer some of these remaining questions, as would reanalysis of the tree rings included in Intcal13.

Chapter 4

A high-resolution record of atmospheric ^{14}C based on Hulu Cave speleothem H82

4.1 Abstract

The development of a calibration of atmospheric radiocarbon ($\Delta^{14}C$) is a significant scientific goal because it provides the means to link the numerous ^{14}C dated paleoclimate records to a common timescale with absolutely dated records, and thereby improve our understanding the relationships between the carbon cycle and climate change. Currently, few calibration datasets that directly sample the atmospheric ^{14}C reservoir are available beyond the end of the dendro-dated Holocene tree ring record at 12.6 kyr BP (Before 1950 AD). In the absence of suitable true atmospheric records, ^{14}C calibrations beyond this age limit are based largely on marine data, that are complicated by the marine reservoir effect, which may have varied over the glacial cycle. In this paper, we present a high-resolution record of U-Th series and

^{14}C measurements from Hulu Cave speleothem H82, spanning 10.6-26.8 kyr BP. Corrections for detrital ^{230}Th are negligible, and the contribution of ^{14}C-free geologic carbon to the speleothem calcite is small (5-6%) and is stable across major climate shifts. The time series provides a 16 kyr record of atmospheric Δ^{14}C as well as an updated age model for the existing Hulu Cave δ^{18}O record. The ^{14}C data are in good overall agreement with existing marine and terrestrial ^{14}C records, but comparisons with the Cariaco Basin marine Δ^{14}C record through the deglacial interval reveal that the Cariaco reservoir age appears to have varied during parts of the Younger Dryas and Heinrich Stadial 1 cold events. This highlights the importance of developing extended high-resolution marine and terrestrial ^{14}C records as a means of detecting changes in ocean circulation over the glacial cycle.

4.2 Introduction

Reconstruction of a high-resolution radiocarbon (^{14}C) record that directly samples atmospheric CO_2 through the last glacial cycle, tied to a robust independent timescale, has been a long-time goal of the scientific community. Atmospheric concentrations of ^{14}C (Δ^{14}C, expressed as per mil deviations from a modern reference standard) have varied over time due to changes in production and the partitioning of ^{14}C between reservoirs of the earth's carbon cycle, and must be calibrated against a calendar timescale for use as a chronometer. Independently dated ^{14}C calibration records provide the means to link the numerous ^{14}C dated paleoclimate records to a common timescale with absolutely dated archives such as layer counted ice cores. Additionally, when corrected for production variations, atmospheric ^{14}C records can be used to trace carbon cycle and ocean circulation changes via comparisons with archives of surface and deep ocean ^{14}C. Such comparisons can lead to an improved understanding of the history of the carbon cycle and a more precise knowledge of its role in climate change.

Few ^{14}C calibration data that directly sample the atmospheric ^{14}C reservoir are available beyond the end of the dendro-dated master tree ring record, which presently extends to 12.6 kyr BP calendar (Reimer *et al.*, 2009). A recently published Huon pine ^{14}C record (Hua *et al.*, 2009) bridges the gap between the master tree ring series and a 1400-year floating Allerød pine sequence (Kromer *et al.*, 2004), extending the tree ring record to approximately 14 kyr BP. A few additional older floating sequences are available back into Marine Isotope Stage 3, most notably New Zealand kauris (Turney *et al.*, 2007), but the distribution of ages for trees recovered so far is patchy (A. Hogg, pers. comm.) and it is unclear whether sufficient trees will be found to produce a continuous record. Terrestrial macrofossils in varve-counted cored sediments from Lake Suigestu in western Japan may ultimately fill this data gap (Nakagawa *et al.*, 2011), but comparison of the existing Suigetsu data (Kitagawa and van der Plicht, 2000) with other records shows that varves are missing and/or that core recovery was incomplete (Staff *et al.*, 2010).

In the absence of suitable true atmospheric records, ^{14}C calibrations beyond 12.6 kyr are largely based on marine data. Several coral data sets with independent ^{234}U-^{230}Th (U-Th) chronologies exist (Bard *et al.*, 1990, 1998, 2004; Edwards *et al.*, 1993; Burr *et al.*, 1998; Burr *et al.*, 2004; Cutler *et al.*, 2004 and Fairbanks *et al.*, 2005), but these are almost all "spot" measurements, and the records contain numerous gaps. In contrast, foraminifera records in marine sediments from the Cariaco Basin (Hughen *et al.*, 2004 and Hughen *et al.*, 2006) and Iberian Margin (Bard *et al.*, 2004) are essentially continuous, but apart from the 10-15 kyr BP interval of the Cariaco record which has its own varve timescale (Hughen *et al.*, 2004), they must be dated indirectly by correlation with other records via sediment color or δ^{18}O stratigraphy. This is particularly difficult for the period 15-24 kyr BP because the δ^{18}O records from the layer counted Greenland ice core (Grootes and Stuiver, 1997 and NGRIP Members, 2004), which provide the chronostratigraphy for so many marine sequences, contain few high resolution features in this interval that can be convincingly correlated with other records.

These marine records are subject to possible variations in the ocean-atmosphere ^{14}C offset (marine ^{14}C reservoir age), which represents a ^{14}C balance between the effects of air-sea gas exchange and the upwelling and mixing of radiocarbon-depleted subsurface waters into the local mixed layer. Records for ^{14}C calibration are chosen from low-latitude locations thought to be least sensitive to possible reservoir age changes (Reimer *et al.*, 2009). However, comparisons of early Younger Dryas ^{14}C data (Muscheler *et al.*, 2008) suggest that the Cariaco record, and perhaps subtropical North Atlantic ^{14}C archives generally, may have been anomalously young when the Atlantic Meridional Overturning Circulation was weakened, as may have occurred in the early Younger Dryas (YD) and Heinrich Stadial 1 (HS1) (McManus *et al.*, 2004). Modeling results (Butzin *et al.*, 2005; Singarayer *et al.*, 2008; Ritz *et al.*, 2008) support this conjecture, though the effect observed in Cariaco is unexpectedly large. In addition, the presence of extremely ^{14}C-depleted waters at depths above 1500 m during the YD and HS 1, at various sites in the North Atlantic, Pacific and Indian Oceans (Voelker *et al.*, 1998; Sikes *et al.*, 2000; Robinson *et al.*, 2005; Marchitto *et al.*, 2007; Stott *et al.*, 2009; and Bryan *et al.*, 2010) suggests that large increases in regional reservoir ages may have occurred at some locations if those waters reached the surface. These variations can potentially give valuable insights into past carbon cycle and ocean circulation changes, but their presence may confound the use of marine-based ^{14}C records for radiocarbon calibration for at least some intervals within the glacial.

This highlights the fact that in the absence of detailed knowledge of how ^{14}C offsets between different carbon reservoirs have varied over time, attempts to derive the history of atmospheric ^{14}C using archives that sample other carbon pools can only succeed for intervals where disparate records are in good agreement. Intervals of disagreement may ultimately provide valuable insights into changes in pool-to-pool ^{14}C gradients and therefore into ocean circulation and carbon cycle dynamics, but it is not possible to know definitively which (if any) of the apparently inconsistent radiocarbon records truly represents atmospheric ^{14}C. However, with a sufficiently large number of datasets it becomes easier to distinguish con-

sensus values. Thus, a key to better understanding of the history of atmospheric ^{14}C, marine reservoir ages, and past carbon cycle dynamics, is the development of multiple records of ^{14}C from different carbon reservoirs with robust independently dated calendar timescales.

Speleothems are cave calcite deposits precipitated from drip water, that represent a potential source of temporally well constrained atmospheric ^{14}C records, because an absolute chronology can be assigned using U-Th series dating with a correction for any detrital Th initially incorporated into the crystal matrix. Meteoric waters above the cave react with soil CO_2, which is present at elevated concentrations (pCO_2) due to biological activity and is in isotopic equilibrium with the atmosphere on annual to decadal timescales (Trumbore, 2000). This reaction forms carbonic acid, which drives carbonate dissolution as the water percolates through the cave host bedrock. As drip waters enter the cave, CO_2 degassing occurs, due to the lower pCO_2 of cave air relative to the drip water, leaving excess carbonate alkalinity that is precipitated as speleothem carbonate. Drip waters will initially be close to saturation for soil CO_2, with ^{14}C values essentially those of the contemporary atmosphere, but as they interact with the host bedrock, they will accumulate a percentage of ^{14}C free or "dead" carbon, which will be reflected in the radiocarbon ages of the speleothem calcite. If the drip waters equilibrate in a closed system, one mole of carbonate is required to neutralize one mole of dissolved CO_2, and the dead carbon fraction (DCF) is 50%; whereas under completely open conditions where drip waters continue to exchange CO_2 with an essentially infinite soil gas reservoir as carbonate dissolution takes place, the DCF approaches zero (Hendy, 1971). In practice, dissolution takes place under conditions that are intermediate between these end points.

A correction of the DCF can be determined in a similar manner to a reservoir age for a marine record, by comparing speleothem ^{14}C measurements on samples of known calendar age with the tree ring record of atmospheric ^{14}C during a period of overlap. The offset between the datasets is then subtracted throughout the remainder of the record to produce

a DCF corrected atmospheric ^{14}C record. This procedure involves the implicit assumption that the correction has remained constant through time. As shown below, comparison with tree ring records indicates that the DCF correction in H82 did remain constant across the Allerød/Younger Dryas and Younger Dryas/Holocene transitions, though the reason for this stability is unclear. Despite the lack of a detailed explanation, the stability of the DCF correction across major climate shifts that likely involved significant changes in hydrology and soil carbon dynamics suggests empirically that a constant DCF correction may be valid for some speleothem records extending further back in time.

The first high-resolution speleothem-based record of atmospheric ^{14}C, spanning 11-45 kyr BP, was measured on speleothem samples from a now submerged cave in the Bahamas (Beck *et al.*, 2001). This stalagmite exhibits relatively high levels of detrital thorium that create significant uncertainty in the absolute chronology, plus a large DCF of 1.5 kyr, and the record deviates significantly from the tree ring data during the Younger Dryas. Nevertheless, agreement with other ^{14}C records is typically within a few ^{14}C hundred years back to 25 kyr BP. Beyond 33 kyr BP, the record displayed very large ^{14}C excursions, whose origin was initially unexplained but ultimately traced to problems with subtraction of laboratory ^{14}C backgrounds (Hoffmann *et al.*, 2010). A new record from the same cave with well characterized blank corrections displays much better agreement with other ^{14}C calibration data beyond 33 kyr BP (Hoffmann *et al.*, 2010) but the uncertainties associated with the large Th and DCF corrections remain high, and the question remains of the precision with which speleothems can be used as meaningful sources of atmospheric ^{14}C records.

To investigate the efficacy of speleothem based reconstructions of atmospheric ^{14}C records, it is clear that studies must be made on speleothems of more pristine calcite. The Hulu Cave speleothems, which are from the region of Eastern China currently influenced by the East Asian Monsoon and have been used to create a high-resolution record of $\delta^{18}O$ as a proxy for monsoon strength (Wang *et al.*, 2001 and Wu *et al.*, 2009), represent an excellent

opportunity to carry out such a test. Here we present a new record of atmospheric ^{14}C based on the Hulu Cave speleothem, H82, spanning 10.7-26.6 kyr BP.

4.3 Materials and Methods

The Hulu Cave site at Tang Shan in eastern China near Nanjing (32 °30′N, 119 °, 90 m asl), is overlain by 30-40 m of limestone, with 30-40 cm of soil consisting mainly of weathered carbonate debris with a <5 cm upper layer of clays and organic matter, that currently supports subtropical C3 vegetation (Kong *et al.*, 2005). 80% of the precipitation at the cave site occurs during the summer monsoon season (Wang *et al.*, 2001), and monitoring by the Nanjing Normal University group has shown that drip rates respond rapidly to changes in rainfall. The 35 cm long speleothem H82 was collected from 35 m depth in Hulu Cave in two sections (A and B + C in Fig. 4.1) that were recovered on separate expeditions led by Y.W. The upper 17 cm of the speleothem is cylindrically shaped with a flat top, and represents the upward extension of one of two fused adjacent stalagmites that together form the lower section. Both sections show wax luster, and well-preserved growth laminations are present from the top of the speleothem through 30 cm (Wu *et al.*, 2009). Previous U-Th work on the upper part of the speleothem (Wang *et al.*, 2001; Yuan *et al.*, 2004 and Wu *et al.*, 2009) has shown that detrital thorium corrections are negligible, which allows a robust U-Th chronology to be constructed.

Prior to the work described here, the H82 stalagmite had already been sectioned into quadrants and extensively sampled for stable isotope analysis and U-Th dating (Wang *et al.*, 2001 and Wu *et al.*, 2009). Most of the sampling for this study was carried out for stalagmite depths 1-138 mm and 131-311 mm in two separate campaigns at University of Minnesota, using a "trench and wall" method that produced series of closely interleaved U-Th and ^{14}C dates (Tables S1 and S2 in Southon *et al.* (2012)). Parallel trenches several mm deep by

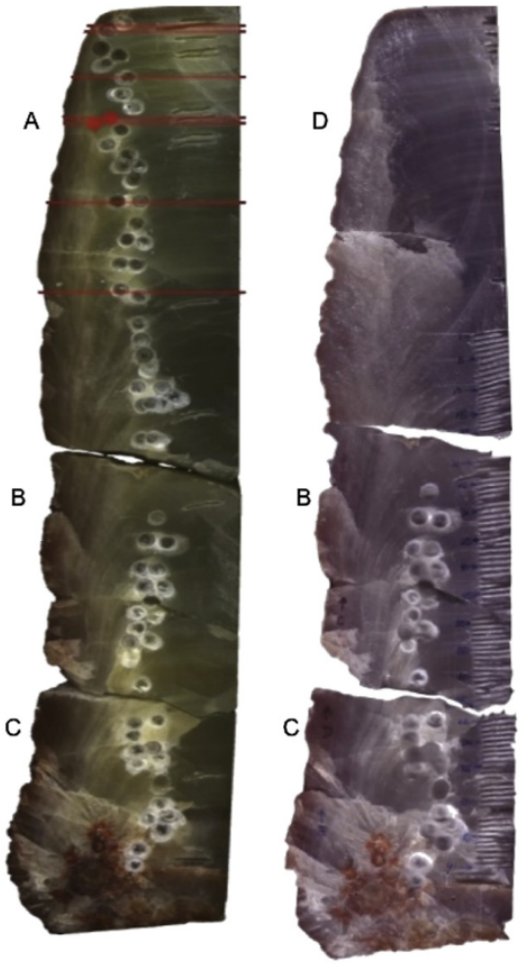

Figure 4.1: The H82 speleothem: two photographs showing sampling done for this project. The speleothem was removed from Hulu Cave in two separate expeditions as Piece A and one continuous Piece B+C, which later broke into two sections. Piece D is a 1 cm slice taken from the right-hand side of piece A, as is evidenced by the matching scars. Pieces B, C, and D were sampled using a trench and wall method as described in the text. Trench and wall sampling for the upper 138mm was carried out on a different quadrant (not shown). Pieces A, B, and C were also sampled off axis using a 3mm ID coring drill.

~1 cm long, separated by 1 mm thick walls, were drilled perpendicular to the growth axis using a Dremel tool, to sample over approximately 1 mm of stalagmite depth (Fig. 4.1). Powdered calcite samples weighing between 100 and 200 mg from the trenches were used for U-Th measurements. The ^{230}Th dating work was performed on a multi-collector inductively coupled plasma mass spectrometer (MC-ICPMS, Thermo-Finnigan Neptune) in the Minnesota isotope laboratory, University of Minnesota. The chemical procedures used to separate the uranium and thorium for ^{230}Th dating are similar to those described in Edwards *et al.* (1987). Uranium and thorium isotopes were analyzed on the multiplier behind the retarding potential quadrupole (RPQ) in peak-jumping mode. Instrumental mass fractionation was determined by measurements of a ^{233}U-^{236}U spike. The details of the technique are similar to those described in Cheng *et al.* (2000), Cheng *et al.* (2009a) and Cheng *et al.* (2009b), and half-life values are described in Cheng *et al.* (2008).

Intervening calcite walls between the trenches were removed as wafers for ^{14}C measurements at University of California Irvine in the Keck Carbon Cycle Accelerator Mass Spectrometry (AMS) Laboratory. Chips from the wafers were used for ^{14}C because we found that drilled powder from the dense H82 calcite gave ^{14}C ages that are systematically younger. This effect has been seen in work on some other speleothems and may be due to pickup of atmospheric CO_2 due to local overheating during drilling (W. Beck, T. Guilderson pers. comm.). A lower resolution wet coring method was used for an earlier ^{14}C sampling series covering the entire stalagmite length, with samples removed as cores 3 mm in diameter, drilled some distance from the growth axis (Fig. 4.1). ^{14}C results from the cores, plus a few measurements on leftover calcite chips sampled for some of the early U-Th work, are given in Table S2 in Southon *et al.* (2012).

Aliquots of calcite wafers or cores for AMS measurements were crushed into sub-millimeter pieces to achieve a desired mass of carbon (typically 12-14 mg of calcite), and pretreated by leaching away 30% of the material in weak HCl. Sample were then hydrolyzed in 85% H_3PO_4

and graphitized by iron catalyzed hydrogen reduction following standard AMS protocols. Prior to graphitization, all sample reactors were baked at 500 °C for 45 min with ∼1 atm. of ^{14}C-free CO_2 to reduce any memory effects from modern carbon (Southon, 2007). ^{14}C measurements were carried out on an NEC Compact (1.5 SDH) AMS system, using six aliquots of Oxalic Acid 1 as the normalizing standard. Each mg-sized carbon sample was measured multiple times (typically 8 to 15 runs) over a 24 h period, and 41 samples out of a total of 260 are duplicate aliquots. Geologic calcite and aliquots of Hulu Cave speleothem MSX (U-Th dated at 135 kyr), of similar size to the H82 samples and similarly processed, were used as procedural blanks. Leftover portions of calcite wafer and core samples taken for ^{14}C were measured for stable isotopes to allow detailed correlations to be made between high-resolution stable isotope records measured previously (Wang *et al.*, 2001 and Wu *et al.*, 2009) and the densely dated records from the present study. Measurements were carried out at UC Irvine on samples of ∼100 µg of powdered calcite, using a Finnigan Delta Plus IRMS equipped with a Kiel IV Carbonate Device.

4.4 Results

4.4.1 H82 Age Model

The U-Th results from the trench and wall samplings for this study, plus earlier lower resolution measurements (Wang *et al.*, 2001; Yuan *et al.*, 2004 and Wu *et al.*, 2009, plus unpublished data) are shown in Table S1 in Southon *et al.* (2012) and Fig. 4.2. Data have been corrected for detrital thorium on the basis of an assumed initial ^{230}Th/^{232}Th atomic ratio of 4.4 ± 2.2×10^{-6} (Wang *et al.*, 2001) and are shown as ages BP (before 1950 AD) with 2σ uncertainties. Fig. 4.2A and B shows, respectively, the speleothem age model before and after small depth adjustments explained in detail section 3.2, required for consistency

between samples from different slabs and quadrants of calcite. No significant age reversals are present, and corrections for detrital Th are a few years above 300 mm, rising to a few decades near the speleothem base. The record displays two periods of very slow stalagmite growth or hiatus: one short gap at 263 mm between ∼19.5 and 20.0 kyr BP and a second longer hiatus at 295 mm, between ∼22.5 and 24.5 kyr BP. The latter corresponds with a hiatus previously identified by Wu *et al.* (2009) at 305 mm in a column cut from another quadrant of H82: the depth difference reflects the irregular nature of the growth surfaces in the bottom few cm. This hiatus occurs during Heinrich Event 2, which appears in the Hulu Cave δ^{18}O record (Wang *et al.*, 2001) as a spike to less negative values. To the extent to which this can be interpreted as a period of especially low summer monsoon intensity, the extreme reduction in growth rate in H82 is consistent with the inferred reduction in precipitation.

4.4.2 Depth Adjustments

Depths measured from the top of H82 to the center of each sample (mid depths) are shown in Tables S1 and S2 in Southon *et al.* (2012). The samplings presented here were done on several different quadrants or slabs of calcite, and comparisons of U-Th and stable isotope (δ^{18}O) data showed that several small adjustments were required to bring the data sets to a common depth scale on the quadrant cutting axis. We stress that these were not required for construction of the ^{14}C record, for which all calendar ages are based on direct interpolation between ^{230}Th ages measured on the same pieces of calcite. Instead, they were used to show consistency between the different samplings, and for placing published high-resolution stable isotope results (Wang *et al.*, 2001 and Wu *et al.*, 2009) on the densely dated age model from the present study. These adjusted depths are also shown in Tables S1 and S2 in Southon *et al.* (2012), and the unadjusted and adjusted age models are shown in Fig. 4.2. The three adjustments required are as follows:

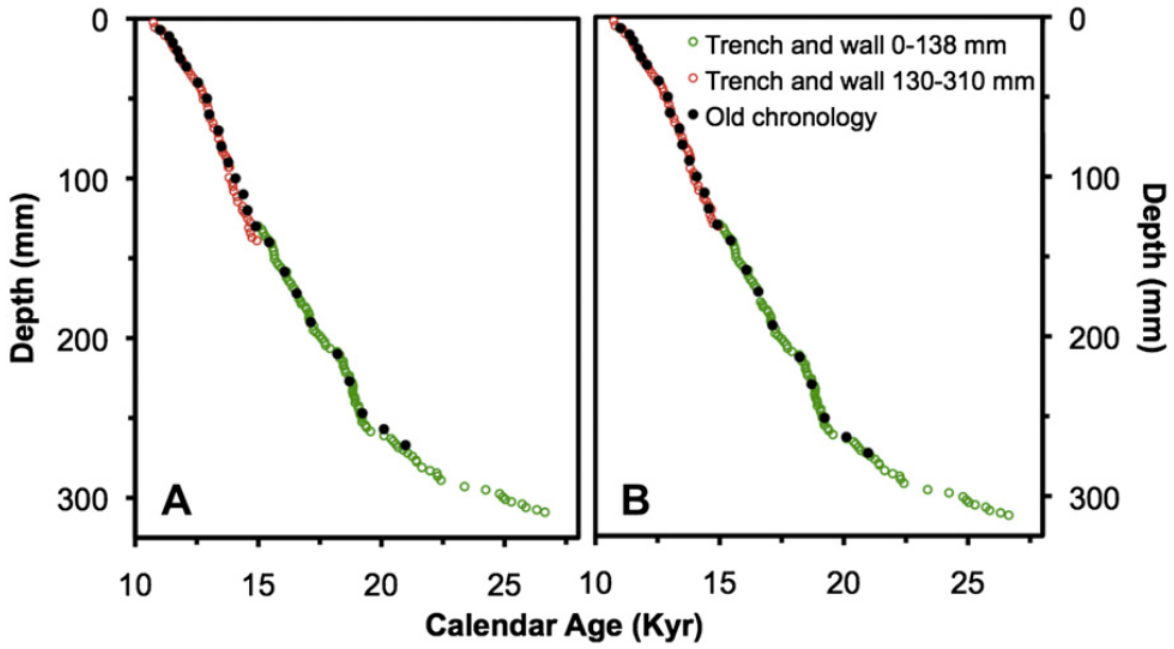

Figure 4.2: A. Age model for H82 based on UeTh measurements from this study (Trench and wall sampling) plus earlier work (Old chronology) e see text. B. Age model after depth adjustments for consistency between samples from different quadrants and slabs of H82 calcite as described in the text.

i The trench and wall sampling for depths 1-138 mm was taken somewhat off axis, where curvature of growth surfaces distorts the on-axis age vs depth relationship. These adjustments become significant for depths below 40 mm where the flat-topped region of H82 rather abruptly becomes significantly smaller and off-axis growth surfaces begin to crowd together and extend down the flanks of the speleothem (Fig. 4.1). The H82-A (^{14}C and δ^{18}O) and H82-B (U-Th) records required compression by 8% below 40 mm to achieve consistency with the upper portions of the old U-Th chronology and the published high resolution δ^{18}O record (Wang *et al.*, 2001).

ii The H82-2 trench and wall samples for depths 130-310 mm were taken on axis, and the depths shown for off-axis core samples in Table S2 in Southon *et al.* (2012) are equivalent on-axis depths determined by visually tracing growth surfaces back to the speleothem axis, hence similar adjustments are not required for these series. However, comparisons of δ^{18}O data from this study and from Wu *et al.* (2009) with a new high-resolution δ^{18}O record (R.L. Edwards pers. comm.) showed that the calcite pieces in Fig. 4.1 and the calcite column sampled by Wu *et al.* (2009) were both missing ∼3 mm at a depth of 172 mm. This represents the break between the upper and lower sections of H82, that were collected from Hulu Cave at different times and sectioned independently, and in retrospect it is not surprising that some of the pieces thought to be contiguous were actually missing a few mm of calcite near the break. The 3 mm of missing calcite was inserted at 172 mm into all of the records used in this study, to ensure consistency with the upcoming new δ^{18}O data.

iii Similar δ^{18}O comparisons suggested that the calcite column sampled for the lower portions of the old U-Th chronology and for the high-resolution Wu *et al.* (2009) δ^{18}O record was also compressed by 3 mm between 245 and 248 mm (248-251 mm after the initial adjustment at 172 mm). Detailed comparisons between the different δ^{18}O records across this interval suggested that it represents a period where different parts of the speleothem

grew at very different rates, rather than actual missing calcite. The cause(s) for such differential growth remain unclear, but might be related to a small change in the drip line. The 245-248 mm interval in the published $\delta^{18}O$ record has been linearly expanded to 6 mm, and depths for the oldest three samples from the old chronology are increased by 3 mm.

4.4.3 ^{14}C Ages

^{14}C results are shown in Table S2 in Southon *et al.* (2012), as conventional radiocarbon ages (Stuiver and Polach, 1977). Uncertainties are shown at 1σ and include contributions from background corrections, normalization to standards, and the scatter in repeated measurements on each sample, as well as counting statistics. A $\pm$ 30% uncertainty was used for all background subtractions, based on scatter between results on different background materials and separate aliquots of the same material, and background variations between measurement runs on different days. Initial ^{14}C ages for three of the samples were significantly older than adjacent data points. The samples were remeasured and the duplicates returned ages consistent with other results, indicating that the aliquots run initially were somehow contaminated with old carbon. These results are retained in Table S2 in Southon *et al.* (2012) but have not been used in the subsequent analyses. Anomalous results on two other samples were traced to mislabeling, and Table S2 in Southon *et al.* (2012) shows the corrected samples ID's. Two pairs of duplicates from regions of very slow growth disagree, probably because the calcite subsamples represented chips of different age.

4.4.4 Interpolated ^{230}Th ages and uncertainties

Interpolated ^{230}Th ages for the ^{14}C record are shown in Table S2 in Southon *et al.* (2012). We stress that the calendar ages for the ^{14}C data are derived exclusively from U-Th measurements

on the same pieces of calcite and are completely independent of the depth adjustments discussed above, ^{14}C measurements on the chip series (Table S2a in Southon *et al.* (2012)) were carried out on aliquots of the same samples used for the old U-Th chronology, and the calendar ages and uncertainties for those samples are those of the corresponding ^{230}Th measurements from Table S1 in Southon *et al.* (2012). Calendar ages for the closely spaced H82-A and H82-2 ^{14}C series are averages of the ^{230}Th ages for adjacent powder samples, and the uncertainties are taken as the standard errors in the means of the bracketing ^{230}Th ages. For the core samples, equivalent on-axis depths found by tracing growth surfaces were used to interpolate among ^{230}Th ages measured on-axis on the same H82 quadrant. For depths below 130 mm, the means of the bracketing H82-2 U-Th series ages were used, and the uncertainty assigned to the calendar age for each ^{14}C datum is once again the uncertainty in the mean ^{230}Th age. However, above 130 mm, linear interpolations between the old chronology ^{230}Th ages spaced 5-10 mm apart were required, because the denser H82-B U-Th series was measured on a different H82 quadrant. Given this coarse spacing, we assumed that the calendar age uncertainties for the interpolated points were comparable with those of the endpoints, and used the means of the uncertainties in the endpoint ages, rather than the more precise uncertainty in the mean.

4.4.5 Depth-based calendar age uncertainties

In addition to the analytically based calendar age uncertainties described above, we also incorporated age uncertainties due to the finite depth ranges spanned by samples taken for ^{14}C (allowing for the possibility of non-uniform sub-sampling for a given ^{14}C measurement) and we also considered possible errors in tracing growth surfaces. Trench and wall ^{14}C samples were approximately 1 mm wide, from which we adopt a maximum depth uncertainty of $\pm$ 0.5 mm for the on-axis H82-2 samples. Similarly, we took the maximum uncertainty for the larger chip samples as $\pm$ 1 mm. For the off-axis H82-A trench and wall series we increased

the depth range by 30% below 40 mm stalagmite depth to take account of the crowding together of curved growth surfaces, which increases the amount of equivalent on-axis depth (and time) represented in each sample. For the 3 mm core samples we assumed a maximum possible error due to finite sample size of ± 1.5 mm above 40 mm and ± 2 mm below that depth, and also factored in an additional uncertainty in tracing growth surfaces back to the stalagmite axis of ± 1 mm above 40 mm and ± 2 mm below 40 mm. For simplicity, and given the relatively coarse sample spacing, we assumed that these tracing errors were uncorrelated between adjacent core samples. Adding these components in quadrature, rounding, and approximating an equivalent 1σ uncertainty as half the maximum possible error, we derive overall 1σ depth uncertainties for the core samples of ± 1 mm from 0-40 mm depth and ± 1.5 mm below 40-mm. Similarly, depth uncertainties for the trench and wall samples are ± 0.25 mm, rising to ± 0.33 mm below 40 mm for the off-axis H82-A series; and ± 0.5 mm for the chips.

These depth uncertainties were converted to age errors using H82 growth rates approximated by piecewise linear fits to short sections of the U-Th age vs. depth record. The resulting age uncertainties were then added in quadrature with those derived from the ^{230}Th ages to produce the total calendar age uncertainties shown in Table S2 in Southon *et al.* (2012). The average growth rate for H82 is approximately 6 mm/kyr from the base of the stalagmite to 260 mm, and increases to an average of 30 mm/kyr above 260 mm. Depth-derived age uncertainties are therefore most significant near the base of the stalagmite, and are especially large during the periods of hiatus. They dominate the overall calendar age uncertainties for the large core samples below 130 mm and contribute significantly over the entire depth range of H82; but only become significant for the much smaller trench and wall samples in the bottom few cm of the speleothem.

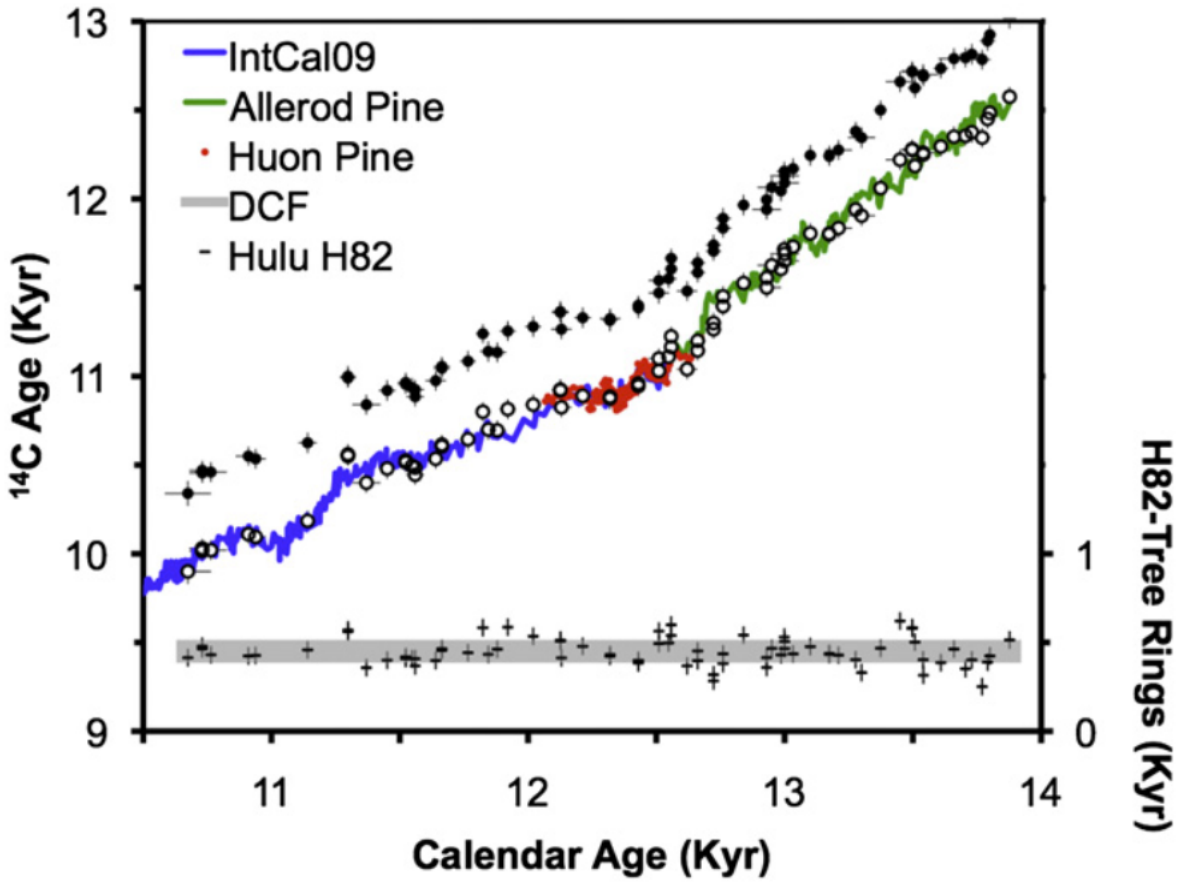

Figure 4.3: ^{14}C measurements on the H82 speleothem plotted with and without DCF correction against an extended tree ring data set: IntCal09 tree rings (Reimer *et al.*, 2009) plus Huon Pine (Hua *et al.*, 2009) and Allerd Pine (Kromer *et al.*, 2004). Tree ring - H82 age differences are shown at the base of the plot, with a grey bar representing the ±50 year DCF uncertainty derived from the H82 - IntCal09 comparison.

4.4.6 DCF correction

The DCF correction was determined by comparing ^{14}C results from the uppermost section of H82 with IntCal09 tree ring data (Reimer *et al.*, 2009), represented by the continuous blue line in Fig. 4.3. The overlap period extends from the start of the German Pine dataset in the mid-YD at 12.6 kyr BP to the end of growth for H82 at 10.7 kyr BP. For simplicity, the H82 data were compared with the smoothed IntCal data rather than the raw tree ring results; and since the ^{14}C calibration curve is relatively flat over most of this interval, the fit is insensitive to small errors in the calibrated ages and no attempt was made to account for uncertainties in the U-Th age model. A DCF correction of 452 yrs was derived from the average of the differences between equivalent H82 and IntCal measurements. Those differences showed substantially greater scatter ($\pm$ 62 years at 1σ) than the $\pm$ 33 years expected from the quoted uncertainties in the H82 and IntCal09 data, suggesting that analytical errors may have been underestimated or that short term DCF variations are present. We have treated the extra variance as arising from rapid DCF variations and therefore assign a value of 450 years for the DCF correction, with an uncertainty $\sim \sqrt{(622 - 332)}$ or $\pm$ 50 years.

In Fig. 4.3 the H82 data are also compared with an extended tree ring record that includes the floating Allerød pine sequence (Kromer *et al.*, 2004), and the recently published Huon pine series (Hua *et al.*, 2009). The positions of the Huon pine and Allerød pine relative to the master series are based on ^{14}C wiggle matching, and are believed to be accurate within decades. This comparison yields a DCF of 450 $\pm$ 70 years, which is slightly more variable than the DCF calculated using only the well-established master series. The agreement with the extended tree ring data indicates that H82 faithfully records atmospheric ^{14}C with a stable DCF across both the Allerød/Younger Dryas and the Younger Dryas/Holocene transitions, i.e., through major monsoonal shifts that correspond to transitions both into and out of a Greenland stadial (Wang *et al.*, 2001). This constancy through significantly different climate

regimes is the basis for our working assumption that the H82 DCF is unchanged throughout the entire H82 record.

4.4.7 Comparison with H82 high-resolution δ^{18}O records

High resolution stable oxygen isotope records from H82 and other Hulu speleothems (Wang *et al.*, 2001 and Wu *et al.*, 2009) have provided a valuable proxy record of changes in the East Asian monsoon on times scales ranging from years to glacial-interglacial cycles. The δ^{18}O data are highly correlated with summer insolation on Milankovich timescales, and with the record of centennial to millennial Greenland stadial/interstadial variations (Wang *et al.*, 2001 and Yuan *et al.*, 2004), consistent with a strong linkage between speleothem δ^{18}O and summer monsoon intensity that is further supported by pollen and other paleoclimate proxy data (Sun and Li, 1999; Xu *et al.*, 2010; Zhu *et al.*, 2010; and Xiao *et al.*, 2004). However, the details of precisely what monsoon parameters are recorded in the stable isotopes are less clear. The coherence of the records over thousands of km in eastern and southern Asia (Wang *et al.*, 2001; Yuan *et al.*, 2004; and Sinha *et al.*, 2005) argues against the idea that speleothem δ^{18}O responds primarily to local variations in temperature or precipitation amount, whether via changes in calcite-water fractionation or in δ^{18}O of meteoric water. Alternative hypotheses attribute δ^{18}O shifts to variations in the summer/winter precipitation ratio (Wang *et al.*, 2001) or changes in the progressive removal of moisture from air masses during transport from tropical Indo-Pacific moisture source regions to sites in Asia (Yuan *et al.*, 2004). Both mechanisms involve relatively direct connections between δ^{18}O and variations in the dominant summer monsoon rainfall, but a recent analysis of δ^{18}O in modern precipitation (Dayem *et al.*, 2010) suggests that the cave δ^{18}O archives may record other effects - variations in the duration of seasonal precipitation regimes or in moisture source regions or transport pathways - that are less directly connected to changes in monthly or total precipitation.

The Hulu δ^{18}O data have played a significant role ^{14}C calibrations, as a means of tying radiocarbon-dated records from other locations (Bard *et al.*, 2004 and Hughen *et al.*, 2006) to the Hulu U-Th timescale. The published high resolution H82 δ^{18}O data were sampled from a different quadrant of H82 from that used here (Wu *et al.*, 2009), and used an earlier U-Th chronology based on ^{230}Th dates at ∼750 year spacing. Stable isotope data from the present study are shown in Table S2 in Southon *et al.* (2012), in standard delta notation relative to Vienna PDB. Instrumental precisions (1σ) are ∼0.06‰ and 0.02‰ for δ^{18}O and δ^{13}C, respectively, based on long-term repeatability for the NBS19 standard. Missing data represent cases where insufficient material remained after the ^{14}C measurement. In Fig. 4.4 we compare δ^{18}O data from our discrete samples with the continuous high resolution records of Wang *et al.* (2001) and Wu *et al.* (2009), having transferred those δ^{18}O datasets to the densely dated U-Th age model from the present investigation with minor depth adjustments as described in Section 3.2. Agreement between the data sets is generally very good, though the high resolution data appear to be offset slightly older than our discrete sample measurements beyond 20.5 kyr BP. Growth surfaces in the bottom few cm of H82 are distinctly more irregular than those higher in the speloethem, so the relationships between depths in different calcite pieces are less obvious and more variable. However, any offsets are less than ∼150 years; and pending availability of high resolution δ^{18}O data extending closer to the speleothem base (R.L. Edwards pers. comm.) we have not attempted additional depth adjustments or δ^{18}O wiggle-matching in this region.

4.5 Discussion

4.5.1 Stability of the H82 dead carbon fraction

Comparisons of the H82 ^{14}C record with tree ring data in the interval 10-14 kyr BP, and with several other calibration records discussed below over the period 14-16 kyr BP (Fig. 5, Fig. 6 and Fig. 7), suggest that any changes in the H82 DCF were less than 100 years, perhaps as small as a few decades. This lack of variation in the DCF may be at least partly a consequence of the small absolute magnitude of the correction, determined by the local environment above the cave. The weak soil development and high infiltration capacity at the Hulu site, and the predominance of carbonate debris in the lower soil horizons (Kong *et al.*, 2005) are consistent with water-carbonate equilibration occurring primarily at shallow depths in an environment that is seldom completely saturated, i.e., under predominantly open system conditions where continuing exchange between meteoric water and soil CO_2 dilutes any geologic carbon contribution.

Nevertheless, the exceptional stability of the H82 DCF remains a puzzle. Pollen records from central and southeastern China (Sun and Li, 1999; Xu *et al.*, 2010; Zhu *et al.*, 2010; and Zhou *et al.*, 2004) show that the deglacial period encompassed major vegetation shifts that are broadly consistent with the record of summer monsoon changes inferred from the speleothem $\delta^{18}O$ data, though in some cases more gradual and prolonged. Widespread increases in broadleaf arboreal taxa indicating shifts to warmer and wetter conditions occurred after 15 kyr and 11.5 kyr BP, consistent with a strengthening of the summer monsoon. The responses to the onset of the YD (weakened summer monsoon) are mixed in the pollen data, with indications of a shift to cooler and wetter climate in southern and eastern China (Sun and Li, 1999; Zhou *et al.*, 2004; and Xu *et al.*, 2010), whereas montane central China experienced cooler and drier conditions (Zhu *et al.*, 2010). The warming and increased precipitation trends from 15 kyr and 11.5 kyr probably acted together to increase soil moisture; and

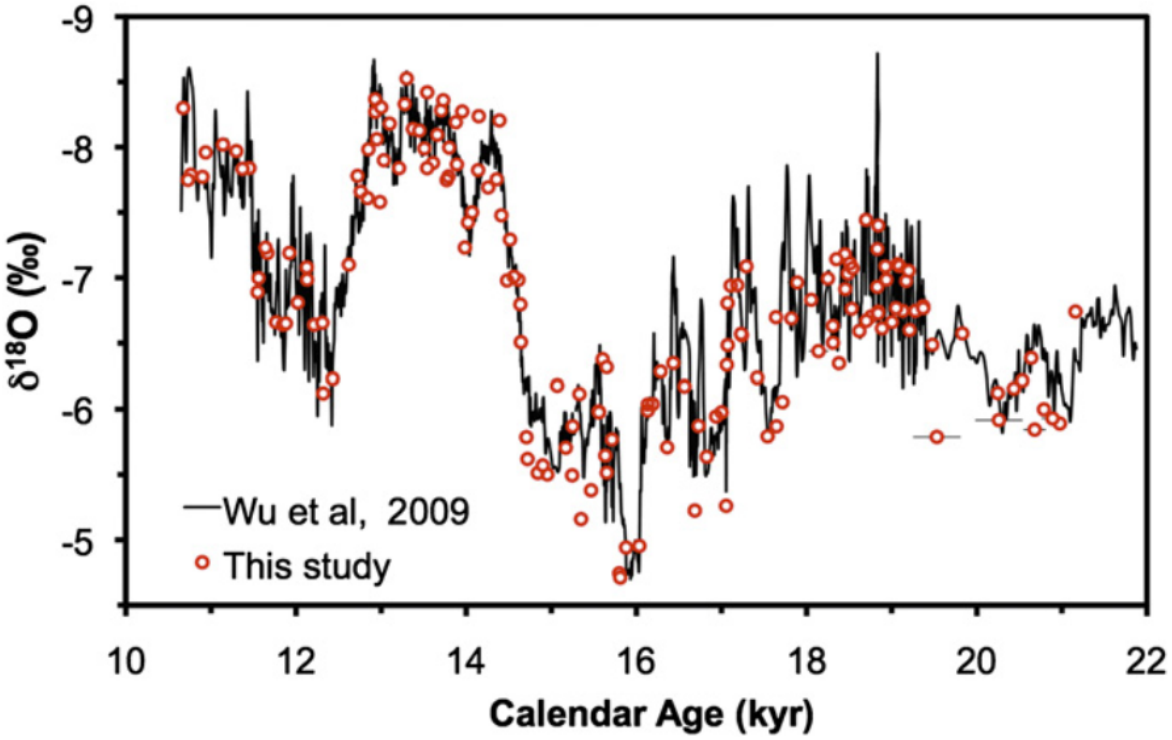

Figure 4.4: High resolution H82 δ^{18}O record from Wu *et al.* (2009), which incorporates the earlier dataset of Wang et al. (2001), plus "spot" H82 d18O data from this study, on a timescale based on the age model shown in Fig. 2B

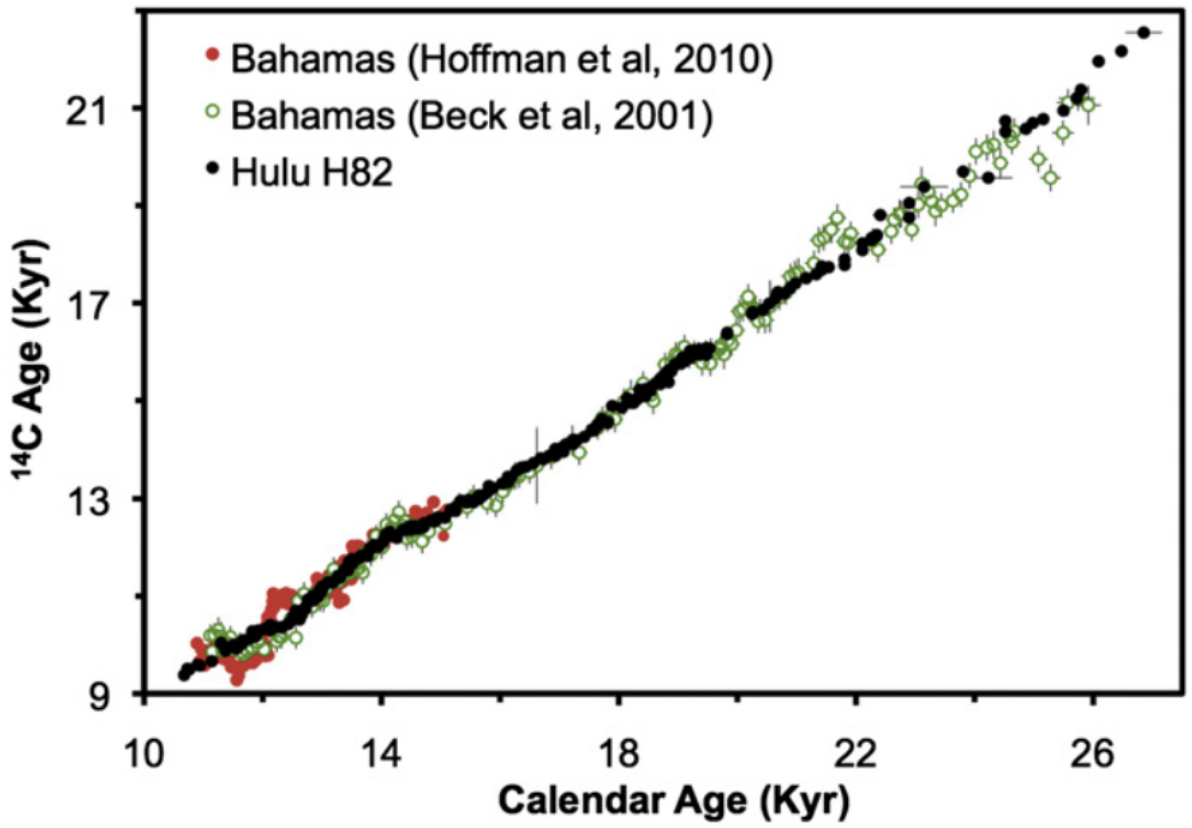

Figure 4.5: Bahamas speleothem (Beck et al., 2001; Hoffmann et al., 2010) and H82 ^{14}C records.

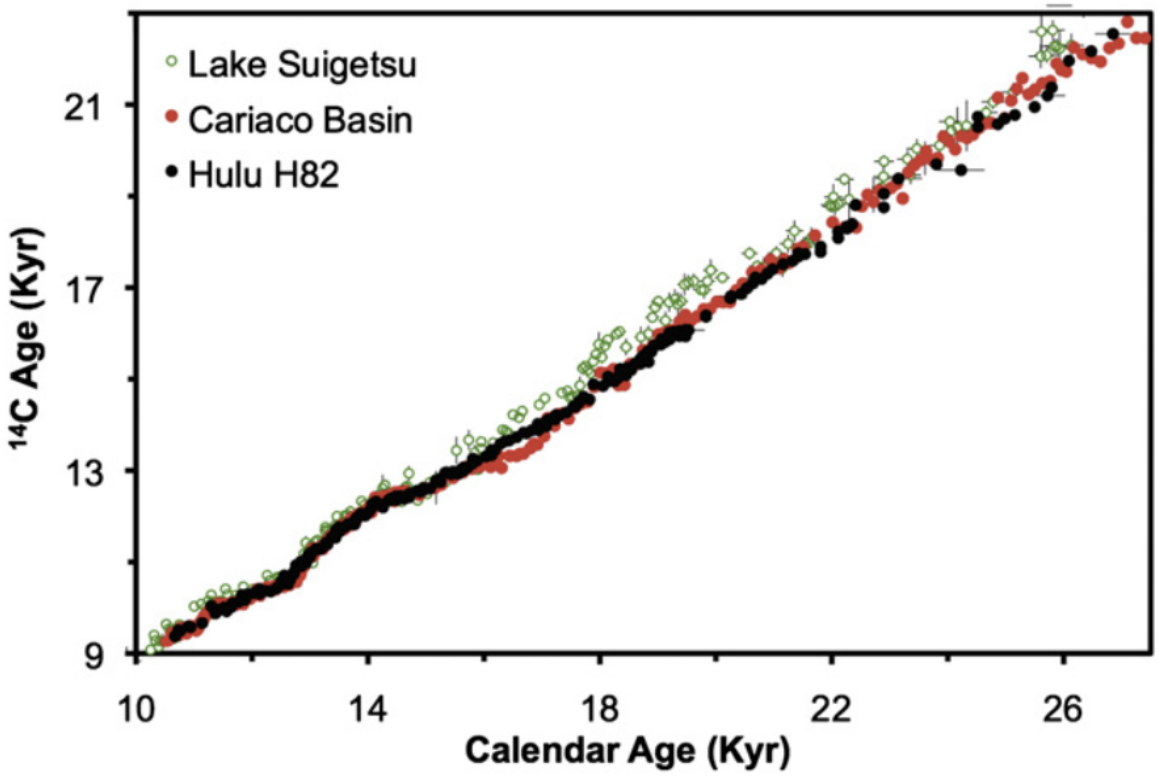

Figure 4.6: ^{14}C from H82, plus sedimentary ^{14}C records from the Cariaco Basin (Hughen *et al.*, 2006) and Lake Suigetsu (Kitagawa and van der Plicht, 2000).

these variations and the associated vegetation shifts to a more subtropical flora would likely have also altered soil carbon turnover and soil gas pCO_2 at the Hulu site, leading in turn to changes in ^{14}C in soil gas, groundwater, and speleothem calcite. In light of the varied wet/dry responses in the pollen data to the initiation of the YD at 13 kyr BP, it is unclear whether overall rainfall varied at Hulu Cave at that time. However, given the weakening of the summer monsoon indicated by the speleothem δ^{18}O, YD cooling at Hulu was certainly accompanied by changes in the seasonality of precipitation, which again must have influenced the local vegetation cover, hydrology, and soil carbon dynamics. While the small overall magnitude of the H82 DCF probably contributed to the lack of variation, the mechanisms by which effects of the various environmental changes on speleothem ^{14}C were attenuated or canceled each other out remain unclear.

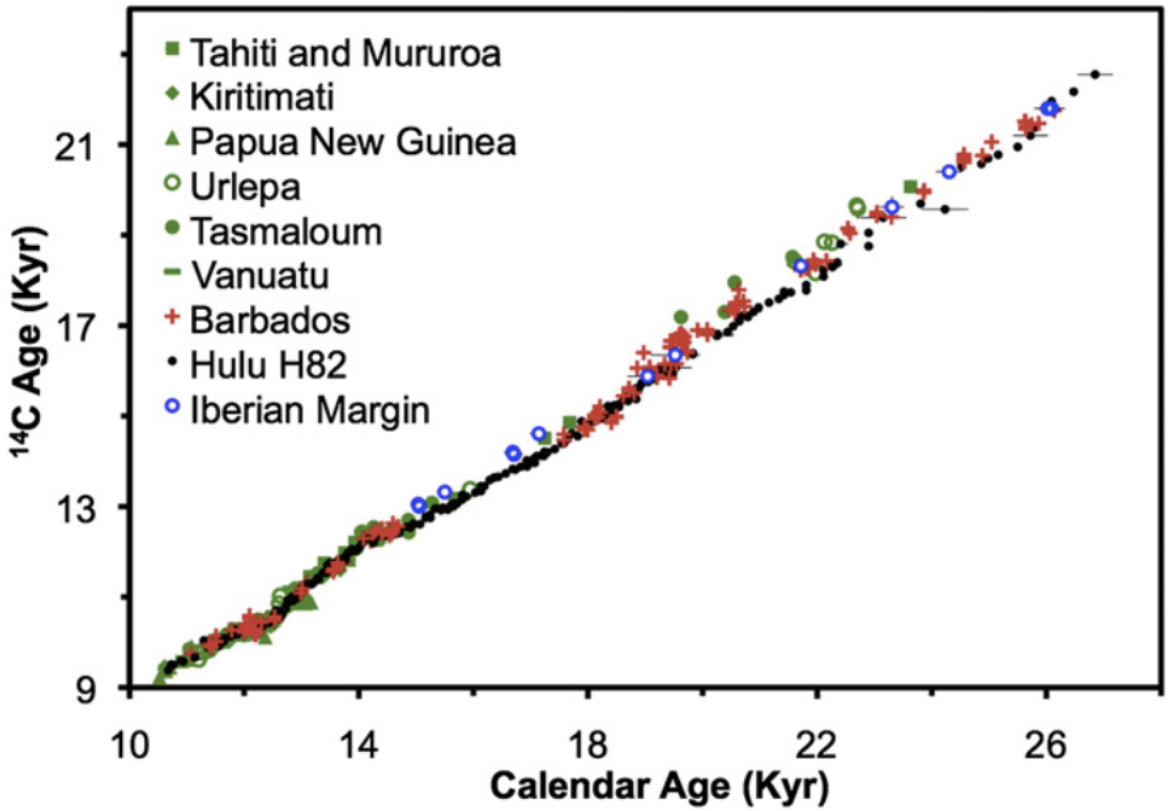

Figure 4.7: All coral ^{14}C records included in IntCal09 (Reimer *et al.*, 2009) plus ^{14}C data from the Iberian Margin sediments (Bard *et al.*, 2004) and H82. Pacific coral records are indicated by green symbols (see legend for details); Atlantic (Barbados) corals are shown in red.

4.5.2 Comparison with other ^{14}C calibration data

^{14}C data from H82 are compared with several existing large-scale calibration datasets in Fig. 4.5, Fig. 4.6 and Fig. 4.7. There is good overall agreement between the Beck *et al.* (2001) Bahamas speleothem ^{14}C record and the Hulu Cave data (Fig. 4.5), though some differences are present, notably before 21 kyr BP. The concordance between the two records for the period 15-21 kyr BP is striking, and indicates that the Bahamas record is accurate over this interval despite the large uncertainties associated with the large DCF and initial thorium corrections. The consistency between the two speleothem records, despite their large differences in location and geochemistry, suggests that there are no major variations in DCF in either record, and that both datasets provide good records of atmospheric ^{14}C over this period. The Hulu record is essentially monotonic over the entire 15-26 kyr BP interval, but the Bahamas record shows some structure around 20 kyr BP and again around 21.5 and 22.5-24.5 kyr BP. Given the large uncertainties in the Bahamas data, these "wiggles" might be statistical artifacts, but since most of them correspond to the periods of hiatus in H82, the Hulu data cannot confirm or refute these results. Before 24.5 kyr BP, the Bahamas data show a large shift to younger ages that is not reproduced in H82.

The overall agreement between the Hulu Cave and Cariaco Basin records shown in Fig. 4.6 is also good, but there are clear systematic differences between 16 and 17 kyr BP, corresponding to part of Heinrich Stadial 1 (HS1). Since the agreement between the Hulu Cave and Bahamas speleothem records in this interval is excellent, the offset between the Hulu Cave and Cariaco records is probably not due to changes in the H82 DCF. The existing Hulu chronology for the Cariaco record (Hughen *et al.*, 2006) is based on correlation of the sediment color record with an earlier lower resolution H82 δ^{18}O dataset (Wang *et al.*, 2001), but comparisons with the new higher resolution H82 δ^{18}O (Wu *et al.*, 2009) data suggest that the Cariaco Basin calendar age chronology is accurate and hence that the offset is not due to an erroneous "warping" of the Cariaco data to older calendar ages. The younger Cariaco ^{14}C

ages in this interval are therefore most likely explained by a remarkable decrease of 300-400 years in the marine reservoir age of the Cariaco Basin during this period.

Whether this was due to local effects within the basin or represents a regional response to ocean circulation changes during HS1 is unclear. A large decrease or total shutdown of North Atlantic Deep Water (NADW) formation associated with HS1 (Seidov and Maslin, 1999; Meissner *et al.*, 2002 and McManus *et al.*, 2004) would likely lead to decreased subsurface turbulence and increased stratification in the North Atlantic, which might allow for air-sea mixing to become the dominant influence on the ^{14}C age of equatorial Atlantic and Caribbean surface waters. However, since the observed drop in Cariaco reservoir age is substantially larger than models predict (Butzin *et al.*, 2005; Ritz *et al.*, 2008; and Singarayer *et al.*, 2008) any regional changes may have been augmented by local effects. Sea level during HS1 was 100-110 meters lower than at present (Peltier and Fairbanks, 2006), reducing the basin sill depths to just 45-35 meters and limiting water exchange with the open Caribbean, though a recent modeling study shows persistent mixing under even shallower LGM conditions (Lane-Serff and Pearce, 2009). Sediment reflectance and Fe and Ti concentration data indicate dry and windy conditions within the basin during HS1 (Peterson *et al.*, 2000), suggesting that increased air-sea gas exchange coupled with reduced input of Caribbean water could have biased local reservoir ages to low values. Recent comparisons of Cariaco data with tree ring data from the early Younger Dryas (Muscheler *et al.*, 2008 and Hua *et al.*, 2009) suggest that a similar (but much briefer) reduction in reservoir age may have occurred at the Allerød/Younger Dryas transition, at a time when sill depths were 60-70 m.

Three other radiocarbon records shown in Fig. 4.6 and Fig. 4.7 and discussed below all contain data that are systematically older than the H82 results over portions of the record beyond 15 kyr BP. One possible explanation is that the H82 DCF was significantly lower in glacial time, so that the plotted H82 ages are too young. However, two lines of evidence suggest that the discrepancies are mostly due to other causes, likely involving changes in

marine reservoir ages or questions about the independent timescales for the other records. First, for intervals where the Bahamas and H82 results agree well, this explanation would require equally large shifts in DCF's for two speleothems in very different locations and geochemical environments, which seems unlikely. Second, in several of these cases the implied decrease in H82 DCF is so large that it would require an extraordinarily low (essentially zero) input of geologic carbonate to Hulu Cave drip waters. However, despite the stability of the H82 DCF over the later period covered by the comparison with the dendro records, the possibility remains open that modest (∼100-200 year) DCF reductions occurred in H82 during the glacial and contributed to these discrepancies.

^{14}C dates on macrofossils from varved Lake Suigetsu (Kitagawa and van der Plicht, 2000) are several hundred years older than our new data over most the period before 16 kyr BP (Fig. 4.6), but this is probably due to problems with the Lake Suigetsu timescale, as opposed to reflecting true carbon cycle changes or a change in H82 DCF. The Lake Suigetsu chronology was based on varve counting in cores from a single borehole and this coring method may have led to the loss of material, particularly from the base of each core section (Staff *et al.*, 2010). New cores were taken from Lake Suigetsu in 2006, using overlapping sections from multiple boreholes to insure continuous coverage, and varve counting and ^{14}C analyses are underway (Nakagawa *et al.*, 2011).

^{14}C results from the Iberian Margin foraminiferal ^{14}C record (Bard *et al.*, 2004) are offset from the new H82 data between 15 and 17 kyr BP (Fig. 4.7), probably due to an increase in Iberian Margin surface reservoir age by ∼350 ^{14}C yr or an offset in calendar timescale of ∼400 yrs younger relative to H82. The latter scenario is possible because the lack of structure in the low-resolution Hulu Cave δ^{18}O record on which the published Iberian Margin calendar timescale is based limits the number of tie points available for correlation in this interval. Correlation to the new high resolution H82 δ^{18}O record is underway (E. Bard, pers. comm.) and this question should be resolved shortly. Alternatively, the Iberian Margin reservoir age

may have increased as proposed by Skinner (2008), though other studies suggest that any large increases in N.E. Atlantic reservoir ages during HS1 were confined to more northern sites (Waelbroeck *et al.*, 2001).

There is good agreement between the Hulu Cave ^{14}C record and published U-Th dated coral data from the end of the Hulu Cave record at 9.5 kyr back to 19.5 kyr BP (with a gap from 16 to 17.5 kyr BP where coral data are absent) but Vanuatu coral data (Cutler *et al.*, 2004) are 350-500 ^{14}C yrs older than equivalent measurements from H82 beyond 19.5 kyr BP (Fig. 4.7). Additionally, Atlantic corals from Barbados (Fairbanks *et al.*, 2005) are systematically $\sim$100-250 ^{14}C yrs older than the H82 data in the interval 19.5-21 kyr BP. This disagreement could indicate either a decrease in H82 DCF, or increased marine reservoir ages in the LGM continuing into early deglacial time. Since a decrease in DCF of the magnitude implied by the Vanuatu data is unlikely, at least some of the discrepancy is probably due to reservoir age variations.

These centennial scale differences between calibration records remain difficult to characterize and explain, particularly in the older portions of the records where uncertainties in both ^{14}C and calendar ages are larger, and especially for intervals that lack robust agreement between any of the datasets. Given current uncertainties concerning glacial ocean circulation and the likelihood of significant hydrologic changes in the tropics during Isotope Stage 2, we cannot rule out the possibility of changes in ^{14}C offsets for both cave and marine systems. More precise apportionment of any changes in marine reservoir ages and speleothem DCF's will rely on the development of other high-resolution records of terrestrial and marine ^{14}C in these intervals.

4.5.3 The timing and origin of deglacial pCO_2 increase

Identifying the magnitude and timing of any changes in ^{14}C offsets between different carbon pools is of particular interest in the so-called Mystery Interval (Broecker and Barker, 2007) between about 15 and 18 kyr BP, which was characterized by a drop of almost 200‰ in atmospheric and surface ocean $\Delta^{14}C$ (Beck *et al.*, 2001; Fairbanks *et al.*, 2005; and Hughen *et al.*, 2006) and a rise of 40 ppm in atmospheric pCO_2 (Monnin *et al.*, 2001). Marchitto *et al.* (2007) linked these changes with a low-$\Delta^{14}C$ excursion in eastern North Pacific intermediate waters, and hypothesized that they represented the ventilation via the Southern Ocean of a previously isolated glacial deep water mass (Adkins *et al.*, 2002), with massive release of sequestered CO_2. Evidence for such a ^{14}C-depleted water mass in the deep glacial Pacific remains elusive (Broecker and Barker, 2007), and the circulation pathways by which any newly ventilated low-^{14}C waters reached intermediate depths in the North Pacific (Marchitto *et al.*, 2007), eastern tropical Pacific (Stott *et al.*, 2009) and Arabian Sea. (Bryan *et al.*, 2010) have not been found (De Pol-Holz *et al.*, 2010). However, if mechanism proposed by Marchitto *et al.* (2007) is correct, the ^{14}C drop is directly related to the problem of glacial-deglacial pCO_2 variations, which are presently poorly understood and are not well simulated by current climate models. Recent studies show intensified upwelling and enhanced biological productivity (Anderson *et al.*, 2009) and a rise in deep ocean $\Delta^{14}C$ (Skinner *et al.*, 2010) within the Southern Ocean, that are coeval (within large uncertainties) with the pCO_2 increase, consistent with the recoupling of a previously isolated deep reservoir with the surface.

The H82 ^{14}C record displays the same ~200‰ atmospheric $\Delta^{14}C$ drop, and the exceptionally high resolution absolute dating of H82 allows for more precise constraints on the timing of the decrease. Fig. 4.8 shows $\Delta^{14}C$ data from the Bahamas, Cariaco and H82 records, plus pCO_2 data from trapped air in the Dome C (Antarctic) ice core (Monnin *et al.*, 2001) plotted on the absolutely dated GISP2 ice core layer counted timescale. The $\Delta^{14}C$ drop in the H82 and

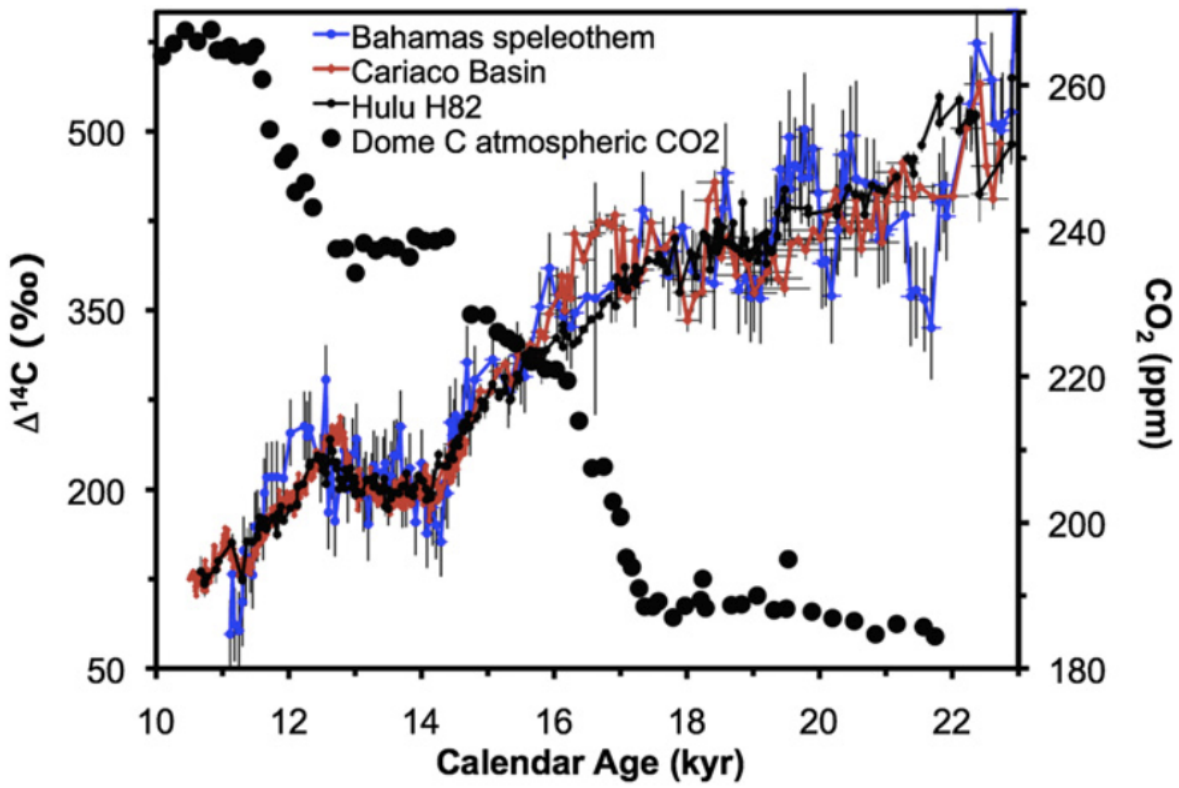

Figure 4.8: $\Delta^{14}C$ for the H82, Bahamas and Cariaco records, plus pCO_2 data from Dome C, Antarctica (Monnin *et al.*, 2001) placed on the layer-counted GISP2 Greenland ice core timescale via synchronization of methane records (Marchitto *et al.*, 2007).

Bahamas data begins more than 1 kyr earlier compared with the Cariaco record, coincides within uncertainties with the atmospheric pCO_2 rise, and closely tracks $\Delta^{14}C$ decreases at intermediate depths in the eastern North Pacific (Marchitto *et al.*, 2007) and the Arabian Sea (Bryan *et al.*, 2010). The new chronology is therefore consistent with the recoupling hypothesis outlined above (though this remains unproven) and underscores the requirement that any hypothesis seeking to explain the glacial-interglacial rise in atmospheric CO_2 must involve strong linkages between atmospheric pCO_2 and terrestrial and marine ^{14}C.

4.5.4 High-resolution $\delta^{18}O$ data

The present study provides a well-constrained age model for the high resolution H82 $\delta^{18}O$ data spanning the deglacial period (Wang *et al.*, 2001 and Wu *et al.*, 2009), with U-Th dates at centennial spacing rather than every 750 years as previously (Table S3). This places the stable isotope data on a more solid chronological framework, though the old and new age models differ very little, typically by 100 years or less. Minor changes primarily reflect "kinks" in the growth rate that were hidden in the lower resolution chronology. The new age model has implications for ^{14}C calibration during early deglaciation, since the rich structure of the high resolution $\delta^{18}O$ data over this interval attests to significant centennial scale monsoon changes (Wu *et al.*, 2009) that provide numerous potential tie points for correlating other climate proxy records with the detailed Hulu chronology.

4.6 Conclusion

This new record of atmospheric ^{14}C is in good overall agreement with existing marine and terrestrial ^{14}C records, suggesting that any changes in the DCF in the H82 speleothem are small, even across major climate transitions that likely involved large perturbations to the

tropical hydrologic cycle. This in turn suggests that the Hulu Cave speleothems may be useful for reconstructing atmospheric ^{14}C back to the radiocarbon detection limit of ∼50 kyr BP. The agreement between the H82 and Bahamas speleothem data over the 15-21 kyr BP interval shows that at least some records with large DCF can provide meaningful records of atmospheric ^{14}C and they should not be a priori excluded from consideration as calibration datasets. The high precision of this Hulu Cave record makes it particularly valuable for recognizing small changes in the paleo-carbon cycle. Comparison with the Cariaco Basin record through the deglacial interval reveals that the marine reservoir age of Cariaco Basin has varied, highlighting the importance of extending high-resolution marine and terrestrial ^{14}C records back to the radiocarbon detection limit to be able to detect changes in ocean circulation over the glacial cycle.

4.7 Acknowledgements

We thank Wally Broecker and the Comer Science and Education Foundation for their support; Julie Ferguson for help with stable isotope measurements; Erik Smith and Ben Hardt for assisting with H82 sampling; Guaciara Santos, Will Beaumont and Kiyo Beverly for laboratory assistance; and two reviewers for thoughtful comments and suggestions that improved the manuscript.

Chapter 5

Assessing influences on speleothem dead carbon variability over the Holocene: Implications for speleothem-based radiocarbon calibration

5.1 Abstract

Recently, it has been shown that U-Th dated speleothems may provide a valuable archive of atmospheric radiocarbon (^{14}C), but the reliability of these records is dependent upon the stability of the dead carbon proportion (DCP) derived from the soil and bedrock. In order to assess climatic influences on speleothem DCP, we have investigated DCP variability over the Holocene interval where atmospheric ^{14}C is well known based on dendrochronologically

dated tree rings by conducting ^{14}C measurements on a U-Th dated stalagmite (HS4) from Heshang Cave, Hubei Province, China (30 °27′N, 110 °25′E; 294 m) spanning 0.5-9.6 ka. We investigated climatic controls on DCP, and found that DCP in HS4 has an average value over the Holocene of 10.3 ± 1.5%, with an average age offset from atmospheric radiocarbon of 875 ± 130 years, and displays a response to both precipitation increases and decreases. HS4 DCP increases during the wetter mid-Holocene interval (∼5.5-7.1 ka), likely reflecting a shift to more closed-system dissolution in response to increased soil moisture. DCP decreases during the 8.2 ka event, a time period of dry conditions at Heshang Cave, though the lower amplitude of this shift indicates that DCP may be less sensitive to dry events. Speleothems are potentially valuable archives of atmospheric radiocarbon, especially in older portions of the ^{14}C calibration curve where knowledge of atmospheric ^{14}C is limited, however minor climatic influences on DCP could introduce uncertainties of several hundred years to calibrated ages.

5.2 Introduction

5.2.1 Calibration of atmospheric radiocarbon

In order to study the causes and effects of past changes in Earth's climate, precise and accurate chronologies and chronometers are key. Many paleoclimate proxy records rely on measurements of the concentration of radiocarbon (^{14}C) in calcite ($CaCO_3$) or organic matter for construction of their calendar age chronologies. However, radiocarbon-based geochronology, which is theoretically possible to at least 50 ka, is complicated by changing atmospheric concentrations of ^{14}C, which are controlled by: (1) non-constant ^{14}C production rates in the upper atmosphere, which vary with geomagnetic field intensity and solar variations over a wide-range of timescales (Bard *et al.*, 1998); and (2) changes in carbon cycling which

redistributes carbon, including ^{14}C, between ocean, atmosphere, and biosphere reservoirs. In order to use ^{14}C as a chronometer, and investigate changes in carbon cycling, the ^{14}C timescale must be calibrated by reconstruction of records of atmospheric ^{14}C tied to robust independent chronologies.

Tree ring records of ^{14}C with calendar ages derived from dendrochronology are considered the most robust records of atmospheric ^{14}C because they directly incorporate atmospheric CO_2 during photosynthesis and have a high-resolution independent chronology. Tree ring records from central and northern Europe are the basis of the most recent IntCal13 radiocarbon calibration curve to 13.9 ka (Reimer *et al.*, 2013). Before this point, regional climate conditions were less hospitable to trees, and the tree ring records are no longer the basis of ^{14}C calibration curves, although there are some floating tree ring chronologies covering earlier intervals (e.g. Turney *et al.*, 2007; Muscheler *et al.*, 2008; Kromer *et al.*, 2004; Hua *et al.*, 2009; and Hogg *et al.*, 2013b).

The only true non-tree ring record of atmospheric ^{14}C extending beyond 13.9 ka is a record from Lake Suigetsu, Japan, which is based on macrofossils paired with a varve counting chronology (Kitagawa and van der Plicht, 1998a, 1998b; 2000; Staff *et al.*, 2010; and Bronk Ramsey *et al.*, 2012) and covers the interval 0-52.8 ka. The Lake Suigetsu record presented by Kitagawa and van der Plicht, 1998a; 1998b; and 2000 showed significant divergence from other atmospheric radiocarbon reconstructions prior to $\sim$25 ka, which was found to be due to errors in the calendar chronology because of incomplete core retrieval during sampling (Staff *et al.*, 2010). A new set of overlapping cores was taken and a new high-resolution record with an improved chronology has been constructed, though the record displays large scatter in the ^{14}C ages in the interval $>$28 ka due to small sample sizes, as well as large uncertainty in the layer-counting age model (Bronk Ramsey *et al.*, 2012). Nonetheless, the Lake Suigetsu ^{14}C record provides a valuable "backbone" for the atmospheric ^{14}C record, which is refined by a variety of other ^{14}C records.

In the absence of true atmospheric records, the majority of calibration efforts have been focused on marine sediment records with a constant correction applied to account for the marine reservoir effect–the offset between the concentration of ^{14}C in the ocean and the atmosphere. The use of marine records for calibration of terrestrial radiocarbon dates is complicated by the potential for climatically driven variations in marine reservoir age. It is well known that large and rapid changes in climate occurred during the deglacial period, which were likely associated with changes in the Atlantic Meridional Overturning Circulation (McManus *et al.*, 2004 and Vellinga and Wood, 2002). These climatic changes were accompanied by large variations in surface ocean ^{14}C (Broecker and Barker, 2007 and Hughen *et al.*, 2000), consistent with the idea that they involved major shifts in the carbon cycle, which would have had large impacts on marine reservoir ages. Despite this complication, the agreement between these reservoir corrected marine records and the Lake Suigetsu record is very good to ∼28 ka. Before 28 ka the divergence between records increases (Reimer *et al.*, 2013); as does the variance in the Lake Suigetsu record (Bronk Ramsey *et al.*, 2012), with differences between records on the order of thousands of years, leading to high uncertainty in the atmospheric ^{14}C record in the earlier intervals.

5.2.2 Speleothem-based records of atmospheric radiocarbon

Recently, there has been interest in using speleothems to create records for radiocarbon calibration, in part because they have many features which may make them valuable sources of records which resolve the calibration curve in older intervals (e.g. Beck *et al.*, 2001; Weyhenmeyer *et al.*, 2003; Dorale *et al.*, 2008; McDermott *et al.*, 2008; Hoffmann *et al.*, 2010; and Southon *et al.*, 2012). Speleothems hold some key advantages over floating tree rings, varved chronologies, and marine records:

1. They can be precisely and absolutely dated using U-Th methods (Richards and Dorale, 2003)

2. Their fast growth rates, highly resolvable stratigraphy, and excellent preservation allow for often continuous high-resolution ^{14}C measurement over the entire ^{14}C dating range

3. They are widely used for paleoclimate reconstruction (Fairchild *et al.*, 2006) so access to numerous U-Th dated samples is possible and will allow for replication of records and direct comparison with climate proxy data. There are, however, several complicating factors affecting speleothem-based radiocarbon calibrations stemming from the way that speleothems are formed.

Formation of speleothem calcite is driven by CO_2 degassing of cave drip water that has accumulated carbon from the soil and bedrock. Meteoric waters equilibrate with soil CO_2 to form carbonic acid, which drives carbonate dissolution as drip water percolates through the limestone cave host bedrock. Consequently, ^{14}C in speleothem calcite is offset from contemporaneous atmospheric ^{14}C because a proportion of speleothem carbon comes from old soil organic matter (SOM) and radiocarbon-free "dead carbon" from the bedrock. To date, the offset between speleothem ^{14}C and contemporaneous atmospheric ^{14}C has been referred to in a variety of different ways across the literature, often using the same acronym to refer to different metrics, which has been a source of some confusion. In this manuscript we will refer to the dead carbon proportion (DCP) as a percentage as defined by Genty and Massault (1997), but we also refer to the DCP as a "correction" or "offset" with units of ^{14}C years.

Hendy (1971) considered two end member scenarios under which dissolution of carbonate bedrock can occur: open and closed system dissolution. In open-system dissolution, the solution dissolving the bedrock is continually in contact with soil CO_2, which leads to speleothem $\Delta^{14}C$ source compositions dominated by a soil CO_2 signature, as isotopic equi-

librium with soil C and the dissolved inorganic carbon (DIC) pool is maintained during dissolution. In closed system dissolution, dissolution of the bedrock takes place in isolation from soil CO_2, leading to $\Delta^{14}C$ source compositions shifted towards a bedrock ^{14}C isotope signature. Therefore, completely open-system dissolution, where soil CO_2 ^{14}C values are identical to atmospheric values would lead to an apparent DCP = 0%, whereas a completely closed-system dissolution wherein one mole of carbonate is required to neutralize one mole of dissolved CO_2 would lead to a theoretical DCP = 50%. However, soil gas $^{14}CO_2$ is rarely equal to atmospheric $^{14}CO_2$, because soil CO_2 is a mixture of atmospheric CO_2, root respiration, and CO_2 from decomposition of aged SOM, leading to the potential for a DCP > 50%, and making a DCP = 0% unlikely. In natural systems, carbonate dissolution usually falls somewhere between the two end member scenarios, with average DCP around 15 ± 5% (Genty *et al.*, 1999). Despite the potential for variable DCP to complicate speleothem-based reconstructions of atmospheric ^{14}C, speleothem radiocarbon records have been used to provide valuable constraints on the calibration curve during intervals where true atmospheric ^{14}C data is limited (Beck *et al.*, 2001; Hoffmann *et al.*, 2010; and Southon *et al.*, 2012).

The speleothem-based records of atmospheric ^{14}C that have been included in IntCal13 are a record spanning 10.6-26.8 ka from Hulu Cave, China (Southon *et al.*, 2012), and a record spanning 11.1-44.1 from the Bahamas (Beck *et al.*, 2001 and Hoffmann *et al.*, 2010). These records were constructed using a trench-and-wall sampling technique, where ^{14}C measurements on intact chips of calcite from the walls are interleaved with U-Th measurements on powder from drilled trenches, resulting in a robust and well-constrained calendar chronology for the ^{14}C record. The record from Hulu Cave, based on speleothem H82, has a very low and stable DCP of 5.4 ± 0.7% (450 ± 50), calculated from the period of overlap between H82 with the master tree ring records spanning 10.7-12.6 ka, which covers the Younger Dryas/Holocene transition - a period of rapid climate change which is likely to have altered cave hydrology (Southon *et al.*, 2012). The Bahamas speleothem record based on GB-89-24-1 spanning 11-45 ka was initially published in Beck *et al.* (2001) and showed extremely large

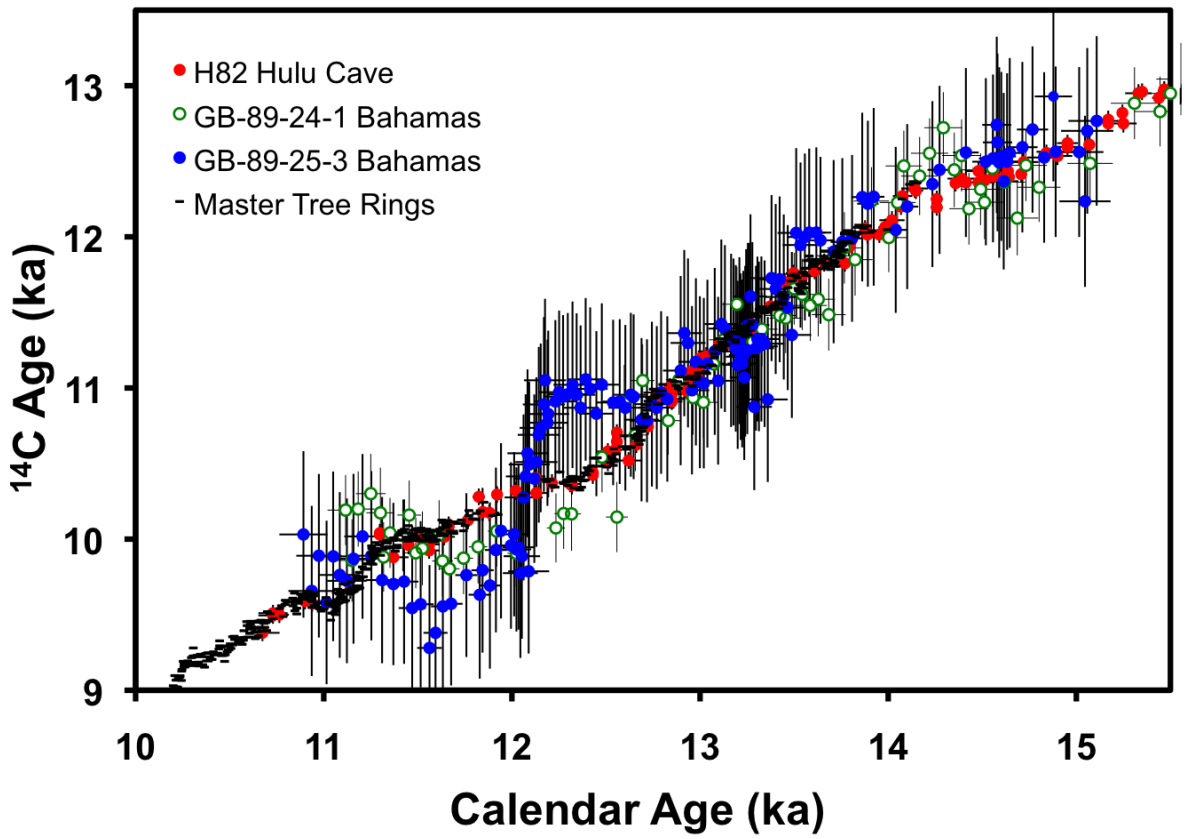

Figure 5.1: Comparison of period of overlap between existing speleothem-based re- constructions of atmospheric ^{14}C H82 Hulu Cave (filled red circles), GB-89-24-1 Bahamas speleothem (open green circles), and GB-89-25-3 Bahamas speleothem (filled blue circles) and tree ring records of atmospheric ^{14}C included in IntCal13 (black dashes))

variations in ^{14}C in the interval 41-44 ka. These variations were found to be an analytical artifact, and a new sampling of GB-89-24-1 covering 41-44 ka as well as a new record based on speleothem GB-89-25-3 spanning 28-44 ka and 11-15 ka to establish the DCP, was constructed by Hoffmann et al. (2010). GB-89-25-3 has a high DCP of 22.7 $\pm$ 5.9% (2075 $\pm$ 540), while GB-89-24-1 has a slightly lower DCP of 16.5 $\pm$ 4.7% (1450 $\pm$ 470).

There has been some hesitation in using speleothems for ^{14}C calibration, because of the potential for undetected variations in DCP, as well as the large variations in DCP seen in the Bahamas speleothem records. However, even with this additional uncertainty, the existing speleothem records of ^{14}C have been instrumental in improving our understanding of the history of the carbon cycle through identifying past changes in ocean circulation, and ma-

rine reservoir age, and therefore improving the ^{14}C calibration curve. Comparison between the Cariaco Basin record and both the Hulu Cave speleothem and Bahamas speleothem ^{14}C records confirmed that the marine reservoir age in Cariaco Basin varied significantly during Heinrich Stadial I (Southon *et al.*, 2012); which resulted in the removal of the Cariaco Basin ^{14}C data during Heinrich Stadial I from IntCal13 (Reimer *et al.*, 2013). Additionally, while the new Lake Suigetsu core has an improved varve counting chronology, complications inherent to varve counting based chronologies still limit the certainty of the calendar chronology, especially in older sections. To address this, the drift in the varve chronology was corrected for by comparison between the Lake Suigetsu record and the U-Th based calendar chronology of Hulu Cave H82 and Bahamas GB-89-25-3 speleothem records (Bronk Ramsey *et al.*, 2012); which resulted in major reductions in the 1σ error of the Lake Suigetsu calendar chronology, ranging from a factor of $\sim$2 at 13 ka to at least a factor of 10 at $>$30 ka. The combination of true atmospheric ^{14}C measurements from Lake Suigetsu with robust absolute U-Th based calendar chronology from speleothems has resulted in significant improvement in the calibration curve.

Speleothem records of ^{14}C have proven to be valuable for improving the calibration curve, but to be able to fully take advantage of speleothems as records of atmospheric ^{14}C, improved understanding of the controls on dead carbon incorporation in speleothems must be developed. Reconstructions of ^{14}C in speleothems over the interval where atmospheric ^{14}C is well known from the tree ring record allows for precise constraint on DCP variability and for investigation of the controls on variability in DCP. The Bahamas and Hulu ^{14}C records included in IntCal13 (Southon *et al.*, 2012; Beck *et al.*, 2001; and Hoffmann *et al.*, 2010) have very short periods of overlap with the tree ring records (Fig. 5.1), of only 2.8 ka in GB-89-24-1, 3.1 ka in GB-89-25-3, and 3.2 ka in H82, which severely limits knowledge of the extent of variability of DCP in these records. To study the variation of DCP in speleothem records over a wide range of climatic conditions and over a range of timescales, we have created a stalagmite-based record of Holocene ^{14}C, as the Holocene represents the interval where at-

mospheric ^{14}C is best known based on dendrochronologically dated trees. This record, based on a Holocene stalagmite referred to as HS4 from Heshang Cave in the Hubei Province of China, is particularly well-suited for this study as it lies in the East Asian Summer Monsoon (EASM) region, a location which has likely experienced large changes in precipitation in response to changing Northern Hemisphere summer insolation (Wang *et al.*, 2008; Morrill *et al.*, 2003; and Hu *et al.*, 2008b) and abrupt events linked to high-latitudes (Liu *et al.*, 2013). Furthermore, as the HS4 stalagmite has been the subject of extensive paleoclimate research (Johnson *et al.*, 2006; Hu *et al.*, 2008b; and Liu *et al.*, 2013) and Heshang Cave is the site of a long-term modern calibration study (Hu *et al.*, 2008b), robust paleoclimate records are available for comparison with the ^{14}C record. In this paper, we present a new speleothem-based atmospheric ^{14}C record spanning 0.5-9.6 ka based on a total of 84 ^{14}C measurements made on HS4 with a calendar age model based on U-Th measurements from Hu *et al.* (2008b) and Liu *et al.* (2013). In addition, to investigate the DCP response to abrupt climate events, we present high-resolution ^{14}C measurements over the 8.2 ka event, a time period characterized by very dry conditions at the cave site (Liu *et al.*, 2013).

5.3 Study location and methods

Heshang Cave is located in the Hubei Provence of China (30.44 °N, 110.42 °E), ∼100 km west of the city of Yichang in the middle reaches of the Yangtze Valley. The cave is 250 m long, roughly horizontal, well ventilated, and overlain with 400 m of Cambrian dolomite. HS4 is a 2.5 m long annually-banded stalagmite that was actively forming when it was collected from Heshang Cave in 2001. HS4 has previously been measured for $\delta^{18}O$ and $\delta^{13}C$ at high resolution and an age model was constructed using 21 U-Th measurements and layer-counting (Hu *et al.*, 2008b). The stalagmite has a high mean growth rate of 0.28 mm/yr.

The stalagmite was cut in half parallel to the growth axis and the surface was polished to reveal laminations consisting of sub-mm scale light and dark couplets, which have been shown to be annual (Hu *et al.*, 2008b). HS4 calcite is milky, opaque, and porous, with a fabric dominantly characterized as open columnar using the terminology of Frisia and Borsato (2010). Fifty-four samples for ^{14}C analysis were taken as intact wafers of calcite using a "moat-and-spall" technique, whereby a small trench is drilled around the desired sample region using a 0.5 mm dental drill and the solid wafer is then snapped off at its base. Similar sampling methods have been employed in this study and previous studies (e.g. Beck *et al.*, 2001; Hoffmann *et al.*, 2010; and Southon *et al.*, 2012) because of concern that contamination of sample material by atmospheric CO_2 may occur, as shifts in isotopic values have been observed in some carbonate samples collected as powder (e.g. Gill *et al.*, 1995). 21 wafer samples were taken from the same depths as the original 21 U-Th dates and an additional 33 were interspersed along the HS4 growth axis to give an average spacing of ∼1 sample every 4 cm. Wafers were subsequently crushed into smaller pieces to achieve the desired mass of carbon for measurements–typically 12-14 mg of calcite for AMS ^{14}C measurements.

A recent study by Liu *et al.* (2013) of the 8.2 ka event in Heshang HS4 indicated a sharp decrease in precipitation over Heshang Cave at that time based on $\delta^{18}O$, Mg/Ca, and annual layer thickness evidence. To investigate how abrupt changes in precipitation affect DCP, an additional 30 samples ranging from 3-7 mg were drilled from this interval at 100 µm resolution with a New Wave Research micromill and measured for ^{14}C. At this high resolution samples must be drilled as powder, but the good agreement between these powder samples and the samples drilled as wafers suggests that there was no atmospheric contamination of these samples.

Carbonate samples for ^{14}C measurements drilled as chunks were pretreated with a 30% leach by reaction with a measured volume of weak HCl to dissolve 30% of the sample mass

while samples drilled with powder were only leached 10%. All carbonate was subsequently hydrolyzed in 85% H3PO4. Samples were graphitized by iron catalyzed hydrogen reduction following standard protocols, and geologic calcite samples were used as procedural blanks. All radiocarbon measurements were made at University of California Irvine on a NEC Compact (1.5 SDH) AMS system, using six aliquots of Oxalic Acid I as the normalizing standard. Each mg-sized carbon sample was measured multiple times (typically 8-15 runs) over a 24 h period.

Due to the aforementioned disparities in terminology used in the literature to describe the offset between speleothem calcite and contemporaneous atmospheric ^{14}C, we undertake a detailed explanation of the metric we use in this paper, in hopes that perhaps a standard can be set in the literature. In this manuscript the term referred to as the DCP is simply the percentage of old ^{14}C-free "dead carbon" incorporated in the speleothem at the time of formation. The percentage is calculated via the procedure of Genty and Massault (1997):

$$DCP = \left[1 - \left(\frac{a^{14}C_{init}}{a^{14}C_{atm.init.}}\right)\right] 100\%$$

where $a^{14}C_{init}$ is the initial activity of the calcite:

$$a^{14}C_{init} = \frac{a^{14}C_{meas}}{e^{\lambda t}}$$

and the atmospheric ^{14}C activity at the time the calcite precipitated, $a^{14}C_{atm.init}$, is obtained from the ^{14}C calibration curve at the calendar age, λ is the decay constant of ^{14}C, using a 5730 a half life, t is the calendar age of the sample in years, and $a^{14}C_{mesa}$ is the ^{14}C concentration measured in the stalagmite. All a^{14}C values are in units of percent modern carbon (pMC). The error in DCP is calculated from the error in the calibration curve, the error in the stalagmite ^{14}C measurement, and the calendar chronology by:

$$\sigma_{DCP} = \left[\left(\frac{a^{14}C_{init.}}{a^{14}C_{atm.init.}} \right) \sqrt{\left(\frac{\sigma_{a^{14}C_{init.}}}{a^{14}C_{init}} \right)^2 + \left(\frac{\sigma_{a^{14}C_{atm.init.}}}{a^{14}C_{atm.init}} \right)^2} \right] 100\%$$

where the error on the initial activity of the calcite ($a^{14}C_{init}$) is:

$$\sigma_{a^{14}C_{init}} = a^{14}C_{init} \sqrt{\left(\frac{\sigma_{a^{14}C_{meas}}}{a^{14}C_{meas}} \right)^2 + (\lambda \sigma_t)^2}$$

When referring to the age offset in ^{14}C years that results from incorporation of dead carbon, we refer to the DCP "correction" or "offset", which is a simple difference between the measured speleothem ^{14}C and the contemporaneous atmospheric ^{14}C. The error is found by propagating the uncertainty in both the calibration curve and the measured value. In these calculations, because the calibration curve has 5-year resolution over the interval defined by the tree rings in practice the atmospheric ^{14}C age used is that of the nearest IntCal point.

Table 5.1: OxCal Bayesian ages.

Distance from top (cm)	Bayes max (yrs BP)	Bayes min (yrs BP)	Bayes age 1σ error (yrs BP)
228	8024	7844	7934 ± 45
229	8084	7875	7979.5 ± 52.25
230.1	8147	7909	8028 ± 59.5
231	8209	7945	8077 ± 66
232	8266	7984	8125 ± 70.5
233	8320	8025	8172.5 ± 73.75
234	8373	8066	8219.5 ± 76.75
235	8432	8117	8274.5 ± 78.75
235.9	8498	8166	8332 ± 83
236.8	8643	8245	8444 ± 99.5

U-Th ages published by Hu *et al.* (2008b) and Liu *et al.* (2013) are the basis of the calendar age model for HS4. Following the methods of Liu *et al.* (2013), the age depth model derived from the 9 U-Th dates covering the 8.2 ka event has been refined by the precise annual layer-counting floating age model for the 8.2 ka event using the OxCal Bayesian software

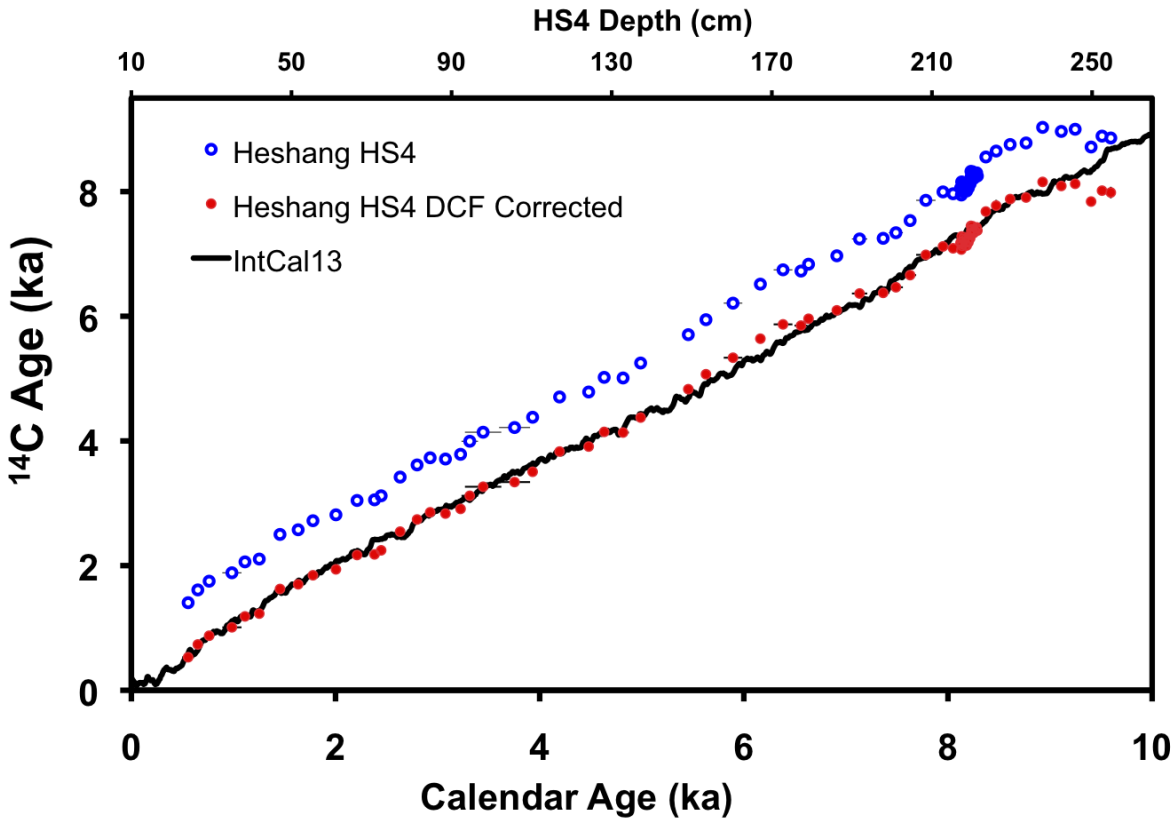

Figure 5.2: Comparison of the HS4 ^{14}C record (open blue circles) and the DCF corrected HS4 ^{14}C record (filled red circles) with IntCal13.)

(Bronk Ramsey, 2008). The OxCal analysis of the U-Th dates for the 8.2 ka event interval was repeated in this study on the 9 U-Th dates with the addition of the U-Th date from Hu *et al.* (2008b) from 238 cm depth, because of its proximity to the high-resolution U-Th dates and smaller uncertainty relative to the nine high-resolution U-Th dates from Liu *et al.* (2013). The resulting Bayesian OxCal ages are shown in Table 1. The age model for the HS4 Holocene ^{14}C record was created using the 10 Bayesian OxCal ages and the remaining 20 U-Th dates from Hu *et al.* (2008b), using the R statistical software program StalAge (Scholz and Hoffmann, 2011) which are shown in Table 2. ^{14}C results are shown in Table 2 as conventional radiocarbon ages (Stuiver and Polach, 1977). Uncertainties are shown at 1σ and include contributions from background corrections, normalization to standards, as well as counting statistics.

5.4 Results

The record spanning 0.5-9.6 ka is plotted in uncalibrated ^{14}C years with IntCal13 in Fig. 5.2. The HS4 data shows reasonably constant offset from the IntCal13 record, but exhibits some interesting non-random structure including, most prominently, a sharp decrease in ^{14}C age before 9.2 ka (250 cm stalagmite depth) that is not seen in IntCal13. This sharp decrease in DCP before 9.2 ka, occurs concurrently with an increase in Mg/Ca, δ^{18}O, δ^{13}C and ^{238}U (Fig 5.5) and is suggestive of mineralogical alteration of this lowest section of HS4 (see Section 5.5.3/Supplementary Discussion of Noronha *et al.* (2014)). Because of this anomalous shift in speleothem geochemistry, measurements below 250 cm were not included in the calculation of the average DCP for the whole Holocene record. The mean DCP and standard deviation were calculated from the difference between each HS4 ^{14}C measurement and equivalent IntCal13 points, giving a mean DCP of 10.3 $\pm$ 1.5% (DCP correction of 875 $\pm$ 130 ^{14}C years). HS4 DCP is higher than Hulu Cave H82's DCP of 5.4 $\pm$ 0.7% (Southon

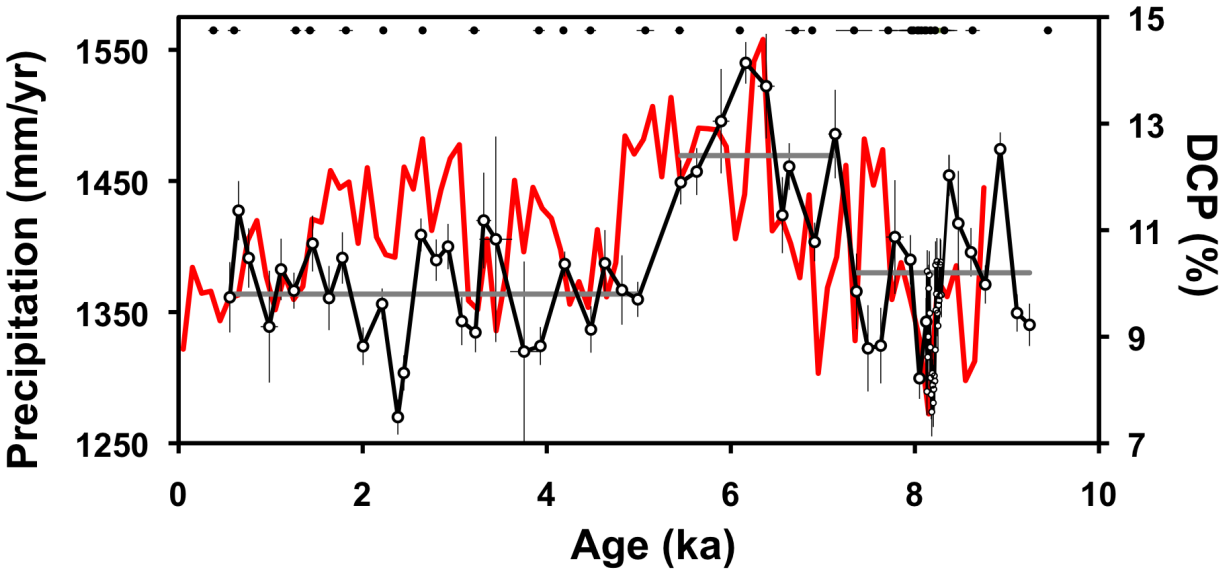

Figure 5.3: Comparison of HS4 DCP (black) and precipitation at HS4 based on the $\Delta\delta^{18}$O record from Hu *et al.* (2008b) (red). $\Delta\delta^{18}$O has been recalculated using HS4 on the StalAge model presented in this text. Grey bars show the means of the regimes identified with the sequential t-test method (Rodionov, 2004)

et al., 2012); but significantly lower and less variable than the DCP of both of the speleothem records from the Bahamas (GB-89-25-3=22.7 $\pm$ 5.9%, GB-89-24-1=16.5 $\pm$ 4.7%) (Beck *et al.*, 2001 and Hoffmann *et al.*, 2010)

To assess whether non-random variability exists in the HS4 DCP record, a runs test utilizing the Matlab "runstest" function was conducted, which rejected the null hypothesis (H_o) that the DCP variability is entirely random ($p<0.0001$). Even if the clearly anomalous data prior to 9.2 ka is excluded, Ho can be rejected at the 90% significance level ($p=0.0982$), suggesting that there is likely some non-random structure to the DCP residuals during other parts of the Holocene that may reflect minor influence of climate or other factors on speleothem DCP. To objectively identify periods of distinct DCP, a sequential t-test method (Rodionov, 2004; cut-off length = 10, α=0.05) was applied to identify statistically significant shifts between one or more DCP regimes. To avoid bias from the dense sampling around the 8.2 ka event, only the low-resolution HS4 DCP data was included in the analysis. Results show four

distinct regimes: 0.556-4.989 ka (mean DCP = 9.8%), 5.456-7.134 ka (mean DCP = 12.4%), 7.365-9.246 ka (mean DCP = 10.2%), and 9.402-9.09 ka (mean DCP = 4.0%). The 8.2 ka event is characterized by decreased DCP values, with a minimum of 7.6% but this event is not recognized by the sequential t-test method, even when the high-resolution data is included in the analysis. Furthermore, z-scores were calculated for each DCP point. During the mid-Holocene period of elevated DCP, the probability of observing the two highest values, z=2.52 and 2.28, is only 0.0058 and 0.0113 respectively, while during the 8.2 event, the probability of observing the lowest DCP value observed is 0.1170. Together, these results suggest that the elevated DCP observed during the mid-Holocene, from ∼5.5 to 7.1 ka, is unlikely to represent random chance and instead may reflect a climatically driven shift in speleothem DCP. The observed DCP decrease during the 8.2 ka event, while it may also reflect a climatically driven shift, is less clear than the mid-Holocene shift.

The rapid decrease in DCP from 10.9% to 7.5% between 2.6-2.4 ka BP lags a peak at 2.7 ka in atmospheric ^{14}C caused by the Homeric Solar Minimum, and is therefore most likely an artifact of the fact that speleothem carbon is not directly sourced from atmospheric CO_2, but from soil CO_2. As was highlighted in Fohlmeister *et al.* (2011a) because of the contribution of old SOM to soil CO_2, centennial scale events in atmospheric ^{14}C, like solar events, will be smoothed in speleothem calcite and create apparent DCP excursions which are caused by comparing a smoothed record (the speleothem) with a higher resolution record (IntCal13).

5.5 Discussion

5.5.1 Climatic influences on DCP during the mid-Holocene

Paleoclimate records indicate that the mid-Holocene was wetter and warmer in central China, suggesting that the increase in DCP seen in HS4 during the mid-Holocene was climatically

or hydrologically driven. Through comparison of the $\delta^{18}O$ record from Heshang Cave with a similar record from speleothem DA from Dongge Cave (25 °17′N, 108 °5′E, 680 m asl) (Wang *et al.*, 2005), 600 km SW and along the same moisture trajectory as Heshang Cave, Hu *et al.* (2008b) showed that annual rainfall in Southwest China was higher than modern values between 8.2 and 3.0 ka, peaking at 8% above the modern value between 6.4 and 5 ka. The period of increased rainfall between 6.4 and 5 ka represents the period of highest rainfall during the Holocene, indicating that the peak in DCP in this interval could be driven by increased precipitation and/or soil moisture (Fig. 5.3). Several modeling studies have confirmed the presence of a strengthened EASM during this interval. The Paleoclimate Modeling Intercomparison Project (PMIP) reported the results of 18 models that showed that amplification of the northern hemispheric seasonal cycle of insolation during the mid-Holocene, specifically at 6 ka, caused a northward shift in monsoon precipitation (Joussaume *et al.*, 1999). A well-dated peat core from Dajiuhu Lake located 125 km north of Heshang Cave (at 31.49 °N, 109.99 °E, 1760 m), has been studied extensively using a variety of paleoclimate proxies including pollen (Zhu *et al.*, 2006; Zhu *et al.*, 2010; Chen *et al.*, 2008; and Zhao and Chen, 2010), minerogenic matter (Zhu *et al.*, 2010), total organic carbon (Ma *et al.*, 2008), and degree of humification (Ma *et al.*, 2009). All proxies from the Dajiuhu peat core show the same general trend of gradually increasing summer monsoon strength from the Late-glacial interval to 6 ka, with interruptions at the Younger Dryas and 8.2 ka event. All proxies show the wettest, warmest, most stable values occurring between ∼4.5-7.0, with an abrupt shift to drier and colder conditions occurring ∼4.2-4.5 ka, and pollen records indicating peak monsoon strength at 6 ka (Zhu *et al.*, 2010). The good agreement between the interval of highest monsoon intensity in the Holocene as shown by the paleoclimate records and the period of increased DCP in HS4 suggests a relationship between rainfall amount and DCP.

The change in DCP due to changing rainfall amount could be caused by accelerating SOM decomposition rates, and therefore increasing mean age of soil gas CO_2, and/or changing

open/closed system dissolution. The mean DCP correction during the mid-Holocene period of increased DCP is 1065 years, while the mean DCP corrections during the early-Holocene and late-Holocene are 845 years and 830 years respectively. If the mid-Holocene increase in DCP was entirely due to increasing decomposition rate of old SOM, and therefore increasing soil CO_2 age, the mean age of soil CO_2 would have had to increase by $\sim$220 years for a period of 1.6 ka during the mid-Holocene. If we make the assumption that SOM was at steady state during the early-Holocene, and no longer at equilibrium during the mid-Holocene when decomposition of the old SOM pools was greatly accelerated causing the mean age of soil CO_2 to increase by 220 years, we can do a simple mass balance calculation to estimate if it is possible for the mid-Holocene increase in DCP to be caused predominately by an increase in the mean age of soil CO_2.

SOM in tropical sites that have been studied using ^{14}C, which may not be analogous to SOM in karst sites, show that $\sim$20% of the SOM has a turnover time of $<$10 years, 60% has a turnover time on the order of decades, and 20% has a turnover time of $>$6000 (Trumbore, 2000). For simplicity, in our mass balance calculations we consider only two SOM pools, an annual pool, and a millennial pool, and assume that the mass of the contribution from the annual pool stays constant between the steady state and the accelerated decomposition modes. Decomposition of a millennial pool with a mean age of $>$5000 years would initially have to be occurring roughly 650 times faster than at steady state if the pool accounted for 25% of the SOM, and 215 times faster if the pool accounted for 50% of the SOM to achieve the 220 year increase in mean age of soil CO_2, and either case would result in the complete consumption of the millennial pool on a timescale on the order of decades - much less than necessary to explain the 1.6 ka long period of increased DCP seen in HS4 at the mid-Holocene.

Moreover, barring a major disturbance event like tilling or fire, which would have effects that are much shorter in duration than the mid-Holocene period of DCP increase, the de-

composition rates of old SOM required for increasing soil CO_2 age to be the primary cause of the increase in DCP seen at the mid-Holocene in HS4 are difficult to explain physically. The Q10 of SOM decomposition, the increase in reaction rates given a 10 °C increase in temperature, is generally thought to be about 2 (Davidson and Janssens, 2006), ruling out warming as the cause of the increase in SOM decomposition rates necessary to increase the mean age of soil CO_2 by 220 years. The increase in precipitation known to have occurred during the mid-Holocene at Heshang Cave would be expected to cause a decrease in SOM decomposition because increased soil moisture would limit oxygen diffusion in the soil, shifting decomposition towards a more anaerobic mode which is a slower process (Davidson and Janssens, 2006). Additionally, observations of soil $^{14}CO_2$ show that soil CO_2 has a mean age of ∼1 year in tropical sites, ∼3 years in temperate sites, and ∼16 years in boreal sites (Trumbore, 2000), suggesting that soil CO_2 mean ages on the order of hundreds of years are unlikely in a sub-tropical site like Heshang Cave.

There has been some effort to understand how changing SOM decomposition affects speleothem DCP (e.g. Genty and Massault, 1999; Fohlmeister *et al.*, 2010, 2011a, 2011b, Griffiths *et al.*, 2012; Rudzka *et al.*, 2011; and Rudzka-Phillips *et al.*, 2013) most often using a simple three-box soil carbon model and the shape of the atmospheric ^{14}C bomb peak in modern speleothems to estimate the relative size and turnover times of three SOM pools. The models employed in these studies require that the soil CO_2 equilibrating with the soil water DIC have mean ages ranging from ∼40 to 500 years during the twentieth century (Rudzka-Phillips *et al.*, 2013), which appears to be at odds with the observations of soil CO_2. This discrepancy between the age distribution of soil carbon incorporated in DIC required by the shape of the bomb peak observed in speleothems, and the observations of soil CO_2 ages is a critical point in our understanding of the role of dead carbon incorporation in speleothems. The discrepancy suggests that it is very likely that processes in soils above karsts are unlike those in sites where soil CO_2 age has been studied to date, therefore limiting our ability to interpret the role of changing age of soil $^{14}CO_2$ on DCP in speleothems.

Given observations of the mean age of soil CO_2 observed in tropical sites (Trumbore, 2000), we tend to favor the explanation that changes in the offset between speleothem calcite and contemporaneous atmospheric ^{14}C of centennial magnitude in observed in the mid-Holocene in HS4 were driven by an increasing proportion of the dripwater DIC derived from the bedrock - that is a more closed system dissolution regime. A similar relationship between rainfall amount and DCP as is observed in HS4 was observed in a record based on an Indonesian speleothem, LR06-B1 from Liang Luar Cave (8 °32′N, 120 °26′W) (Griffiths *et al.*, 2012). Griffiths *et al.* (2012) hypothesized that increased precipitation at the cave site would increase saturation of the voids in the soil zone, thereby limiting exchange between soil gas and soil moisture. Lower CO_2 diffusion in the soil zone due to soil saturation would shift dissolution to a more closed system, increasing speleothem DCP by increasing the relative proportion of carbon sourced from the radiocarbon-free limestone host rock. Conversely, periods of decreased rainfall should lead to lower DCP as soil would be less saturated, allowing for more CO_2 diffusion, and would lead to more open system dissolution. The increased DCP observed in HS4 during the mid-Holocene (∼5.5-7.1 ka) is consistent with this mechanism and indicates that increases in precipitation may in fact lead to more closed system dissolution and a higher DCP.

5.5.2 Climatic influences on DCP during the 8.2 ka event

Hu *et al.* (2008b) showed that the most pronounced dry event at Heshang Cave occurred at 8.2 ka, when rainfall was ∼7% lower than present. This interval was identified by Liu *et al.* (2013) as having synchronous onset and similar duration to the 8.2 ka event seen in the Greenland ice core record. HS4 $\delta^{18}O$, Mg/Ca, and layer thickness data demonstrate that the 8.2 ka event at Heshang Cave was characterized by an abrupt decrease in precipitation that lasted for 150 years. To investigate the effect of abrupt precipitation decreases on DCP, the 8.2 ka interval was sampled for ^{14}C at high resolution. These high-resolution

^{14}C measurements show a rapid decrease in DCP to a minimum of 7.6% (Fig. 5.4), but the interval is not significantly different than the proceeding early Holocene DCP values as demonstrated by a sequential t-test method (Rodionov, 2004). If the relationship between rainfall amount and DCP described by Griffiths *et al.* (2012) controls DCP in HS4, we might expect a more pronounced drop in DCP at the 8.2 ka event. Under this mechanism, decreases in DCP during periods of lower rainfall are driven by more open system dissolution because of increased exchange between soil CO_2 and DIC in soil moisture relative to the exchange that would occur in a saturated soil zone. A possible explanation of the muted DCP response to the 8.2 ka dry event at Heshang Cave is that the relationship between closed-vs-open system dissolution and rainfall amount may be non-linear. A completely closed system dissolution regime would result in DCP of 50%, indicating that even during the mid-Holocene when DCP reached a high of 14.1%, carbonate dissolution took place in a largely open system. There is likely a limit to how much the lack of saturation of voids in the soil zone increases exchange between soil CO_2 and soil moisture, i.e. once soil reaches a specific level of dryness, the degree of open-system dissolution will be less sensitive to further decreases in soil moisture. Moreover, even in a completely open system, where all speleothem carbon is derived from soil CO_2, there will be some contribution of ^{14}C-depleted carbon from aged SOM, putting a lower limit on speleothem DCP. The lack of a significant decrease in DCP in HS4 at the 8.2 ka event suggests that DCP in speleothems formed in relatively open system regimes, i.e. speleothems with low average DCP, may be less affected by dry events than by wet events.

Consistent with this hypothesis, DCP is remarkably stable in Hulu Cave speleothem H82 throughout the Younger Dryas (YD) climate event, which was likely a period of reduced EASM intensity (Wang *et al.*, 2001 and Yancheva *et al.*, 2007). The Bahamas speleothem GB-89-24-1 is also stable over the Younger Dryas interval, though GB-89-25-3, which has a much higher average DCP, shows large fluctuations in DCP at the YD suggesting that climate did have an effect on DCP in some speleothems in the region during the YD interval. Rudzka *et al.* (2011) produced records of DCP over the YD interval in three stalagmites: So-1 from

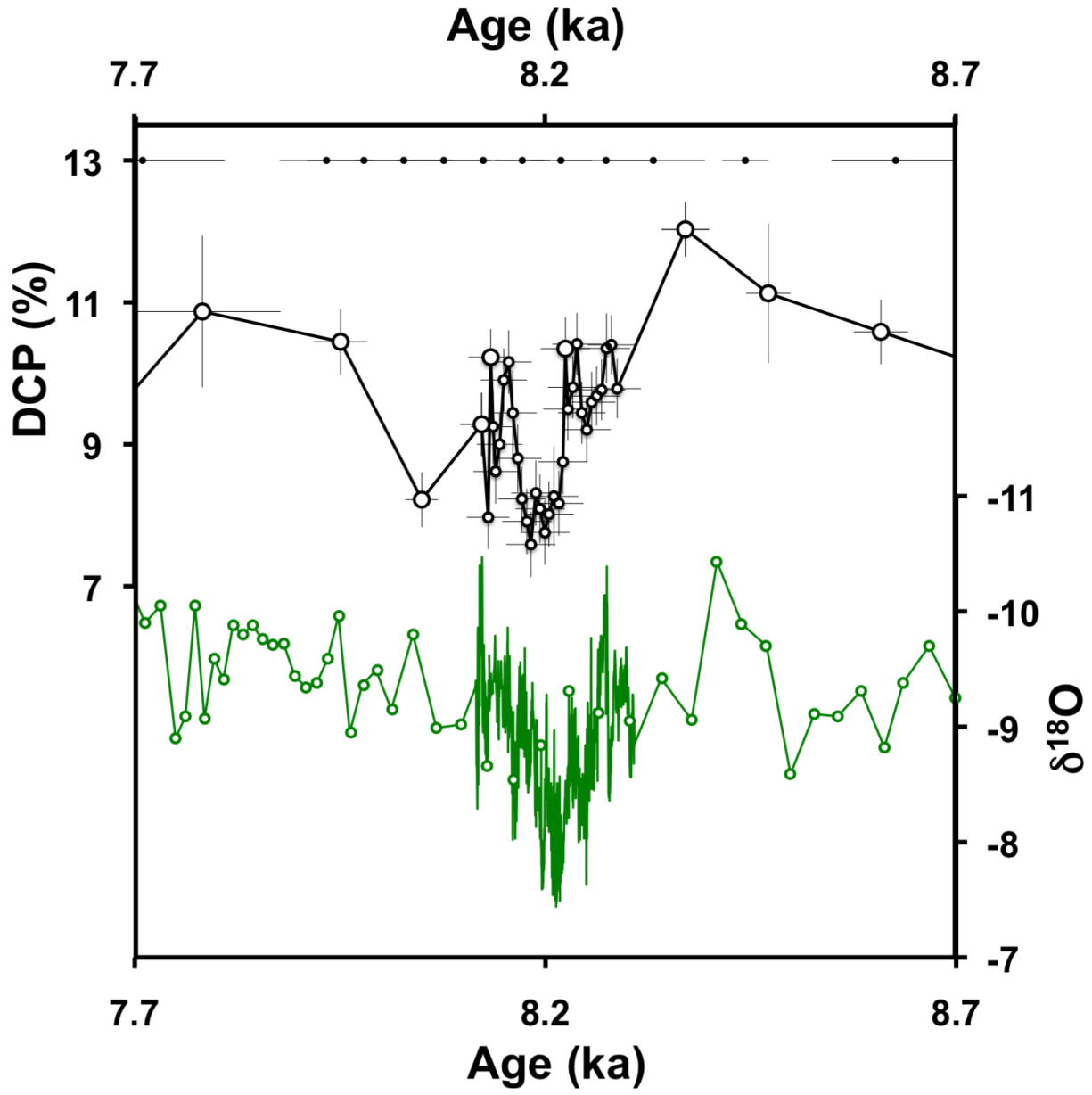

Figure 5.4: Plot of DCP and δ^{18}O in the interval defined by the 8.2 ka event. Top panel shows high-resolution measurements of DCP at 8.2 ka event as small open circles and lower resolution measurements as larger open circles. Bottom panel shows high-resolution δ^{18}O measurements covering the 8.2 ka event (Liu *et al.*, 2013) without markers and lower resolution δ^{18}O measurements in the interval (Hu *et al.*, 2008b) shown with open circles. Both δ^{18}O records are plotted on the StalAge age model presented in this manuscript. U-Th ages defining this interval, including the 10 Bayesian OxCal corrected ages,are shown at the top of the figure.

Sofular Cave in northwestern Turkey (41 °25′N, 31 °56′E), stalagmite Candela from El Pindal Cave in northern Spain (43 °23′N, 4 °30′W), and stalagmite GAR-01 from La Garma Cave in northern Spain (43 °24′N, 3 °39′W) which also show muted responses to the YD in DCP. There is a decrease of $3.24 \pm 2.27\%$ (1σ) in DCP in the Turkish speleothem, So-1, between the two measurements bracketing the Blling-Allerd/YD transition (from $9.58 \pm 1.87\%$ at 13.1 ka to $6.34 \pm 1.29\%$ at 12.8 ka), but DCP rebounds to pre-YD values by the next measurement at 12.4 ka. The two speleothems from Northern Spain, Candela and GAR-01, are separated by only 70 km but display very different responses to the YD climate event. Candela shows a largely stable DCP over the YD interval, with some indication of a slight increasing trend in DCP. GAR-01 shows a decrease in DCP of $4.43 \pm 1.77\%$ (pre-YD maximum of $6.13 \pm 1.15\%$ to a mean of $1.7 \pm 1.72\%$) at the onset of the YD, but DCP rebounds to $5.42 \pm 0.92\%$ at 12.2 ka and drops back to a mean of $1.93 \pm 1.34\%$ for the remainder of the YD interval. Given the high uncertainty, low resolution, and lack of knowledge of what the range of variability is in DCP in GAR-01 over stable climate intervals, it is difficult to assess whether the decreases in GAR-01 are significant. We interpret HS4, H82, GB-89-24-1, So-1 and Candela as speleothems with low average DCP without pronounced drops in DCP during dry events, lending support to the hypothesis that DCP in some speleothems with low DCP may be somewhat less sensitive to decreases in rainfall amount. However, many of these records are limited in duration and do not span periods of precipitation increase so it is difficult to discern with certainty whether this asymmetric response of DCP to rainfall amount observed in Heshang Cave exists in other speleothems, and more speleothem records covering both stable climate intervals and abrupt climate transitions need to be investigated to verify this hypothesis.

5.5.3 Mineralogically-driven shifts in DCP

The dramatic shift to lower DCP values before 9.2 ka, or ∼250 cm stalagmite depth, occurs simultaneously with rapid changes in other geochemical parameters including $\delta^{18}O$, $\delta^{13}C$, Mg/Ca and ^{238}U concentration (Fig 5.5). Below ∼250 cm, $\delta^{18}O$, $\delta^{13}C$, and Mg/Ca values reach a maximum of −8.01‰, −3.65‰, and 0.037 compared to average of the proceeding stable ∼1ka interval preceding the 8.2ka event of −9.40‰, −9.44‰, and 0.029 respectively. ^{238}U concentration below 250 cm is 3.79 ppm compared to the average of 0.50 ppm of the rest of the stalagmite. The fact that all of these large and rapid changes in speleothem geochemistry, occur concurrently during an interval which is not known to represent an abrupt climate change, and that these changes are confined to the base of the stalagmite suggests that this portion of the sample may have originally been deposited as aragonite. To test this, material from the three samples that yielded low DCP was collected and checked via XRD to determine the polymorph. XRD results confirmed that the sample from 255.4 cm, the oldest sample measured for ^{14}C, is 98% aragonite, though the samples from 252.35 and 254.05 cm, which also yielded low DCP, are both primarily calcite, though trace element, stable isotope, and thin section analysis suggests that these sections may have also been originally deposited as aragonite and subsequently recrystallized. The low DCP during this time may therefore reflect a primary signal unique to aragonite speleothems, that could also be climatically linked, or could simply be an artifact caused by post-depositional alteration.

Aragonite speleothems have been found in cave environments with source waters with high Mg/Ca concentrations (Frisia *et al.*, 2002), as Mg^{2+} is a strong inhibitor of calcite nucleation and growth (Bischoff and Fyfe, 1968 and Burton and Walter, 1987). Heshang Cave is located in a dolomite ($CaMg(CO_3)_2$) host rock, providing a major source for higher Mg^{2+} concentrations in drip water. Frisia *et al.* (2002), however, observe that aragonite does not always form from very high Mg/Ca ratio waters and hypothesizes that low drip rate, which can lead to increases in super-saturation through prolonged degassing, may be a controlling factor in

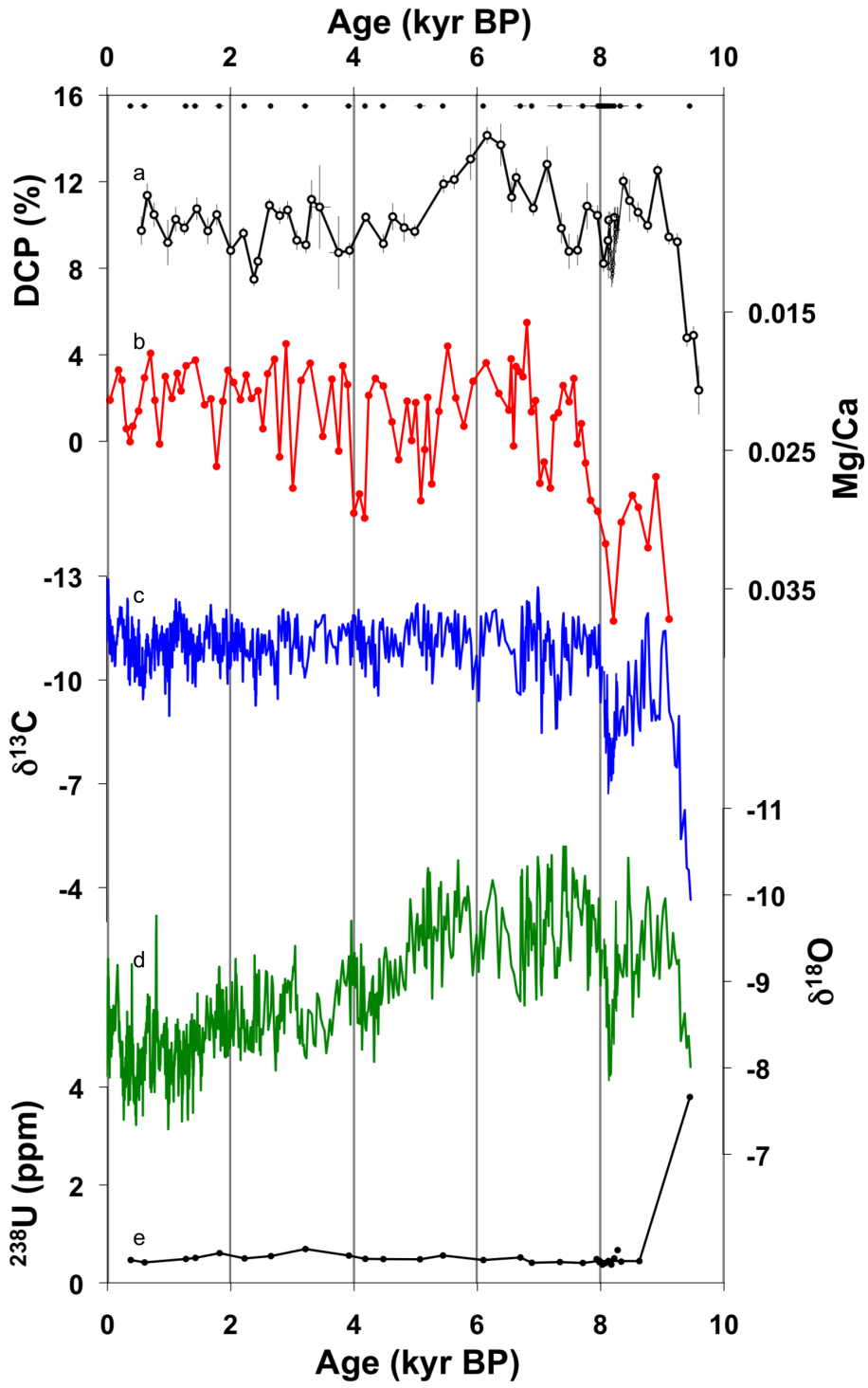

Figure 5.5: Comparison of (a) HS4 DCP, (b) Mg/Ca concentration (g/g), (c) δ^{13}C (‰V-PDB), (d) δ^{18}O (‰V-PDB), and (e) ^{238}U concentration (ppm). U-Th dates with 2σ error bars are shown at the top of the figure. All data sets are plotted using the StalAge age model presented in this text.

aragonite precipitation. Exceptionally low drip rates during the period of initial formation of HS4, perhaps due to incomplete development of fractures feeding the stalagmite drip, could potentially explain the very low DCP seen in this interval if the drip rate was low enough to allow for exchange between cave drip water and cave air CO_2, though recent modeling studies suggest that this would require drip intervals on the order of 1000s of seconds (Scholz *et al.*, 2009 and Deininger *et al.*, 2012). Furthermore, this would be expected to lead to decreased speleothem growth rates which are not observed in this section of HS4. Nevertheless, recent cave studies have suggested that CO_2 exchange between cave atmosphere and speleothem solution films does likely influence the carbon isotope composition of speleothem calcite in some cases (Frisia *et al.*, 2011 and Tremaine *et al.*, 2011), but clearly more work is needed to assess the importance of this mechanism. One alternative possibility is that in the initial stages of HS4 deposition, water was able to pool on the speleothem surface during all or part of the year. In this case, speleothem source water and/or water driving recrystallization would have had sufficient time to exchange with the contemporaneous cave air, shifting $\Delta^{14}C$ of the DIC towards the contemporaneous modern atmosphere $\Delta^{14}CO_2$ values and leading to anomalously low apparent DCP values. Finally, we cannot rule out the possibility that the DCP shift does reflect a true climate-related shift towards an open-system dissolution regime in response to decreased rainfall which would have coincided with increased prior calcite precipitation, increased dripwater Mg/Ca, and, hence, aragonite precipitation.

The result that two of the samples with anomalous geochemistry are calcite is unsurprising, because aragonite is not stable at Earth surface temperatures and pressures and is often diagenetically replaced with or overgrown by calcite, which can inherit textural and chemical properties from the precursor aragonite (Frisia *et al.*, 2002). Diagenetic replacement of aragonite by calcite could be driven by condensation or pooling of cave moisture on the speleothem surface - a process that could also contribute to the decreased DCP seen in this portion of HS4 if the water was in isotopic equilibrium with cave atmosphere CO_2. There is only one U-Th measurement in this interval, at 253 cm, but it does not display any

age reversal, which suggests that diagenetic replacement of aragonite occurred soon after deposition. We examined thin sections of this part of HS4 for evidence of relict aragonite or other signs of aragonite to calcite transformation. The speleothem fabric is suggestive of aragonite and fossil aragonite that has been transformed to calcite, with a mixture of acicular crystals, some with square terminations, consistent with aragonite, and a mosaic fabric with some fibrous precursor phase that has been replaced by equant crystals and calcite rhombs. While it is possible that the very low DCP signal in this section of HS4 does reflect very dry conditions at Heshang Cave at this time, this signal could also reflect enhanced equilibration between cave air and speleothem source waters and/or introduction of contemporaneous atmosphere ^{14}C through post-depositional alteration processes. Because of the complex diagenetic history in this section of HS4, and the lack of additional evidence for very dry conditions at this time, we do not utilize this portion of HS4 to interpret climate or atmospheric ^{14}C history at this time. A speleothem composed of intact aragonite would theoretically be suitable for paleoclimate or ^{14}C reconstructions, but in situations where diagenetic replacement has taken place, both the U-Th age, ^{14}C age, and isotopic compositions are likely to be altered, causing changes in the calendar chronology and proxy concentrations.

5.6 Conclusions

This new high-resolution record of ^{14}C from speleothem HS4 from Heshang Cave, China, contributes to the developing understanding of the controls on variability of dead carbon incorporation in speleothems, which is critically important to our ability to use speleothems as records of atmospheric ^{14}C. This record shows evidence of climatically controlled variation in DCP, with an increase in DCP during the warmer and wetter mid-Holocene interval, and a smaller shift towards lower DCP during the 8.2 ka dry event. We suggest that the

increase in precipitation during the mid-Holocene caused increased soil moisture, which limited diffusion of soil CO_2 and equilibration between soil moisture and soil CO_2, therefore shifting carbonate dissolution towards a more closed system regime and increasing DCP. The lower amplitude change in DCP during the very dry 8.2 ka event suggests that there may be an asymmetric response of speleothem DCP to rainfall amount. Development of other speleothem ^{14}C records that span both wet and dry events is necessary to confirm this mechanism, and continue to develop understanding of the controls on variability in dead carbon incorporation in speleothems.

5.7 Acknowledgements

We would like to thank Yuhui Liu and Gideon Henderson for information regarding the 8.2 ka event in HS4, Silvia Frisia for assistance with thin section interpretation, and David Richards, and two anonymous reviewers for their suggestions that greatly improved this manuscript. This research was supported by NSFAGS-0903101 to KRJ, an NSF EAPSI grant number 1107922 to ALN, and NSFC41072262 to HCY.

Table 5.2: StalAge age model and radiocarbon measurements.

UCI AMS #	Distance from top (cm)	StalAge model (Yrs BP)	StalAge 1σ Error	Fraction Modern	$\Delta^{14}C$ (‰)	^{14}C age (Yrs BP)	^{14}C Age DCF corrected (Yrs BP)	DCP (%)
93902	24.65	556	58	0.8394 ± 0.0012	−102.2 ± 1.2	1405 ± 15	530 ± 131	9.74 ± 0.66
77412	28.5	651	49	0.8182 ± 0.0011	−114.8 ± 1.1	1610 ± 15	735 ± 131	11.37 ± 0.56
93903	33	762	47	0.8043 ± 0.0016	−118.1 ± 1.6	1750 ± 20	875 ± 132	10.48 ± 0.56
77413	43	985	94	0.7908 ± 0.0012	−109.2 ± 1.2	1885 ± 15	1010 ± 131	9.19 ± 1.05
93904	48.25	1113	50	0.7740 ± 0.0011	−114.4 ± 1.1	2060 ± 15	1185 ± 131	10.26 ± 0.58
77414	52.85	1253	25	0.7696 ± 0.0011	−104.5 ± 1.1	2105 ± 15	1230 ± 131	9.86 ± 0.34
77415	59	1456	45	0.7324 ± 0.0011	−126.5 ± 1.1	2500 ± 15	1625 ± 131	10.75 ± 0.52
93905	63.25	1634	48	0.7258 ± 0.0019	−115.5 ± 1.9	2575 ± 25	1700 ± 132	9.73 ± 0.60
77416	67	1779	39	0.7127 ± 0.0012	−116.2 ± 1.2	2720 ± 15	1845 ± 131	10.48 ± 0.48
77417	73	2004	27	0.7046 ± 0.0010	−102.2 ± 1.0	2815 ± 15	1940 ± 131	8.82 ± 0.35
77418	78.6	2211	17	0.6844 ± 0.0010	−105.8 ± 1.0	3045 ± 15	2170 ± 131	9.61 ± 0.29
93906	83.4	2382	23	0.6836 ± 0.0009	−88.1 ± 0.9	3055 ± 15	2180 ± 131	7.49 ± 0.33
77421	85.25	2447	24	0.6781 ± 0.0010	−88.3 ± 1.0	3120 ± 15	2245 ± 131	8.32 ± 0.33
77422	90.6	2633	21	0.6532 ± 0.0011	−101.7 ± 1.1	3420 ± 15	2545 ± 131	10.91 ± 0.31
93907	95.45	2799	31	0.6375 ± 0.0009	−105.7 ± 0.9	3615 ± 15	2740 ± 131	10.44 ± 0.39

77423	99.9	2927	35	0.6287 ± 0.0009	−104.3 ± 0.9	3730 ± 15	2855 ± 131	10.69 ± 0.43
93908	104.5	3077	23	0.6300 ± 0.0023	−85.9 ± 2.3	3710 ± 30	2835 ± 133	9.29 ± 0.45
77424	109	3225	27	0.6242 ± 0.0010	−78.0 ± 1.0	3785 ± 15	2910 ± 131	9.08 ± 0.37
93909	111.7	3315	81	0.6081 ± 0.0010	−92.0 ± 1.0	3995 ± 15	3120 ± 131	11.18 ± 0.90
77425	115	3446	178	0.5973 ± 0.0009	−93.8 ± 0.9	4140 ± 15	3265 ± 131	10.83 ± 1.93
93910	118.35	3754	152	0.5917 ± 0.0009	−68.2 ± 0.9	4215 ± 15	3340 ± 131	8.72 ± 1.69
77426	121.7	3931	26	0.5798 ± 0.0009	−67.2 ± 0.9	4380 ± 15	3505 ± 131	8.83 ± 0.36
77427	131.5	4195	11	0.5568 ± 0.0010	−75.1 ± 1.0	4705 ± 15	3830 ± 131	10.36 ± 0.23
77428	141.75	4480	34	0.5513 ± 0.0011	−52.1 ± 1.1	4785 ± 20	3910 ± 132	9.14 ± 0.44
93913	145.85	4632	54	0.5353 ± 0.0009	−62.5 ± 0.9	5020 ± 15	4145 ± 131	10.38 ± 0.62
93914	149.8	4817	57	0.5361 ± 0.0008	−39.9 ± 0.8	5010 ± 15	4135 ± 131	9.88 ± 0.65
77429	154	4989	23	0.5201 ± 0.0009	−49.0 ± 0.9	5250 ± 15	4375 ± 131	9.70 ± 0.33
77430	166	5456	29	0.4915 ± 0.0014	−49.1 ± 1.4	5705 ± 25	4830 ± 132	11.90 ± 0.41
93915	169.1	5629	37	0.4772 ± 0.0008	−57.2 ± 0.8	5945 ± 15	5070 ± 131	12.10 ± 0.44
93916	172.8	5894	91	0.4616 ± 0.0008	−58.2 ± 0.8	6210 ± 15	5335 ± 131	13.05 ± 0.98
77433	176.7	6162	31	0.4443 ± 0.0008	−63.7 ± 0.8	6515 ± 15	5640 ± 131	14.14 ± 0.39
93917	179	6384	92	0.4318 ± 0.0007	−65.3 ± 0.7	6745 ± 15	5870 ± 131	13.70 ± 0.98
93918	181.15	6560	63	0.4329 ± 0.0007	−42.7 ± 0.7	6725 ± 15	5850 ± 131	11.28 ± 0.71
77434	183.6	6634	36	0.4270 ± 0.0008	−47.3 ± 0.8	6835 ± 15	5960 ± 131	12.19 ± 0.44
77464	193.25	6911	23	0.4198 ± 0.0010	−31.4 ± 1.0	6970 ± 20	6095 ± 132	10.78 ± 0.36
77470	200.5	7134	75	0.4062 ± 0.0010	−37.4 ± 1.0	7240 ± 20	6365 ± 132	12.80 ± 0.83
77435	208.1	7365	61	0.4055 ± 0.0007	−11.8 ± 0.7	7250 ± 15	6375 ± 131	9.85 ± 0.71
77471	212.2	7490	68	0.4011 ± 0.0010	−7.6 ± 1.0	7340 ± 25	6465 ± 132	8.78 ± 0.81
77465	216.7	7629	59	0.3914 ± 0.0009	−15.1 ± 0.9	7535 ± 20	6660 ± 132	8.83 ± 0.71
77472	222	7783	95	0.3760 ± 0.0010	−36.0 ± 1.0	7860 ± 25	6985 ± 132	10.87 ± 1.07
77466	228	7951	33	0.3696 ± 0.0009	−33.0 ± 0.9	7995 ± 25	7120 ± 132	10.45 ± 0.46
93919	230.6	8050	20	0.3709 ± 0.0006	−17.9 ± 0.6	7965 ± 15	7090 ± 131	8.22 ± 0.39
94750	232.05	8123	26	0.3668 ± 0.0012	−20.1 ± 1.2	8055 ± 30	7180 ± 133	9.28 ± 0.45
94751	232.2	8131	26	0.3719 ± 0.0016	−5.5 ± 1.6	7945 ± 35	7070 ± 135	7.97 ± 0.45
93920	232.25	8134	27	0.3624 ± 0.0008	−30.5 ± 0.8	8155 ± 20	7280 ± 132	10.23 ± 0.40
94752	232.3	8137	27	0.3663 ± 0.0012	−19.9 ± 1.2	8070 ± 30	7195 ± 133	9.25 ± 0.53
94753	232.35	8140	27	0.3692 ± 0.0009	−11.9 ± 0.9	8005 ± 20	7130 ± 132	8.62 ± 0.45
94754	232.45	8145	28	0.3680 ± 0.0009	−14.3 ± 0.9	8030 ± 20	7155 ± 132	9.00 ± 0.45
94755	232.55	8150	28	0.3642 ± 0.0016	−23.7 ± 1.6	8115 ± 35	7240 ± 135	9.91 ± 0.45
94756	232.65	8156	28	0.3627 ± 0.0015	−27.2 ± 1.5	8145 ± 35	7270 ± 135	10.16 ± 0.45
94757	232.75	8161	29	0.3651 ± 0.0009	−20.2 ± 0.9	8095 ± 20	7220 ± 132	9.44 ± 0.60
94758	232.85	8167	29	0.3669 ± 0.0009	−14.6 ± 0.9	8055 ± 20	7180 ± 132	8.80 ± 0.48
94759	232.95	8172	29	0.3686 ± 0.0009	−9.4 ± 0.9	8015 ± 25	7140 ± 132	8.23 ± 0.45
94760	233.05	8178	30	0.3684 ± 0.0008	−9.3 ± 0.8	8020 ± 20	7145 ± 132	7.91 ± 0.46
94761	233.15	8183	30	0.3689 ± 0.0008	−7.4 ± 0.8	8010 ± 20	7135 ± 132	7.59 ± 0.46
94762	233.25	8189	30	0.3654 ± 0.0008	−16.2 ± 0.8	8090 ± 20	7215 ± 132	8.31 ± 0.46
94763	233.35	8194	30	0.3659 ± 0.0009	−14.2 ± 0.9	8075 ± 25	7200 ± 132	8.09 ± 0.48
94750	233.45	8200	30	0.3667 ± 0.0008	−11.3 ± 0.8	8060 ± 20	7185 ± 132	7.76 ± 0.45
94751	233.55	8205	30	0.3652 ± 0.0012	−14.6 ± 1.2	8090 ± 30	7215 ± 133	8.01 ± 0.46
94752	233.65	8211	30	0.3638 ± 0.0009	−17.8 ± 0.9	8125 ± 20	7250 ± 132	8.27 ± 0.70
94753	233.75	8217	30	0.3638 ± 0.0016	−17.1 ± 1.6	8125 ± 40	7250 ± 136	8.17 ± 0.46
94754	233.85	8222	30	0.3613 ± 0.0009	−23.3 ± 0.9	8180 ± 20	7305 ± 132	8.75 ± 0.46
77473	233.9	8225	30	0.3548 ± 0.0009	−40.3 ± 0.9	8325 ± 20	7450 ± 132	10.35 ± 0.44
94764	233.95	8228	30	0.3584 ± 0.0009	−30.5 ± 0.9	8245 ± 25	7370 ± 132	9.50 ± 0.45
94765	234.05	8234	30	0.3572 ± 0.0008	−33.0 ± 0.8	8270 ± 20	7395 ± 132	9.80 ± 0.44
94766	234.15	8239	30	0.3549 ± 0.0008	−38.5 ± 0.8	8320 ± 20	7445 ± 132	10.41 ± 0.44
94767	234.25	8245	29	0.3590 ± 0.0008	−26.8 ± 0.8	8230 ± 20	7355 ± 132	9.44 ± 0.44
94768	234.35	8251	29	0.3598 ± 0.0008	−23.8 ± 0.8	8210 ± 20	7335 ± 132	9.21 ± 0.45
94769	234.45	8257	29	0.3581 ± 0.0009	−27.8 ± 0.9	8250 ± 20	7375 ± 132	9.59 ± 0.43

94770	234.55	8263	29	0.3589 ± 0.0009	−24.9 ± 0.9	8230 ± 20	7355 ± 132	9.68 ± 0.42
94771	234.65	8269	29	0.3588 ± 0.0010	−24.3 ± 1.0	8235 ± 25	7360 ± 132	9.77 ± 0.43
94772	234.75	8275	29	0.3565 ± 0.0009	−30.1 ± 0.9	8285 ± 20	7410 ± 132	10.35 ± 0.49
94773	234.85	8281	29	0.3559 ± 0.0009	−30.9 ± 0.9	8300 ± 20	7425 ± 132	10.40 ± 0.42
94774	234.95	8288	29	0.3582 ± 0.0012	−23.9 ± 1.2	8250 ± 30	7375 ± 133	9.78 ± 0.42
94775	236.2	8371	29	0.3448 ± 0.0006	−50.8 ± 0.6	8555 ± 15	7680 ± 131	12.03 ± 0.38
94776	237.7	8472	27	0.3406 ± 0.0035	−50.9 ± 3.5	8650 ± 90	7775 ± 158	11.13 ± 0.98
94777	239.85	8609	33	0.3363 ± 0.0008	−47.1 ± 0.8	8755 ± 20	7880 ± 132	10.59 ± 0.46
94778	242.3	8765	25	0.3353 ± 0.0006	−31.9 ± 0.6	8780 ± 15	7905 ± 131	9.98 ± 0.36
94779	244.85	8927	16	0.3249 ± 0.0007	−43.5 ± 0.7	9030 ± 20	8155 ± 132	12.52 ± 0.32
77468	247.75	9110	18	0.3276 ± 0.0008	−13.7 ± 0.8	8965 ± 20	8090 ± 132	9.45 ± 0.35
93926	249.9	9246	21	0.3261 ± 0.0006	−2.1 ± 0.6	9000 ± 20	8125 ± 132	9.22 ± 0.40
93927	252.35	9402	23	0.3379 ± 0.0008	53.8 ± 0.8	8715 ± 20	7840 ± 132	4.78 ± 0.41
77469	254.05	9509	26	0.3307 ± 0.0008	44.7 ± 0.8	8890 ± 25	8015 ± 132	4.89 ± 0.43
93928	255.4	9595	28	0.3318 ± 0.0036	58.9 ± 3.6	8860 ± 90	7985 ± 158	2.36 ± 1.13

Chapter 6

Speleothem ^{14}C bomb peak evidence for subterranean microbial production of CO_2 as the dominant source of speleothem carbon

6.1 Introduction

Reconstructing the history of atmospheric radiocarbon (^{14}C) concentrations through the detection limit of ^{14}C has been a long-term goal of the scientific community, because of the usefulness of ^{14}C for creating calendar chronologies and as a tracer of carbon through the reservoirs of the carbon cycle. Speleothems have recently become important sources of records of atmospheric ^{14}C, and speleothem-based ^{14}C records from Hulu Cave, China (Southon *et al.*, 2012) and a submerged cave in the Bahamas (Beck *et al.*, 2001 and Hoffmann *et al.*, 2010) were incorporated in the latest version of the official ^{14}C calibration curve,

IntCal13. These records provide valuable constraints on atmospheric ^{14}C in the intervals of the calibration curve where true atmospheric records are lacking, holding two key advantages over the marine and terrestrial sediment records and corals that define the interval beyond the robust dendrochronologically dated master tree ring records:

1. They can be precisely and absolutely dated using U-Th methods (Richards and Dorale, 2003), resulting in a robust calendar chronology.

2. They often have very fast growth rates, highly resolvable stratigraphy, and excellent preservation, which allows for continuous high-resolution ^{14}C measurement over the entire ^{14}C dating range.

Speleothems are, however, complicated as records of atmospheric ^{14}C because speleothem carbon is not derived directly from atmospheric CO_2. Speleothem carbon is derived from several organic and inorganic carbon sources, some of which are older than the contemporaneous atmosphere, creating an offset between speleothem carbonate ^{14}C and contemporaneous atmosphere ^{14}C that is referred to as the dead carbon fraction (DCF) or dead carbon proportion (DCP). This offset is similar in nature to the marine reservoir correction applied to marine sediment records of atmospheric ^{14}C, but to date is not as well understood nor constrained.

The most simple model of carbon incorporation in speleothems was described by Hendy (1971), who considered two end member scenarios under which carbon incorporation in dissolved inorganic carbon (DIC) of waters that will ultimately feed speleothem drip water can occur: open and closed-system dissolution. In open-system dissolution, the solution dissolving the carbonate bedrock is continually in contact with soil CO_2, which leads to speleothem ^{14}C activities identical to the soil $^{14}CO_2$ activities, as isotopic equilibrium with soil carbon and the DIC pool is maintained during dissolution. In a closed-system, dissolution of the bedrock takes place in isolation from soil CO_2, leading to speleothem ^{14}C activities

shifted towards a bedrock ^{14}C activities. Therefore, completely open-system dissolution, where soil $^{14}CO_2$ activities are identical to atmospheric values would lead to an apparent DCP = 0%, whereas a completely closed-system dissolution wherein one mole of carbonate is required to neutralize one mole of dissolved CO_2 would lead to a theoretical DCP = 50%. However, soil gas $^{14}CO_2$ is rarely equal to atmospheric $^{14}CO_2$, because soil CO_2 is a mixture of atmospheric CO_2, root respiration, and CO_2 from decomposition of aged soil organic matter (SOM), leading to the potential for a DCP >50%, and making a DCP = 0% unlikely. In natural systems, carbonate dissolution usually falls somewhere between the two end member scenarios, with average DCP around 15 ± 5% (Genty *et al.*, 1999).

The range of DCP observed in speleothems suggests that dissolution regimes are generally more open than they are closed, which, under this model, suggests that soil CO_2 is the dominant source of speleothem C, and that therefore changes in soil $^{14}CO_2$ activities due to changes in root respiration and/or SOM decomposition rates could have a significant impact on speleothem DCP. Operating on the assumption that the degree of open/closed-system dissolution can be taken to be constant over to 20^{th} century, several previous studies have interpreted speleothem-based ^{14}C records of the 20^{th} century atmospheric ^{14}C bomb peak as records of soil $^{14}CO_2$ actives (e.g. Genty and Massault, 1999; Fohlmeister *et al.*, 2010; Fohlmeister *et al.*, 2011a; Griffiths *et al.*, 2012; and Rudzka-Phillips *et al.*, 2013). Under this assumption, the degree of attenuation of the 20^{th} century atmospheric ^{14}C bomb peak in soil CO_2 as it is recorded in speleothems, is controlled by the turnover time of SOM pools. Employing a simple soil carbon model to estimate the relative sizes and turnover times of SOM pools necessary to generate the best fit to speleothem bomb peak records, these studies have attempted to understand the contribution of soil CO_2 to speleothem DCP, as well as investigate the potential of speleothem ^{14}C records as sensitive recorders of past SOM dynamics.

The results of these modeling studies have suggested that soil CO_2 at infiltration sites in karst settings has pre-bomb mean ages ranging from decades to centuries (Rudzka-Phillips *et al.*, 2013). However these predictions are at odds with observations of soil CO_2 ages, which are typically on the order of years, with CO_2 derived from root respiration and decomposition of organic matter with a turnover time of <1 yr comprising 60-50% of soil CO_2 in boreal and temperate sites and >80% in tropical sites (Trumbore, 2000). This discrepancy between observed soil CO_2 ages and the mean age of soil CO_2 required by the shape of the bomb peak in speleothems suggest that:

1. soil carbon in karst settings may have very different dynamics than sites that have been studied previously and/or
2. soil CO_2 is not the predominant source of modern and slightly aged carbon that is incorporated in drip water DIC.

Both of these hypotheses have major implications for interpretation of $\delta^{13}C$ and $\Delta^{14}C$ records in speleothems, as well as for understanding the role of karst soils in the global carbon cycle.

In this study, we attempt to resolve the cause of the discrepancy between observations of soil CO_2 and speleothem bomb peak records through observations of soil carbon $\Delta^{14}C$ and $\delta^{13}C$ in Heshang Cave, China. We present a new bomb peak record from speleothem HS4 from Heshang Cave, China and a geochemical box model that builds on previous attempts to understand dead carbon incorporation in speleothems. We use this model to evaluate the age spectrum of SOM required to produce the speleothem bomb peak at HS4 and 13 other speleothem bomb peak records in the literature (Table 6.1).

6.2 Site and sample description

Heshang Cave is located in the Hubei Provence of China (30.44 °N, 110.42 °E, 294 m asl), ∼100 km west of the city of Yichang in the middle reaches of the Yangtze Valley. The cave is 250 m long, roughly horizontal, and overlain with ∼400 m of Cambrian dolomite. The hillside has a very thin soil cover of 5-30 cm of well-developed soil derived from dolomite bedrock, wind-blown silicate dust, and organic matter from the dense local vegetation. The cave has a large entrance with a height of about 20 m and is well ventilated. Annual average temperature in the study area is ∼18 °C, with daily averages ranging from 5 °C to 28 °C. Unlike many caves, cave temperature at Heshang Cave exhibits a seasonal cycle, ranging from 16 °C to 22 °C, lagging the local temperature cycle by 2-3 months (Johnson *et al.*, 2006).

HS4 is a 2.5 m long annually banded stalagmite that was actively forming when it was collected from Heshang Cave in 2001. The HS4 site is located ∼150 m from the entrance of the cave, and was still actively dripping when this study was undertaken. Records of $\delta^{18}O$, $\delta^{13}C$, and ^{14}C covering the Holocene measured on HS4 have been previously reported by Hu *et al.* (2008b), Liu *et al.* (2013), and Noronha *et al.* (2014). The age model for the final 150 years of stalagmite growth is well-defined by annual layer counting (Hu *et al.*, 2008b). Previous work reporting Heshang Cave speleothem HS4 ^{14}C showed that HS4 Holocene average DCP was 10.3 ± 1.5%. DCP increased significantly during the warmer, wetter, mid-Holocene spanning ∼5-7.5 ka (Noronha *et al.*, 2014) to a maximum of 14.1 ± 0.4% at 6 ka. This increase in DCP was interpreted as a shift to more closed-system dissolution regime, likely in response to increased precipitation at this time.

6.3 Methods

6.3.1 Speleothem calcite

The stalagmite, HS4, was previously cut in half parallel to the growth axis and the surface was polished to reveal laminations consisting of sub-mm scale light and dark couplets, which has been shown to be annual (Hu *et al.*, 2008b). HS4 calcite is milky, opaque, and porous, with a fabric dominantly characterized as open columnar using the terminology of Frisia and Borsato (2010). Speleothem calcite for the 20th century record of ^{14}C was drilled parallel to growth lamina as powder using a New Wave Research micromill. The age model for the 20^{th}century is based on annual layer counting described in Hu *et al.* (2008a).

Beginning in 2007, calcite precipitated from the drip that previously fed HS4 was grown on etched glass plates. Plates were collected and replaced during each trip to the cave site, each sample representing an average of 40 days of calcite growth. Samples nearest the center of the glass plate are preferred for measurements of stable isotopes and trace elements, as isotope and element ratios change with distance from the drip axis. Because reported ^{14}C measurements are corrected for isotopic fractionation (Stuiver and Polach, 1977), calcite for ^{14}C measurements was collected from calcite scraped from the funnel above the glass plate in effort to preserve the calcite precipitated on the glass plate for stable isotope and trace element analyses. For simplicity we refer to this calcite as "glass plate calcite" throughout the manuscript. Measurements of ^{14}C have been made on glass plate calcite during the interval spanning from April 2007 to March 2012.

Speleothem and glass plate calcite samples for ^{14}C measurements were pretreated with a 10% HCl leach, and subsequently hydrolyzed in 85% H_3PO_4. After conversion to CO_2, calcite samples were converted to graphite via iron catalyzed hydrogen reduction following standard protocols as described in Santos *et al.* (2007).

6.3.2 Soil organic matter

Because access to the recharge zone is difficult, all soil sampling was conducted at a site near the entrance of the cave. One expedition to the recharge zone in August 2004 described the soil at the recharge zone as 30 cm deep with reasonably dense vegetation (Hu *et al.*, 2008a), which is consistent with the site at which sampling was conducted. Soil was collected from a site near the cave entrance during the field trip in March 2010, in 5 cm depth intervals until the bedrock was reached. Prior to measurement, visible roots were picked out and soil samples were dried in an oven at 65 °C for 12-24 hrs.

Both samples of bulk SOM and SOM separated by size fraction were measured for ^{14}C and $\delta^{13}C$. Samples of soil from intermediate depths (5-10 cm) were separated by size fractions, defined as coarse sand (>425 μm), medium sand (425-250 μm), fine sand (250-63 μm), and silt (<63 μm). All SOM samples were ground to powder because of the presence of dolomite, ($CaMgCO_3$) which is more resistant to acid hydrolysis than calcite. Soil samples were acidified with 1N HCl overnight to remove carbonate. Following acidification, SOM samples were converted to CO_2 via combustion in evacuated sealed quartz tubes at 900 °C for 3.5 hrs, cryogenically purified, and graphitized via hydrogen reduction.

6.3.3 Soil CO_2

Soil CO_2 from depth was sampled using stainless steel gas wells, which were installed in the soil at a variety of depths. CO_2 was sampled 12-24 hrs after installation of wells, and wells removed at the end of each field trip. CO_2 concentrations were measured with a portable infra-red gas analyzer (LI-820 CO_2 Analyzer, LICOR Inc., Lincoln, NE, USA). When pCO_2 concentrations were above 2,000 ppm sample was collected in 0.5 L evacuated stainless steel canisters to achieve the in desired sample size of ∼1 mg C. When sampling with stainless steel canisters, flow was restricted by stainless steel capillary (0.010 cm × 0.063 cm × 30 cm,

Fisher). When pCO_2 was below 2,000 ppm, samples were collected by pumping atmosphere for ∼15 minutes through steel traps containing activated molecular sieves (13× powder-free 133 8/12 beads, Grace) using a diaphragm pump (Hargraves Fluidics BTC Series miniature). Samples were filtered through Drierite desiccant (W.A. Hammond Drierite Co. Ltd., Xenia, OH, USA), and flow rate was measured as 1 L/min. One sample of atmospheric CO_2 was collected in a steel trap at the cave site during the field trip in March 2010. To prevent ^{14}C memory effects traps were pre-conditioned by baking at 630 °C for 45 mins under vacuum.

Soil CO_2 samples collected in evacuated flasks were extracted on line, and CO_2 collected in steel traps was released for isotopic analysis by baking the traps at 475 °C. All CO_2 samples were cryogenically purified and converted to graphite via the sealed tube zinc reduction method (Xu *et al.*, 2007).

6.3.4 Tree ring record of atmospheric ^{14}C

A pine tree of unknown species from a location across the river from Heshang Cave was felled in July 2011 to create a record of local atmospheric ^{14}C. We selected a tree that was located ∼50 m away from the road to avoid bias from point sources of fossil fuels. The 25 rings were assumed to be annual, and were counted to create a calendar age model for a record of local atmospheric ^{14}C. The tree appeared to be colonized by blue-stain fungus, but a study by English *et al.* (2011) showed that blue-stain fungus colonization did not detectably alter whole wood or α-cellulose $\delta^{18}O$ or $\delta^{13}C$, suggesting that translocation effects are minimal. The tree was sampled annually, and pretreated to α-cellulose using the methods described in Southon and Magana (2010). Briefly, ∼30 mg of shaved wood was treated with a standard acid-base-acid treatment, followed by a bleaching treatment to isolate hollocellulose, and a strong base treatment to isolate α-cellulose. All samples were treated in individual 13 mm glass test tubes.

Tree cellulose was converted to CO_2 via combustion in evacuated sealed quartz tubes at 900 °C for 3.5 hrs, cryogenically purified, and graphitized by iron catalyzed hydrogen reduction.

6.3.5 Isotope analysis

After conversion to graphite, all ^{14}C measurements were made at University of California Irvine on a NEC Compact (1.5 SDH) AMS system, using six aliquots of Oxalic Acid I as the normalizing standard. Each mg-sized carbon sample was measured multiple times (typically 8 to 15 runs) over a 24 hr period.

$\delta^{13}C$ were measured by isotope ratio mass spectrometry at University of California, Irvine. Measurements on samples collected as gas were made on splits of CO_2 injected into He-filled vials to a target concentration of 3,500 ppm CO_2 using a Thermo Finnigan DeltaPlus equipped with a GasBench II autosampler. $\delta^{13}C$ measurements on SOM were made by placing acidified, ground soil in tin capsules that are combusted to CO_2 and analyzed by isotope ratio mass spectrometry on a Thermo Finnigan DeltaPlus equipped with a Fisons NA1500NC elemental analyzer. Replicate measurement errors on known standards were approximately ± 0.1‰.

6.3.6 Soil Carbon Model

Previous attempts to evaluate the age spectrum of soil carbon above caves using speleothem bomb peak records (e.g. Genty and Massault, 1999; Fohlmeister *et al.*, 2010; Fohlmeister *et al.*, 2011a; Griffiths *et al.*, 2012; and Rudzka-Phillips *et al.*, 2013) estimated soil $^{14}CO_2$

using the mass balance equation originally proposed by Genty and Massault (1999):

$$a^{14}C_g = C_1\left(a^{14}C_{atm-y_1}\right) + C_2\left(a^{14}C_{atm-y_2}\right) + C_3\left(a^{14}C_{atm-y_3}\right)$$

where C_1, C_2, and C_3 are the relative proportion of three SOM pools such that:

$$C_1 + C_2 + C_3 = 1$$

and the $a^{14}C_{atm-y_j}$ is the ^{14}C activity of the pool approximated by a simple moving average, with a window, y, equal to the turnover time of the SOM pool:

$$a^{14}C_{atm-y} = \frac{\sum_{i=1}^{y} a^{14}C_{atm_i}}{y}$$

Approximating soil carbon ^{14}C activity via moving average results in modeling SOM pools as heterogenous, and decomposition of SOM as a zero-order process. That is, a moving average assumes the inputs to the SOM pool from each year contribute a constant mass to the CO_2 flux at every time step until the inputs are exhausted after y time steps. This deviates from typical geochemical box modeling approaches, where SOM within a given pool is homogenized, and the homogenized pool decomposes as a first-order process (Six and Jastrow, 2002). Additionally, these models did not include a pool with a turnover time of one year, essentially allowing for the possibility of soils where no root respiration was occurring.

Accordingly, in this study, we build on these previous works by modeling SOM using a more typical geochemical box modeling approach with a total of 4 boxes - 3 homogenous SOM pools which decompose as a first-order process, and and a pool with a turnover time (τ) equal to one year which represents root respiration and decomposition of organic matter of annual age. We implement this model using the Matlab Global Optimization solver tool, `MultiStart`, to generate 1000 sets of random start points for the parameters P_j and τ_j,

where j=1:4 and P_j represents the relative proportions of four pools, and τ_j is the associated turnover time for each pool. We constrain the parameters P_j to satisfy the requirements, $\sum P_j = 1$ and $1 > P_j > 0$. The first pool is fixed as an annual pool (i.e. $\tau_1 = 1$), and the rest of the pools are constrained to represent pools with turnover times on the order of decades, centuries, and millennia (i.e. $100 > \tau_2 > 1$; $1000 > \tau_3 > 100$; $10000 > \tau_4 > 1000$). We initialize the model by starting 100 years before the first speleothem ^{14}C measurement, and set the initial ^{14}C activity of each SOM pool equal to the average of the decay corrected ^{14}C activity of the atmosphere over the last τ years.

We take these parameters (P_j) to represent the relative proportions and turnover times of SOM pools, and derive the relative proportion of the soil CO_2 fluxes from them, instead of estimating the relative proportions of SOM contributions to the soil CO_2 directly. We make this distinction because, in part due to the use of the moving average approach to estimating ^{14}C activity of soil carbon pools, the language in previous studies was ambiguous and at times erroneously implied that the contribution of a SOM pool to the total amount of SOM is equal to the contribution of CO_2 of that pool to the soil gas e.g. a pool with $\tau = 5$ yr that comprises 50% of the SOM is taken to generate 50% of the total soil CO_2. In reality, at steady state, making the assumption that the only loss pathway for a SOM is decomposition, the size of a flux of CO_2 from a SOM pool is a function of its turnover time τ:

$$F = \frac{M}{\tau}$$

where F is the flux from a pool, and M is the mass of the pool. Continuing in our example of a pool that comprises 50% of the SOM, with a τ of 5 years, at steady state the annual flux out of the pool will be equal to 1/5 of its mass. If we imagine the the rest of the SOM as a single pool with a τ of 100 years, the steady state loss of the pool is equal to 1/100 of its mass each year, which means that the flux from the pool with a τ of 5 years will make

up 95% of the soil CO_2. In this study, we refer to the relative parameters representing the proportions of the CO_2 fluxes as F_j.

After calculating the steady state fluxes from the SOM pools and their relative contributions to the CO_2, we calculate the ^{14}C activity of the SOM pool at each time step via:

$$a^{14}C_{j_{y_i}} = a^{14}C_{j_{y_{i-1}}}\left(1 - \frac{1}{\tau}\right) + a^{14}C_{(j-1)_{y_i}}\left(\frac{1}{\tau}\right)$$

where i is the current model step year and j refers to the SOM pool 1-4. The inputs to the pools with longer τ are derived from the younger pools, and the inputs into pool 1 are equal to the decay corrected ^{14}C activity of the atmosphere at the given model step year $\left(a^{14}C_{atm_{y_i}}\right)$.

We then multiply the fluxes by the ^{14}C activity of the pools at the model step and sum them together to find the $^{14}CO_2$ activity at the model step:

$$a^{14}CO_{2(y_i)} = F_1\left(a^{14}C_{pool1_{y_i}}\right) + F_2\left(a^{14}C_{pool2_{y_i}}\right) + F_3\left(a^{14}C_{pool3_{y_i}}\right) + F_4\left(a^{14}C_{pool4_{y_i}}\right)$$

Once the entire 20^{th} century soil $^{14}CO_2$ record is calculated from the start points generated, we find the offset between the pre-bomb interval (y<1955) of the calculated curve to the measured speleothem bomb peak curve to estimate the contribution from ^{14}C dead sources, and subtract this difference from the entire curve. After this step, the residuals are computed and using the Matlab optimization function, `fmincon`, we iteratively calculate the parameters that yield the best fit with the measured speleothem bomb peak from each set of start points.

In contrast to previous studies, we opt to ignore fractionation effects in our calculations for several reasons:

- Measured speleothem a^{14}C activities already account for fractionation effects, as they are reported as fractionation corrected values following the standard outlined in Stuiver and Polach (1977).

- There has been significant confusion in the speleothem literature recently about the correct formulae to correct for fractionation. Some previous modeling studies have used a value of 2.3 for fractionation changes in $^{14}C/^{12}C$ vs. $^{13}C/^{12}C$ based on an attempt to determine the fractionation of ^{14}C relative to ^{13}C in photosynthesis (Saliege and Fontes, 1984). The experiment was probably compromised by contributions of fossil fuel and the value of 2.3 has no support from quantum theory (Southon, 2011).

- At the range of observed surface temperatures and bomb/post-bomb speleothem ^{14}C activities, fractionation effects are small, on the order of 2-4%.

- Because we, and others, do not allow for variable temperature in our model, fractionation affects all time steps by the same constant term. Therefore ignoring fractionation does not affect the shape of the bomb peak curve generated by the model, only the contribution of aged carbon from dead sources.

For atmospheric ^{14}C activity for the post-bomb era we use the Hua *et al.* (2013) reconstructions of regional atmospheric ^{14}C at annual resolution, and for the pre-bomb era linearly interpolated the IntCal13 Northern and Southern Hemisphere curves to annual resolution (Reimer *et al.*, 2013). In addition to modeling the soil gas age at the infiltration site for HS4, we apply this model to 13 speleothem bomb peak records (shown in Table 6.1) from the literature which have published age models which are based on independent methods. In order words, we exclude from our modeling speleothem bomb peak records with published age models that rely primarily on ^{14}C bomb peak evidence as well as modifications made to age models made on the basis of the results of previous modeling studies. In practice this

means we exclude the records of Hua *et al.* (2013) and Hodge *et al.* (2011) and use the layer counting age models in Rudzka-Phillips *et al.* (2013).

Table 6.1: Speleothem bomb peak records referred to in this text. Modified from Table 1 in Rudzka-Phillips *et al.*, 2013

Speleothem	Cave	Location	^{14}C Zone	Altitude (m asl)	MAT (°C)	MAP (mm/yr)	Soil cover (m)	Overburden thickness (m)	Reference
Asfa-3	Rukiessa	Ethiopia	NHZ3		20-25		<1	30	Baker *et al.*, 2007
CC-Bil	Crag	SW Ireland	NHZ1	60	9.6	1465	<0.5	20	Rudzka-Phillips *et al.*, 2013
ER-77	Grotta di Ernesto	NE Italy	NHZ1	1167	6.6	1300	<1.5	5-30	Fohlmeister *et al.*, 2011a
Fau-stm14	La Faurie	SW France	NHZ1	225	12.9	860	0.2	10	Genty and Massault, 1999
GAR-02	La Garma	N Spain	NHZ1	80	13.7	1278	0.6-1.5	60-80	Rudzka-Phillips *et al.*, 2013
Gib04a	New St. Michaels	Gibraltar	NHZ2	325	18.3	767	<0.5	60	Mattey *et al.*, 2008
Han-stm5	Han-sur-Lesse	Belgium	NHZ1	180	8.9	790	<0.3	50	Genty *et al.*, 1998
HS4	Heshang	Central China	NHZ3	294	18	1144	<0.3	400	this publication
LR06-B1	Liang Luar	Indonesia	SHZ3	550	26	1200	1-2	30-50	Griffiths *et al.*, 2012
Merc-1	Rukiessa	Ethiopia	NHZ3		20-25		<1	25	Baker *et al.*, 2007
Obi84	Obir	Austria	NHZ1	1090	6.9	1350	<0.3	70	Smith *et al.*, 2009
Pos-stm4	Postojna	Slovenia	NHZ1	529	8	1500	<0.1	30	Genty *et al.*, 1998
So-11	Sofular	N Turkey	NHZ2	400	13.81	1200	0.5-1	10-30	Rudzka-Phillips *et al.*, 2013
T7	Cold Air	South Africa	SHZ3	1420	18.8	512	<0.3	20	Sundqvist *et al.*, 2013

6.4 Results

6.4.1 Measurements

The results of the tree ring record of local atmospheric ^{14}C and the single measurement of atmospheric $^{14}CO_2$ are shown in Figure 6.1 and suggest that atmospheric ^{14}C at the study site is similar to, though slightly lower than, the regional atmospheric ^{14}C as approximated by the NHZ3 reconstruction from Hua *et al.* (2013). There appears to be an increasing divergence with time between the tree ring record and the NHZ3 reconstruction, which is probably a regional offset due to the rapid increase in emission of ^{14}C-free fossil fuel derived CO_2 in China during the beginning of the 21st century. Given the good agreement between the tree ring record and the NHZ3 reconstruction before 2000 AD, we consider the NHZ3 reconstruction to be an appropriate approximation of atmospheric $^{14}CO_2$ at Heshang Cave for our soil carbon model. The mean DCP calculated for HS4 from the 20^{th} century pre-bomb points is 9.45 ± 0.21‰, which is lower than the Holocene average of 10.3 ± 1.5‰, but

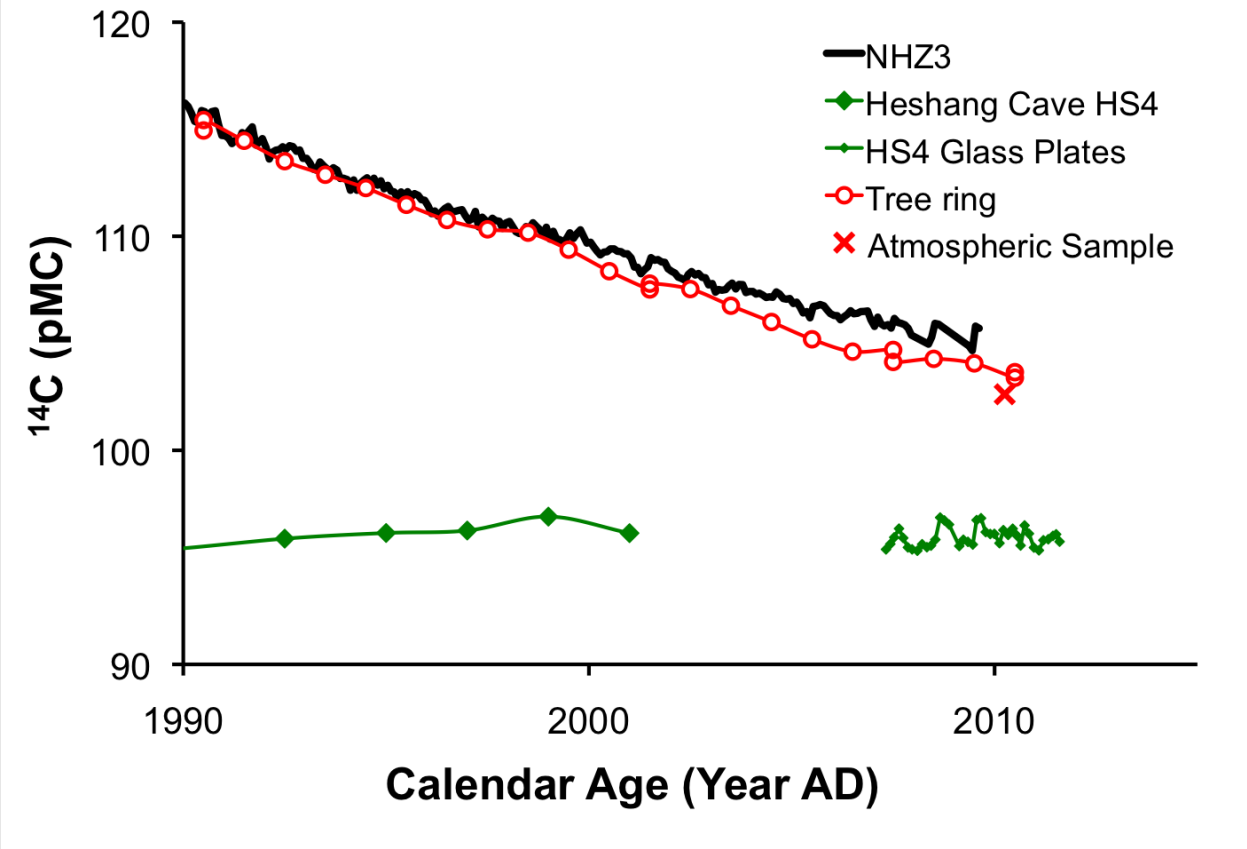

Figure 6.1: Results of local tree ring record and atmospheric $^{14}CO_2$ at Heshang Cave, and speleothem and glass plate calcite $^{14}CO_2$.

well within the Holocene 1σ uncertainty. HS4 speleothem calcite ^{14}C begins to increase in response to the atmospheric ^{14}C bomb peak by 1959 from the pre-bomb average value of 88.30 $\pm$ 0.18 pMC and increases gradually to a maximum of 96.90 $\pm$ 0.24 pMC in 1999. The total increase in speleothem ^{14}C in response to the atmospheric ^{14}C bomb peak increase in NHZ3 of $\sim$70 pMC is 8.6 pMC. Glass plate calcite has an average value of 95.92 $\pm$ 0.41 pMC, and appears to have a seasonal cycle with an amplitude of $\sim$1 pMC over the 5 year interval sampled.

Soil $^{14}CO_2$ activities range from 96.20 $\pm$ 0.16 to 105.34 $\pm$ 0.38 pMC and do not show any consistent trend with depth as shown in Figure 6.2a. Soil CO_2 $\delta^{13}C$ range from -22.7 to -12.8‰, and are shown in Figure 6.2b. The mean $\delta^{13}C$ of the CO_2 sampled during the cold dry month, March 2010, is -15.7‰, which is significantly more positive than $\delta^{13}C$ of soil

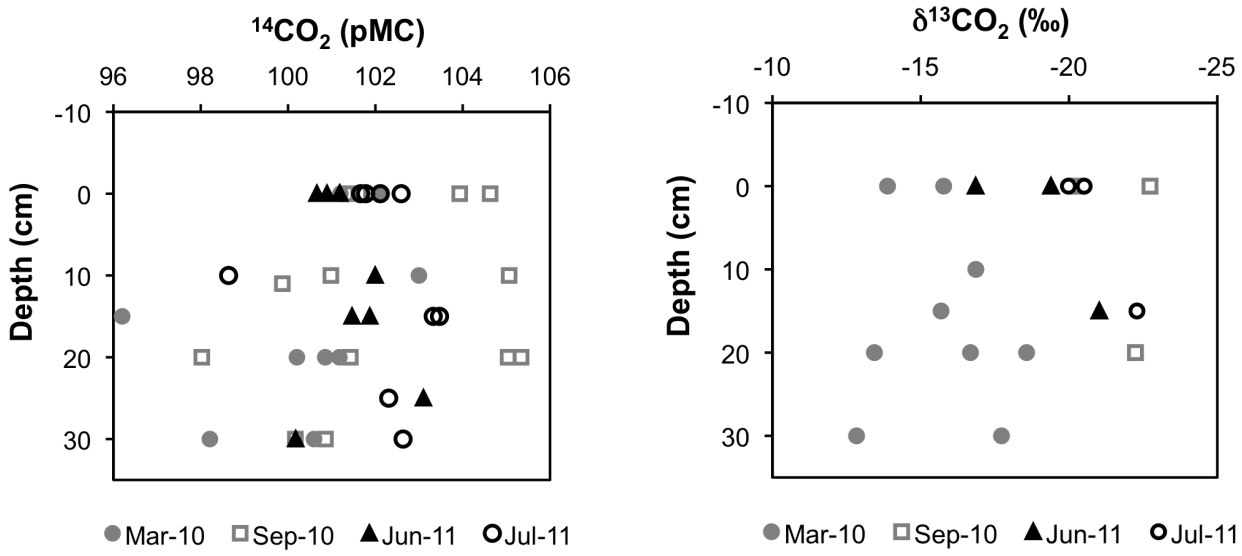

Figure 6.2: Isotopic measurements of soil CO_2. a) $^{14}CO_2$ by depth b) $\delta^{13}C$ of soil CO_2 by depth

CO_2 sampled during warm wet months (Sep 2010 = -21.8‰, June 2011 = -19.1‰, July = -20.9‰). Soil pCO_2 is typically <5,000 ppm and generally increases with depth as shown in Fig 6.4. Soil pCO_2 was lowest in March, with 2435 ppm being highest value observed occurring at 30 cm depth, and the maximum observed value of 15,005 ppm observed in July at 30 cm depth.

Bulk SOM ^{14}C is shown in Figure 6.3, and generally decreases with depth with an average value of 44 ± 12 pMC in the 0-5 cm depth interval, 27 ± 5 pMC in the 5-10 cm interval, and 29 ± 16 pMC in the 10-15 cm interval. Soil from 10-15 cm depth was analyzed for ^{14}C by size fractions. Sand fractions typically each accounted for ∼1/3 of the SOM by mass while silt accounted for only ∼1%. Coarser size fractions have lower ^{14}C activities than finer size fractions. Coarse sand has an average value = 25 ± 3, medium sand = 38 ± 15, fine sand = 54 ± 16, and silt = 73 ± 20. This is opposite to the trend expected when separating out SOM by size fractions - typically coarse material is composed of younger material and finer fractions account for the occluded recalcitrant carbon. All of these SOM ^{14}C measurements are much lower than is typically found in measurements of ^{14}C in shallow intervals of tropical

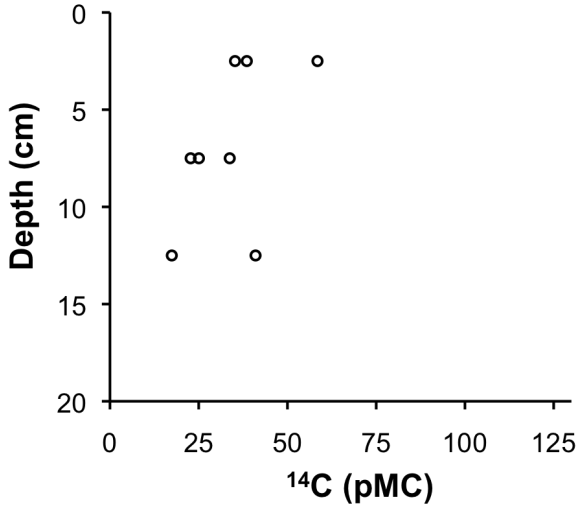

Figure 6.3: Heshang Cave bulk SOM ^{14}C activities.

soils. Becker-Heidmann *et al.* (1988) measured ^{14}C on the silt fraction of SOM of a Chinese mollisol, finding maximum ^{14}C activities of 96.6 ± 0.6 pMC in the 0-19 cm depth interval with decreasing ^{14}C activities with depth to 49.43 ± 0.46 pMC in the depth interval 65-105 cm. Ding *et al.* (2010) measured SOM in the 0-30 cm interval ranging from 109.49 ±0.43 to 95.58 ±0.49 pMC in a South China forest soil. Hobley *et al.* (2014) measured ^{14}C activities of 96.8 ± 0.6 pMC on bulk SOM from the 0-30 cm depth interval of an Australian karst soil.

Soil samples from Heshang Cave were carbonate rich - with an average value of ∼45% carbonate by mass. It is possible that dolomite was not completely removed during pretreatment, therefore biasing SOM ^{14}C activities lower. However, the δ^{13}C values of the bulk SOM samples ranged from −23.7 to −25.9‰, which is typical of SOM suggesting that dolomite was successfully removed by pretreatment with 1N HCl overnight. Furthermore, even if we assume that SOM samples did contain some residual dolomite with a δ^{13}C of 0‰, assuming SOM should have a δ^{13}C value typically observed in C3 plants of −27‰ (Cerling and Harris, 1999), dolomite would account for a maximum of 12% of the sample C, which would shift the range of ^{14}C activities for the bulk measurements from 17 - 58 pMC to at most 19 - 66 pMC. This latter range still represents very old carbon (3,400 to 13,300 yrs), so regardless

of whether traces of residual dolomite were present the results show that SOM at this site is very old.

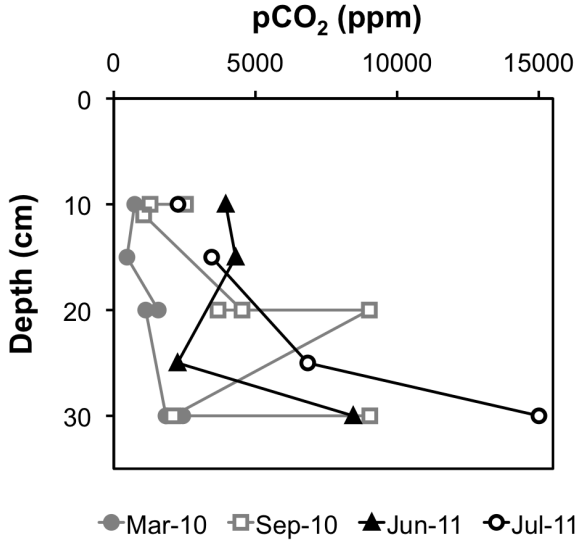

Figure 6.4: Soil pCO_2 v depth

6.4.2 Geochemical box model

Results of the soil carbon geochemical box modeling of speleothem bomb peak records are shown in Table 6.2. The values shown are the mean and standard deviation of the DCP values generated by the model results that yield fits with residuals <5% larger than the best fit, following the practice of Rudzka-Phillips *et al.* (2013), and refer to these solutions as the "good solutions." The number of good solutions is shown in Table 6.2, as well as the average percentage of CO_2 derived from the annual pool (F_1) in the good solutions, and the minimum age of the soil CO_2 for the good solutions.

Modeled F_1 range from <1% to 33%, with most speleothems suggesting a contribution from root respiration and decomposition of organic matter of annual age accounting for <10% of the total CO_2 flux. Gib04a is the only speleothem record that yielded parameters that are similar to observations of typical soil gas sources of CO_2, with ∼30% of CO_2 derived

from a pool of annual age. Model results show Pos-stm4 and ER-77 speleothem carbon is derived predominately from a pool of decadal age, and Han-stm5 is a mixture of decadal and centennially aged pools. All other records showed a dominance of the flux of CO_2 derived from organic carbon with a τ >70 yr. The minimum age of soil CO_2 predicted by the good solutions is consistently on the order of decades or centuries, which contrasts starkly with observations of soil gas in temperate and tropical sites observed to have mean soil gas ages on the order of years (Trumbore, 2000).

6.5 Discussion

6.5.1 Heshang Cave soil carbon

Measurements of ^{14}C in both Heshang Cave SOM and soil CO_2 are both very different than published observations of ^{14}C in shallow tropical soils. Trumbore (1993) observed Brazilian SOM is composed of a mixture of large stocks of carbon of multi-millennial age and carbon with post-bomb ^{14}C activities. $^{14}CO_2$ measurements of tropical soils show that they are dominated by root respiration and decomposition of decadal age SOM, which has post-bomb ^{14}C activities, yielding a soil $^{14}CO_2$ activity higher than that of atmospheric $^{14}CO_2$ (e.g. Ding *et al.*, 2010 and Trumbore, 2000). ^{14}C measurements of SOM at Heshang Cave shows that SOM at Heshang Cave contains carbon of multi-millennial age, but the absence of bulk or size fractionated SOM measurements with post-bomb ^{14}C activities suggests that the annual inputs of organic carbon to the soil are very low. If annual carbon inputs to soil are low, most carbon fixed in a given year must be respired in that same year, which would yield very large fluxes of CO_2 with ^{14}C activities close to atmospheric, and soil $^{14}CO_2$ would be roughly equal to atmospheric $^{14}CO_2$. However, soil $^{14}CO_2$ measured at Heshang Cave generally is lower than clean atmospheric $^{14}CO_2$, as well as the atmospheric measurement

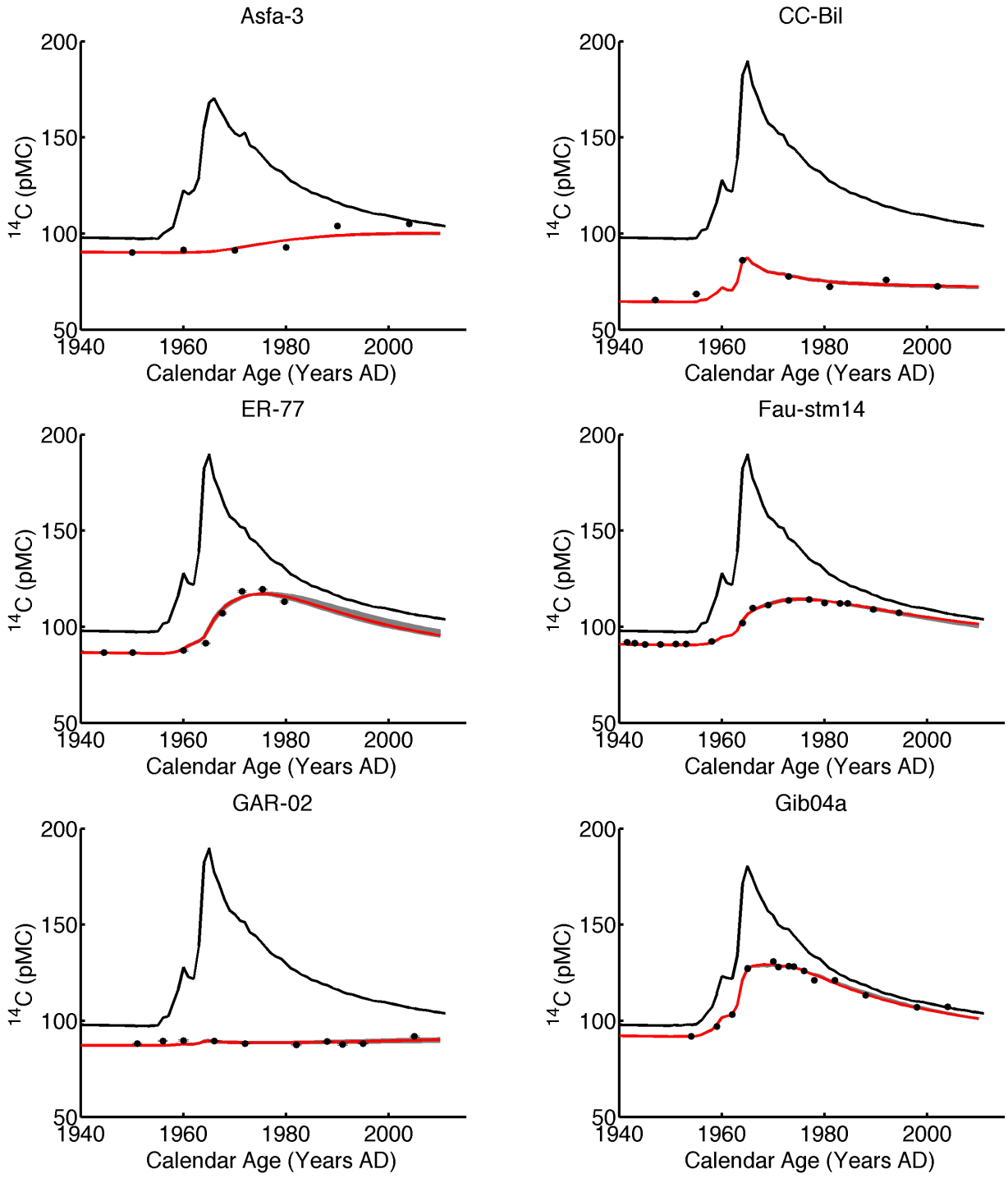

Figure 6.5: Results of speleothem ^{14}C bomb peak modeling. Black line is regional atmospheric ^{14}C record from Hua *et al.* (2013) used for the bomb peak record shown on the same plot. Speleothem measurements are shown in black circles. Redline shows the modeled best fit and grey lines are the good fits.

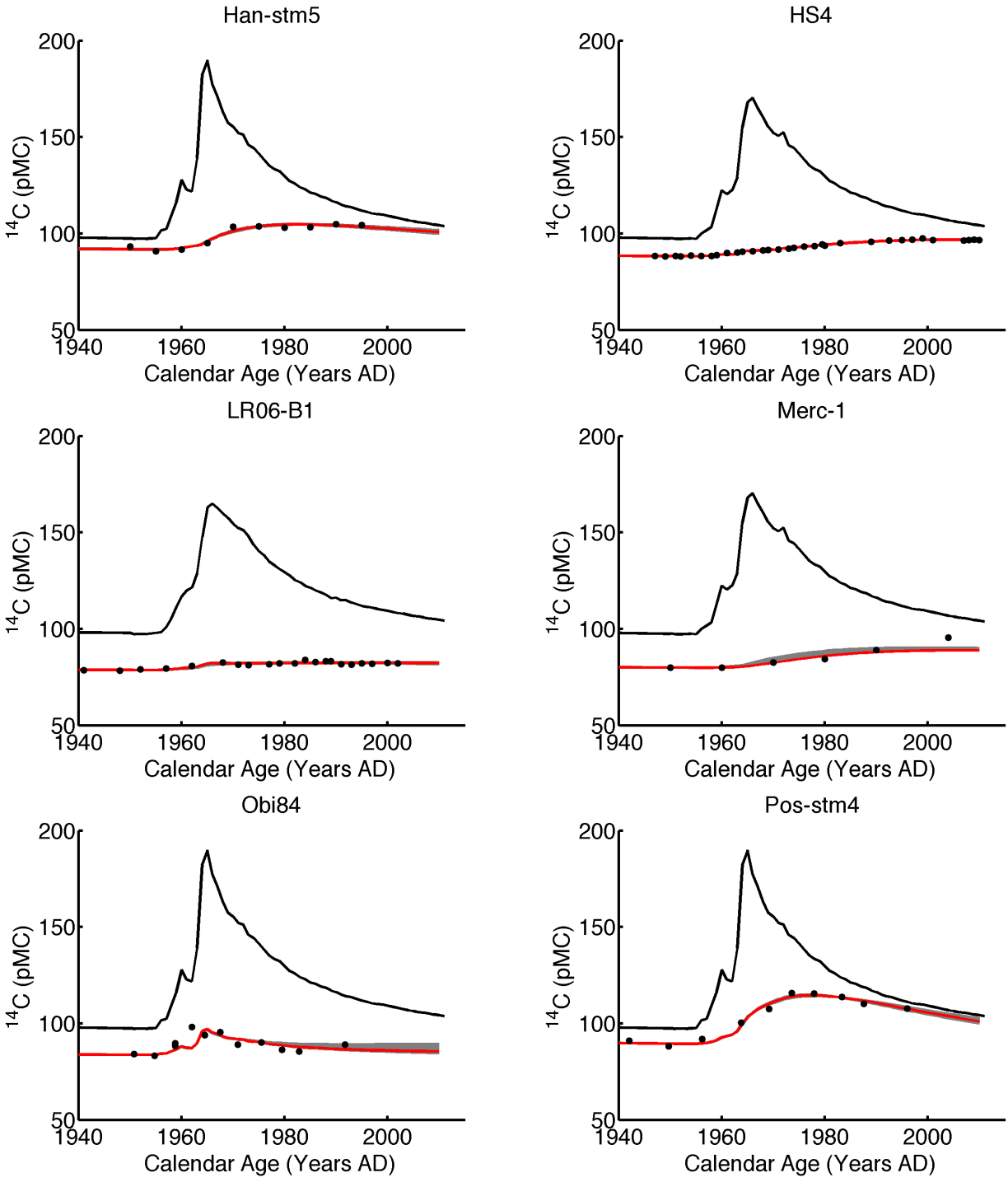
Han-stm5
HS4
LR06-B1
Merc-1
Obi84
Pos-stm4
200
150
100
50
1940
1960
1980
2000
^{14}C (pMC)
Calendar Age (Years AD)

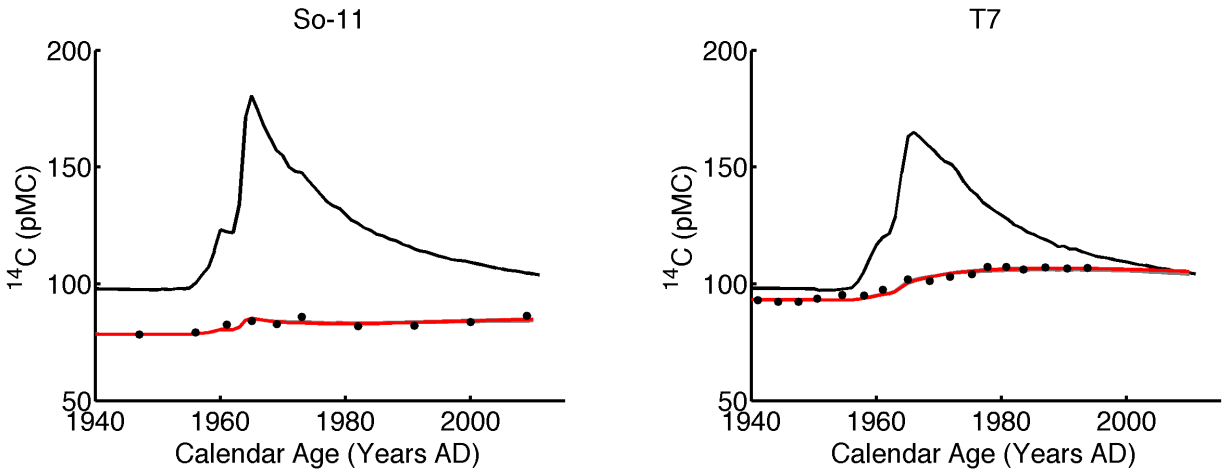

taken at the cave site in March 2010 and the trend predicted by the tree ring record of atmospheric ^{14}C (Fig 6.6).

There are several potential sources of depleted $^{14}CO_2$ observed in Heshang Cave soil, both because of sampling methods and properties of the system. The installation of wells used to sample soil CO_2 at depth causes disturbance of the soil profile and the ecosystem, which could potentially bias soil gas ^{14}C activities, though this contribution would most likely increase decomposition of labile carbon with contemporaneous and post-bomb ^{14}C activities and therefore increase the measured $^{14}CO_2$ activities. However, given the especially low ^{14}C activity of SOM and the apparent absence of decadal aged carbon, a small flux of decomposition of multi-millennial aged SOM found at Heshang Cave could achieve the observed offset of soil $^{14}CO_2$ from atmospheric $^{14}CO_2$.

Given the range of δ^{13}C observed in the soil, and very high carbonate concentration of the soil, it is also possible that some of the soil CO_2 is derived from ^{14}C-free carbonates in the soil. The open system model of carbon incorporation in speleothems relies on continuous equilibration of soil water DIC with soil CO_2, replacing carbon derived from dissolution of the carbonate bedrock with carbon derived from the atmosphere. The loss of carbon derived from the bedrock to soil CO_2 during equilibration in open system carbonate dissolution could

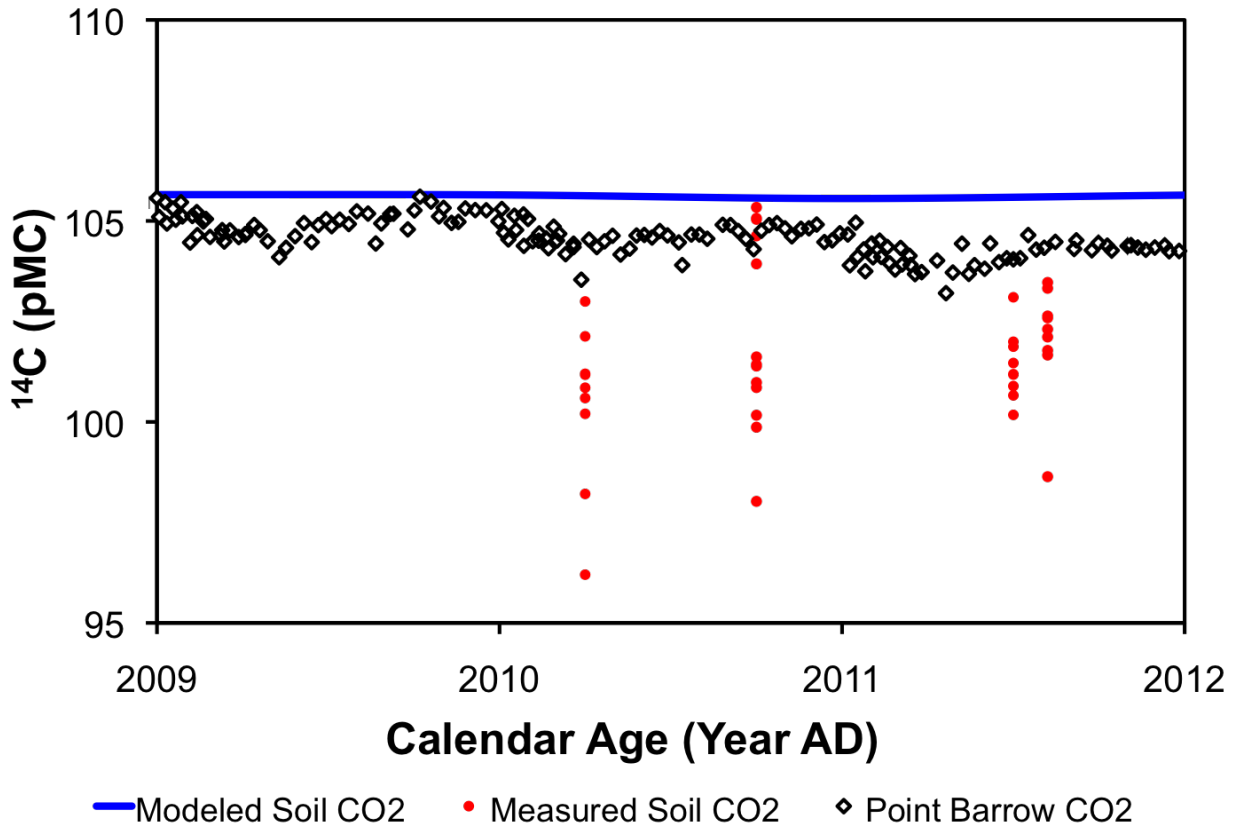

Figure 6.6: Observed clean atmospheric $^{14}CO_2$ (courtesy of X. Xu) and local atmospheric $^{14}CO_2$ with Heshang Cave soil $^{14}CO_2$.

contribute to the depletion of soil $^{14}CO_2$ activities. Additionally, calcite precipitation in the soil zone could also be a source of ^{14}C-free CO_2 to the soil atmosphere above Heshang Cave.

According to Roland *et al.* (2013), several recent studies in regions with carbonate bedrock have observed a cycle of CO_2 where daytime CO_2 fluxes are orders of magnitude higher than what could be expected from biological principles, and drawdown of CO_2 occurs during nighttime when there is no photosynthesis occurring. Roland *et al.* (2013) suggested that daytime ventilation of the soil zone disturbs carbonate equilibria by driving evaporation of soil moisture and down-mixing of lower pCO_2 atmosphere, therefore inducing calcite supersaturation conditions, driving calcite precipitation, and daytime production of CO_2. At night, cooler temperatures allow condensation, driving calcite dissolution and consumption

of CO_2. Through the process described by Roland *et al.* (2013), a significant portion of day time CO_2 flux could be ^{14}C-free, which would offset soil $^{14}CO_2$ from atmospheric $^{14}CO_2$.

Modeling results suggest that the CO_2 from which speleothem carbon in HS4 is derived predominately from decomposition of a single pool with a $\tau = 108$ yr. This results predicts that soil $^{14}CO_2$ activities would be 105.65 pMC in 2010, which is essentially indistinguishable from contemporaneous atmospheric $^{14}CO_2$ (Fig 6.6). It is not possible to determine isotopically if soil CO_2 is dominated by a flux from a centennial pool, as predicted by the modeling results, or is mostly root respiration and decomposition of young SOM as would be expected from observations of soil $^{14}CO_2$ activities in shallow tropical soils, with a contribution from an inorganic ^{14}C-free source. Given the dense local vegetation, absence of post-bomb ^{14}C activities in the SOM, high soil carbonate concentration, and observations of the dominance of root respiration at other tropical sites (Trumbore, 2000), we believe the most likely scenario is that soil CO_2 at Heshang Cave is derived predominately from carbon fixed during the current year with a contribution from a ^{14}C-free source. However, the measurements made in this study point to soil carbon dynamics being very complicated at this site, and perhaps across karst sites in general, highlighting the need for further investigations of soil carbon in karst sites to determine if they are consistently storing large quantities of very old SOM and how SOM decomposition at these sites responds to global climate change.

6.5.2 The sources of speleothem carbon

Modeling results suggest that CO_2 derived from root respiration and decomposition of organic matter with τ <1 year does not represent a significant portion of speleothem carbon, which is similar to the results of previous modeling studies. Genty and Massault (1997) referred to the soil $^{14}CO_2$ measurements of Dorr and Münnich (1986) which suggested that under forested soil in Germany decomposition of SOM with $\tau = 100$ years composes 25% of

soil CO_2 flux in the summer and 75% of the flux in the winter. Under the assumption that the bulk of infiltration of waters that feed speleothems in temperate settings occurs during the winter months when photosynthesis is at a minimum, previous modeling studies have accepted modeling results that suggest that speleothem carbon is derived from soil CO_2 that is dominated by decomposition of old SOM in good agreement with observations of winter soil $^{14}CO_2$ activity.

However, even if this assumption is accurate for sites where the growing season is out of phase with the rainy season, it is certainly not the case in tropical and sub-tropical sites with monsoon climates where the growing season and rainy season are in phase. Indeed our modeling results show that the speleothems from subtropical and tropical sites, LR06-B1 and HS4, both show some of the lowest contributions of carbon with τ <1 year. Moreover, the assumption that speleothem carbon is predominantly derived from winter soil CO_2 is difficult to reconcile even in temperate sites because of the particularly low soil pCO_2 in temperate sites during the winter. Dorr and Münnich (1986) showed winter pCO_2 in the forested soil of <3,000 ppm, and Tegen and Dorr (1996) typically saw concentrations of <2,000 ppm in German forest during cold seasons. Measurements of soil pCO_2 at Grotto di Ernesto also showed values of ∼2,000 ppm in winter. If the majority of speleothem carbon is derived from soil CO_2 during the winter, the combination of very low pCO_2 and high soil moisture, which would limit diffusion of CO_2, would reduce open system behavior and result in very high speleothem DCP, which is not generally observed in speleothems from temperate sites.

The assumption that open system dissolution is occurring under these low soil pCO_2 conditions also makes it difficult to explain observed drip water Ca^{2+} concentrations. Fohlmeister *et al.* (2011b) used a calcite dissolution model to calculate Grotto di Ernesto ER-G1 drip water carbon isotopes using the annual average soil pCO_2 observed above Grotto di Ernesto of 4,000 ppm. When the model was able to accurately reproduce drip water ^{14}C activity, it underestimated the $\delta^{13}C$ value by ∼1‰, and the Ca^{2+} concentration by a factor of ∼2. The

discrepancy in $\delta^{13}C$ isotopes is very likely a result of the fact that the model did not consider calcite precipitation that may have occurred before or after the drip water entered the cave, or equilibration with cave atmospheric CO_2 - both of which are processes which would likely shift $\delta^{13}C$ values higher. The discrepancy in Ca^{2+} is harder to explain. Fohlmeister *et al.* (2011b) suggested that the discrepancy could be due to the longer time necessary to establish equilibrium between soil water and soil gas for carbon isotopes than Ca^{2+}, however, another possibility is that the initial pCO_2 used in the model was too low.

A higher initial pCO_2 would increase the Ca^{2+} concentration of the water at the transition from open to closed system, which is the phase during which the majority of the Ca^{2+} is acquired. However, when Fohlmeister *et al.* (2011b) forced their model to fit observed drip water Ca^{2+} values, calculated drip water ^{14}C activity was higher than observed drip water ^{14}C activity by 6.5 pMC. The initial value used for the soil $^{14}CO_2$ activity was 110.6 pMC, based on the results of a previous bomb-peak modeling study on ER-77 which used the moving average approach to calculate soil carbon ^{14}C activity Fohlmeister *et al.* (2011a). The best fit to ER-77 in the geochemical box modeling results of this study suggest that the a lower initial $^{14}CO_2$ activity of 99.5 pMC is appropriate for the carbon source for ER-77, which could help bring the modeled speleothem ^{14}C activities in line with the observed speleothem ^{14}C activities. This initial $^{14}CO_2$ activity predicted from the model best fit to the ER-77 bomb peak record is lower than the ^{14}C activities measured in ER-G1 drip water, suggesting that the this estimate is too low for ER-G1, and the possibility that ER-G1 and ER-77 do not assimilate carbon from the same source. Nonetheless, the use of a higher initial pCO_2 and a lower initial ^{14}C activity as predicted by this study could potentially improve the performance of the Fohlmeister *et al.* (2011b) model in estimating drip water geochemistry.

Given the low pCO_2 observed in shallow karst soils, and the disagreement between observations of soil $^{14}CO_2$ activity and the $^{14}CO_2$ activity necessary to reproduce the speleothem

bomb peak records as predicted by the geochemical box model, we suggest that CO_2 in the soil zone is not the dominant source of speleothem carbon. The near absence of root respiration signal in speleothem carbon and the predicted dominance of decomposition of very old SOM suggests the possibility of a source of CO_2 that is removed from the soil zone, where decomposition of aged SOM occurs in isolation.

Transport of SOM to depth, both as particulate and dissolved organic matter, is known to be an important loss pathway for soil carbon (Kindler *et al.*, 2011). Organic matter incorporated in speleothem calcite has long been studied via fluorescence (McGarry and Baker, 2000) and recently has been studied for lipid biomarkers and $\delta^{13}C$ (e.g. Blyth *et al.*, 2006, Huang *et al.*, 2008, Xie *et al.*, 2003, Perrette *et al.*, 2008). Although the the extent of any transformation of this organic matter has not been well studied, there exists evidence of alteration of organic matter during transit through the vadose zone. Drip water organic matter fluorescence has been observed to have a lower emission wavelength than SOM, suggesting that in karst settings transformations of organic matter is occurring in the vadose zone (Baker *et al.*, 1998). Pabich *et al.* (2001) showed that thicker the vadose zones had lower the organic concentration at the water table, and a strong inverse relationship between organic concentrations and nitrate concentrations suggests that the loss is through microbial transformations. Studies of organic matter in Heshang Cave drip water have shown that drip water *n*-alkanes are dominated by low molecular weight fatty acids, in contrast *n*-alkanes in the soil which are dominated by high molecular weight fatty acids (Xie *et al.*, 2003 and Li *et al.*, 2011), which also suggests SOM undergoes microbial transformation during transit from the soil to the cave.

Very high vadose zone pCO_2 concentrations have long been known to occur in both carbonate and carbonate-free settings, (e.g. Bacon and Keller, 1998; Murphy *et al.*, 1992; Keller, 1991; Keller and Bacon, 1998; Wood and Petraitis, 1984; Wood *et al.*, 1993; Hendry *et al.*, 1993; Hendry and Wassenaar, 2005; Lawrence *et al.*, 2000; and Sanchez-Cañete *et al.*, 2011), and

isotopic evidence suggest that microbial respiration of organic material is the dominant source of subterranean CO_2. Most relevant to karst settings, Benavente *et al.* (2010) measured soil and vadose zone pCO_2 and $\delta^{13}C$ in a Mediterranian karst. Benavente *et al.* (2010) measured pCO_2 concentrations of <2,000 ppm with a $\delta^{13}C$ of -11.2 to -20.6 in the soil, and pCO_2 concentrations of >20,000 ppm in wells at depths of >10 m, with a $\delta^{13}C$ ranging from -19.7 to -22.1, suggesting an the CO_2 was derived from an organic matter source. Peyraube *et al.* (2013) estimated vadose zone pCO_2 based on carbon isotopic evidence in cave drip water and CO_2, and suggests vadose zone pCO_2 values of 4.4% (44,000 ppm) in winter and 10% in summer with $\delta^{13}C$ values of $-22.31‰$ and $-24.20‰$, which is in good agreement with the observations presented by Benavente *et al.* (2010). A study of the sources of cave CO_2 by Breecker *et al.* (2012) also hypothesized that the majority of cave CO_2 is advected from a deep biogenic source.

Several lines of evidence suggest that in at least some karst terrains, SOM is transported to depth in the vadose zone and microbial decomposition of this SOM produces high levels of subterranean CO_2. In settings where this process occurs, it must have some influence on speleothem C, and could explain the absence of root respiration derived carbon and dominance of carbon derived from decomposition of aged SOM seen in speleothem bomb peaks records. However, the hypothesis that speleothems are reflecting predominately the ^{14}C activity of this microbial produced subterranean CO_2 is hard to reconcile with carbonate chemistry. If waters are encountering large reservoirs of CO_2 during percolation, carbonate chemistry dictates that $CaCO_3$ must be consumed. Several studies have suggested that generation of subterranean CO_2 is an important, and possibly necessary, driver of carbonate dissolution and karst development (e.g. Wood, 1985; Atkinson, 1977; Gabrovšek *et al.*, 2000; and Gulley *et al.*, 2014). This process would be expected to result in speleothems formed in essentially closed systems, with DCP=50%. However, we consistently observe speleothems with DCP<50% and bomb peak profiles that do not reflect observed soil $^{14}CO_2$ activity, suggesting that open-system dissolution is occurring even at significant depth in the vadose

zone. Understanding how/if open-system dissolution occurs in the deep epikarst region is a key to confirming this hypothesis.

6.6 Implications for speleothem-based ^{14}C calibration

The apparent stability of speleothem DCP observed across major climate transitions has been both the most promising and puzzling result of attempts to produce speleothem-based records of atmospheric ^{14}C. Several speleothem records have been observed to have muted changes in DCP throughout the Younger Dryas climate event (Noronha *et al.*, 2014), and most exceptionally in the Hulu Cave speleothem, H82, DCP showed no response throughout the Younger Dryas despite the changes in summer monsoon intensity inferred from speleothem $\delta^{18}O$, and vegetation changes inferred by pollen evidence (Southon *et al.*, 2012). The hypothesis that speleothems are formed predominately from CO_2 in the vadose zone derived from microbial decomposition of aged organic matter could potentially begin to explain the apparent stability of DCP in speleothems through major climate transitions. Relative to temperature and moisture conditions at the surface, the climate variability over the last glacial cycle would be expected to induce less variability in the conditions the deep vadose zone.

The fact that speleothem carbon is derived predominately from SOM acts as something like a low pass filter, through which both abrupt changes in global atmospheric ^{14}C, and regional changes in soil dynamics are smoothed. In many speleothems, abrupt changes in surface ^{14}C, like the 20^{th} century atmospheric ^{14}C bomb peak are barely distinguishable in speleothem calcite because the signal is diluted by the very long turnover time of the SOM which dominates the CO_2 flux from which drip water DIC is acquired. Changes in hydrology appear to have the most important driver of speleothem DCP (Griffiths *et al.*, 2012 and Noronha *et al.*, 2014), with a working hypothesis that higher precipitation increases

soil moisture, therefore limiting CO_2 diffusion and open system behavior, and leading to a higher proportion of carbon derived from the ^{14}C-free bedrock. In a system where most drip water DIC is acquired during open system dissolution occurring at depth in the vadose zone, open system dissolution, which relies on the assumption of a functionally infinite supply of CO_2 could only occur when voids in the bedrock are filled with more gas than water. During periods of higher infiltration this condition would be met less often, and the kind of closed system dissolution that produces karst would dominate, leading to higher speleothem DCP.

6.7 Conclusion

We have developed an improved model based on previous attempts to model the sources of speleothem carbon which allows us to predict the SOM age distribution required to produce the shape of the speleothem 20^{th}century bomb peak. The results of this modeling work confirm the results of previous studies, which suggest that a large flux of CO_2 derived from organic material with turnover times on the order of centuries is necessary to produce the observed speleothem ^{14}C bomb peak. We believe this result suggests that soil CO_2 is not the dominant source of speleothem C, and suggest that CO_2 produced by microbial decomposition of leached SOM in the deep vadose zone is the main source of speleothem C.

Our observations of soil carbon at Heshang Cave, China indicate that soil carbon dynamics at karst sites are complicated and unlike sites that have been studied previously. Karst soils appear to be a unique system that may respond differently to global climate change that sites studies previously, meriting continued study of carbon cycling in karst settings to continue to our understanding of the role of karst soils in the global carbon-climate feedback cycle and the sources of speleothem C.

Table 6.2: Modeling results for the 14 speleothem records described in Table 6.1. P_j=Percent of total SOM, F_j=Percent of total CO_2 flux, τ_j=Turnover time in years, P_j, F_j, τ represent the parameters for the best model fit. Mean F_1 are the mean and standard deviation of the percentage of the CO_2 flux derived from root respiration and organic material with τ <1 year for the model solutions with residuals that were <5% greater than the best fit. n<5%=the number of model solutions with residuals <5% greater than the best fit. n<1955 is the number of stalagmite ^{14}C measurements in the pre-bomb interval. Speleothems that have only one measurement in the pre-bomb interval have DCP values given with no associated uncertainty, as the given uncertainties in DCP are the standard deviation of the differences between atmospheric ^{14}C and pre-bomb speleothem ^{14}C. Min soil CO_2 is the minimum age of soil CO_2 of the good fits.

Speleothem	P_j (%)	F_j (%)	τ_j (%)	DCP (%)	Mean F_1 (%)	Min soil CO_2 Age (yr)	n<5%	n<1955
Asfa3	<1	<1	1	7.50	0.00	102	3	1
	<1	<1	6					
	100	100	102					
	<1	<1	4358					
CC-Bil	<1	25	1	34.13 ± 1.62	24.52 ± 0.29	74	6	3
	<1	<1	14					
	98	75	126					
	2	<1	2104					
ER-77	<1	<1	1	11.85 ± 0.77	0.01 ± 0.01	67	37	11
	<1	71	11					
	<1	1	557					
	99	28	7238					
Fau-stm14	<1	9	1	7.28 ± 1.01	9.58 ± 0.44	79	35	11
	7	46	13					
	65	44	130					
	27	1	4450					
Gar02	<1	3	1	11.35 ± 1.37	2.7 ± 0.15	124	232	3
	<1	<1	96					
	10	89	111					
	90	9	9912					
Gib04a	1	31	1	6.18	32.55 ± 1.04	32	3	1
	11	43	8					
	82	25	104					
	7	<1	1043					
Han-stm5	<1	<1	1	4.36	0.35 ± 0.24	1029	27	1
	1	37	20					
	5	45	159					
	94	19	7214					
HS4	<1	3	1	9.43 ± 0.23	3.46 ± 0.07	367	2	5
	<1	<1	7					
	19	88	109					
	81	9	4655					
LR06-B1	<1	5	1	19.56 ± 0.78	3.47 ± 0.26	231	758	3
	<1	<1	6					
	2	34	103					
	98	62	3461					
Merc1	<1	<1	1	18.01	0 ± 0.01	81	232	1

	<1	1	6					
	95	98	117					
	5	<1	9094					
Obi84	<1	14	1	14.14 ± 0.91	14.49 ± 0.09	210	972	2
	<1	<1	83					
	4	52	243					
	96	34	9460					
Pos-stm4	<1	6	1	8.26 ± 1.88	6.51 ± 0.6	75	79	2
	1	67	18					
	1	5	375					
	98	22	7428					
So-11	<1	8	1	19.70	7.99 ± 0.29	92	18	1
	<1	<1	38					
	99	91	103					
	1	<1	5773					
T7	<1	8	1	4.88 ± 1.33	7.79 ± 0.28	63	557	3
	100	92	70					
	<1	<1	278					
	<1	<1	4430					

Chapter 7

Conclusions and Future Work

While this disseration spans a broad variety of work on ^{14}C in the Earth system, the most significant results of this dissertation are the works that concern development of speleothem-based ^{14}C calibration. The speleothem works included in this dissertation demonstrate the utility of speleothems as records of atmospheric ^{14}C, and begin to deconvolve the controls on speleothem dead carbon incorporation. Our understanding of carbon incorporation in speleothems is still being developed, and the results presenting in this dissertation have wide-reaching applications across Earth science. Potential continuations of the work presented in this dissertation include:

- **A study of soil carbon at karst sites**

  The results presented in Chapter 6 highlight that soil carbon in karst sites might be much older than soil carbon at sites studied previously, and may have very different dynamics. Despite the surface soil being very shallow in karst settings, the "soil zone" likely extends very deep where organic matter is stored in voids in the bedrock. Karst terrains make up ∼10% of global land surface area, and have often been subject to desertification due to human impacts. The fate of organic carbon eroded from karst

terrains, and response of soils in karst terrains to global climate change is largely unknown and a highly important research topic.

- **A study of the seasonal ^{14}C signal in speleothem glass plate calcite**

  Chemical kinetics predict that speleothem calcite crystallization generally happens very quickly - too quickly for significant exchange between drip water and cave atmosphere. However, the glass plate calcite ^{14}C measurements at Heshang Cave show a clear seasonal cycle. The 20^{th} century bomb peak record indicates that root respiration is not an important contribution to speleothem carbon in HS4, and the lack of the overall declining trend seen in atmospheric $^{14}CO_2$ in the glass plate calcite suggests that this is still the case at HS4. The seasonal cycle in ^{14}C in HS4 suggests that there is some equilibration with cave atmosphere occurring before calcite deposition. Combined with measurements of ^{14}C in glass plates from other caves, there is potential for a study investigating the mechanisms and importance of in cave gas exchange in speleothem calcite isotopic composition.

- **A 20^{th}century speleothem age model algorithm**

  There is a growing interest in high-resolution paleo reconstructions of changes in the Earth system in the period since the Industrial Revolution as well as the past two thousand years - the so called "Common Era." The position of the bomb peak in speleothems is a useful chronological tool for precisely identifying the year 1955, and defining chronologies for records of the Common Era. The model used in Chapter 6 of this dissertation could be modified to accept a speleothem ^{14}C bomb peak record, with depths and ^{14}C concentrations (and potentially sampling date), and output the most probable position of the year 1955 and estimate a constant growth rate for the post-bomb interval. This would be a useful tool, that would likely be widely used. Accordingly I would modify the program to use a free programming language, like R,

as at present it runs in Matlab, which is expensive software, and uses an expensive Matlab add-on package.

- **Reconstruction of atmospheric ^{14}C using the remaining Hulu Cave speleothems**

  Hulu Cave speleothem H82 produced a remarkable speleothem-based record of atmospheric ^{14}C with a robust calendar chronology and a stable DCP that has contributed significantly to refining the ^{14}C calibration curve. Reconstruction of atmospheric ^{14}C based on the remaining Hulu Cave speleothems is highly desirable goal for studies of Earth system history.

- **A Hulu Cave ^{14}C bomb peak record**

  The exceptional stability of DCP, and simultaneous responsiveness of Hulu Cave H82 to changes in atmospheric ^{14}C is both the most promising and puzzling characteristic of Hulu Cave speleothems as records of atmospheric ^{14}C. A ^{14}C bomb peak record from Hulu Cave would be a valuable record for understanding carbon cycling in Hulu Cave, which could improve interoperation of the Hulu Cave speleothem records as a record of atmospheric ^{14}C. Understanding carbon cycling at Hulu Cave could also help with interpretations of the δ^{13}C record at Hulu Cave, which has millennial scale structure but at present remains largely unstudied.

Bibliography

Adkins, J. F., K. McIntyre, and D. P. Schrag (2002). The salinity, temperature, and $\delta^{18}O$ of the glacial deep ocean. *Science*, 298(5599):1769–73. doi:10.1126/science.1076252.

Alley, R., R. C. Finkel, K. Nishiizumi, S. Anadakrishnan, C. A. Shuman, G. Mershon, G. A. Zielinski, and P. A. Mayewski (1995). Changes in continental and sea-salt atmospheric loadings in central Greenland during the most recent deglaciation: Model-based estimates. *Journal of Glaciology*, 41(139):503–514.

Anderson, R., S. Ali, L. I. Bradtmiller, S. H. H. Nielsen, M. Q. Fleisher, B. E. Anderson, and L. H. Burckle (2009). Wind-driven upwelling in the Southern Ocean and the deglacial rise in atmospheric CO_2. *Science*, 323(5920):1443–8. doi:10.1126/science.1167441.

Atkinson, T. C. (1977). Carbon dioxide in the atmosphere of the unsaturated zone: an important control of groundwater hardness in limestones. *Journal of Hydrology*, 35:111–123.

Bacon, D. H. and C. K. Keller (1998). Carbon dioxide respiration in the deep vadose zone: Implications for groundwater age dating. *Water Resources Research*, 34(11):3069–3077. doi:10.1029/98WR02045.

Baker, A., A. Asrat, I. J. Fairchild, M. J. Leng, P. M. Wynn, C. L. Bryant, D. Genty, and M. Umer (2007). Analysis of the climate signal contained within $\delta^{18}O$ and growth rate parameters in two Ethiopian stalagmites. *Geochimica et Cosmochimica Acta*, 71(12):2975–2988. doi:10.1016/j.gca.2007.03.029.

Baker, A., D. Genty, W. Dreybrodt, W. L. Barnes, N. J. Mockler, and J. Grapes (1998). Testing theoretically predicted stalagmite growth rate with recent annually laminated samples: Implications for past stalagmite deposition. *Geochimica et Cosmochimica Acta*, 62(3):393–404.

Bard, E. (1998). Geochemical and geophysical implications of the radiocarbon calibration. *Geochimica et Cosmochimica Acta*, 62(12):2025–2038.

Bard, E., M. Arnold, B. Hamelin, N. Tisnerat-Laborde, and G. Cabioch (1998). Radiocarbon calibration by means of mass spectrometric $^{230}Th/^{234}U$ and ^{14}C ages of corals. An updated data base including samples from Barbados Mururoa and Tahiti. *Radiocarbon*, 40(3):1085–1092.

Bard, E., B. Hamelin, R. G. Fairbanks, and A. Zindler (1990). Calibration of the ^{14}C timescale over the past 30,000 years using mass spectrometric U-Th ages from Barbados corals. *Nature*, 345(6274):405–410. doi:10.1038/345405a0.

Bard, E., G. Ménot, F. Rostek, L. Licari, P. Böning, R. L. Edwards, H. Cheng, Y. Wang, and T. J. Heaton (2013). Radiocarbon Calibration/Comparision Records Based on Marine Sediments From The Pakistan and Iberian Margins. *Radiocarbon*, 55(4):1999–2019.

Bard, E., G. Ménot-Combes, F. Rostek, and G. Menot-Combes (2004). Present status of radiocarbon calibration and comparison records based on Polynesian corals and Iberian Margin sediments. *Radiocarbon*, 46(3):1189–1202.

Barker, S., M. Greaves, and H. Elderfield (2003). A study of cleaning procedures used for foraminiferal Mg/Ca paleothermometry. *Geochemistry, Geophysics, Geosystems*, 4(9). doi:10.1029/2003GC000559.

Bauer, J. and E. R. M. Druffel (1998). Ocean margins as a significant source of organic matter to the deep open ocean. *Nature*, 392:20–23.

Beck, J. W., D. A. Richards, R. L. Edwards, B. W. Silverman, P. L. Smart, D. J. Donahue, S. Hererra-Osterheld, G. S. Burr, L. Calsoyas, A. J. T. Jull, and D. Biddulph (2001). Extremely large variations of atmospheric ^{14}C concentration during the last glacial period. *Science*, 292(5526):2453–2458. doi:10.1126/science.1056649.

Becker-Heidmann, P., L. Liang-wu, and H.-W. Scharpenseel (1988). Radiocarbon Dating of Organic Matter Fractions of a Chinese Mollisol. *Zeitschrift für Pflanzenernährung und Bodenkunde*, 151(1):37–39. doi:10.1002/jpln.19881510109.

Beer, J., F. Joos, C. Lukasczyk, W. Mende, J. Rodriguez, U. Siegenthaler, and R. Stellmacher (1993). 10Be as an indicator of solar variability and climate. In E. Nesme-Ribes, editor, *The Solar Engine and Its Influence on Terrestrial Atmosphere and Climate*, 221–233. Springer Berlin Heidelberg, Berlin, Heidelberg. ISBN 978-3-642-79259-5. doi:10.1007/978-3-642-79257-1.

Behl, R. (1995). Sedimentary Facies And Sedimentology Of The Late Quaternary Santa Barbara Basin, SITE 893. *Proceedings of the Ocean Drilling Program, Scientific Results*, 146(2).

Benavente, J., I. Vadillo, F. Carrasco, a. Soler, C. Liñán, and F. Moral (2010). Air Carbon Dioxide Contents in the Vadose Zone of a Mediterranean Karst. *Vadose Zone Journal*, 9(1):126. doi:10.2136/vzj2009.0027.

Bischoff, J. L. and W. S. Fyfe (1968). Catalysis, inhibition, and the calcite-aragonite problem; [Part] 1, The aragonite-calcite transformation. *American Journal of Science*, 266(2):65–79. doi:10.2475/ajs.266.2.65.

Blyth, A. J., P. Farrimond, and M. Jones (2006). An optimised method for the extraction and analysis of lipid biomarkers from stalagmites. *Organic Geochemistry*, 37(8):882–890. doi:10.1016/j.orggeochem.2006.05.003.

Boden, T. and B. Andres (2013). Global CO_2 Emissions from Fossil-Fuel Burning, Cement Manufacture, and Gas Flaring: 1751-2010.

Breecker, D. O., A. E. Payne, J. Quade, J. L. Banner, C. E. Ball, K. W. Meyer, and B. D. Cowan (2012). The sources and sinks of CO_2 in caves under mixed woodland and grassland vegetation. *Geochimica et Cosmochimica Acta*, 96:230–246. doi:10.1016/j.gca.2012.08.023.

Broecker, W. S. (2009). The Mysterious ^{14}C decline. *Radiocarbon*, 51(1):105–119.

Broecker, W. S. and S. Barker (2007). A 190 per mil drop in atmosphere's Δ^{14}C during the "Mystery Interval" (17.5 to 14.5 kyr). *Earth and Planetary Science Letters*, 256(1-2):90–99. doi:10.1016/j.epsl.2007.01.015.

Bronk Ramsey, C. (2008). Deposition models for chronological records. *Quaternary Science Reviews*, 27(1-2):42–60. doi:10.1016/j.quascirev.2007.01.019.

Bronk Ramsey, C., R. a. Staff, C. L. Bryant, F. Brock, H. Kitagawa, J. van der Plicht, G. Schlolaut, M. H. Marshall, A. Brauer, H. F. Lamb, R. L. Payne, P. E. Tarasov, T. Haraguchi, K. Gotanda, H. Yonenobu, Y. Yokoyama, R. Tada, and T. Nakagawa (2012). A complete terrestrial radiocarbon record for 11.2 to 52.8 kyr B.P. *Science*, 338(6105):370–374. doi:10.1126/science.1226660.

Bryan, S. P., T. M. Marchitto, and S. J. Lehman (2010). The release of ^{14}C-depleted carbon from the deep ocean during the last deglaciation: Evidence from the Arabian Sea. *Earth and Planetary Science Letters*, 298(1-2):244–254. doi:10.1016/j.epsl.2010.08.025.

Burr, G. S., J. W. Beck, F. W. Taylor, J. Récy, R. L. Edwards, G. Cabioch, T. Correge, D. J. Donahue, and J. M. O'Malley (1998). High-resolution radiocarbon calibration between 11,700 and 12,400 Calendar Years BP Derived From ^{230}Th Ages of Corals from Espiritu Santo Island, Vanuatu. *Radiocarbon*, 40(3):1093–1105.

Burr, G. S., C. Galang, F. Taylor, C. Gallup, R. L. Edwards, K. Cutler, and B. Quirk (2004). Radiocarbon results from a 13-kyr BP coral from the Huon Peninsula, Papua New Guinea. *Radiocarbon*, 46(3):1211–1224.

Burton, E. A. and L. M. Walter (1987). Relative precipitation rates of aragonite and Mg calcite from seawater: Temperature or carbonate ion control? *Geology*, 15(2):111.

Butzin, M., M. Prange, and G. Lohmann (2005). Radiocarbon simulations for the glacial ocean: The effects of wind stress, Southern Ocean sea ice and Heinrich events. *Earth and Planetary Science Letters*, 235(1-2):45–61. doi:10.1016/j.epsl.2005.03.003.

Cannariato, K. G., J. P. Kennett, and R. J. Behl (1999). Biotic response to late Quaternary rapid climate switches in Santa Barbara Basin : Ecological and evolutionary implications. *Geology*, 27:63–66.

Cerling, T. E. and J. M. Harris (1999). Carbon isotope fractionation between diet and bioapatite in ungulate mammals and implications for ecological and paleoecological studies. *Oecologia*, 120(3):347–363. doi:10.1007/s004420050868.

Chen, X., C. Zhu, C. Ma, and C. Fan (2008). Sensitivity of pollen factors in the climate transfer function. *Chinese Science Bulletin*, 53(S1):50–57. doi:10.1007/s11434-008-5002-y.

Cheng, H., R. L. Edwards, W. S. Broecker, G. H. Denton, X. Kong, Y. Wang, R. Zhang, and X. Wang (2009a). Ice age terminations. *Science*, 326(5950):248–52. doi:10.1126/science.1177840.

Cheng, H., R. L. Edwards, J. Hoff, C. Gallup, D. A. Richards, and Y. Asmerom (2000). The half-lives of uranium-234 and thorium-230. *Chemical Geology*, 169(1-2):17–33. doi:10.1016/S0009-2541(99)00157-6.

Cheng, H., R. L. Edwards, X. F. Wang, J. Woodhead, J. Hellstrom, Y. J. Wang, and X. G. Kong (2008). A new generation of ^{230}Th dating techniques: Tests of precision and accuracy. *Geochimica et Cosmochimica Acta Supplement*, 72:157.

Cheng, H., D. Fleitmann, R. L. Edwards, X. Wang, F. W. Cruz, a. S. Auler, A. Mangini, Y. Wang, X. Kong, S. J. Burns, and A. Matter (2009b). Timing and structure of the 8.2 kyr B.P. event inferred from ^{18}O records of stalagmites from China, Oman, and Brazil. *Geology*, 37(11):1007–1010. doi:10.1130/G30126A.1.

Cutler, K. B., S. C. Gray, G. S. Burr, R. L. Edwards, F. W. Taylor, G. Cabioch, J. W. Beck, H. Cheng, and J. Moore (2004). Radiocarbon calibration and comparison to 50 kyr BP with paired C-14 and Th-230 dating of corals from Vanuatu and Papua New Guinea. *Radiocarbon*, 46(3):1127–1160.

Davidson, E. A. and I. A. Janssens (2006). Temperature sensitivity of soil carbon decomposition and feedbacks to climate change. *Nature*, 440(7081):165–73. doi:10.1038/nature04514.

Dayem, K. E., P. Molnar, D. S. Battisti, and G. H. Roe (2010). Lessons learned from oxygen isotopes in modern precipitation applied to interpretation of speleothem records of paleoclimate from eastern Asia. *Earth and Planetary Science Letters*, 295(1-2):219–230. doi:10.1016/j.epsl.2010.04.003.

De Pol-Holz, R., L. D. Keigwin, J. R. Southon, D. Hebbeln, and M. Mohtadi (2010). No signature of abyssal carbon in intermediate waters off Chile during deglaciation. *Nature Geoscience*, 3(3):192–195. doi:10.1038/ngeo745.

Deininger, M., J. Fohlmeister, D. Scholz, and A. Mangini (2012). Isotope disequilibrium effects: The influence of evaporation and ventilation effects on the carbon and oxygen isotope composition of speleothems - A model approach. *Geochimica et Cosmochimica Acta*, 96:57–79. doi:10.1016/j.gca.2012.08.013.

Denton, G. H., T. V. Lowell, C. J. Heusser, P. I. Moreno, G. Andersen, L. E. Heusser, C. Schlüchter, and D. R. Marchant (1999). Interhemispheric Linkage of Paleocliamte During the Last Glaciation. *Geografiska Annaler Series A*, 81(2):107–153.

Ding, P., C. D. Shen, N. Wang, W. X. Yi, X. F. Ding, D. P. Fu, K. X. Liu, and L. P. Zhou (2010). Turnover Rate Of Soil Organic Matter And Origin Of Soil $^{14}CO_2$ In Deep Soil

From A Subtropical Forest In Dinghushan Biosphere Reserve, South China. *Radiocarbon*, 52(2):1422–1434.

Dorale, J. A., J. R. Southon, and R. L. Edwards (2008). High-resolution radiocarbon calibration from 30-50 ka based on stalagmite ^{14}C and ^{230}Th ages. *Geochimica et Cosmochimica Acta*, 72(12):A224.

Dorr, H. and K. O. Münnich (1986). Annual varitions of the ^{14}C Content of Soil CO_2. *Radiocarbon*, 28(2A):338–345.

Drenzek, N. J., K. A. Hughen, D. B. Montlucon, J. R. Southon, G. M. dos Santos, E. R. M. Druffel, L. Giosan, and T. I. Eglinton (2009). A new look at old carbon in active margin sediments. *Geology*, 37(3):239–242. doi:10.1130/G25351A.1.

Durand, N., P. Deschamps, E. Bard, B. Hamelin, G. Camoin, A. L. Thomas, G. M. Henderson, Y. Yokoyama, and H. Matsuzaki (2013). Comparison of ^{14}C and U-Th Ages in Corals from IODP #310 cores offshore Tahiti. *Radiocarbon*, 55(4):1947–1974.

Edwards, R. L., J. W. Beck, G. S. Burr, D. J. Donahue, J. M. Chappell, A. L. Bloom, E. R. M. Druffel, and F. W. Taylor (1993). A Large Drop in Atmospheric ^{14}C/^{12}C and Reduced Melting in the Younger Dryas, Documented with ^{230}Th Ages of Corals. *Science*, 260(5110):962–968.

Edwards, R. L., J. H. Chen, and G. J. Wasserburg (1987). 238U, ^{234}U, ^{230}Th, 232Th systematics and the precise measurement of time over the past 500,000 years. *Earth and Planetary Science Letters*, 81:175–192.

English, N. B., N. G. McDowell, C. D. Allen, and C. Mora (2011). The effects of α-cellulose extraction and blue-stain fungus on retrospective studies of carbon and oxygen isotope variation in live and dead trees. *Rapid Communications in Mass Spectrometry*, 25(20):3083–3090. doi:10.1002/rcm.5192.

Etheridge, D. M., L. P. Steele, R. L. Langenfelds, R. J. Francey, J.-M. Barnola, and V. I. Morgan (1996). Natural and anthropogenic changes in atmospheric CO_2 over the last 1000 years from air in Antarctic ice and firn. *Journal of Geophysical Research*, 101:4115–4128.

Fairbanks, R. G., R. A. Mortlock, T.-C. Chiu, L. Cao, A. Kaplan, T. P. Guilderson, T. W. Fairbanks, A. L. Bloom, P. M. Grootes, and M.-J. Nadeau (2005). Radiocarbon calibration curve spanning 0 to 50,000 years BP based on paired ^{230}Th/^{234}U/238U and ^{14}C dates on pristine corals. *Quaternary Science Reviews*, 24(16-17):1781–1796. doi:10.1016/j.quascirev.2005.04.007.

Fairchild, I. J., C. L. Smith, A. Baker, L. Fuller, C. Spötl, D. P. Mattey, and F. McDermott (2006). Modification and preservation of environmental signals in speleothems. *Earth-Science Reviews*, 75(1-4):105–153. doi:10.1016/j.earscirev.2005.08.003.

Finkel, R. C. and K. Nishiizumi (1997). Beryllium 10 concentrations in the Greenland Ice Sheet Project 2 ice core from 3-40 ka. *Journal of Geophysical Research*, 102(C12):699–706.

Fohlmeister, J., B. Kromer, and A. Mangini (2011a). The Influence Of Soil Organic Matter Age Spectrum On The Reconstruction Of Atmospheric ^{14}C Levels Via Stalagmites. *Radiocarbon*, 53(1):99–115.

Fohlmeister, J., D. Scholz, B. Kromer, and A. Mangini (2011b). Modelling carbon isotopes of carbonates in cave drip water. *Geochimica et Cosmochimica Acta*, 75(18):5219–5228. doi:10.1016/j.gca.2011.06.023.

Fohlmeister, J., A. Schröder-Ritzrau, and C. Spötl (2010). The Influences Of Hydrology On The Radiogenic And Stable Carbon Isotope Composition Of Cave Drip Wter, Grotta Di Ernesto (Italy). *Radiocarbon*, 52(4):1529–1544.

Frisia, S. and A. Borsato (2010). Chapter 6: Karst. In A. M. Alonso-Zarza and L. H. Tanner, editors, *Carbonates in Continental Settings: Facies, Environments, and Processes*, volume 61, 61, 269–318. Elsevier. doi:10.1016/S0070-4571(09)06106-8.

Frisia, S., A. Borsato, I. J. Fairchild, F. McDermott, and E. M. Selmo (2002). Aragonite-Calcite Relationships in Speleothems (Grotte De Clamouse, France): Environment, Fabrics, and Carbonate Geochemistry. *Journal of Sedimentary Research*, 72(5):687–699. doi: 10.1306/020702720687.

Frisia, S., I. J. Fairchild, J. Fohlmeister, R. Miorandi, C. Spötl, and A. Borsato (2011). Carbon mass-balance modelling and carbon isotope exchange processes in dynamic caves. *Geochimica et Cosmochimica Acta*, 75(2):380–400. doi:10.1016/j.gca.2010.10.021.

Gabrovšek, F., B. Menne, and W. Dreybrodt (2000). A model of early evolution of karst conduits affected by subterranean CO_2 sources. *Environmental Geology*, 39(6):531–543.

Galbraith, E. D., S. L. Jaccard, T. F. Pedersen, D. M. Sigman, G. H. Haug, M. Cook, J. R. Southon, and R. Francois (2007). Carbon dioxide release from the North Pacific abyss during the last deglaciation. *Nature*, 449(7164):890–3. doi:10.1038/nature06227.

Genty, D. and M. Massault (1997). Bomb ^{14}C Recorded in laminated Speleothems: Calculations of Dead Carbon Proportion. *Radiocarbon*, 39(1):33–48.

Genty, D. and M. Massault (1999). Carbon transfer dynamics from bomb-^{14}C and δ^{13}C time series of a laminated stalagmite from SW France - modelling and comparison with other stalagmite records. *Geochimica et Cosmochimica Acta*, 63(10):1537–1548. doi:10.1016/S0016-7037(99)00122-2.

Genty, D., M. Massaultl, M. Gilmour, A. Baker, S. Verheyden, and E. Kepens (1999). Calculation of past Dead Carbon Proportion and variablity by the comparision of AMS ^{14}C and TIMS U/Th Ages on Two Holocen Stalagmites. *Radiocarbon*, 41(3).

Genty, D., B. Vokal, and B. Obelić (1998). Bomb ^{14}C time history recorded in two modern stalagmites - importance for soil organic matter dynamics and bomb ^{14}C distribution over continents. *Earth and Planetary Science Letters*, 160:795–809.

Gill, I., J. J. Olson, and D. K. Hubbard (1995). Corals, paleotemperature records, and the aragonite-calcite transformation. *Geology*, 23(4):333. doi:10.1130/0091-7613(1995)023⟨0333:CPRATA⟩2.3.CO;2.

Graham, D. W., B. H. Corliss, M. L. Bender, and L. D. Keigwin (1981). Carbon and oxygen isotopic disequilibria of recent deep-sea benthic foraminifera. *Marine Micropaleontology*, 6:483–497.

Green, J. (1963). *Methods in carbohydrate chemistry*. Academic Press, New York. ISBN 9780127462066.

Griffiths, M., J. Fohlmeister, R. Drysdale, Q. Hua, K. R. Johnson, J. Hellstrom, M. Gagan, and J.-X. Zhao (2012). Hydrological control of the dead carbon fraction in a Holocene tropical speleothem. *Quaternary Geochronology*, 14:81–93. doi:10.1016/j.quageo.2012.04.001.

Grootes, P. and M. Stuiver (1997). Oxygen 18/16 variability in Greenland snow and ice with 10ˆ3- to 10ˆ5-year time resolution. *Journal of Geophysical Research*, 102.

Gulley, J., J. Martin, and P. Moore (2014). Vadose CO_2 gas drives dissolution at water tables in eogenetic karst aquifers more than mixing dissolution. *Earth Surface Processes and Landforms*. doi:10.1002/esp.3571.

Hendry, M. J., J. R. Lawrence, B. N. Zanyk, and R. Kirkland (1993). Microbial Production of CO_2 in Unsaturated Geologic Media in a Geologic Media in a Mesoscale Model. *Water Resources Research*, 29(4):973–984.

Hendry, M. J. and L. I. Wassenaar (2005). Origin and migration of dissolved organic carbon fractions in a clay-rich aquitard: ^{14}C and $\delta^{13}C$ evidence. *Water Resources Research*, 41(2):n/a–n/a. doi:10.1029/2004WR003157.

Hendy, C. (1971). The isotopic geochemistry of speleothems - I. The calculation of the effects of different modes of formation on the isotopic composition of speleothems and their applicability as palaeoclimatic indicators. *Geochimica et Cosmochimica Acta*, 35(8):801–824. doi:10.1016/0016-7037(71)90127-X.

Hendy, I. L., J. P. Kennett, E. B. Roark, and B. L. Ingram (2002). Apparent synchroneity of submillennial scale climate events between Greenland and Santa Barbara Basin , California from 30 - 10 ka. *Quaternary Science Reviews*, 21:1167–1184.

Hill, T. M., J. P. Kennett, D. L. Valentine, Z. Yang, C. M. Reddy, R. K. Nelson, R. J. Behl, C. Robert, and L. Beaufort (2006). Climatically driven emissions of hydrocarbons from marine sediments during deglaciation. *Proceedings of the National Academy of Sciences*, 103(37):13570–4. doi:10.1073/pnas.0601304103.

Hobley, E., G. R. Willgoose, S. Frisia, and G. Jacobsen (2014). Stability and storage of soil organic carbon in a heavy-textured Karst soil from south-eastern Australia. *Soil Research*. doi:10.1071/SR13296.

Hodge, E., J. McDonald, M. Fischer, D. Redwood, Q. Hua, V. A. Levchenko, R. Drysdale, C. Waring, and D. Fink (2011). Using the ^{14}C bomb pulse to date young speleothems. *Radiocarbon*, 53(2):345–357.

Hoffmann, D. L., J. W. Beck, D. A. Richards, P. L. Smart, J. S. Singarayer, T. Ketchmark, and C. J. Hawkesworth (2010). Towards radiocarbon calibration beyond 28ka using speleothems from the Bahamas. *Earth and Planetary Science Letters*, 289(1-2):1–10. doi: 10.1016/j.epsl.2009.10.004.

Hogg, A. G., Q. Hua, P. G. Blackwell, M. Niu, C. E. Buck, T. P. Guilderson, T. J. Heaton, J. G. Palmer, P. J. Reimer, R. W. Reimer, C. S. M. Turney, and S. R. H. Zimmerman (2013a). SHCal13 Southern Hemisphere Calibration, 0-50,000 Years Cal BP. *Radiocarbon*, 55(4):1889–1903.

Hogg, A. G., C. S. M. Turney, J. G. Palmer, J. R. Southon, B. Kromer, C. B. Ramsey, G. Boswijk, P. Fenwick, A. L. Noronha, R. Staff, M. Friedrich, L. Reynard, D. Guetter, L. Wacker, and R. Jones (2013b). The New Zealand Kauri (Agathis Australis) Research Project: A Radiocarbon Dating Intercomparison Of Younger Dryas Wood And Implications For IntCal13. *Radiocarbon*, 55(2).

Holsten, J., L. D. Stott, and W. Berelson (2004). Reconstructing benthic carbon oxidation rates using δ^{13}C of benthic foraminifers. *Marine Micropaleontology*, 53(1-2):117–132. doi: 10.1016/j.marmicro.2004.05.006.

Hu, C., G. Henderson, J. Huang, Z. Chen, and K. R. Johnson (2008a). Report of a three-year monitoring programme at Heshang Cave , Central China. *International Journal of Speleology*, 37(3):143–151.

Hu, C., G. M. Henderson, J. Huang, S. Xie, Y. Sun, and K. R. Johnson (2008b). Quantification of Holocene Asian monsoon rainfall from spatially separated cave records. *Earth and Planetary Science Letters*, 266(3-4):221–232. doi:10.1016/j.epsl.2007.10.015.

Hua, Q., M. Barbetti, D. Fink, K. F. Kaiser, M. Friedrich, B. Kromer, V. a. Levchenko, U. Zoppi, A. M. Smith, F. Bertuch, and K. Felix (2009). Atmospheric ^{14}C variations derived from tree rings during the early Younger Dryas. *Quaternary Science Reviews*, 28(25-26):2982–2990. doi:10.1016/j.quascirev.2009.08.013.

Hua, Q., M. Barbetti, and A. Rakowski (2013). Atmospheric radiocarbon for the period 1950-2010. *Radiocarbon*, 55(4):2059–2072.

Huang, X., J. Cui, Y. Pu, J. Huang, and A. J. Blyth (2008). Identifying "free" and "bound" lipid fractions in stalagmite samples: An example from Heshang Cave, Southern China. *Applied Geochemistry*, 23(9):2589–2595. doi:10.1016/j.apgeochem.2008.05.008.

Hughen, K. A., S. Lehman, J. R. Southon, J. Overpeck, O. Marchal, C. Herring, and J. Turnbull (2004). ^{14}C activity and global carbon cycle changes over the past 50,000 years. *Science*, 303(5655):202–7. doi:10.1126/science.1090300.

Hughen, K. A., J. R. Southon, S. Lehman, C. Bertrand, and J. Turnbull (2006). Marine-derived ^{14}C calibration and activity record for the past 50,000 years updated from the Cariaco Basin. *Quaternary Science Reviews*, 25(23-24):3216–3227. doi:10.1016/j.quascirev.2006.03.014.

Hughen, K. A., J. R. Southon, S. J. Lehman, and J. T. Overpeck (2000). Synchronous Radiocarbon and Climate Shifts During the Last Deglaciation. *Science*, 290(5498):1951–1954. doi:10.1126/science.290.5498.1951.

Hwang, J., E. R. M. Druffel, and J. E. Bauer (2006). Incorporation of aged dissolved organic carbon (DOC) by oceanic particulate organic carbon (POC): An experimental approach using natural carbon isotopes. *Marine Chemistry*, 98(2-4):315–322. doi:10.1016/j.marchem.2005.10.008.

Hwang, J., E. R. M. Druffel, and T. Komada (2005). Transport of organic carbon from the California coast to the slope region: A study of Δ^{14}C and δ^{13}C signatures of organic compound classes. *Global Biogeochemical Cycles*, 19(2). doi:10.1029/2004GB002422.

Ingram, B. L. and J. P. Kennett (1995). Radiocarbon Chronology and Planktonic-Benthic Foraminiferal ^{14}C Age Differences in Santa Barbara Basin Sediments, Hole 893A. *Proceedings of the Ocean Drilling Program, Scientific Results*, 146(2):19–27.

Ingram, B. L. and J. R. Southon (1996). Reservoir ages in Eastern Pacific coastal and estuarine water. *Radiocarbon*, 38(3):573–582.

Johnson, K. R., C. Hu, N. Belshaw, and G. Henderson (2006). Seasonal trace-element and stable-isotope variations in a Chinese speleothem: The potential for high-resolution paleomonsoon reconstruction. *Earth and Planetary Science Letters*, 244(1-2):394–407. doi:10.1016/j.epsl.2006.01.064.

Joussaume, S., K. E. Taylor, P. Braconnot, J. F. B. Mitchell, J. E. Kutzbach, S. P. Harrison, I. C. Prentice, A. J. Broccoli, A. Abe-Ouchi, P. J. Bartlein, C. Bonfils, B. Dong, J. Guiot, K. Herterich, C. D. Hewitt, D. Jolly, J. W. Kim, A. Kislov, A. Kitoh, M. F. Loutre, V. Masson, B. McAvaney, N. McFarlane, N. de Noblet, W. R. Peltier, J. Y. Peterschmitt, D. Pollard, D. Rind, J. F. Royer, M. E. Schlesinger, J. Syktus, S. Thompson, P. Valdes, G. Vettoretti, R. S. Webb, and U. Wyputta (1999). Monsoon changes for 6000 years ago: Results of 18 simulations from the Paleoclimate Modeling Intercomparison Project (PMIP). *Geophysical Research Letters*, 26(7):859–862. doi:10.1029/1999GL900126.

Kaiser, K. F., M. Friedrich, C. Miramont, B. Kromer, M. Sgier, M. Schaub, I. Boeren, S. Remmele, S. Talamo, F. Guibal, and O. Sivan (2012). Challenging process to make the Lateglacial tree-ring chronologies from Europe absolute - an inventory. *Quaternary Science Reviews*, 36:78–90. doi:10.1016/j.quascirev.2010.07.009.

Keller, C. K. (1991). Hydrogeochemistry of a Clayey Till - Sources of CO_2. *Water Resources Research*, 27(10):2555–2564.

Keller, C. K. and D. H. Bacon (1998). Soil respiration and georespiration distinguished by transport analyses of vadose CO_2, $^{13}CO_2$, and $^{14}CO_2$. *Global Biogeochemical Cycles*, 12(2):361–372.

Kennett, J. P., K. G. Cannariato, I. L. Hendy, and R. J. Behl (2000). Carbon Isotopic Evidence for Methane Hydrate Instability During Quaternary Interstadials. *Science*, 288(5463):128–133. doi:10.1126/science.288.5463.128.

Kindler, R., J. Siemens, K. Kaiser, D. C. Walmsley, C. Bernhofer, N. Buchmann, P. Cellier, W. Eugster, G. Gleixner, T. Gr?nwald, A. Heim, A. Ibrom, S. K. Jones, M. Jones, K. Klumpp, W. Kutsch, K. S. Larsen, S. Lehuger, B. Loubet, R. Mckenzie, E. Moors, B. Osborne, K. Pilegaard, C. Rebmann, M. Saunders, M. W. I. Schmidt, M. Schrumpf, J. Seyfferth, U. Skiba, J.-F. Soussana, M. a. Sutton, C. Tefs, B. Vowinckel, M. J. Zeeman, and M. Kaupenjohann (2011). Dissolved carbon leaching from soil is a crucial component of the net ecosystem carbon balance. *Global Change Biology*, 17(2):1167–1185. doi:10.1111/j.1365-2486.2010.02282.x.

Kitagawa, H. and J. van der Plicht (1998a). A 40,000-year varve chronology from Lake Suigetsu, Japan: Extension of the ^{14}C Calibration Curve. *Radiocarbon*, 40(1):505–515.

Kitagawa, H. and J. van der Plicht (1998b). Atmospheric Radiocarbon Calibration to 45,000 yr B.P.: Late Glacial Fluctuations and Cosmogenic Isotope Production. *Science*, 279(5354):1187–1190. doi:10.1126/science.279.5354.1187.

Kitagawa, H. and J. van der Plicht (2000). Atmospheric radiocarbon calibration beyond 11,900 cal BP from Lake Suigetsu laminated sediments. *Radiocarbon*, 42(3):369–380.

Komada, T., E. R. M. Druffel, and S. E. Trumbore (2004). Oceanic export of relict carbon by small mountainous rivers. *Geophysical Research Letters*, 31(7):L07504. doi:10.1029/2004GL019512.

Kong, X. G., Y. J. Wang, J. Y. Wu, H. Cheng, R. L. Edwards, and X. F. Wang (2005). Complicated responses of stalagmite $\delta^{13}C$ to climate change during the last glaciation from Hulu Cave, Nanjing, China. *Science in China Series D: Earth Sciences*, 48(12):2174. doi:10.1360/04yd0140.

Kromer, B., M. Friedrich, K. A. Hughen, K. F. Kaiser, S. Remmele, M. Schaub, and S. Talamo (2004). Late Glacial ^{14}C ages from a floating, 1382-ring pine chronology. *Radiocarbon*, 46(3):1203–1209.

Kvenvolden, K. A. and F. D. Hostettler (2004). *Geochemical Investigations in Earth and Space Science: A Tribute to Isaac R. Kaplan*, volume 9 of *The Geochemical Society Special Publications*. Elsevier. ISBN 9780444516473. doi:10.1016/S1873-9881(04)80016-6.

Laj, C., C. Kissel, A. Mazaud, E. Michel, R. Muscheler, and J. Beer (2002). Geomagnetic field intensity, North Atlantic Deep Water circulation and atmospheric $\Delta^{14}C$ during the last 50 kyr. *Earth and Planetary Science Letters*, 200(1-2):177–190. doi:10.1016/S0012-821X(02)00618-0.

Lane-Serff, G. F. and R. B. Pearce (2009). Modeling hydrography and marine sedimentation in the Cariaco Basin since the Last Glacial Maximum. *Journal of Geophysical Research*, 114(C4). doi:10.1029/2008JC005076.

Lawrence, J., M. Hendry, L. I. Wassenaar, J. Germida, G. Wolfaardt, N. Fortin, and C. Greer (2000). Distribution and Biogeochemical Importance of Bacterial Populations in a Thick Clay-Rich Aquitard System. *Microbial Ecology*, 40(4):273–291. doi:10.1007/s002480000073.

Leavitt, S. W. and S. R. Danzer (1993). Method for batch processing small wood samples to holocellulose for stable-carbon isotope analysis. *Analytical Chemistry*, 6:87–89.

Li, X., C. Wang, J. Huang, C. Hu, and S. Xie (2011). Seasonal variation of fatty acids from drip water in Heshang Cave, central China. *Applied Geochemistry*, 26(3):341–347. doi:10.1016/j.apgeochem.2010.12.007.

Linke, P. and G. Lutze (1993). Microhabitat preferences of benthic foraminifera-a static concept or a dynamic adaptation to optimize food acquisition? *Marine Micropaleontology*, 20(3-4):215–234. doi:10.1016/0377-8398(93)90034-U.

Liu, Y.-H., G. M. Henderson, C.-Y. Hu, a. J. Mason, N. Charnley, K. R. Johnson, and S.-C. Xie (2013). Links between the East Asian monsoon and North Atlantic climate during the 8,200 year event. *Nature Geoscience*, 6(2):117–120. doi:10.1038/ngeo1708.

Ma, C., C. Zhu, C. Zheng, C. Wu, Y. Guan, Z. Zhao, L. Huang, and R. Huang (2008). High-resolution geochemistry records of climate changes since late-glacial from Dajiuhu peat in Shennongjia Mountains, Central China. *Chinese Science Bulletin*, 53(S1):28–41. doi:10.1007/s11434-008-5007-6.

Ma, C., C. Zhu, C. Zheng, Q. Yin, and Z. Zhao (2009). Climate changes in East China since the Late-glacial inferred from high-resolution mountain peat humification records. *Science in China Series D: Earth Sciences*, 52(1):118–131. doi:10.1007/s11430-009-0003-5.

Magana, A. L., J. R. Southon, J. P. Kennett, E. B. Roark, M. Sarnthein, and L. D. Stott (2010). Resolving the cause of large differences between deglacial benthic foraminifera radiocarbon measurements in Santa Barbara Basin. *Paleoceanography*, 25(4):PA4102.

Marchitto, T. M., S. J. Lehman, J. D. Ortiz, J. Flückiger, and A. van Geen (2007). Marine radiocarbon evidence for the mechanism of deglacial atmospheric CO_2 rise. *Science*, 316(5830):1456–9. doi:10.1126/science.1138679.

Masiello, C. A. and E. R. M. Druffel (2001). Carbon isotope geochemistry of the Santa Clara River. *Global Biogeochemical Cycles*, 15(2):407–416.

Matsumoto, K. and Y. Yokoyama (2013). Atmospheric $\Delta^{14}C$ reduction in simulations of Atlantic overturning circulation shutdown. *Global Biogeochemical Cycles*, 27(2):296–304. doi:10.1002/gbc.20035.

Mattey, D. P., D. Lowry, J. Duffet, R. Fisher, E. Hodge, and S. Frisia (2008). A 53year seasonally resolved oxygen and carbon isotope record from a modern Gibraltar speleothem: Reconstructed drip water and relationship to local precipitation. *Earth and Planetary Science Letters*, 269(1-2):80–95. doi:10.1016/j.epsl.2008.01.051.

McCormac, F. G., P. J. Reimer, A. G. Hogg, T. G. Higham, M. L. Baillie, J. G. Palmer, and M. Stuiver (2002). Calibration of the radiocarbon time scale for the Southern Hemisphere; AD 1850-950. *Radiocarbon*, 44(3):641–651. doi:10.2458/azu_js_rc.44.4063.

McDermott, F., A. S. Jackson, A. Mangini, D. P. Mattey, and S. Frisia (2008). ^{14}C variability in two late Holocene stalagmites and the implications for climate forcing mechanisms. *Geochimica et Cosmochimica Acta*, 72(12):A612.

McGarry, S. F. and A. Baker (2000). Organic acid fluorescence: applications to speleothem palaeoenvironmental reconstruction. *Quaternary Science Reviews*, 19(11):1087–1101. doi: 10.1016/S0277-3791(99)00087-6.

McManus, J. F., R. Francois, J.-M. Gherardi, L. D. Keigwin, and S. Brown-Leger (2004). Collapse and rapid resumption of Atlantic meridional circulation linked to deglacial climate changes. *Nature*, 428(6985):834–7. doi:10.1038/nature02494.

Meissner, K. J., A. Schmittner, E. C. Wiebe, and A. J. Weaver (2002). Simulations of Heinrich Events in a coupled ocean-atmosphere-sea ice model. *Geophysical Research Letters*, 29(14):14–16. doi:10.1029/2001GL013514.

Merrill, R. B. and J. W. Beck (1995). The ODP Color Digital Imaging System: Color Logs of Quaternary Sediments From The Santa Barbara Basin, Sit 893. In *Proceedings of the Ocean Drilling Program, Scientific Results*, volume 146, 25–59.

Monnin, E., A. Indermühle, A. Dällenbach, J. Flückiger, B. Stauffer, T. F. Stocker, D. Raynaud, and J. M. Barnola (2001). Atmospheric CO_2 concentrations over the last glacial termination. *Science*, 291(5501):112–114. doi:10.1126/science.291.5501.112.

Morrill, C., J. T. Overpeck, and J. E. Cole (2003). A synthesis of abrupt changes in the Asian summer monsoon since the last deglaciation. *The Holocene*, 13(4):465–476. doi: 10.1191/0959683603hl639ft.

Murphy, E. M., J. A. Schramke, J. K. Fredrickson, H. W. Bledsoe, A. J. Francis, D. Sklarew, and J. C. Linehan (1992). The influence of microbial activity and sedimentary organic carbon on the isotope geochemistry of the Middendorf aquifer. *Water Resources Research*, 28(3):723–740.

Muscheler, R., B. Kromer, S. Björck, A. Svensson, M. Friedrich, K. F. Kaiser, and J. R. Southon (2008). Tree rings and ice cores reveal ^{14}C calibration uncertainties during the Younger Dryas. *Nature Geoscience*, 1(4):263–267. doi:10.1038/ngeo128.

Nakagawa, T., K. Gotanda, T. Haraguchi, T. Danhara, H. Yonenobu, A. Brauer, Y. Yokoyama, R. Tada, K. Takemura, R. a. Staff, R. Payne, C. B. Ramsey, C. Bryant,

F. Brock, G. Schlolaut, M. Marshall, P. Tarasov, H. Lamb, and C. Bronk Ramsey (2011). SG06, a fully continuous and varved sediment core from Lake Suigetsu, Japan: stratigraphy and potential for improving the radiocarbon calibration model and understanding of late Quaternary climate changes. *Quaternary Science Reviews*, 36:1–13. doi: 10.1016/j.quascirev.2010.12.013.

NGRIP Members (2004). High-resolution record of Northern Hemisphere climate extending into the last interglacial period. doi:10.1038/nature02805.

Noronha, A. L., K. R. Johnson, C. Hu, J. Ruan, J. R. Southon, and J. E. Ferguson (2014). Assessing influences on speleothem dead carbon variability over the Holocene: Implications for speleothem-based radiocarbon calibration. *Earth and Planetary Science Letters*, 394:20–29. doi:10.1016/j.epsl.2014.03.015.

Ogden, J., A. Wilson, C. Hendy, and R. M. Newnham (1992). The Late Quaternary history of kauri (*Agathis australis*) in New Zealand and its climatic significance. *Journal of Biogeography*, 19:611–622.

Ostlund, H. and M. Stuiver (1980). GEOSECS Pacific Radiocarbon. *Radiocarbon*, 22(1):25–53.

Pabich, W., I. Valiela, and H. Hemond (2001). Relationship between DOC concentration and vadose zone thickness and depth below water table in groundwater of Cape Cod, USA. *Biogeochemistry*, 247–268.

Palmer, J., A. Lorrey, C. S. M. Turney, A. Hogg, M. Baillie, K. Fifield, and J. Ogden (2006). Extension of New Zealand kauri (Agathis australis) tree-ring chronologies into Oxygen Isotope Stage (OIS) 3. *Journal of Quaternary Science*, 21(7):779–787. doi:10.1002/jqs.1075.

Peltier, W. R. and R. G. Fairbanks (2006). Global glacial ice volume and Last Glacial Maximum duration from an extended Barbados sea level record. *Quaternary Science Reviews*, 25(23-24):3322–3337. doi:10.1016/j.quascirev.2006.04.010.

Perrette, Y., J. Poulenard, A.-I. Saber, B. Fanget, S. Guittonneau, B. Ghaleb, and S. Garaudee (2008). Polycyclic Aromatic Hydrocarbons in stalagmites: Occurrence and use for analyzing past environments. *Chemical Geology*, 251(1-4):67–76. doi:10.1016/j.chemgeo.2008.02.013.

Peterson, L. C., G. H. Haug, K. A. Hughen, and U. Röhl (2000). Rapid Changes in the Hydrologic Cycle of the Tropical Atlantic During the Last Glacial. *Science*, 290(5498):1947–1951. doi:10.1126/science.290.5498.1947.

Peyraube, N., R. Lastennet, a. Denis, and P. Malaurent (2013). Estimation of epikarst air pCO_2 using measurements of water $\delta^{13}C_{TDIC}$, cave air pCO_2 and $\delta^{13}C_{CO_2}$. *Geochimica et Cosmochimica Acta*, 118:1–17. doi:10.1016/j.gca.2013.03.046.

Raisbeck, G. M., F. Yiou, M. Fruneau, J. M. Loiseaux, M. Lieuvin, and J. C. Ravel (1981). Cosmogenic 10Be/7Be as a probe of atmospheric transport porcesses. *Geophysical Research Letters*, 8(1):1015–1018.

Reimer, P. J., M. G. L. Baillie, E. Bard, A. Bayliss, J. W. Beck, P. G. Blackwell, C. B. Ramsey, C. E. Buck, G. S. Burr, R. L. Edwards, M. Friedrich, P. M. Grootes, T. P. Guilderson, I. Hajdas, T. J. Heaton, A. G. Hogg, K. A. Hughen, K. F. Kaiser, B. Kromer, F. G. McCormac, S. W. Manning, R. W. Reimer, D. A. Richards, J. R. Southon, S. Talamo, C. S. M. Turney, J. van der Plicht, C. E. Weyhenmeyer, C. Bronk Ramsey, and J. van der Plicht (2009). IntCal09 and Marine09 Radiocarbon Age Calibration Curves, 0-50,000 Years cal BP. *Radiocarbon*, 51(4):1111–1150.

Reimer, P. J., E. Bard, A. Bayliss, J. W. Beck, P. G. Blackwell, C. B. Ramsey, C. E. Buck, H. Cheng, R. L. Edwards, M. Friedrich, P. M. Grootes, T. P. Guilderson, H. Haflidason, I. Hajdas, C. Hatte, T. J. Heaton, D. L. Hoffmann, A. G. Hogg, K. A. Hughen, K. F. Kaiser, B. Kromer, S. W. Manning, M. Niu, R. W. Reimer, D. A. Richards, E. M. Scott, J. R. Southon, R. Staff, C. S. M. Turney, and J. van der Plicht (2013). IntCal13 and Marine13 Radiocarbon Age Calibration Curves 0-50,000 years cal BP. *Radiocarbon*, 55(4):1869–1887.

Richards, D. A. and J. A. Dorale (2003). Uranium-series Chronology and Environmental Applications of Speleothems. *Reviews in Mineralogy and Geochemistry*, 52(1):407–460. doi:10.2113/0520407.

Ritz, S. P., T. F. Stocker, and S. A. Müller (2008). Modeling the effect of abrupt ocean circulation change on marine reservoir age. *Earth and Planetary Science Letters*, 268(1-2):202–211. doi:10.1016/j.epsl.2008.01.024.

Robinson, L. F., J. F. Adkins, L. D. Keigwin, J. R. Southon, D. P. Fernandez, S.-L. Wang, and D. S. Scheirer (2005). Radiocarbon variability in the western North Atlantic during the last deglaciation. *Science*, 310(5753):1469. doi:10.1126/science.1114832.

Rodionov, S. N. (2004). A sequential algorithm for testing climate regime shifts. *Geophysical Research Letters*, 31(9):L09204. doi:10.1029/2004GL019448.

Roland, M., P. Serrano-Ortiz, A. S. Kowalski, Y. Goddéris, E. P. Sánchez-Cañete, P. Ciais, F. Domingo, S. Cuezva, S. Sanchez-Moral, B. Longdoz, D. Yakir, R. Van Grieken, J. Schott, C. Cardell, and I. A. Janssens (2013). Atmospheric turbulence triggers pronounced diel pattern in karst carbonate geochemistry. *Biogeosciences*, 10(7):5009–5017. doi:10.5194/bg-10-5009-2013.

Romanek, C. S., E. L. Grossman, and J. W. Morse (1992). Carbon isotopic fractionation in synthetic aragonite and calcite: Effects of temperature and precipitation rate. *Geochimica et Cosmochimica Acta*, 56(1):419–430. doi:10.1016/0016-7037(92)90142-6.

Rose, K. A., E. L. Sikes, T. P. Guilderson, P. Shane, T. M. Hill, R. Zahn, and H. J. Spero (2010). Upper-ocean-to-atmosphere radiocarbon offsets imply fast deglacial carbon dioxide release. *Nature*, 466(7310):1093–1097.

Rudzka, D., F. McDermott, L. M. Baldini, D. Fleitmann, A. Moreno, and H. Stoll (2011). The coupled δ^{13}C-radiocarbon systematics of three Late Glacial/early Holocene speleothems; insights into soil and cave processes at climatic transitions. *Geochimica et Cosmochimica Acta*, 75(15):4321–4339. doi:10.1016/j.gca.2011.05.022.

Rudzka-Phillips, D., F. McDermott, a. Jackson, and D. Fleitmann (2013). Inverse modelling of the ^{14}C bomb pulse in stalagmites to constrain the dynamics of soil carbon cycling at selected European cave sites. *Geochimica et Cosmochimica Acta*, 112:32–51. doi:10.1016/j.gca.2013.02.032.

Saliege, J. and J. Fontes (1984). Essai de détermination expérimentale du fractionnement des isotopes ^{13}C et ^{14}C du carbone au cours de processus naturels. *The International Journal of Applied Radiation and Isotopes*, 35(1):55–62. doi:10.1016/0020-708X(84)90132-7.

Sanchez-Cañete, E. P., P. Serrano-Ortiz, a. S. Kowalski, C. Oyonarte, and F. Domingo (2011). Subterranean CO_2 ventilation and its role in the net ecosystem carbon balance of a karstic shrubland. *Geophysical Research Letters*, 38(9). doi:10.1029/2011GL047077.

Santos, G., R. B. Moore, J. R. Southon, S. Griffin, E. Hinger, and D. Zhang (2007). AMS ^{14}C Sample preparation at the KCCAMS/UCI Facility: Status Report and Performance of Small Samples. *Radiocarbon*, 49(2):255–269.

Sarnthein, M., P. M. Grootes, J. P. Kennett, and M.-J. Nadeau (2007). ^{14}C Reservoir Ages Show Deglacial Changes in Ocean Currents and Carbon Cycle. In A. Schmittner, J. C. H. Chiang, and S. R. Hemming, editors, *Ocean Circulation: Mechanisms and Impacts-Past and Future Changes of Meridional Overturning*. American Geophysical Union. doi:10.1029/173GM13.

Scholz, D. and D. L. Hoffmann (2011). StalAge - An algorithm designed for construction of speleothem age models. *Quaternary Geochronology*, 6(3-4):369–382. doi:10.1016/j.quageo.2011.02.002.

Scholz, D., C. Mühlinghaus, and A. Mangini (2009). Modelling δ^{13}C and δ^{18}O in the solution layer on stalagmite surfaces. *Geochimica et Cosmochimica Acta*, 73(9):2592–2602. doi:10.1016/j.gca.2009.02.015.

Seidov, D. and M. Maslin (1999). North Atlantic deep water circulation collapse during Heinrich events. *Geology*, 27(1):23.

Sikes, E. L., C. R. Samson, T. P. Guilderson, and W. R. Howard (2000). Old radiocarbon ages in the southwest Pacific Ocean during the last glacial period and deglaciation. *Nature*, 405(6786):555–559. doi:10.1038/35014581.

Singarayer, J. S., D. A. Richards, A. Ridgwell, P. J. Valdes, W. E. N. Austin, and J. W. Beck (2008). An oceanic origin for the increase of atmospheric radiocarbon during the Younger Dryas. *Geophysical Research Letters*, 35(14):1–6. doi:10.1029/2008GL034074.

Sinha, A., K. G. Cannariato, L. D. Stott, H.-C. Li, C.-F. You, H. Cheng, R. L. Edwards, and I. B. Singh (2005). Variability of Southwest Indian summer monsoon precipitation during the Bølling-Ållerød. *Geology*, 33(10):813. doi:10.1130/G21498.1.

Six, J. and J. D. Jastrow (2002). Organic Matter Turnover. In *Encyclopedia of Soil Science*, 936–942.

Skinner, L. C. (2008). Revisiting the absolute calibration of the Greenland ice-core age-scales. *Climate of the Past Discussions*, 4(3):791–807. doi:10.5194/cpd-4-791-2008.

Skinner, L. C., S. Fallon, C. Waelbroeck, E. Michel, and S. Barker (2010). Ventilation of the deep Southern Ocean and deglacial CO_2 rise. *Science*, 328(5982):1147–1151. doi:10.1126/science.1183627.

Smith, C. L., I. J. Fairchild, C. Spötl, S. Frisia, A. Borsato, S. G. Moreton, and P. M. Wynn (2009). Chronology building using objective identification of annual signals in trace element profiles of stalagmites. *Quaternary Geochronology*, 4(1):11–21. doi:10.1016/j.quageo.2008.06.005.

Southon, J. R. (2007). Graphite reactor memory - Where is it from and how to minimize it? *Nuclear Instruments and Methods in Physics Research Section B: Beam Interactions with Materials and Atoms*, 259(1):288–292. doi:10.1016/j.nimb.2007.01.251.

Southon, J. R. (2011). Are the Fractionation Corrections Correct: Are the isotopic shifts for $^{14}C/^{12}C$ ratios in physical processes and chemical reactions really twice those for $13/^{12}C$? *Radiocarbon*, 53(4):691–704.

Southon, J. R. and A. L. Magana (2010). A Comparison Of Cellulose Extraction And ABA Pretreatment Methods For AMS ^{14}C Dating Of Ancient Wood. *Radiocarbon*, 52(3):1371–1379.

Southon, J. R., A. L. Noronha, H. Cheng, R. L. Edwards, and Y. Wang (2012). A high-resolution record of atmospheric ^{14}C based on Hulu Cave speleothem H82. *Quaternary Science Reviews*, 33:32–41. doi:10.1016/j.quascirev.2011.11.022.

Staff, R., C. Bronk Ramsey, and T. Nakagawa (2010). A re-analysis of the Lake Suigetsu terrestrial radiocarbon calibration dataset. *Nuclear Instruments and Methods in Physics Research Section B: Beam Interactions with Materials and Atoms*, 268(7-8):960–965. doi:10.1016/j.nimb.2009.10.074.

Stott, L. D., T. Bunn, M. Prokopenko, C. Mahn, J. Gieskes, and J. M. Bernhard (2002). Does the oxidation of methane leave an isotopic fingerprint in the geologic record? *Geochemistry, Geophysics, Geosystems*, 3(2). doi:10.1029/2001GC000196.

Stott, L. D., J. R. Southon, A. Timmermann, and A. Koutavas (2009). Radiocarbon age anomaly at intermediate water depth in the Pacific Ocean during the last deglaciation. *Paleoceanography*, 24(2):1–10. doi:10.1029/2008PA001690.

Stuiver, M. and H. A. Polach (1977). Reporting of C-14 data. *Radiocarbon*, 19(3):355–363.

Stuiver, M. and P. D. Quay (1980). Changes in atmospheric carbon-14 attributed to a variable sun. *Science*, 207(4426):11–9. doi:10.1126/science.207.4426.11.

Suess, A. H. E. and T. W. Linick (1990). The ^{14}C record in bristlecone pine wood of the past 8000 years based on the dendrochronology of the late C . W . Ferguson. *Philosophical Transactions of the Royal Society of London*, 330:430–412.

Sun, X. and X. Li (1999). A pollen record of the last 37 ka in deep sea core 17940 from the northern slope of the South China Sea. *Marine Geology*, 156(1-4):227–244. doi: 10.1016/S0025-3227(98)00181-9.

Sundqvist, H. S., K. Holmgren, J. Fohlmeister, Q. Zhang, M. B. Matthews, C. Spötl, and H. Körnich (2013). Evidence of a large cooling between 1690 and 1740 AD in southern Africa. *Scientific Reports*, 3:1767. doi:10.1038/srep01767.

Tegen, I. and H. Dorr (1996). ^{14}C measurements of soil organic matter, soil CO_2 and dissolved organic carbon (1987-1992). *Radiocarbon*, 38(2):247–251.

Tremaine, D. M., P. N. Froelich, and Y. Wang (2011). Speleothem calcite farmed in situ: Modern calibration of δ^{18}O and δ^{13}C paleoclimate proxies in a continuously-monitored natural cave system. *Geochimica et Cosmochimica Acta*, 75(17):4929–4950. doi:10.1016/j.gca.2011.06.005.

Trumbore, S. E. (1993). Comparison of carbon dynamics in tropical and temperate soils using radiocarbon measurements. *Global Biogeochemical Cycles*, 7(2):275–290.

Trumbore, S. E. (2000). Age of soil organic matter and soil respiration: Radiocarbon constraints on belowground C dynamics. *Ecological Applications*, 10(2):399–411.

Turney, C. S. M., L. Fifield, and J. Palmer (2007). Towards A Radiocarbon Calibration For Oxygen Isotope Stage 3 Using New Zealand Kauri (Agathis Australis). *Radiocarbon*, 49(2):447–457.

van Geen, A., R. G. Fairbanks, P. Dartnell, M. McGann, J. V. Gardner, and M. Kashgarian (1996). Ventilation changes in the northeast Pacific during the last deglaciation. *Paleoceanography*, 11(5):519–528.

Vellinga, M. and R. A. Wood (2002). Global climatic impacts of a collapse of the Atlantic thermohaline circulation. *Climatic Change*, 54:251–267. doi:10.1023/A:1016168827653.

Voelker, A. H. L., M. Sarnthein, P. M. Grootes, H. Erlenkeuser, C. Laj, A. Mazaud, M. Schleicher, and M.-J. Nadeau (1998). Correlation of marine ^{14}C ages from the Nordic Seas with the GISP2 isotope record: Implications for C-14 calibration beyond 25 ka BP. *Radiocarbon*, 40(1):517–534.

Waelbroeck, C., J. C. Duplessy, E. Michel, L. Labeyrie, D. Paillard, and J. Duprat (2001). The timing of the last deglaciation in North Atlantic climate records. *Nature*, 412(6848):724–727.

Wang, Y., H. Cheng, R. L. Edwards, Y. He, X. Kong, Z. An, J. Wu, M. J. Kelly, C. a. Dykoski, and X. Li (2005). The Holocene Asian monsoon: links to solar changes and North Atlantic climate. *Science*, 308(5723):854–7. doi:10.1126/science.1106296.

Wang, Y., H. Cheng, R. L. Edwards, X. Kong, X. Shao, S. Chen, J. Wu, X. Jiang, X. Wang, and Z. An (2008). Millennial- and orbital-scale changes in the East Asian monsoon over the past 224,000 years. *Nature*, 451(7182):1090–3. doi:10.1038/nature06692.

Wang, Y. J., H. Cheng, R. L. Edwards, Z. S. An, J. Y. Wu, C. C. Shen, and J. a. Dorale (2001). A high-resolution absolute-dated late Pleistocene Monsoon record from Hulu Cave, China. *Science*, 294(5550):2345–8. doi:10.1126/science.1064618.

Weyhenmeyer, C. E., S. J. Burns, D. Fleitmann, J. D. Kramers, A. Matter, H. N. Waber, and P. J. Reimer (2003). Changes in Atmospheric ^{14}C Between 55 and 42 ky BP Recorded in a Stalagmite From Socotra Island, Indian Ocean. *EOS Transactions AGU*, 84(46):Fall Meeting Supplement Abstract PP32B–0289.

Wood, B. D., C. K. Keller, and D. L. Johnston (1993). In Situ Measurement of Microbial Activity and Controls on Microbial CO_2 Production in the Unsaturated Zone. *Water Resources Research*, 29(3).

Wood, W. W. (1985). Origin of caves and other solution openings in the unsaturated (vadose) zone of carbonate rocks: A model. *Geology*, 13:822–824. doi:10.1130/0091-7613(1985)13⟨822.

Wood, W. W. and M. J. Petraitis (1984). Origin and Distribution of Carbon Dioxide in the Unsaturated Zone of the Southern High Plains of Texas. *Water Resources Research*, 20(9):1193–1208.

Wu, J. Y., Y. J. Wang, H. Cheng, and L. R. Edwards (2009). An exceptionally strengthened East Asian summer monsoon event between 19.9 and 17.1 ka BP recorded in a Hulu stalagmite. *Science in China Series D: Earth Sciences*, 52(3):360–368.

Xiao, J., Q. Xu, T. Nakamura, X. Yang, W. Liang, and Y. Inouchi (2004). Holocene vegetation variation in the Daihai Lake region of north-central China: a direct indication of the Asian monsoon climatic history. *Quaternary Science Reviews*, 23(14-15):1669–1679. doi:10.1016/j.quascirev.2004.01.005.

Xie, S., Y. Yi, J. Huang, C. Hu, Y. Cai, M. Collins, and A. Baker (2003). Lipid distribution in a subtropical southern China stalagmite as a record of soil ecosystem response to paleoclimate change. *Quaternary Research*, 60:340–347. doi:10.1016/j.qres.2003.07.010.

Xu, D., H. Lu, N. Wu, and Z. Liu (2010). 30 000-Year vegetation and climate change around the East China Sea shelf inferred from a high-resolution pollen record. *Quaternary International*, 227(1):53–60. doi:10.1016/j.quaint.2010.04.015.

Xu, X., S. E. Trumbore, S. Zheng, J. R. Southon, K. E. McDuffee, M. Luttgen, and J. C. Liu (2007). Modifying a sealed tube zinc reduction method for preparation of AMS graphite

targets: Reducing background and attaining high precision. *Nuclear Instruments and Methods in Physics Research Section B: Beam Interactions with Materials and Atoms*, 259(1):320–329. doi:10.1016/j.nimb.2007.01.175.

Yancheva, G., N. R. Nowaczyk, J. Mingram, P. Dulski, G. Schettler, J. F. W. Negendank, J. Liu, D. M. Sigman, L. C. Peterson, and G. H. Haug (2007). Influence of the intertropical convergence zone on the East Asian monsoon. *Nature*, 445(7123):74–7. doi:10.1038/nature05431.

Yuan, D.-X., H. Cheng, R. L. Edwards, C. A. Dykoski, M. J. Kelly, M. Zhang, J. Qing, Y. Lin, Y. Wang, J. Wu, J. A. Dorale, Z. An, and Y. Cai (2004). Timing, duration, and transitions of the last interglacial Asian monsoon. *Science*, 304(5670):575–578.

Zhao, C. and X. Chen (2010). Climatological Significance of Pollen Factors Revealed by Pollen-Climate Response Surface Functions in Dajiuhu, Shennongjia. *Acta Meteorologica Sinica*, 24(6):699–712.

Zhou, W., X. Yu, A. J. T. Jull, G. S. Burr, J. Xiao, X. Lu, and F. Xian (2004). High-resolution evidence from southern China of an early Holocene optimum and a mid-Holocene dry event during the past 18,000 years. *Quaternary Research*, 62(1):39–48. doi:10.1016/j.yqres.2004.05.004.

Zhu, C., C. Ma, S.-Y. Yu, L. Tang, W. Zhang, and X. Lu (2010). A detailed pollen record of vegetation and climate changes in Central China during the past 16000 years. *Boreas*, 39(1):69–76. doi:10.1111/j.1502-3885.2009.00098.x.

Zhu, C., C. Ma, W. Zhang, C. Zheng, L. Tang, X. Lu, K. Liu, and H. Chen (2006). Pollen Record From Dajiuhu Basin OF Shennongjia and Environmental Changes 15.753 Ka BP. *Quaternary Sciences*, 26(5):814–826.

Appendix A

A comparison of cellulose extraction and ABA pretreatment methods for AMS ^{14}C dating of ancient wood

A.1 Abstract

We have compared accelerator mass spectrometry (AMS) radiocarbon results on wood samples at or near the limit of ^{14}C dating, pretreated with a standard acid-base-acid (ABA) protocol, with those obtained from cellulose prepared from the same samples by several modifications of the Jayme-Wise cellulose extraction method (Green 1963). These tests were carried out to determine the most efficient way to ensure low backgrounds in ^{14}C measurements of well-preserved ancient wood samples.

A.2 Introduction

Cellulose is a long polysaccharide chain that does not translocate within a tree or exchange carbon with the atmosphere following its formation. Radiocarbon dates performed on cellulose alone are therefore thought to be a good measure of past atmospheric ^{14}C. A study by Gaudinski et al. (2005) indicated that the Jayme-Wise method produces extracts that are most chemically similar to pure cellulose as compared to other cellulose extraction methods

A batch processing protocol for Jayme-Wise cellulose extraction, developed by Leavitt and Danzer (1993) and commonly used for stable isotope measurements, involves 3 steps to isolate α-cellulose, each step followed by multiple water washes:

1. Cleaning: treatment in a Soxhlet system with toluene and ethanol to remove waxes, fats, oils, resins, and other compounds soluble in organic solvents.

2. Isolation of holocellulose: bleaching with a mixture of sodium chlorite and acetic acid to remove lignins.

3. Isolation of α-cellulose: treatment with strong base followed by a neutralizing acetic acid wash.

In ^{14}C studies, a major driver for using cellulose extractions has been the need to quantitatively remove resins, lignins, and other mobile wood fractions when studying ^{14}C in post-bomb and immediately pre-bomb wood. These fractions can contaminate tree rings with translocated carbon from subsequent years, which can have very different $\Delta^{14}C$ and may not be not completely removed by more conventional pretreatments, though the overall effect on measured $\Delta^{14}C$ values is relatively small (Cain and Suess 1976; Stuiver and Quay 1981).

Translocation effects are less important in studies of ancient wood where decadal or centennial scale $\Delta^{14}C$ changes were a few tens of per mil at most. In those contexts, cellulose extraction can be viewed as one of several strong ^{14}C pretreatment methods for removal of exogenous contamination from pollen and organic sediment fines (Brown et al. 1989; Gillespie 1990), charcoal (Bird et al. 1999), and wood (Santos et al. 2001), developed as more rigorous alternatives to the conventional acid-base-acid (ABA) or de Vries protocol (Stuiver and Quay 1981). The other techniques typically employ a variety of initial acid and base treatments rather than Soxhlet extractions, but a common feature of all of these methods is a very strong acid/oxidation step. Gillespie (1990) used dilute Schutze reagent (10% $KClO_3$ in 35% HNO_3); the ABOX method (Bird et al. 1999; Santos et al. 2001; Pigati et al. 2007) employs acid-dichromate solution (0.1M $K_2Cr_2O_7$ in 2M H_2SO_4); and acid chlorite or hypochlorite bleaching is used in cellulose extractions and in pollen preparation for ^{14}C dating (Brown et al. 1989).

As used in many labs today, ABA involves treatment at 60 °C-90 °C with 1N HCl and 1N NaOH, with the base washes repeated until the solutions remain clear. ABA pretreatment of wood has historically resulted in varied results and is sometimes viewed as inadequate, but comparisons of ABA with other pretreatment methods have not always involved the full rigor of the ABA protocol. For example, in radiometric labs where large volumes of reagents are required, a single long-duration base treatment may be employed (A Hogg, personal communication), as opposed to repeated washes that at least in principle might be more effective. Additionally, in some comparisons between ABA and ABOX (Bird et al. 1999; Santos et al. 2001) the acid and base treatments (AB) were carried out at room temperature (G M Santos, personal communication), and the final acid step of ABA–potentially important for removing any CO_2 absorbed under alkaline conditions–was sometimes omitted. In one study (Hatt et al. 2001) that was subsequently cited elsewhere as showing the levels of contamination remaining after ABA, the ABA was in fact deliberately carried out in a way

that would maximize the uptake of modern CO_2, in order to test subsequent decontamination procedures.

In this study, we compared several variations of the Jayme-Wise cellulose extraction method against ABA pretreatment to see whether rigorous ABA could produce ^{14}C backgrounds from wood samples comparable with those obtained from cellulose. In addition, we attempted to streamline the Jayme-Wise method and thus reduce processing times for wood samples for ^{14}C measurements, to eliminate the unnecessary exposure of samples to carbon-containing reagents, and to test cellulose extraction procedures that did not require specialized Soxhlet apparatus. This report reflects the current state of an ongoing study, and the methods described here may be subject to further development and do not necessarily represent "best" techniques.

A.3 Methods

Samples tested were well-preserved wood samples beyond or close to the limit of ^{14}C dating. Three were New Zealand kauri: cellulose from two of these (Wk5383, Wk5385) had been previously dated to >50 kyr (Turney et al. 2007) and one (OIS7) was known from stratigraphy to be >140 kyr (Marra et al. 2006). The Wk5385 sample was chosen for this study because earlier work at the Waikato ^{14}C laboratory suggested that it could not be fully cleaned even when rigorous ABA treatment was used (A Hogg, F Petchey, personal communications). The other 2 samples were woods used as background materials in our laboratory: a "Patagonia" spruce sample of unknown stratigraphic provenance from northeast Iowa, USA (S Stine, personal communication) previously dated to >50 kyr (CAMS-50039), and a conifer (probably spruce) sample collected near the Queets River mouth, Olympic Peninsula, Washington, USA, from a stratigraphic unit corresponding to oxygen isotope stage 5a or 5c (G Thackray, personal communication).

The woods were sampled as fine shavings ¡0.5 mm thick, cut from wood blocks with an X-Acto knife. We typically used samples of 20-40 mg of wood–much more than we would normally use for ABA treatment–because we anticipated significant losses in the cellulose extractions. The kauri samples strongly resembled newly cut wood and produced no dust when sliced, but the Queets-A and Patagonia woods, though well preserved, were noticeably more friable.

The ABA pretreatment was carried out in 13 100 mm test tubes covered with vented Fisher KimKap closures, on a heat block at 70 °C. Ultra-fine tip plastic pipets (Samco #233) were used throughout to minimize pipetting losses. Samples were treated with aliquots of ∼6 mL of 1N HCl for 30 min, followed by successive 30-min treatments with 1N NaOH until the liquid remained clear, ending with another 30-min 1N HCl wash. Samples were then washed several times in Milli-Q water (15 min, 70 °C) to pH >6 to remove remaining acid, dried for 30 min at 50 °C in a vacuum oven, and the tubes were capped with gas-tight closures (Fisher TainerTop). Processing times for batches of 10-25 samples were typically 5 to 6 hr.

Isolation of holocellulose was carried out in 13-mm test tubes at 70 °C in a fume hood. Early workers recommended that acid chlorite treatment be carried out at pH 2.4 or greater for maximum bleaching efficiency (Skelly 1960), which may be why weak (buffered) acids such as CH_3COOH have traditionally been used in Jayme-Wise extractions for stable isotope measurements. However, more recent studies (Kaczur and Cawlfield 2000; Svensson et al. 2006) indicate that there is little loss of efficiency even at very low pH. The acid decomposition of sodium chlorite in the presence of chloride ion was summarized by Gordon (1982) as:

$$5\,NaClO_2 + 4\,HCl \longrightarrow 4\,ClO_2 + 5\,NaCl + 2\,H_2O$$

Using equal volumes of 1N HCl and 1M NaClO2 solution simplifies the procedure and ensures that the reaction takes place under strongly acidic conditions (pH ∼1) where contamination by atmospheric CO_2 is unlikely. We found that 2.5 mL of bleaching agent and 2.5 mL of

acid was sufficient to bleach up to 40 mg of wood over 4-6 hr in most cases, though bleaching times varied. For a few of the larger samples, the ClO_2 was exhausted (indicated by the disappearance of the characteristic gold color of the solution) and a second short treatment was required to fully bleach some of the larger pieces. Some ClO_2 was initially evolved into the head space of the vented caps, but very little escaped.

After bleaching, the holocellulose was washed several times with Milli-Q water (30 min, 70 °C) to pH >6. Samples that had separated into fine fibers required centrifuging for several minutes before pipetting to help separate cellulose from liquid and thus reduce losses. The samples were then dried at 50 °C for 30 min in a vacuum oven, and the tubes were capped with gas-tight closures. For αcellulose extractions, the bleached holocellulose was washed once with Milli-Q, then treated with 6 mL of 5N NaOH for 1 hr at room temperature. This was followed by a 30-min treatment with 1N HCl at 70 °C to remove any absorbed atmospheric CO_2, then multiple Milli-Q washes and drying as above.

These procedures were compared with a more traditional batch processing cellulose extraction method (X Xu, personal communication), based on the work of Leavitt and Danzer (1993) and similar to techniques used previously for ^{14}C by Linick et al. (1986). Samples were processed in Ankom™F57 Dacron filter bags (25 µm effective pore size). Each bag was subdivided into 2 heatsealed pouches containing individual samples, and bags were identified by unique patterns of heatsealing lines. Up to 25 bags were placed in a 50-mm-ID (200 mL) Soxhlet apparatus and extracted with 600 mL of 2:1 mixture of ¿99.5% toluene and HPLC-grade ethanol and then with 600 mL of HPLC ethanol, each for ∼18 hr. Subsequent processing of the bags was carried out in a 2-L beaker covered with a watch glass, on a hot plate with a magnetic stirrer. Samples were boiled gently for 2 hr in Milli-Q water and then placed in a bleaching solution (4 g of sodium chlorite and 2 mL of glacial acetic acid added to 600 mL of water) at 70 °C. An additional 4 g of chlorite and 2 mL of acetic acid were added after 3-4 hr and the treatment was continued overnight, after which the samples were

washed several times with 600 mL of Milli-Q water over 3-4 hr and dried at 50 °C for 2-3 hr in a vacuum oven. For α-cellulose extraction, washed holocellulose samples were treated in 600 mL of 17% (weight/volume) NaOH for 1 hr at room temperature, treated at 70 °C with 1N HCl and then washed repeatedly with water and dried as above.

Further variations of the holocellulose isolation step were made by modifying both the bleaching agent and the activating acid. A 5% sodium hypochlorite solution (Chlorox), which is the traditional source of Cl_2 for chlorine-based bleaching (Long and Kalin 1992), was tested briefly as an alternative to sodium chlorite in the test tube-based protocol, though chlorite is now strongly preferred for extracting cellulose because the ClO2 produced attacks lignin only and the reaction does not generate harmful free Cl_2. The standard batch processing Jayme-Wise method (Leavitt and Danzer 1993) uses glacial acetic acid to activate the chlorite, but mineral acids such as H_3PO_4 and HCl have been used in some ^{14}C studies (Pearson and Stuiver 1986; Long and Kalin 1992; A Hogg, personal communication), reducing the exposure of samples to carbon-containing reagents. We tested the use of H_3PO_4 and HCl as alternatives to acetic acid and ultimately chose HCl for the test tube-based method described above. We also checked whether baking ABA-treated samples immediately prior to combustion was effective for reducing backgrounds. Samples in unsealed quartz combustion tubes prefilled with CuO and Ag, were baked in air for 1 hr or 3 hr in a muffle furnace at 160 °C or 300 °C, prior to sealing in vacuum and combustion at 900 °C. The 300 °C bake caused actual charring of the wood, and was intended to approximate the low-temperature stage of the stepped-combustion protocol of Bird et al. (1999), who found that a 330 °C combustion with a limited quantity of oxygen gas was very effective at removing contaminants remaining after ABOX.

A.4 Results

A surprising result of our initial cellulose extraction tests was to reveal that a small but significant source of contamination existed: results for holoor α-cellulose samples showed substantial scatter and some were elevated (by 0.1-0.5 pMC) compared to ABA-only results on the same wood. The source of the contamination was ultimately shown to be the NaClO2 when a new batch was purchased, but the contamination mechanism remains unclear.

Within the obvious limitations imposed by this problem, we found no differences in ^{14}C results for OIS7 kauri, Patagonia spruce, Queets-A, and Wk5383 kauri for several variations of the cellulose extraction procedures (Table 1). Samples treated with the full Jayme-Wise α-cellulose protocol described above, including 2 days of Soxhlet extractions, returned results similar to those where ABA-treated wood was transferred to the Ankom bags for subsequent holo or α-cellulose extractions, or samples where all processing was carried out in test tubes. In addition, we saw no significant differences between results for cellulose extractions where acetic acid, H_3PO_4, and HCl were used as chlorite activators. We also tested using a stronger acid for the final neutralization step after NaOH treatment for α-cellulose: 2M H_2SO_4, 2 hr at 70 °C, used by Hattè et al. (2001) to enhance the effectiveness of the final step of ABA; but saw no improvement.

In spite of the presence of low-level contamination from the chlorite, these results suggested strongly that ABA treatment followed by cellulose extraction in the 13-mm test tubes was as effective as the full Jayme-Wise treatment, while taking far less time overall. Subsequent tests were therefore aimed at optimizing the test tube method described above. ABA-treated samples destined for cellulose extraction were treated with HCl and chlorite solution immediately after the last acid wash of ABA, and left overnight at room temperature. This reduced the subsequent 70 °C bleaching time to 2-3 hr and the overall processing time for holo or α-cellulose production to 24-30 hr: typically from the late morning of one day to the after-

Table A.1: Initial ^{14}C results for OIS7 kauri, Patagonia spruce, Queets-A, and QK5383.

	Cellulose extraction[a]			^{14}C results	
Pretreatment	Activating acid/ processed in:	Cellulose fraction	Neutralizing acid for alpha-cellulose	pMC	±
ABA		None		0.20	0.13
Soxhlet	HAc/bags	Alpha	HCl	0.23	0.07
ABA	HAc/bags	Alpha	HCl	0.37	0.13
ABA	H_3PO_4	Alpha	HCl	0.34	0.04
ABA	HCl/bags	Holo		0.35	0.05
ABA	HCl/tubes	Holo		0.28	0.11
ABA	HCl/tubes	Alpha	HCl	0.27	0.10
ABA	HCl/tubes	Alpah	HCl	0.31	0.12

[a]HAc: acetic acid. Note: all cellulose samples were extracted with the first (contaminated) batch of chlorite.

noon of the next. An obvious next step would be to leave the samples at higher temperature overnight, but we have not yet tested this for fear of sample losses. (Note: we have since determined that yields for samples left bleaching overnight at 70 °C are indistinguishable from those for samples treated as above).

We tested weaker HCl and chlorite mixtures (2.5 mL of 0.25N HCl with 2.5 mL of 0.25M $NaClO_2$) but found that bleaching times increased and that 30-40 mg wood samples often required a second application of bleaching solutions. Bleaching with HCl-activated Chlorox (Long and Kalin 1992) required numerous applications of bleaching solutions following an overnight soak at room temperature, was obviously more destructive to some samples than chlorite, produced free chlorine, and left samples still only partially bleached after a full working day.

Backgrounds for holo and α-cellulose extractions using the optimized test tube procedure with the new chlorite were gratifyingly lower; data from these experiments and from samples treated with ABA are shown in Figure 1. (In comparing our results with data from other studies, it is important to note that all data shown here are raw ^{14}C results: no processing line blanks or AMS "machine" backgrounds have been subtracted.) For OIS7 kauri, Patagonia

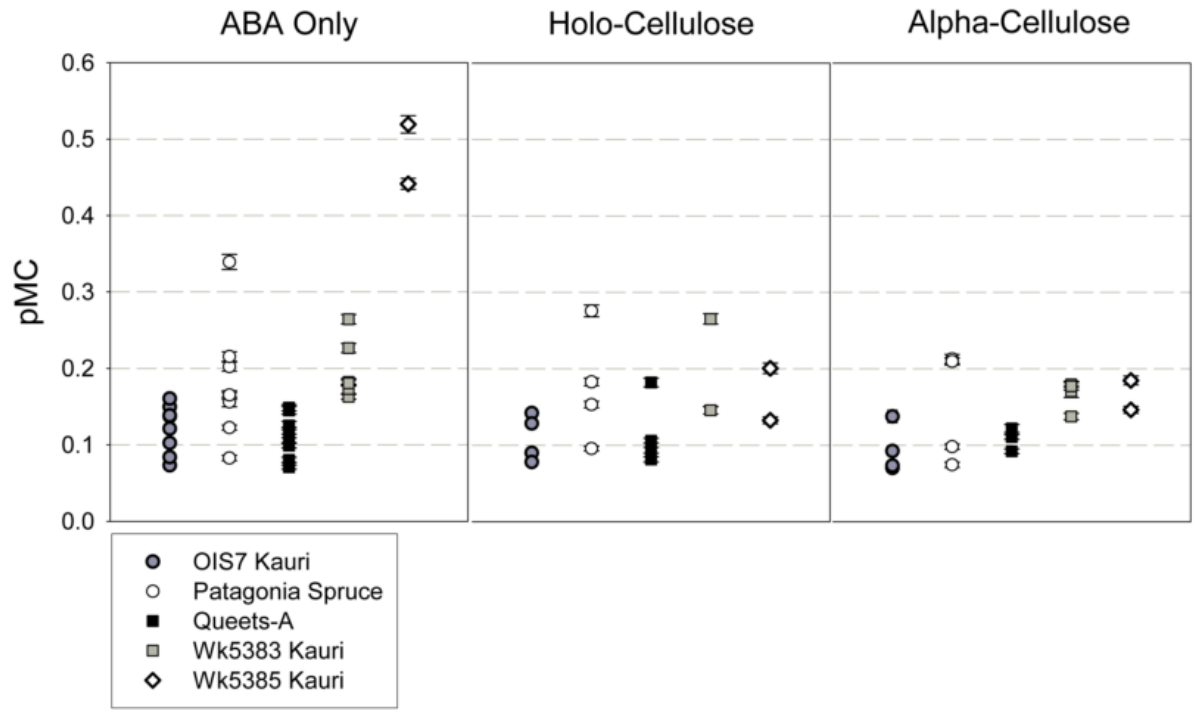

Figure A.1: ^{14}C results (pMC) for wood samples treated with the standard ABA protocol, and ABA plus holo- and alpha-cellulose extractions. Note that all data are shown as raw values: no backgrounds have been subtracted.

spruce, Queets-A, and Wk5383 kauri, the results show little difference between pretreatment methods. Wk5383 consistently displayed slightly higher pMC values than the samples known from stratigraphy to be beyond the limit of ^{14}C dating, and may indeed be younger. Wk5385 kauri was previously measured at Waikato and found to be difficult to clean by ABA, even when treated with multiple base washes. In our tests, we found that by isolating holocellulose the background for this sample was significantly improved, though further processing to α-cellulose had little effect.

Yields from ABA were uniformly high, but large decreases in sample mass were observed with increased processing to holo and α-cellulose, particularly for the less well-preserved Queets-A and Patagonia samples. Table 2 shows average yields from test tube processing. In some cases, 30 mg or more of wood was required to produce 3 mg of α-cellulose, which in turn would yield about 1 mg of graphite for AMS. Furthermore, cellulose yields for a given type of

wood showed significant scatter about these mean values, suggesting that wood preservation can vary significantly even within a single wood block.

Table A.2: Average percent yield for samples by treatment method

	ABA	Holocellulose	Alpha-cellulose
OIS7 kauri	79	35	30
Patagonia	73	16	11
Queets-A	71	15	10
WK5383	77	36	27
WK5385	76	44	33

Samples of holocellulose (and α-cellulose to an even greater extent) were very fluffy compared to ABA-treated wood, and sample handling problems due to static were correspondingly severe. The cellulose was particularly difficult to load into 6-mm quartz tubes for combustion, and in many cases cellulose fibers were left on the tube walls in the area where the tubes are sealed. This can lead to sealing problems as the adhering cellulose pyrolyzes in vacuum and effectively increases the melting point of the quartz. An effective solution to this problem is to burn off the stray fibers from the portion of the tubes where sealing takes place, by heating this area in air with a gas torch before attaching the tubes to the combustion vacuum line (X Xu, personal communication).

Samples that were baked just prior to combustion showed slight improvement in backgrounds in some cases (Figure 2), but the differences were small and may simply reflect random scatter. Baking for 3 hr versus 1 hr at each temperature produced no obvious increases in the ^{14}C ages. Carbon losses due to charring in the 300 °C bake (calculated from the CO_2 yields per initial mass of ABA-treated wood for charred and uncharred samples) were significant, and increased from ∼30% for a 1-hr bake to ∼40% after 3 hr. In marked contrast to the effect of the post-ABOX low-temperature oxygen combustion of Bird et al. (1999), charring in air had little effect on ^{14}C ages from these ABA-treated samples.

A.5 Discussion

One possible candidate for the puzzling contamination of the first batch of $NaClO_2$ is absorption of atmospheric CO_2, since the jar of chlorite had been in general use in another laboratory for several months and could conceivably have been left open for extended periods. Prior to our experiments, it was used only for extractions on modern and post-bomb samples, and so the contamination was not detected. However, it is difficult to understand how any absorbed CO_2 could have been transferred to the cellulose, since the bleaching protocols involved activation under acidic conditions (strongly acidic in some cases) in part to minimize this possibility.

Hatt et al. (2001) pointed out that replacement of hydroxyl groups in wood structures by Cl^- (which does occur to some extent during chlorite delignification at low pH, e.g. Svensson et al. 2006) might lead to subsequent carboxylation via a further replacement of Cl^- by carbonate ions, but again, this second step requires alkaline conditions that were not present in our experiments. Furthermore, Hatt et al. also found that any bound CO_2 was effectively removed by subsequent treatment with 2M H_2SO_4, which did not remove the contamination we encountered.

Our tests of cellulose extraction methods indicate that pretreatment of samples in individual 13-mm test tubes by ABA plus bleaching is effective, and appears to have several advantages over Soxhlet/ bleach batch processing in the Ankom filter bags. No specialized Soxhlet equipment is required, the process takes significantly less time, any possibility of cross-contamination is removed, and labeling of samples is easier. Furthermore, the Dacron bag material consists of white matted fibers that are sometimes difficult to distinguish from adhering cellulose, which can complicate the removal of samples when the bags are cut apart after processing.

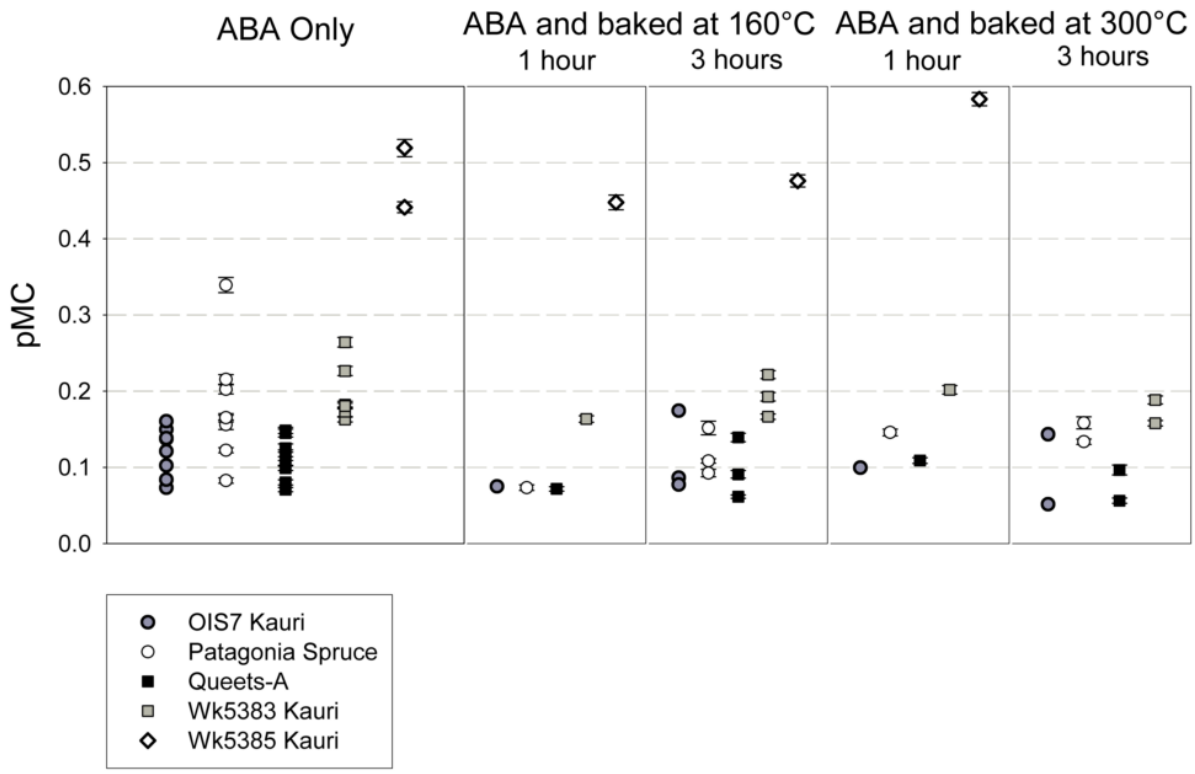

Figure A.2: ^{14}C results (pMC) for ABA-treated wood samples baked in air in quartz combustion tubes just prior to sealing. (The Wk5385 sample baked for 3 hr at 400 °C was lost during graphitization.)

However, while the test tube method seems superior for the well-preserved woods used here, we recognize that this may not be true for more degraded samples. Processing in tubes requires many pipetting steps, and these may also require centrifugation if the samples begin to disintegrate, so that for samples with marginal preservation, batch processing in filter bags may actually be less labor intensive, and therefore preferable. If the conventional Jayme-Wise method is used for such cases, it would seem prudent to adapt it for the special requirements of ^{14}C, though the excellent cellulose ^{14}C results obtained in previous studies suggests that few serious problems exist. Nevertheless, since concerns have been raised about possible contamination by solvent residues (Long and Kalin 1992), using only ^{14}C-dead solvents rather than modern ethanol in any Soxhlet processing of old samples seems desirable (Hogg et al. 2006), though we did not test this. Our results show no disadvantages to using mineral acids for bleaching, thus avoiding unnecessary exposure of samples to organic acids.

For 4 of the 5 woods tested (OIS7 kauri, Patagonia spruce, Queets-A, and Wk5383 kauri), ^{14}C values for wood pretreated with ABA were not significantly different from ^{14}C values for holo or α-cellulose extractions. However, our results for the Wk5385 kauri sample (Figure 3) clearly confirm the earlier findings of the Waikato ^{14}C laboratory. This wood contains younger contaminating material that could not be completely removed by ABA, even with multiple base treatments at high temperature, and was unaffected by subsequent 160 °C baking or 300 °C charring in air. The contamination was effectively removed by holocellulose extraction, and further processing to αcellulose did not produce significantly older ages.

These tests have therefore confirmed that a subset of old wood does exist for which even rigorous ABA treatment is ineffective and more elaborate/harsh treatments are required. Given that those methods involve significant extra work and result in lower processing yields than ABA, a useful strategy for projects involving large numbers of measurements on single logs (e.g. calibration studies) would be to carry out spot-checks on inner and outer rings of

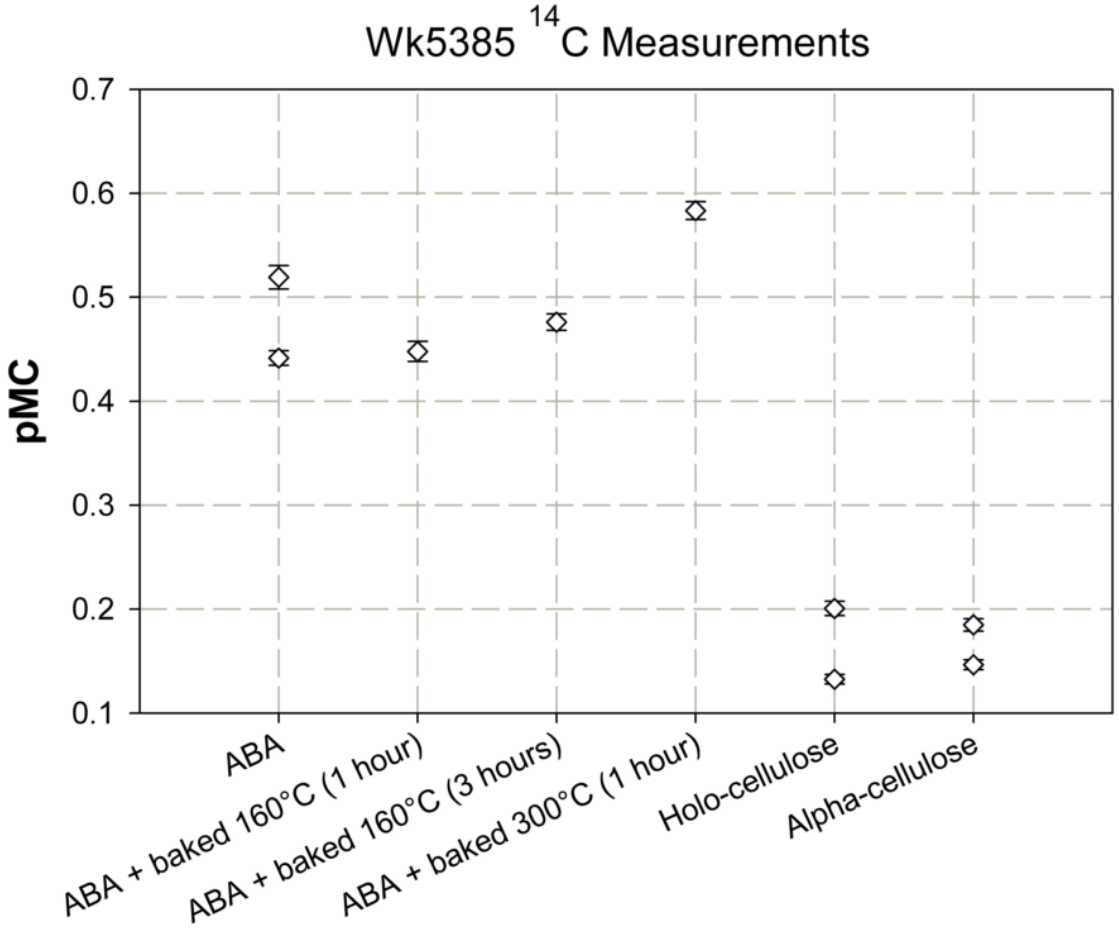

Figure A.3: ^{14}C measurements on Wk5385 showed that cellulose extraction was required for removal of young contamination from this sample: ABA with or without subsequent baking was ineffective.

ABA versus holocellulose or other pretreatment of choice. If ABA proved effective, as it did for 4 of the 5 woods tested here, it could then be used with confidence for the large-scale study.

A.6 Acknowledgements

We thank Xiaomei Xu for laboratory assistance, and Glenn Thackray, Scott Stine, Alan Hogg, and Fiona Petchey for information on wood samples, pretreatment methods used in the Waikato radiocarbon lab, and previous ^{14}C results.

A.7 References

Bird MI, Ayliffe LK, Fifield LK, Turney CSM, Cresswell RG, Barrows TT, David B. 1999. Radiocarbon dating of "old?" charcoal using a wet oxidation, stepped-combustion procedure. Radiocarbon 41(2):127?40.

Brown TA, Nelson DE, Matthewes RW, Vogel JS, Southon JR. 1989. Radiocarbon dating of pollen by accelerator mass spectrometry. Quaternary Research 32(2):205-12.

Cain WF, Suess HE. 1976. Carbon 14 in tree rings. Journal of Geophysical Research 81(21):3688-94. Gaudinski JB, Dawson TE, Quideau S, Schuur EAG, Roden JS, Trumbore SE, Sandquist DR, Oh S-W, Wasylishen RE. 2005. Comparative analysis of cellulose preparation techniques for use with 13C, 14C and 18O isotopic measurements. Analytical Chemistry 77(22): 7212-24.

Gillespie R. 1990. On the use of oxidation for AMS sample pretreatment. Nuclear Instruments and Methods in Physics Research B 52(3-4):345-7.

Gordon G. 1982. Improved methods of analysis for chlorate, chlorite, and hypochlorite ions at the sub-mg/L level. In: Proceedings of the Water Quality Technology Conference. American Water Works Association, Nashville, Tennessee, USA. p 175-89.

Green JW. 1963. Methods of Carbohydrate Chemistry. New York: Academic Press. p 9-21.

Hatt C, Morvan J, Noury C, Paterne M. 2001. Is classical acid-alkali-acid treatment responsible for contamination? An alternative proposition. Radiocarbon 43(2A):177-82.

Hogg AG, Fifield LK, Turney CSM, Palmer JG, Galbraith R, Baillie MGK. 2006. Dating ancient wood by high sensitivity liquid scintillation counting and accelerator mass spectrometry-pushing the boundaries. Quaternary Geochronology 1(4):241-8.

Kaczur JJ, Cawlfield DW. 2000. Chlorine oxygen acids and salts, chlorous acid, chlorites and chlorine dioxide. In: Kirk-Othmer Encyclopedia of Chemical Technology. 5th edition. New York: John Wiley and Sons.

Leavitt SW, Danzer SR. 1993. Method for processing small wood samples to holocellulose for stable-carbon isotope analysis. Analytical Chemistry 65(1):87-89.

Linick TW, Long A, Damon PE, Ferguson CW. 1986. High-precision radiocarbon dating of bristlecone pine from 6554 to 5350 BC. Radiocarbon 28(2B): 943-53.

Long A, Kalin RM. 1992. High-sensitivity radiocarbon dating in the 50,000 to 70,000 BP range without isotopic enrichment. Radiocarbon 34(2):351-9.

Marra MJ, Alloway BV, Newnham RM. 2006. Paleoenvironmental reconstruction of a well-preserved Stage 7 forest sequence catastrophically buried by basaltic eruptive deposits, northern New Zealand. Quaternary Science Reviews 25(17-18):2143-61.

Pearson GW, Stuiver M. 1986. High-precision calibration of the radiocarbon time scale 500-2500 BC. Radiocarbon 28(2B):839-62.

Pigati JS, Quade J, Wilson J, Jull AJT, Lifton NA. 2007. Development of low-background vacuum extraction and graphitization systems for 14C dating of old (4060 ka) samples. Quaternary International 166(1):414.

Santos GM, Bird MI, Pillans B, Fifield LK, Alloway BV, Chappell J, Hausladen PA, Arneth A. 2001. Radiocarbon dating of wood using different pretreatment procedures: application to the chronology of Rotoehu Ash, New Zealand. Radiocarbon 43(2A):239-48.

Skelly JK. 1960. The theory and practice of sodium chlorite bleaching. The Journal of the Society of Dyers and Colorists 76(8):469-79.

Stuiver M, Quay PD. 1981 Atmospheric 14C changes resulting from fossil fuel CO2 release and cosmic ray flux variability. Earth and Planetary Science 53(3): 349-62.

Svensson DR, Jameel H, Chang H-M, Kadla JF. 2006. Inorganic reactions in chlorine dioxide bleaching of softwood kraft pulp. Journal of Wood Chemistry and Technology 26(3):201-13.

Turney CSM, Fifield LK, Palmer JG, Hogg AG, Baillie MGL, Galbraith R, Ogden J, Lorrey A, Tims SG. 2007. Towards a radiocarbon calibration for oxygen isotope stage 3 using New Zealand kauri (Agathis Australis). Radiocarbon 49(2):447-57.